With a bright young mind and a map to see: Imaging topographic map reorganization in the developing visual system

Vanessa Junyang Li

Integrated Program in Neuroscience

McGill University, Montreal

January 2025

A thesis submitted to McGill University in partial fulfillment of the requirements of the degree of Doctor of Philosophy.

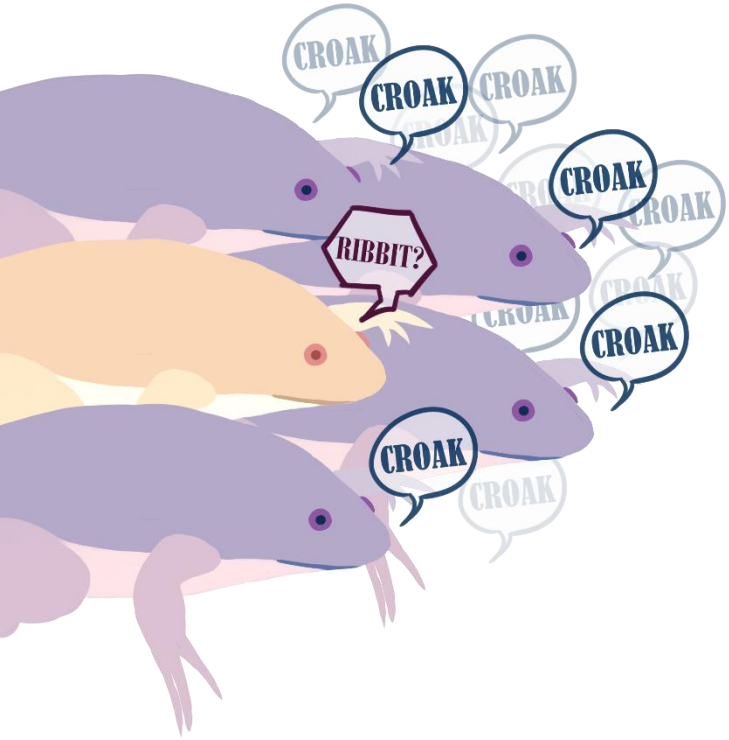

……To all of you who fired together with me
and gave me a place to belong.

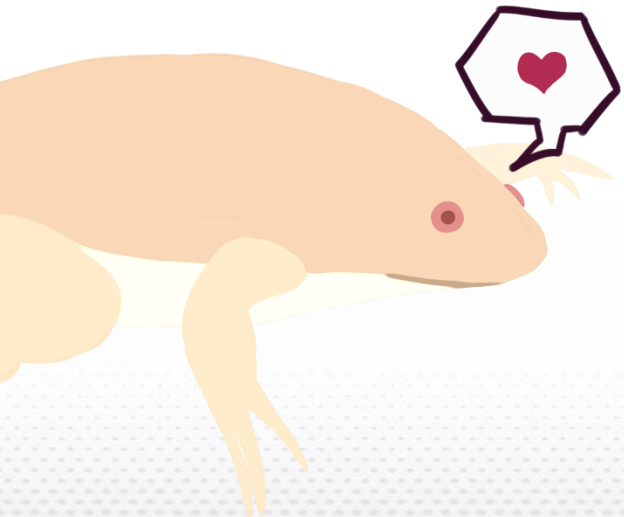

Table of Contents

*Chapters II and III are published manuscripts, thus reference formatting will differ from the rest of the thesis.

Acknowledgements

I would like to express my thanks to all who have guided and supported me on my journey thus far.

To Mom, Dad and Aunt Sally: despite the distance between us you've always been right behind me, and I've never felt far away from home. To Auntie Dawn, thank you for your guidance and inspiration. To Auntie Grace, your warmth and kindness will always be missed. To Luyang, thanks for feeding me and listening to all my rants, I am incredibly lucky to have you as a roommate and friend.

To members of the Ruthazer lab, past and present: Thank you for being my family through all these years. To Anne, thanks for working all the miracles. To Cynthia, your cupcakes are the best in the world. To Phil, Tony, Elena, Stephen, Marion and Tasnia, thanks for showing me the ropes and kicking my time with the tadpoles off with a blast. To Zahraa, the most wonderful collaborator, thanks for dragging me across the finish line for the Neuroscience review after I've been out of commission. To Nick, Ryan, Sarah, Andrew and Weihang, thanks for sharing time with me in the lab and making it truly special. To David, Finnley and Anna, my *kouhais* whom I find myself relying on all the time, especially while trudging out this thesis – thanks for having my back. To William and Natasha, my most recent co-occupants in the office with all the snacks – I count on you to bring in the future of Team Tadpole.

To Dr. Jesper Sjöström, Dr. Christopher Pack, Dr. Curtis Baker and Dr. Kenneth Hastings: Thank you for your kind guidance and mentorship. Thanks to the IPN, the Neuro, the McGill Faculty of Medicine and NSERC for providing funding and resources.

To Ed, from whom I've aspired to learn all about how to become a proper scientist: Thanks for being the best supervisor I could ever ask for.

List of abbreviations

3D	three-dimensional
AMPA	*α*-amino-3-hydroxy-5-methyl-4-isoxazolepropionic acid
AMPAR	*α*-amino-3-hydroxy-5-methyl-4-isoxazolepropionic acid receptor
ANOVA	analysis of variance
APV	(2*R*)-amino-5-phosphonovaleric acid
BMP	bone morphogenic protein
Ca^{2+}	calcium ion
CaM	calmodulin
CldU	5-chloro-2'-deoxyuridine
cpGFP	circularly permuted green fluorescent protein
dpf	days post fertilization
DSGC	direction-selective ganglion cell
GABA	*gamma*-Aminobutyric acid
GECI	genetically encoded calcium indicator
GFP	green fluorescent protein
GluN1	glutamate receptor NMDA type subunit 1
GluN2	glutamate receptor NMDA type subunit 2
GluN3	glutamate receptor NMDA type subunit 3
hCG	human chorionic gonadotropin
HEPES	4-(2-hydroxyethyl)-1-piperazineethanesulfonic acid
LGN	lateral geniculate nucleus
LTP	long-term potentiation
LTD	long-term depression
MBSH	modified Barth’s saline
MK-801	dizocilpine
mRNA	messenger RNA
MT	middle temporal area
NC	noise correlation

NMDA	*N*-methyl-D-aspartate
NMDAR	*N*-methyl-D-aspartate receptor
PMSG	pregnant mare serum gonadotropin
PMT	photomultiplier tube
PTU	phenylthiourea
RF	receptive field
RGC	retinal ganglion cell
ROI	region of interest
SC	superior colliculus
Shh	Sonic Hedgehog
STDP	spike-timing-dependent plasticity
V1	primary visual cortex
WGA-HRP	wheat germ agglutinin-horseradish peroxidase

Abstract

Topographic organization in sensory systems has been a long-standing topic of interest in circuit and developmental neuroscience, thanks to its ubiquitous presence across species and sensory modalities. Advances in fluorescence microscopy *in vivo* have opened opportunities to study the emergence and evolution of topographic maps in developing sensory systems at a new level of resolution and precision. Here we used two-photon calcium imaging to perform retinotopic mapping in the optic tectum of *Xenopus laevis* tadpoles, permitting a three-dimensional view of the functional retinotopic map at sub-cellular resolution that could be followed in the same animal over several days. We focused our observations on a time window between developmental stages 43 and 48 when the visual system of the tadpole is known to undergo robust growth and refinement. Injecting GCaMP6s mRNA into one blastomere of two-cell stage embryos yielded mosaic tadpoles with GCaMP expression restricted to one lateral half of the animal, labelling postsynaptic tectal neurons in one hemisphere and retinal ganglion cell axons crossing over to the opposite hemisphere. This provides a model to separately observe presynaptic and postsynaptic retinotopic maps in the same animal. Longitudinal imaging revealed a marked change in the 3D map gradient between stage 45 and 48, as well as an increase in the smoothness of local map gradients that was partially reduced by NMDA receptor blockade. We further performed retinotopic mapping in GCaMP6s-expressing tadpoles with sparse Alexa594-dextran dye labelling of postsynaptic tectal neurons. This allowed us to quantify developmental changes in the position and dendritic field morphology of the dextran-labelled cells and compare them to volumetric changes in the whole tectum. We made a parallel comparison in the functional aspect, comparing receptive field inputs to individual cells versus the span of visual field representations covered by the whole tectum. The results of these investigations provide us a bridge to understanding the relationship between morphological and functional changes in an actively growing immature visual system.

Résumé

L'organisation topographique dans les systèmes sensoriels est depuis longtemps un sujet d'intérêt dans les neurosciences des circuits et du développement en raison de son omniprésence chez toutes les espèces et dans toutes les modalités sensorielles. Les progrès de la microscopie à fluorescence in-vivo ont permis d'étudier l'émergence et l'évolution des cartes topographiques dans les systèmes sensoriels en développement à un nouveau niveau de résolution et de précision. Ici, nous avons utilisé l'imagerie calcique à deux photons pour réaliser une cartographie rétinotopique dans le tectum optique de têtards de Xenopus laevis, ce qui nous a permis d'obtenir une vue tridimensionnelle de la carte rétinotopique fonctionnelle à une résolution subcellulaire suivie chez le même animal sur multiple jours consécutifs. Nous avons concentré nos observations sur une fenêtre temporelle située entre les stades de développement 43 et 48, période pendant laquelle le système visuel de ces têtards connaît une croissance et un raffinement importants. L'injection de l'ARNm GCaMP6s dans un blastomère d'embryons au stade deux-cellules produit des têtards mosaïques avec une expression de GCaMP limitée à une moitié latérale de l'animal, marquant les neurones tectaux postsynaptiques dans un hémisphère et les axones des cellules ganglionnaires de la rétine traversant jusqu'à l'hémisphère opposé, nous fournissant un modèle pour observer séparément les cartes rétinotopiques présynaptiques et postsynaptiques dans le même animal. L'imagerie longitudinale a révélé un changement marqué dans le gradient de la carte 3D entre les stades 45 et 48, ainsi qu'une augmentation de la continuité des gradients locaux de la carte qui a été partiellement réduite par le blocage des récepteurs NMDA. Nous avons procédé à une cartographie rétinotopique chez des têtards exprimant le GCaMP6s avec un marquage au traceur Alexa594-dextran des neurones tectaux post-synaptiques. Cela nous a permis de quantifier les changements développementaux dans la position et la morphologie du champ dendritique des cellules marquées au dextran et de les comparer aux changements volumétriques de l'ensemble du tectum. Nous avons effectué une comparaison parallèle sur le plan fonctionnel, en comparant les champs

réceptifs entrants aux cellules individuelles à l'étendue des représentations du champ visuel couvertes par l'ensemble du tectum. Les résultats de ces recherches nous permettent de comprendre la relation entre les changements morphologiques et fonctionnels dans le système visuel immature et en croissance.

Contribution to original knowledge

The assembly of neural circuits in early development to form sensory maps has been a topic well documented and researched, yet much of the process and its underlying mechanisms remains to be elucidated. Recent advances in *in vivo* fluorescence microscopy and genetic manipulation provide powerful tools to characterize the developmental progression of sensory map formation with unprecedented clarity and resolution. What was previously described by traditional methods such as histological staining or electrophysiology focusing on a limited subset of cells can now be re-examined with non-invasive imaging procedures that offer a whole-brain, subcellular-resolution view of both morphology and functional activity. Innovations in labelling techniques also enable the targeting of specific cells or components in the circuit with enhanced specificity.

The research projects documented in this thesis take advantage of cutting-edge imaging tools and techniques to characterize topographic map formation in the visual system of *Xenopus laevis*, the African clawed frog, an animal model for circuit development with a wealth of historical studies to build upon and many advantageous traits that make it highly compatible with *in vivo* fluorescence microscopy.

In Chapter III, we used the genetically encoded calcium indicator GCaMP6s to visualize neuronal activity in the larval Xenopus tectum with two-photon calcium imaging, and developed a pipeline to perform retinotopic mapping to extract the three-dimensional layout of visual field representations in the tectum and quantify fine-scale properties of the retinotopic maps. Characterizations of the retinotopic map in the developing Xenopus tectum in prior studies were performed with anatomical tracing (Sakaguchi & Murphey, 1985) or coarse multiunit electrophysiology recordings (Gaze et al., 1974; Holt & Harris, 1983), limiting scale and resolution to a subset of cells or recording points. Our approach expanded the range of measurements to the whole tectum while resolving subcellular details. The non-invasive nature of the imaging procedures also made it possible to perform multiple imaging sessions on the same animal over several days.

We showed the existence of coarse retinotopic gradients in animals as young as developmental stage 42 (following Nieuwkoop and Faber (1994)), only a day after retinal ganglion cells (RGCs) first reach the tectum (Holt & Harris, 1983). Retinotopic maps extracted at stage 45 and 48 showed more pronounced retinotopic gradients, and we noted a striking change in the 3D orientation of the gradients between the two stages, pointing to extensive circuit rewiring occurring during this period.

Two properties are often associated with the degree of refinement in visual circuits: the smoothness of topographic gradients, considering one of the hallmarks of mature visual maps is a high degree of order in their spatial patterning; another being receptive field sizes of individual units in the circuit, as smaller receptive field sizes translate to higher visual acuity. We designed two measures to characterize these properties: “local discontinuity” to quantify the neighborhood smoothness of the map gradient, and “receptive field sharpness” to approximate receptive field size. We applied these measures to our longitudinal imaging data recording from the same animals at different developmental stages and found a stage-dependent difference in both measures, quantitatively demonstrating functional map refinement as animals mature.

Visually driven activity guide circuit wiring in the retinotectal system through the Hebbian mechanism of “neurons that fire together wire together" (Kutsarova et al., 2017), and the *N*-methyl-D-aspartate receptor (NMDAR), an ion channel found at synapses and function as a coincidence detector for concurrent pre- and postsynaptic activity, has been shown to play a role in this visual activity-dependent refinement process (Dong et al., 2009; Rajan et al., 1999; Zhang et al., 1998). We treated tadpoles with the NMDAR antagonist dizocilpine (MK-801) and measured a significant change in both “local discontinuity” and “receptive field sharpness” in the retinotopic maps of these tadpoles compared to untreated animals, demonstrating the involvement of NMDARs in the outcome of map refinement (Li et al., 2022).

To follow up with the observation of marked changes in the retinotopic gradient between developmental stages 45 and 48 and gain a clearer picture of how the changes occur, in Chapter IV, we labelled individual tectal neurons in GCaMP-expressing tadpoles to serve as fiducial markers in longitudinal imaging experiments, allowing us a side-by-side

comparison to examine how developmental changes in morphology relate to changes in functional visual representations, and how changes in single neurons sum up to changes seen in the whole tectum.

In both Chapter III and Chapter IV, we employed a technique developed in the Ruthazer laboratory of injecting GCaMP mRNA into one blastomere of two-cell stage embryos to generate hemi-mosaic tadpoles with GCaMP expression limited to one lateral half of the animal (Benfey et al., 2021). As retinal projections in Xenopus at this stage cross over entirely to innervate the tectal hemisphere on the opposite side, these hemi-mosaic animals will have GCaMP expression in only RGC axon terminals in one tectal hemisphere and only tectal cells in the other, effectively separating pre- and postsynaptic components of the retinotectal pathway. We took advantage of this unique property to separately visualise pre- and postsynaptic retinotopic maps in the same animals in Chapter III, and restrict our functional analyses to the postsynaptic component of the retinotectal system in Chapter IV.

In all, the studies in this thesis contributed new pieces to the current understanding of circuit formation in the Xenopus retinotectal system, and demonstrated the application of various novel tools and techniques in functional imaging and analysis that can be transferred to future research in similar topics.

References

Benfey, N. J., Li, V. J., Schohl, A., & Ruthazer, E. S. (2021). Sodium-calcium exchanger mediates sensory-evoked glial calcium transients in the developing retinotectal system. *Cell Reports*, *37*(1).

Dong, W., Lee, R. H., Xu, H., Yang, S., Pratt, K. G., Cao, V., Song, Y.-K., Nurmikko, A., & Aizenman, C. D. (2009). Visual avoidance in Xenopus tadpoles is correlated with the maturation of visual responses in the optic tectum. *Journal of neurophysiology*, *101*(2), 803-815. https://doi.org/10.1152/jn.90848.2008

Gaze, R. M., Keating, M., & Chung, S. (1974). The evolution of the retinotectal map during development in Xenopus. *Proceedings of the Royal Society of London. Series B. Biological Sciences*, *185*(1080), 301-330.

Holt, C. E., & Harris, W. A. (1983). Order in the initial retinotectal map in Xenopus: a new technique for labelling growing nerve fibres. *Nature*, *301*(5896), 150-152. https://doi.org/10.1038/301150a0

Kutsarova, E., Munz, M., & Ruthazer, E. S. (2017). Rules for Shaping Neural Connections in the Developing Brain. *Frontiers in neural circuits*, *10*, 111-111. https://doi.org/10.3389/fncir.2016.00111

Li, V. J., Schohl, A., & Ruthazer, E. S. (2022). Topographic map formation and the effects of NMDA receptor blockade in the developing visual system. *Proceedings of the National Academy of Sciences*, *119*(8), e2107899119.

Nieuwkoop, P. D., & Faber, J. (1994). *Normal Table of Xenopus Laevis (Daudin): A Systematical and Chronological Survey of the Development from the Fertilized Egg Till the End of Metamorphosis*. Garland Pub.

Rajan, I., Witte, S., & Cline, H. T. (1999). NMDA receptor activity stabilizes presynaptic retinotectal axons and postsynaptic optic tectal cell dendritesin vivo. *Journal of Neurobiology*, *38*(3), 357-368. https://doi.org/10.1002/(sici)1097-4695(19990215)38:3<357::aid-neu5>3.0.co;2-#

Sakaguchi, D. S., & Murphey, R. K. (1985). Map formation in the developing Xenopus retinotectal system: an examination of ganglion cell terminal arborizations. *Journal of Neuroscience*, *5*(12), 3228-3245. https://doi.org/10.1523/JNEUROSCI.05-12-03228.1985

Zhang, L. I., Tao, H. W., Holt, C. E., Harris, W. A., & Poo, M.-m. (1998). A critical window for cooperation and competition among developing retinotectal synapses. *Nature*, *395*(6697), 37-44. https://doi.org/10.1038/25665

Chapter I: Introduction

Author contributions

Vanessa Li wrote this chapter, with revisions by Edward Ruthazer.

Overview

Neural circuits in vertebrate brain areas responsible for sensory processing often display topographic organization, where neurons encoding similar sensory features are spatially organized in close proximity. The organization of sensory maps is closely linked to the structure and function of sensory circuits (Fritzsch et al., 2019; Kaas, 1997; Young, 1998), making the formation of maps a topic of wide interest in developmental neuroscience. The work in this thesis revolves around understanding principles and mechanisms underlying the developmental formation of sensory maps, specifically in the visual system of *Xenopus laevis*. In this chapter, we aim to provide a primer on key concepts that will be relevant for understanding the rest of the thesis. We will start with an overview of sensory maps and what is known about the mechanisms guiding circuit formation, further expanded on in Chapter II. This will be followed by a brief introduction to Xenopus and the Xenopus retinotectal system as a model for studying sensory map development, as well as two-photon microscopy and the genetically encoded calcium indicator GCaMP, tools that were prominently used in the work in Chapters III~IV.

Sensory maps and the retinotectal system

Sensory maps are areas of the brain that respond to sensory stimulation from the environment, in which neurons are spatially organized according to features of the stimulus they encode. Sensory maps are often topographically organized to reflect the sensory surface from which they receive their inputs, examples being visual maps that spatially mirror the retina (Dhande & Huberman, 2014; Hubel & Wiesel, 1977), and

auditory maps that mirror the cochlea (Schreiner & Winer, 2007).

The retinotectal system is the pathway from the retina to the optic tectum in birds, reptiles and amphibians, and the superior colliculus (SC) in mammals. In non-mammalian vertebrates such as Xenopus, the optic tectum is the main processor of visual information. Retinal projections form topographically ordered terminations in the tectum, with the dorsal-ventral (D-V) axis of the retina mapped to the lateral-medial (L-M) axis of the tectum, and the temporal-nasal (T-N) axis of the retina mapped to the rostral-caudal (R-C) axis of the tectum (Fig.I.1).

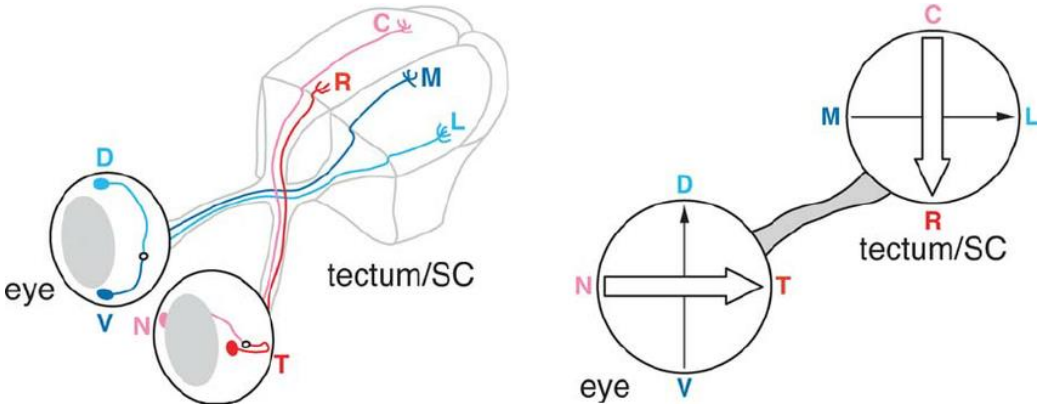

Figure I.1. Configuration of the retinotectal map.
Reprinted from Lemke and Reber (2005) with permission from the publisher.

Mechanisms guiding map formation

The developmental wiring of sensory circuits relies on two broad sources for guidance: molecular guidance cues and neuronal activity.

Molecular guidance cues are distributed in gradients in the developing brain and are generally considered to establish the coarse layout of sensory maps (Triplett, 2014). The prominent molecular guidance cues in the retinotectal system are molecules from the ephrin/Eph family, with ephrin-A/EphA mediating axon targeting along the rostrocaudal axis of the tectum, and ephrin-B/EphB mediating axon targeting along the mediolateral axis (McLaughlin, Hindges, et al., 2003). Ephrin and Eph gradients are

present in the Xenopus tectum starting from very early stages and remain to the time of metamorphosis (Higenell et al., 2012; Mann et al., 2002), providing guidance for axonal targeting before the onset of vision.

Neuronal activity modifies axonal projections and synaptic connections through activity-dependent plasticity. Activity-dependent plasticity is generally considered to provide fine-scale tuning to the initially coarse topography from molecular guidance, refining topographic order in the map and reducing receptive field sizes to yield higher sensory acuity (Kutsarova et al., 2017; Vislay-Meltzer et al., 2006). A well-known form of activity-dependent plasticity is Hebbian plasticity, named for its basic characteristics that were first postulated by Donald Hebb (1949). In Hebbian plasticity, synapses between two neurons are strengthened when the timing of activity in these two neurons is consistent with the first cell driving the second to fire. A corollary to Hebbian plasticity is Stentian plasticity (Stent, 1973), where the connections between two neurons that repeatedly fire out of sync with each other are destabilized. The most common examples of synaptic strengthening and weakening via Hebbian and Stentian mechanisms are long-term potentiation (LTP) and long-term depression (LTD), first studied in the hippocampus (Bliss & Lømo, 1973; Dudek & Bear, 1992) and subsequently characterized in different forms across different brain areas and neuron types (reviewed in Malenka and Bear (2004), Citri and Malenka (2008)). LTP is a persistent increase in synaptic strength between two neurons that can be induced by prolonged high-frequency stimulation in the presynaptic neuron, or by pairing low-frequency stimulation in the presynaptic neuron with depolarization of the postsynaptic neuron. LTD is a persistent reduction in synaptic strength that can be induced by prolonged low-frequency stimulation in the presynaptic neuron. Both LTP and LTD can also be induced by precise timing of activation in presynaptic and postsynaptic neurons, a paradigm termed spike-timing dependent plasticity (STDP) (Bi & Poo, 1998; Levy & Steward, 1983; Magee & Johnston, 1997; Markram et al., 1997; Sjöström et al., 2001; Zhang et al., 1998) (reviewed in (Dan & Poo, 2006)).

Both Hebbian and Stentian plasticity have been demonstrated in the Xenopus retinotectal system (Khakhalin et al., 2014; Munz et al., 2014; Pratt et al., 2008;

Rahman et al., 2020). Hebbian plasticity stabilizes connections between neurons sharing similar sensory representations, and by extension, similar response profiles, while Stentian plasticity destabilizes connections between neurons with different sensory representations. Both mechanisms push neurons to preferably wire with other neurons that share similar sensory representations, enhancing topographic organization.

However, one may note that Hebbian and Stentian mechanisms acting alone can form a feedback loop that will not reach a stable state as long as any differences between neurons remain, and some form of regulation must be in place to limit the propagation of this feedback loop so that a stable map with a varied array of sensory representations can be formed. The brain has been found to achieve this by limiting the overall strength of synaptic transmission within a certain dynamic range through an additional set of mechanisms generally known as homeostatic plasticity (reviewed in Turrigiano and Nelson (2004), Tien and Kerschensteiner (2018)). Homeostatic plasticity has been demonstrated in the Xenopus retinotectal system, in which tectal neurons have been found to adapt their intrinsic excitability so that the total level of synaptic input and tectal neuron spike output is conserved (Pratt & Aizenman, 2007).

The neuronal activity that leads to activity-dependent plasticity can either be evoked by sensory stimulation or arise spontaneously. In the tadpole retinotectal system, the tectum becomes responsive to visual stimuli as soon as the first RGCs arrive from the retina (Holt & Harris, 1983), and visually evoked activity leads to robust activity-dependent refinement in the retinotectal circuit (Munz et al., 2014; Rahman et al., 2020). In mammals, wiring in the retinotectal circuit occur before eye opening, and refinement is guided by spontaneously occurring waves of activity in the retina (Ackman et al., 2012; McLaughlin, Torborg, et al., 2003).

In addition to molecular guidance and activity-dependent plasticity, competition between sensory afferents for target space serve as a third mechanism that act in parallel to determine the final product of circuit wiring. Axons in the retinotectal pathway project to fill available target space, as shown by experiments ablating parts of the retina or tectum/superior colliculus. When the tectum is partially ablated, RGC axons form a

compressed topographic map in the remaining tectal fragment (Finlay et al., 1979; Schmidt & Coen, 1995; Yoon, 1976), and when the retina is partially ablated, RGCs from the remaining retina project to fill the space in the tectum that would have been innervated by the missing retinal projections (Schmidt & Easter, 1978). The involvement of competitive mechanisms is emphasized in extreme cases where a severe reduction of RGC inputs reduces competition between the remaining RGCs for target space, and where a partial tectal lesion leaves insufficient target space to accommodate all incoming RGC inputs. In Math5 (Atoh7) mutant mice, which have severely reduced numbers of RGCs, the remaining retinal axons project predominantly to the anteromedial portion of the SC despite originating from locations dispersed throughout the retina (Triplett et al., 2011). While moderate lesions to the SC in hamsters lead to RGCs forming a compressed map in the remaining tectal space, in the case of large lesions, parts of the RGC projections representing peripheral visual field are lost (Finlay et al., 1979; Pallas & Finlay, 1989). Extreme cases aside, under normal circumstances, axon competition and the resulting space-filling tendency of axonal projections has the effect of filling in any gaps in the sensory map to promote a smooth and continuous topographic organization.

NMDA receptors

One of the most relevant and widely studied participants in activity-dependent plasticity is the *N*-methyl-D-aspartate (NMDA) receptor. NMDA receptors are glutamate receptors involved in excitatory synaptic transmission, along with *α*-amino-3-hydroxy-5-methyl-4-isoxazolepropionic acid (AMPA) receptors. While AMPARs can be activated and generate excitatory synaptic responses when the neuron is at hyperpolarized resting potentials, NMDARs are only active when the neuron is depolarized (Mayer et al., 1984; Nowak et al., 1984). The distinctive activation mechanism of NMDARs makes them a perfect candidate for mediating Hebbian type plasticity.

NMDA receptors are calcium-permeable cation channels with glutamate and glycine (or D-serine) as their binding ligands. At hyperpolarized potentials, the NMDAR channel

pore is blocked by a magnesium ion, which only dissociates when the neuron is depolarized. Therefore, NMDARs are usually only activated when the binding of ligands occurs at the same time as neuronal depolarization. This property of NMDARs allows them to act as coincidence detectors for activity in pairs of connected neurons. Indeed, NMDAR activation has been identified as a key mechanism underlying classical LTP and LTD (Bear & Malenka, 1994) as well as their spike-dependent forms (Dan & Poo, 2006). NMDARs are known to be involved in activity-dependent modification of neuronal afferents in development, as evidenced by reduced pruning in RGC axons when NMDAR activity is blocked (Cline & Constantine-Paton, 1989; Hua et al., 2005; Munz et al., 2014; Simon et al., 1992). In Chapter III, we followed this line of investigation to explore whether NMDAR blockade affects functional properties of the developing topographic map.

NMDARs are tetrameric complexes consisting of different combinations of three families of subunits: GluN1, GluN2 and GluN3, also known as NR1, NR2 and NR3 (Monyer et al., 1992; Moriyoshi et al., 1991; Sucher et al., 1995) (Fig.1.2). GluN1 is encoded by the gene GRIN1 and have eight variants produced by alternative splicing (Zukin & Bennett, 1995). GluN2 can be further categorized into four types (A~D) (Monyer et al., 1992) and GluN3 can be further categorized into two types (A~B) (Chatterton et al., 2002). Each GluN2 and GluN3 subtype is encoded by a different gene (GRIN2A, GRIN2B, GRIN2C, GRIN2D, and GRIN3A, GRIN3B). GluN1 subunits are considered obligatory, as they are necessary for the trafficking of NMDAR subunits from the endoplasmic reticulum to the surface of neurons (Fukaya et al., 2003; Standley et al., 2000). Each NMDAR contains two GluN1 subunits, which are either assembled with two GluN2 subunits of the same type to form canonical diheteromeric NMDARs, or two different subunits from the GluN2 and GluN3 families to create triheteromeric NMDARs. GluN1 and GluN3 subunits contain glycine binding sites, while GluN2 subunits have glutamate binding sites. Different combinations of subunit types grant different properties to the assembled NMDAR, determining its functional attributes including permeation and gating properties, pharmacological activation, trafficking properties and coupling to downstream cascades (reviewed in Paoletti et al. (2013)).

A large body of work has closely associated NMDAR activity with synapse maturation and the progression of neonatal development. The neonatal brain contains many synapses that express only NMDARs, making them functionally “silent”, as the lack of AMPARs means they are unable to activate from normal hyperpolarized resting potentials (Isaac et al., 1997; Isaac et al., 1995; Kerchner & Nicoll, 2008). These synapses eventually mature to gain AMPAR conductance, as AMPARs are transported to their surface (Wu et al., 1996) – a process that has been shown to follow the activation of NMDARs in these synapses (Shi, Hayashi et al. 1999, Hayashi, Shi et al. 2000). The ratio of AMPAR to NMDAR transmission increases over the course of development (Zhu & Malinow, 2002), corresponding to increased numbers of mature AMPAR-expressing synapses.

Immature synapses are also associated with higher levels of GluN2B compared to GluN2A (Tovar & Westbrook, 1999), which gives them an overall slower response decay time compared to mature synapses with higher levels of GluN2A (Vicini et al., 1998). During neonatal development, there is a brain-wide switch in NMDAR subunit composition from predominantly GluN2B to predominantly GluN2A (Bar-Shira et al., 2015; Liu et al., 2004; Monyer et al., 1994).

The activity of NMDARs can be modulated by a wide variety of compounds that bind at various sites on the receptor (Fig.I.2). Common NMDAR agonists that increase NMDAR activity upon binding include NMDA, the glutamate site agonist from which NMDARs derived their name (Curtis & Watkins, 1960), and D-serine, a glycine site agonist (Mothet et al., 2000). Exogenous application of D-serine at chronic, saturating levels in Xenopus tadpoles has been found to promote stability in both pre- and postsynaptic arbors, leading to less complex RGC axon terminals (Van Horn et al., 2017) and more compact tectal dendritic arbors with increased synapse density (Chorghay et al., 2023). Common NMDAR antagonists that block or reduce NMDAR transmission upon binding include APV, a competitive glutamate site antagonist, and MK-801, a noncompetitive channel pore blocker (Watkins & Olverman, 1987). Blockade of NMDAR activity in Xenopus tadpoles has been found to reduce arbor stability and lead to enlarged RGC terminals (Cline & Constantine-Paton, 1990; Rajan et al., 1999).

Though the bulk of the work on NMDAR-dependent plasticity has been done in the context of postsynaptic NMDARs, NMDARs have also been found in presynaptic terminals and play unique roles in synaptic plasticity (Bouvier et al., 2015; Corlew et al., 2008; Dore et al., 2017). Work in the Ruthazer lab selectively knocking down pre- or postsynaptic NMDARs in the Xenopus retinotectal pathway has shown that NMDARs in pre- and postsynaptic partners impact neuronal morphology in opposite ways, with knockdown of postsynaptic NMDARs increasing RGC axonal arbor complexity and reducing tectal dendritic arbor complexity, and knockdown of presynaptic NMDARs reducing axonal arbor complexity and increasing tectal dendritic arbor complexity (Kesner et al., 2020).

NMDARs have been classically understood to function ionotropically by increasing cation conductance upon activation, raising intracellular Ca^{2+} levels to trigger downstream mechanisms, but recent studies have shown that NMDARs also signal non-ionotropically, independent of Ca^{2+} conduction (Dore et al., 2015; Dore et al., 2017; Nabavi et al., 2013). Non-ionotropic activity of NMDARs has been implicated in multiple aspects of activity-dependent plasticity including LTD induction (Carter & Jahr, 2016; Nabavi et al., 2013), presynaptic NMDAR control of spontaneous release (Abrahamsson et al., 2017), and structural plasticity in dendritic spines (Aow et al., 2015).

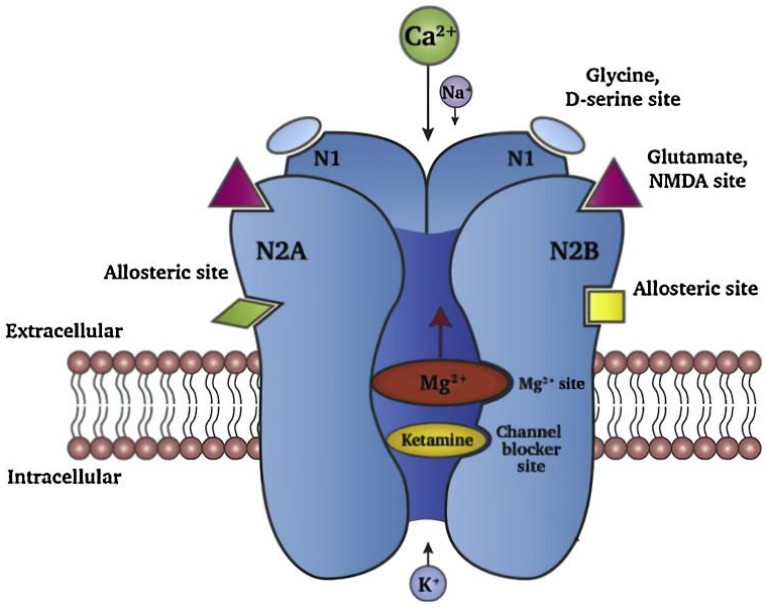

Figure I.2. Schematic of an NMDA receptor.
An NMDA receptor is comprised of two GluN1 subunits and two other subunits, which can be GluN2 or GluN3. Several types of non-competitive NMDAR antagonists, including ketamine and MK-801, act by binding at sites inside the NMDAR channel pore and preventing ion flow through the channel. Other NMDAR antagonists act competitively by binding to the glycine or glutamate sites (e.g. APV, phenylalanine), or noncompetitively by binding at the allosteric sites (e.g. polyamines, zinc).

Reprinted from Kokane et al. (2020) with permission from the publisher.

Studying retinotopic map formation in *Xenopus laevis*

The retinotectal system of *Xenopus laevis* is a well-studied animal model in the field of developmental neuroscience (Cline & Kelly, 2012). Here we will give a brief introduction to the Xenopus tadpole, and highlight strengths of this model that we used to our advantage in the research on map formation presented in this thesis.

Xenopus embryos develop externally from oocytes. In laboratory environments, Xenopus eggs can either be acquired by inducing amplexus between a pair of male and female frogs and collecting the resulting fertilized eggs, or by inducing ovulation in females, collecting unfertilized eggs and fertilizing them *in vitro* with sperm. *In vitro* fertilization facilitates the introduction of mRNA into early-stage embryos via microinjection, which will result in expression of the translated protein throughout the animal. We have also exploited the ability to freeze and ship sperm from transgenic frogs to perform *in vitro* fertilization to produce heterozygous transgenic offspring without requiring the costly and resource-intensive maintenance of multiple transgenic lines in our facility.

The pace of early developmental progression in tadpoles is affected by environmental factors such as temperature. For this reason, developmental stages of tadpoles are determined using a set of anatomical criteria (Nieuwkoop & Faber, 1994; Zahn et al., 2022). Key developmental stages for the scope of this thesis are stage 38/39, when the first RGC axons from the dorsal retina arrive at the tectum and the first visual responses

can be recorded by electrophysiology; stage 40, when RGC axons reach caudal tectum and complete the nascent retinotopic map; stage 45, when the optics in the tadpole eye transforms from hyperopic to emmetropic, and visual responses recorded in the tectum become more robust and display clearer topographic order; stage 48, when the pace of maturation in the tadpole slows and the tadpole must start feeding to continue developing into later stages (Gaze et al., 1974; Holt & Harris, 1983; Richards et al., 2012). At 20°C, stages 38~40 occur at roughly 3 days post fertilization (dpf), stage 45 at 5 dpf, and stage 48 starts at 8 dpf and can last for over a week until the tadpole starts to feed.

The retinotectal circuit in the tadpole tectum consists of RGC axons from the retina terminating in a neuropil region in the tectum and synapsing with dendrites from tectal cells (Fig.I.3 right). Adult Xenopus have been shown to have 14 morphologically distinct types of tectal cells (Lazar, 1973; Lázár & Székely, 1967) and 12 morphologically distinct types of RGCs (Straznicky & Straznicky, 1988), but all cell types present in the developing tadpole tectum have not been conclusively determined (Richards et al., 2010). Functionally, tectal neurons are known to have subtypes expressing different receptors and displaying distinct response properties, with some being glutamatergic (excitatory) and some being *gamma*-Aminobutyric acid (GABA)ergic (inhibitory) (Ciarleglio et al., 2015; Gambrill et al., 2016; Hickmott & Constantine-Paton, 1993; Miraucourt et al., 2012).

During development, new cells in the tectum are added linearly at the caudomedial edge of the tectum, but new cells in the retina are added in concentric rings at the ciliary margin, resulting in a mismatch in proliferative axes that necessarily requires compensatory adjustments in the retinotectal circuit throughout the course of development to maintain intact topographic order and visual processing functions (Gaze et al., 1979). This is an interesting problem that can lead to deeper insights into the baseline logic of developmental circuit assembly, which we explore in Chapter IV.

Within the retinotectal system, RGC axons from each eye cross the optic chiasm and project almost exclusively to the contralateral tectum, with very rare cases of single mistargeted axons projecting to the ipsilateral tectum (Munz et al., 2014; Sakaguchi &

Murphey, 1985). We take advantage of this anatomical feature of Xenopus in the mRNA microinjection technique applied in Chapter III and IV that generates tadpoles expressing the genetically encoded calcium indicator GCaMP6s in only one lateral half of the animal. In these hemimosaic animals, the tectal hemisphere in the labelled side of the animal will have GCaMP fluorescence in its tectal cells but not in the RGC axon terminals projecting in from the eye in the unlabelled side; on the other hand, RGC axons from the eye in the labelled side will project to the contralateral, unlabelled tectal hemisphere, becoming the only source of GCaMP fluorescence in that tectal hemisphere. This effectively allows us to separately visualize activity in RGC axon terminals and postsynaptic tectal neurons by imaging the two tectal hemispheres of these hemimosaic animals.

In the Ruthazer lab we mainly use Xenopus tadpoles with the periodic albino mutation for imaging experiments. The period albino mutation in these tadpoles reduces melanin synthesis in the melanophores that cover their skin (Hoperskaya, 1975), greatly reducing pigmentation and making their skin appear transparent (Fig. I.3 left). This enables non-invasive *in vivo* microscopy without the need to perform surgery to gain access to the tectum. As the periodic albino mutation is a recessive trait (Fukuzawa, 2021), tadpoles developed from eggs from albino frogs fertilized with sperm from non-albino frogs will display melanin pigmentation similar to wild type animals, but the pigmentation can be reduced to a level that permits optical imaging by application of phenylthiourea (PTU) to the rearing medium, which inhibits tyrosinase activity required for pigmentation.

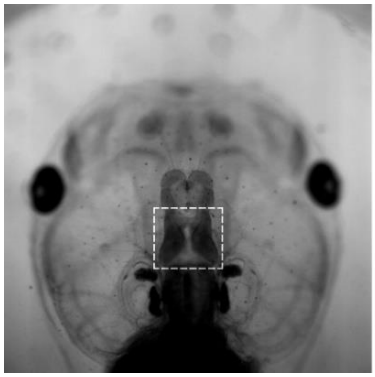

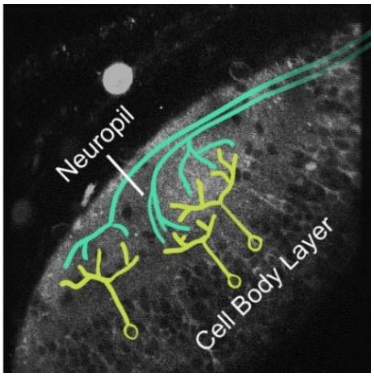

Figure I.3. The Xenopus optic tectum.
(Left) Widefield image of the head of a stage 48 albino Xenopus tadpole. The tectum is marked with a white box. Image from Dr. Philip Kesner.

(Right) Two-photon optical section of the left tectal hemisphere of a Xenopus tadpole, with schematic depictions of RGC axons projecting into the tectum from the contralateral eye and contacting the dendrites of tectal cells. The tectum can be visually separated into two regions: a neuropil region that consists mostly of RGC terminals and dendrites of tectal cells, and a cell body layer that consists mostly of cell somata of tectal cells, lined with radial glial somata on the ventricular surface. *Adapted from Li et al. (2022).*

Two-photon microscopy

Two-photon excitation microscopy is a fluorescence imaging technique that allows fast, high-resolution imaging of living organisms and tissue. A laser beam of excitation light in a specific wavelength (usually near-infrared) is focused on a specific location in the specimen. Each photon from the excitation light carries approximately half the energy necessary to excite one molecule of fluorophore present in the specimen, and when two photons are simultaneously absorbed by the fluorophore molecule, the fluorophore is activated and produces emission. The excitation laser is scanned sequentially at high speed across the specimen, and the resulting emission is captured by a photomultiplier tube (PMT) that converts the light signal to a digital signal to produce an image. The distribution of optical signal (known as the point-spread function) from two-photon excitation has a peak intensity concentrated within a micrometer scale volume (Fig.I.4), which results in an optical sectioning effect that produces sharp images restricted to the focal plane of imaging. The long excitation wavelengths used in two-photon microscopy penetrate well through thick tissue and create less damage and phototoxicity compared to traditional fluorescence microscopy techniques such as confocal microscopy that use shorter excitation wavelengths, making it suitable for imaging live organisms and tissue over extended periods of time. In addition, because two-photon microscopy, unlike

conventional confocal microscopy, relies on non-linear fluorescence excitation, all excitation outside the focal plane is eliminated, permitting non-descanned detection of emitted light. This allows for lower excitation intensities and results in significantly less photodynamic damage when imaging 3D volumes.

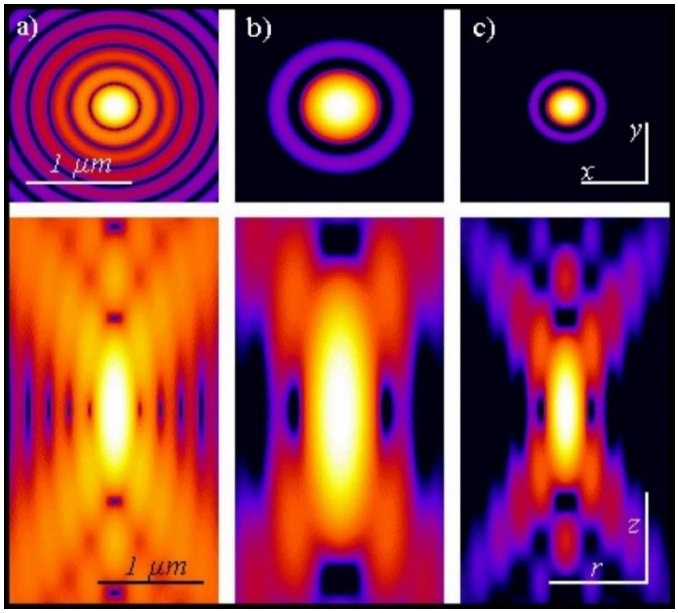

Figure I.4. Point spread functions of widefield, two-photon excitation, and confocal microscopy.
Calculated intensity distributions for optical responses from a point source imaged by (a) wide field, (b) two-photon excitation microscopy, and (c) confocal microscopy. *Reprinted from Diaspro et al. (2006) under CC BY 2.0.* *https://creativecommons.org/licenses/by/2.0/*

GCaMP

GCaMP is a version of genetically-encoded calcium indicator (GECI) proteins that can be expressed in cells and exhibits changes in fluorescence when bound to calcium ions (Ca^{2+}). GECIs are typically used to detect changes in intracellular calcium levels that accompany neuronal activity. GCaMP proteins consist of three interconnected domains: a circularly permuted green fluorescent protein (cpGFP), a calmodulin (CaM) domain that binds to Ca^{2+}, and a M13 calmodulin-binding domain of skeletal muscle myosin

light chain kinase that interacts with calcium-bound CaM (Fig.I.5). In the absence of Ca^{2+}, the GFP fluorophore domain is protonated and gives off low basal fluorescence. Upon Ca^{2+} binding, the CaM domain undergoes a conformation change and forms a complex with M13 that blocks water molecules from the GFP domain, causing the GFP protein to deprotonate and convert to an anionic form with bright fluorescence (Wang et al., 2008).

The GCaMP6 family is a recent generation of GCaMP widely used in research for their improved sensitivity compared to previous generations. There are three commonly-utilized variants in this family: GCaMP6s, GCaMP6m, and GCaMP6f, each with different kinetics and sensitivity profiles, with GCaMP6f having the fastest dynamics and GCaMP6s having the slowest dynamics but highest sensitivity (Chen et al., 2013). We chose GCaMP6s for use in the receptive field mapping experiments presented in Chapter III~IV due to the need for high signal-to-noise ratio for more reliable mapping results. GCaMP6s expression can be driven in tadpoles by injecting mRNA containing the GCaMP6s encoding sequence into *in vitro* fertilized embryos. There is also a transgenic GCaMP6s Xenopus line available from National Xenopus Resource (Horb et al., 2019), and for some experiments we used sperm from male frogs in this line to produce tadpoles expressing GCaMP6s via *in vitro* fertilization. In general, we found tadpoles expressing GCaMP6s transgenically versus through mRNA blastomere injection showed similar levels of GCaMP basal fluorescence and signal strength in response to calcium activity under two-photon illumination.

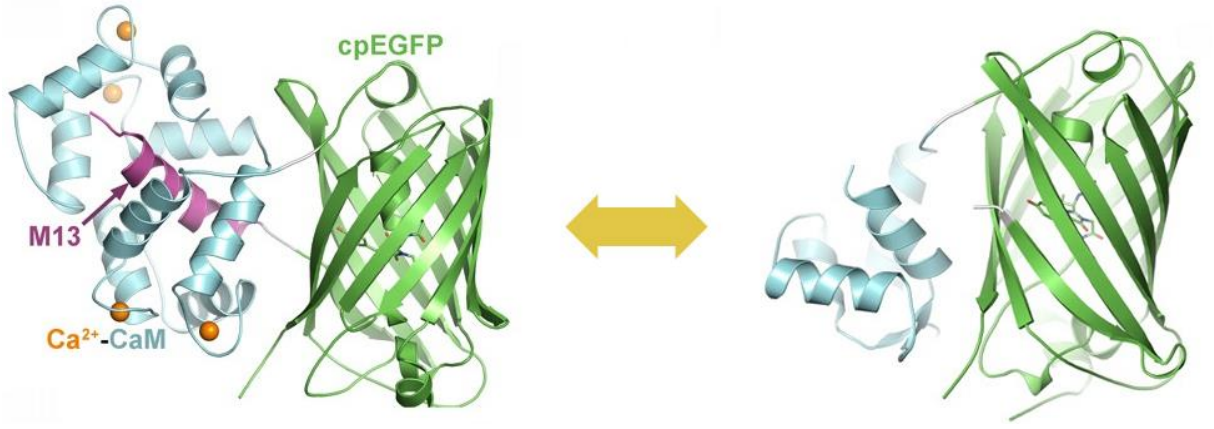

Figure I.5. Crystal structure of GCaMP2 in bound (left) and unbound (right) states.
Reprinted from Akerboom et al. (2009) under CC BY 4.0.
https://creativecommons.org/licenses/by/4.0/

Summary

In this chapter, we gave a brief overview of sensory maps and mechanisms guiding their formation, with a focus on mechanisms found to be active in the Xenopus retinotectal system. We will expand the scope of discussion to visual systems across species and delve into the functional and computational significance of sensory maps in Chapter II.

We provided details about *Xenopus laevis*, including the structure of their retinotectal system as well as the developmental progression of tadpoles during the stages where we examined changes in the tectal retinotopic map in Chapter III and IV. Also provided were details on the NMDA receptor, one of the molecular players involved in activity-dependent refinement that we focused on in Chapter III, and details on the genetically encoded calcium indicator GCaMP and two-photon microscopy, which were the primary tool used to visualize neuronal activity in the tectum and perform receptive field mapping in Chapter III~IV.

References

Abrahamsson, T., Chou, C. Y. C., Li, S. Y., Mancino, A., Costa, R. P., Brock, J. A., Nuro, E., Buchanan, K. A., Elgar, D., & Blackman, A. V. (2017). Differential regulation of evoked and spontaneous release by presynaptic NMDA receptors. *Neuron*, *96*(4), 839-855. e835.

Ackman, J. B., Burbridge, T. J., & Crair, M. C. (2012). Retinal waves coordinate patterned activity throughout the developing visual system. *Nature*, *490*(7419), 219-225. https://doi.org/10.1038/nature11529

Akerboom, J., Rivera, J. D. V., Guilbe, M. M. R., Malavé, E. C. A., Hernandez, H. H., Tian, L., Hires, S. A., Marvin, J. S., Looger, L. L., & Schreiter, E. R. (2009). Crystal structures of the GCaMP calcium sensor reveal the mechanism of fluorescence signal change and aid rational design. *Journal of biological chemistry*, *284*(10), 6455-6464.

Aow, J., Dore, K., & Malinow, R. (2015). Conformational signaling required for synaptic plasticity by the NMDA receptor complex. *Proceedings of the National Academy of Sciences*, *112*(47), 14711-14716.

Bar-Shira, O., Maor, R., & Chechik, G. (2015). Gene expression switching of receptor subunits in human brain development. *PLoS computational biology*, *11*(12), e1004559.

Bear, M. F., & Malenka, R. C. (1994). Synaptic plasticity: LTP and LTD. *Current Opinion in Neurobiology*, *4*(3), 389-399.

Bi, G.-q., & Poo, M.-m. (1998). Synaptic modifications in cultured hippocampal neurons: dependence on spike timing, synaptic strength, and postsynaptic cell type. *Journal of neuroscience*, *18*(24), 10464-10472.

Bliss, T. V., & Lømo, T. (1973). Long‐lasting potentiation of synaptic transmission in the dentate area of the anaesthetized rabbit following stimulation of the perforant path. *The Journal of Physiology*, *232*(2), 331-356.

Bouvier, G., Bidoret, C., Casado, M., & Paoletti, P. (2015). Presynaptic NMDA receptors: roles and rules. *Neuroscience*, *311*, 322-340.

Carter, B. C., & Jahr, C. E. (2016). Postsynaptic, not presynaptic NMDA receptors are required for spike-timing-dependent LTD induction. *Nature neuroscience*, *19*(9), 1218-1224.

Chatterton, J. E., Awobuluyi, M., Premkumar, L. S., Takahashi, H., Talantova, M., Shin, Y., Cui, J., Tu, S., Sevarino, K. A., & Nakanishi, N. (2002). Excitatory glycine

receptors containing the NR3 family of NMDA receptor subunits. *Nature*, *415*(6873), 793-798.

Chen, T.-W., Wardill, T. J., Sun, Y., Pulver, S. R., Renninger, S. L., Baohan, A., Schreiter, E. R., Kerr, R. A., Orger, M. B., Jayaraman, V., Looger, L. L., Svoboda, K., & Kim, D. S. (2013). Ultrasensitive fluorescent proteins for imaging neuronal activity. *Nature*, *499*(7458), 295-300. https://doi.org/10.1038/nature12354

Chorghay, Z., Li, V. J., Schohl, A., Ghosh, A., & Ruthazer, E. S. (2023). The effects of the NMDAR co-agonist d-serine on the structure and function of optic tectal neurons in the developing visual system. *Scientific Reports*, *13*(1), 13383.

Ciarleglio, C. M., Khakhalin, A. S., Wang, A. F., Constantino, A. C., Yip, S. P., & Aizenman, C. D. (2015). Multivariate analysis of electrophysiological diversity of Xenopus visual neurons during development and plasticity. *elife*, *4*, e11351.

Citri, A., & Malenka, R. C. (2008). Synaptic plasticity: multiple forms, functions, and mechanisms. *Neuropsychopharmacology*, *33*(1), 18-41.

Cline, H. T., & Constantine-Paton, M. (1989). NMDA receptor antagonists disrupt the retinotectal topographic map. *Neuron*, *3*(4), 413-426. https://doi.org/10.1016/0896-6273(89)90201-8

Cline, H. T., & Constantine-Paton, M. (1990). NMDA receptor agonist and antagonists alter retinal ganglion cell arbor structure in the developing frog retinotectal projection. *Journal of Neuroscience*, *10*(4), 1197-1216.

Cline, H. T., & Kelly, D. (2012). Xenopus as an experimental system for developmental neuroscience: introduction to a special issue. In (Vol. 72, pp. 463-464).

Corlew, R., Brasier, D. J., Feldman, D. E., & Philpot, B. D. (2008). Presynaptic NMDA Receptors: Newly Appreciated Roles in Cortical Synaptic Function and Plasticity. *The Neuroscientist*, *14*(6), 609-625. https://doi.org/10.1177/1073858408322675

Curtis, D. R., & Watkins, J. C. (1960). THE EXCITATION AND DEPRESSION OF SPINAL NEURONES BY STRUCTURALLY RELATED AMINO ACIDS. *Journal of Neurochemistry*, *6*(2), 117-141. https://doi.org/https://doi.org/10.1111/j.1471-4159.1960.tb13458.x

Dan, Y., & Poo, M.-M. (2006). Spike timing-dependent plasticity: from synapse to perception. *Physiological reviews*, *86*(3), 1033-1048.

Dhande, O. S., & Huberman, A. D. (2014). Retinal ganglion cell maps in the brain: implications for visual processing. *Current Opinion in Neurobiology*, *24*, 133-142.

Diaspro, A., Bianchini, P., Vicidomini, G., Faretta, M., Ramoino, P., & Usai, C. (2006). Multi-photon excitation microscopy. *Biomedical engineering online*, *5*, 1-14.

Dore, K., Aow, J., & Malinow, R. (2015). Agonist binding to the NMDA receptor drives movement of its cytoplasmic domain without ion flow. *Proceedings of the National Academy of Sciences*, *112*(47), 14705-14710.

Dore, K., Stein, I. S., Brock, J. A., Castillo, P. E., Zito, K., & Sjöström, P. J. (2017). Unconventional NMDA receptor signaling. *Journal of Neuroscience*, *37*(45), 10800-10807.

Dudek, S. M., & Bear, M. F. (1992). Homosynaptic long-term depression in area CA1 of hippocampus and effects of N-methyl-D-aspartate receptor blockade. *Proceedings of the National Academy of Sciences*, *89*(10), 4363-4367.

Finlay, B. L., Schneps, S. E., & Schneider, G. E. (1979). Orderly compression of the retinotectal projection following partial tectal ablation in the newborn hamster. *Nature*, *280*(5718), 153-155.

Fritzsch, B., Elliott, K. L., & Pavlinkova, G. (2019). Primary sensory map formations reflect unique needs and molecular cues specific to each sensory system. *F1000Research*, *8*.

Fukaya, M., Kato, A., Lovett, C., Tonegawa, S., & Watanabe, M. (2003). Retention of NMDA receptor NR2 subunits in the lumen of endoplasmic reticulum in targeted NR1 knockout mice. *Proceedings of the National Academy of Sciences*, *100*(8), 4855-4860.

Fukuzawa, T. (2021). Periodic albinism of a widely used albino mutant of Xenopus laevis caused by deletion of two exons in the Hermansky–Pudlak syndrome type 4 gene. *Genes to Cells*, *26*(1), 31-39.

Gambrill, A. C., Faulkner, R. L., & Cline, H. T. (2016). Experience-dependent plasticity of excitatory and inhibitory intertectal inputs in Xenopus tadpoles. *Journal of Neurophysiology*, *116*(5), 2281-2297.

Gaze, R., Keating, M., Ostberg, A., & Chung, S. (1979). The relationship between retinal and tectal growth in larval Xenopus: implications for the development of the retino-tectal projection. *Development*, *53*(1), 103-143.

Gaze, R. M., Keating, M., & Chung, S. (1974). The evolution of the retinotectal map during development in Xenopus. *Proceedings of the Royal Society of London. Series B. Biological Sciences*, *185*(1080), 301-330.

Hebb, D. O. (1949). *The Organization of Behavior*. John Wiley and Sons.

Hickmott, P. W., & Constantine-Paton, M. (1993). The contributions of NMDA, non-NMDA, and GABA receptors to postsynaptic responses in neurons of the optic tectum. *Journal of Neuroscience*, *13*(10), 4339-4353.

Higenell, V., Han, S. M., Feldheim, D. A., Scalia, F., & Ruthazer, E. S. (2012). Expression patterns of Ephs and ephrins throughout retinotectal development in Xenopus laevis. *Developmental neurobiology*, *72*(4), 547-563. https://doi.org/10.1002/dneu.20930

Holt, C. E., & Harris, W. A. (1983). Order in the initial retinotectal map in Xenopus: a new technique for labelling growing nerve fibres. *Nature*, *301*(5896), 150-152. https://doi.org/10.1038/301150a0

Hoperskaya, O. A. (1975). The development of animals homozygous for a mutation causing periodic albinism (ap) in Xenopus laevis. *Development*, *34*(1), 253-264.

Horb, M., Wlizla, M., Abu-Daya, A., McNamara, S., Gajdasik, D., Igawa, T., Suzuki, A., Ogino, H., Noble, A., & France, C. d. R. B. X. t. i. (2019). Xenopus resources: transgenic, inbred and mutant animals, training opportunities, and web-based support. *Frontiers in physiology*, *10*, 387.

Hua, J. Y., Smear, M. C., Baier, H., & Smith, S. J. (2005). Regulation of axon growth in vivo by activity-based competition. *Nature*, *434*(7036), 1022-1026.

Hubel, D. H., & Wiesel, T. N. (1977). Ferrier lecture-Functional architecture of macaque monkey visual cortex. *Proceedings of the Royal Society of London. Series B. Biological Sciences*, *198*(1130), 1-59.

Isaac, J. T., Crair, M. C., Nicoll, R. A., & Malenka, R. C. (1997). Silent synapses during development of thalamocortical inputs. *Neuron*, *18*(2), 269-280.

Isaac, J. T., Nicoll, R. A., & Malenka, R. C. (1995). Evidence for silent synapses: implications for the expression of LTP. *Neuron*, *15*(2), 427-434.

Kaas, J. H. (1997). Topographic maps are fundamental to sensory processing. *Brain research bulletin*, *44*(2), 107-112.

Kerchner, G. A., & Nicoll, R. A. (2008). Silent synapses and the emergence of a postsynaptic mechanism for LTP. *Nature reviews neuroscience*, *9*(11), 813-825.

Kesner, P., Schohl, A., Warren, E. C., Ma, F., & Ruthazer, E. S. (2020). Postsynaptic and Presynaptic NMDARs Have Distinct Roles in Visual Circuit Development. *Cell Reports*, *32*(4), 107955. https://doi.org/10.1016/j.celrep.2020.107955

Khakhalin, A. S., Koren, D., Gu, J., Xu, H., & Aizenman, C. D. (2014). Excitation and inhibition in recurrent networks mediate collision avoidance in X enopus tadpoles. *European Journal of Neuroscience*, *40*(6), 2948-2962.

Kokane, S. S., Armant, R. J., Bolaños-Guzmán, C. A., & Perrotti, L. I. (2020). Overlap in the neural circuitry and molecular mechanisms underlying ketamine abuse and its use as an antidepressant. *Behavioural brain research*, *384*, 112548.

Kutsarova, E., Munz, M., & Ruthazer, E. S. (2017). Rules for Shaping Neural Connections in the Developing Brain. *Frontiers in neural circuits*, *10*, 111-111. https://doi.org/10.3389/fncir.2016.00111

Lazar, G. (1973). The development of the optic tectum in Xenopus laevis: a Golgi study. *Journal of anatomy*, *116*(Pt 3), 347.

Lázár, G., & Székely, G. (1967). Golgi studies on the optic center of the frog. *J. Hirnforsch*, *9*(32), 344.

Lemke, G., & Reber, M. (2005). Retinotectal mapping: new insights from molecular genetics. *Annu. Rev. Cell Dev. Biol.*, *21*(1), 551-580.

Levy, W., & Steward, O. (1983). Temporal contiguity requirements for long-term associative potentiation/depression in the hippocampus. *Neuroscience*, *8*(4), 791-797.

Li, V. J., Schohl, A., & Ruthazer, E. S. (2022). Topographic map formation and the effects of NMDA receptor blockade in the developing visual system. *Proceedings of the National Academy of Sciences*, *119*(8), e2107899119.

Liu, X.-B., Murray, K. D., & Jones, E. G. (2004). Switching of NMDA receptor 2A and 2B subunits at thalamic and cortical synapses during early postnatal development. *Journal of Neuroscience*, *24*(40), 8885-8895.

Magee, J. C., & Johnston, D. (1997). A synaptically controlled, associative signal for Hebbian plasticity in hippocampal neurons. *Science*, *275*(5297), 209-213.

Malenka, R. C., & Bear, M. F. (2004). LTP and LTD: an embarrassment of riches. *Neuron*, *44*(1), 5-21.

Mann, F., Ray, S., Harris, W. A., & Holt, C. E. (2002). Topographic mapping in dorsoventral axis of the Xenopus retinotectal system depends on signaling through ephrin-B ligands. *Neuron*, *35*(3), 461-473.

Markram, H., Lübke, J., Frotscher, M., & Sakmann, B. (1997). Regulation of synaptic efficacy by coincidence of postsynaptic APs and EPSPs. *Science*, *275*(5297), 213-215.

Mayer, M. L., Westbrook, G. L., & Guthrie, P. B. (1984). Voltage-dependent block by Mg2+ of NMDA responses in spinal cord neurones. *Nature*, *309*(5965), 261-263.

McLaughlin, T., Hindges, R., & O'Leary, D. D. (2003). Regulation of axial patterning of the retina and its topographic mapping in the brain. *Current Opinion in Neurobiology*, *13*(1), 57-69.

McLaughlin, T., Torborg, C. L., Feller, M. B., & O'Leary, D. D. (2003). Retinotopic map refinement requires spontaneous retinal waves during a brief critical period of development. *Neuron*, *40*(6), 1147-1160.

Miraucourt, L. S., da Silva, J. S., Burgos, K., Li, J., Abe, H., Ruthazer, E. S., & Cline, H. T. (2012). GABA expression and regulation by sensory experience in the developing visual system. *PLoS One*, *7*(1), e29086.

Monyer, H., Burnashev, N., Laurie, D. J., Sakmann, B., & Seeburg, P. H. (1994). Developmental and regional expression in the rat brain and functional properties of four NMDA receptors. *Neuron*, *12*(3), 529-540.

Monyer, H., Sprengel, R., Schoepfer, R., Herb, A., Higuchi, M., Lomeli, H., Burnashev, N., Sakmann, B., & Seeburg, P. H. (1992). Heteromeric NMDA receptors: molecular and functional distinction of subtypes. *Science*, *256*(5060), 1217-1221.

Moriyoshi, K., Masu, M., Ishii, T., Shigemoto, R., Mizuno, N., & Nakanishi, S. (1991). Molecular cloning and characterization of the rat NMDA receptor. *Nature*, *354*(6348), 31-37.

Mothet, J.-P., Parent, A. T., Wolosker, H., Brady Jr, R. O., Linden, D. J., Ferris, C. D., Rogawski, M. A., & Snyder, S. H. (2000). D-serine is an endogenous ligand for the glycine site of the N-methyl-D-aspartate receptor. *Proceedings of the National Academy of Sciences*, *97*(9), 4926-4931.

Munz, M., Gobert, D., Schohl, A., Poquerusse, J., Podgorski, K., Spratt, P., & Ruthazer, E. S. (2014). Rapid Hebbian axonal remodeling mediated by visual stimulation. *Science*, *344*(6186), 904-909. https://doi.org/10.1126/science.1251593

Nabavi, S., Kessels, H. W., Alfonso, S., Aow, J., Fox, R., & Malinow, R. (2013). Metabotropic NMDA receptor function is required for NMDA receptor-dependent long-term depression. *Proceedings of the National Academy of Sciences*, *110*(10), 4027-4032.

Nieuwkoop, P. D., & Faber, J. (1994). *Normal Table of Xenopus Laevis (Daudin): A Systematical and Chronological Survey of the Development from the Fertilized Egg Till the End of Metamorphosis*. Garland Pub.

Nowak, L., Bregestovski, P., Ascher, P., Herbet, A., & Prochiantz, A. (1984). Magnesium gates glutamate-activated channels in mouse central neurones. *Nature*, *307*(5950), 462-465.

Pallas, S., & Finlay, B. (1989). Conservation of receptive-field properties of superior colliculus cells after developmental rearrangements of retinal input. *Visual neuroscience*, *2*(2), 121-135.

Paoletti, P., Bellone, C., & Zhou, Q. (2013). NMDA receptor subunit diversity: impact on receptor properties, synaptic plasticity and disease. *Nature reviews neuroscience*, *14*(6), 383-400.

Pratt, K. G., & Aizenman, C. D. (2007). Homeostatic regulation of intrinsic excitability and synaptic transmission in a developing visual circuit. *Journal of Neuroscience*, *27*(31), 8268-8277.

Pratt, K. G., Dong, W., & Aizenman, C. D. (2008). Development and spike timing–dependent plasticity of recurrent excitation in the Xenopus optic tectum. *Nature neuroscience*, *11*(4), 467-475.

Rahman, T. N., Munz, M., Kutsarova, E., Bilash, O. M., & Ruthazer, E. S. (2020). Stentian structural plasticity in the developing visual system. *Proceedings of the National Academy of Sciences*, *117*(20), 10636-10638.

Rajan, I., Witte, S., & Cline, H. T. (1999). NMDA receptor activity stabilizes presynaptic retinotectal axons and postsynaptic optic tectal cell dendritesin vivo. *Journal of Neurobiology*, *38*(3), 357-368. https://doi.org/10.1002/(sici)1097-4695(19990215)38:3<357::aid-neu5>3.0.co;2-#

Richards, B. A., Aizenman, C. D., & Akerman, C. J. (2010). In vivo spike-timing-dependent plasticity in the optic tectum of Xenopus laevis. *Frontiers in synaptic neuroscience*, *2*, 1439.

Richards, B. A., van Rheede, J. J., & Akerman, C. J. (2012). Visuospatial information in the retinotectal system of xenopus before correct image formation by the developing eye. *Developmental Neurobiology*, *72*(4), 507-519. https://doi.org/10.1002/dneu.20943

Sakaguchi, D. S., & Murphey, R. K. (1985). Map formation in the developing Xenopus retinotectal system: an examination of ganglion cell terminal arborizations. *Journal of Neuroscience*, *5*(12), 3228-3245. https://doi.org/10.1523/JNEUROSCI.05-12-03228.1985

Schmidt, J., & Coen, T. (1995). Changes in retinal arbors in compressed projections to half tecta in goldfish. *Journal of Neurobiology*, *28*(4), 409-418.

Schmidt, J. T., & Easter, S. S. (1978). Independent biaxial reorganization of the retinotectal projection: a reassessment. *Experimental Brain Research*, *31*, 155-162.

Schreiner, C. E., & Winer, J. A. (2007). Auditory cortex mapmaking: principles, projections, and plasticity. *Neuron*, *56*(2), 356-365.

Simon, D. K., Prusky, G. T., O'leary, D., & Constantine-Paton, M. (1992). N-methyl-D-aspartate receptor antagonists disrupt the formation of a mammalian neural map. *Proceedings of the National Academy of Sciences*, *89*(22), 10593-10597.

Sjöström, P. J., Turrigiano, G. G., & Nelson, S. B. (2001). Rate, timing, and cooperativity jointly determine cortical synaptic plasticity. *Neuron*, *32*(6), 1149-1164.

Standley, S., Roche, K. W., McCallum, J., Sans, N., & Wenthold, R. J. (2000). PDZ domain suppression of an ER retention signal in NMDA receptor NR1 splice variants. *Neuron*, *28*(3), 887-898.

Stent, G. S. (1973). A physiological mechanism for Hebb's postulate of learning. *Proceedings of the National Academy of Sciences*, *70*(4), 997-1001.

Straznicky, C., & Straznicky, I. T. (1988). Morphological classification of retinal ganglion cells in adult Xenopus laevis. *Anatomy and Embryology*, *178*, 143-153.

Sucher, N. J., Akbarian, S., Chi, C. L., Leclerc, C. L., Awobuluyi, M., Deitcher, D. L., Wu, M. K., Yuan, J. P., Jones, E. G., & Lipton, S. A. (1995). Developmental and regional expression pattern of a novel NMDA receptor-like subunit (NMDAR-L) in the rodent brain. *Journal of Neuroscience*, *15*(10), 6509-6520.

Tien, N.-W., & Kerschensteiner, D. (2018). Homeostatic plasticity in neural development. *Neural development*, *13*, 1-7.

Tovar, K. R., & Westbrook, G. L. (1999). The incorporation of NMDA receptors with a distinct subunit composition at nascent hippocampal synapses in vitro. *Journal of Neuroscience*, *19*(10), 4180-4188.

Triplett, J. W. (2014). Molecular guidance of retinotopic map development in the midbrain. *Current Opinion in Neurobiology*, *24*, 7-12.

Triplett, J. W., Pfeiffenberger, C., Yamada, J., Stafford, B. K., Sweeney, N. T., Litke, A. M., Sher, A., Koulakov, A. A., & Feldheim, D. A. (2011). Competition is a driving force in topographic mapping. *Proceedings of the National Academy of Sciences*, *108*(47), 19060-19065.

Turrigiano, G. G., & Nelson, S. B. (2004). Homeostatic plasticity in the developing nervous system. *Nature reviews neuroscience*, *5*(2), 97-107.

Van Horn, M. R., Strasser, A., Miraucourt, L. S., Pollegioni, L., & Ruthazer, E. S. (2017). The gliotransmitter d-serine promotes synapse maturation and axonal stabilization in vivo. *Journal of Neuroscience*, *37*(26), 6277-6288.

Vicini, S., Wang, J. F., Li, J. H., Zhu, W. J., Wang, Y. H., Luo, J. H., Wolfe, B. B., & Grayson, D. R. (1998). Functional and pharmacological differences between recombinant N-methyl-D-aspartate receptors. *Journal of neurophysiology*, *79*(2), 555-566.

Vislay-Meltzer, R. L., Kampff, A. R., & Engert, F. (2006). Spatiotemporal Specificity of Neuronal Activity Directs the Modification of Receptive Fields in the Developing Retinotectal System. *Neuron*, *50*(1), 101-114. https://doi.org/10.1016/j.neuron.2006.02.016

Wang, Q., Shui, B., Kotlikoff, M. I., & Sondermann, H. (2008). Structural basis for calcium sensing by GCaMP2. *Structure*, *16*(12), 1817-1827.

Watkins, J. C., & Olverman, H. J. (1987). Agonists and antagonists for excitatory amino acid receptors. *Trends in neurosciences*, *10*(7), 265-272. https://doi.org/10.1016/0166-2236(87)90171-8

Wu, G.-Y., Malinow, R., & Cline, H. (1996). Maturation of a central glutamatergic synapse. *Science*, *274*(5289), 972-976.

Yoon, M. (1976). Progress of topographic regulation of the visual projection in the halved optic tectum of adult goldfish. *The Journal of Physiology*, *257*(3), 621-643.

Young, E. D. (1998). Parallel processing in the nervous system: evidence from sensory maps. *Proceedings of the National Academy of Sciences*, *95*(3), 933-934.

Zahn, N., James-Zorn, C., Ponferrada, V. G., Adams, D. S., Grzymkowski, J., Buchholz, D. R., Nascone-Yoder, N. M., Horb, M., Moody, S. A., & Vize, P. D. (2022). Normal Table of Xenopus development: a new graphical resource. *Development*, *149*(14), dev200356.

Zhang, L. I., Tao, H. W., Holt, C. E., Harris, W. A., & Poo, M.-m. (1998). A critical window for cooperation and competition among developing retinotectal synapses. *Nature*, *395*(6697), 37-44. https://doi.org/10.1038/25665

Zhu, J. J., & Malinow, R. (2002). Acute versus chronic NMDA receptor blockade and synaptic AMPA receptor delivery. *Nature neuroscience*, *5*(6), 513-514.

Zukin, R. S., & Bennett, M. V. (1995). Alternatively spliced isoforms of the NMDARI receptor subunit. *Trends in neurosciences*, *18*(7), 306-313.

Preface to Chapter II

This chapter is a review of literature on sensory maps across species, with a focus on the visual system. We delve into mechanisms guiding map formation in early development, and discuss theories on how maps are involved in sensory processing by routing sensory information and performing computation.

Author contributions

Chapter II has been published as: Li, V. J., Z. Chorghay and E. S. Ruthazer (2023). "A guide for the multiplexed: the development of visual feature maps in the brain." Neuroscience **508**: 62-75. https://doi.org/10.1016/j.neuroscience.2022.07.026.

The manuscript was collaboratively written by VJL, ZC and ESR.

Chapter II

A Guide for the Multiplexed: The development of visual feature maps in the brain

Authors: *Vanessa J. Li, *Zahraa Chorghay, Edward S. Ruthazer

**these authors contributed equally*

Highlights:

- Neural maps convert complex environments into neural space in the brain
- Maps form by molecular guidance, competition, and activity-dependent plasticity
- Maps exhibit a nested structure that allows multiplexing of information
- Fine-scale heterogeneity enhances the computational capacity of the neural circuit

Keywords: cortex, thalamus, superior colliculus, optic tectum, retina, orientation, ocular dominance, topographic map

Abstract

Neural maps are found ubiquitously in the brain, where they encode a wide range of behaviourally relevant features into neural space. Developmental studies have shown that animals devote a great deal of resources to establish consistently patterned organization in neural circuits throughout the nervous system, but what purposes maps serve beneath their often intricate appearance and composition is a topic of active debate and exploration. In this article, we review the general mechanisms of map formation, with a focus on the visual system, and then survey notable organizational properties of neural maps: the multiplexing of feature representations through a nested architecture, the interspersing of fine-scale heterogeneity within a globally smooth organization, and the complex integration at the microcircuit level that enables a high dimensionality of information encoding. Finally, we discuss the roles of maps in cortical functions, including input segregation, feature extraction and routing of circuit outputs

for higher order processing, as well as the evolutionary basis for the properties we observe in neural maps.

What is a map?

The orderly organization of functionally related neurons in the brain, commonly known as neural maps, has captivated the intrigue of neuroscientists since their first observations in the late 19th century (Fritsch and Hitzig, 1870, Jackson, 1875, Grünbaum and Sherrington, 1902, Holmes, 1918, Penfield and Boldrey, 1937). Subsequent research solidified the idea that neural maps hold a biological significance. A striking ubiquity of maps in nervous systems has been observed -- neural maps are found throughout the nervous system in a vast range of species, representing properties ranging from sensory modalities to cognitive abstractions to motor commands. Moreover, researchers have uncovered an elaborate set of mechanisms underlying the development of neural maps, including intricate attractive and repulsive interactions of axons with molecular guidance cues in work that was pioneered by Friedrich Bonhoeffer and colleagues (Bonhoeffer and Huf, 1980, 1982, 1985, Walter, Henke-Fahle, et al., 1987, Walter, Kern-Veits, et al., 1987). The prevalence of maps as well as the metabolic resources devoted to their formation in developing circuits suggests that neural maps are necessary for brain function. While a connection between map organization and brain function is widely accepted, a detailed understanding of this connection continues to undergo thorough investigation and speculation. An important scientific question is how do neural maps facilitate information processing in the brain.

At first glance, maps appear to be a straightforward solution for the brain to encode and process complex, multidimensional information during an organism’s interaction with its environment. Neural maps conform to the mathematical definition of functions: they uniquely assign elements from the input set X to elements of the output set Y, where X is feature space in the environment and Y is neuroanatomical space in the brain. The form of a neural map reflects the feature space it represents (Fig.II.1A). Some maps are continuous, such as retinotopic maps representing visual space and tonotopic maps for

auditory frequencies. In these maps, neurons that are closer to each other tend to represent stimulus features that are closer to each other in the input space. Other neural maps are discrete, such as glomerular maps for odorants. Here, receptors distributed throughout the olfactory epithelium project to corresponding glomeruli in the olfactory bulb, with each type of olfactory receptor associating with a discrete set of olfactory glomeruli. Somatosensory, motor, and higher-order maps tend to be a combination of continuous and discrete maps.

A fundamental property of neural maps is the possibility for multiple features to be coextensively represented within the same anatomical area. A prominent example of this is found in the mammalian visual cortex (Fig.II.1B). The primary visual cortex (V1) receives topographically organized input from the lateral geniculate nucleus, and serves as a first stop in the visual cortex where various properties of visual stimuli are extracted and distributed for further processing in higher order visual areas. Within the framework of retinotopy, in many mammalian species the population of V1 neurons further displays modular organization of properties like ocular dominance, orientation, and direction selectivity. The overlay of these feature maps in V1 not only presents an elegant solution to the encoding, parallel processing, and distribution of a vast amount of information, but also allows neural computations to be performed locally within circuits of V1 itself.

In this review we will analyze the significance of neural maps as an effective scheme for information encoding. We will approach this subject from two aspects, drawing from examples in the visual system. We first discuss the mechanisms underlying map development, highlighting how they drive the formation of maps with complex structure. We then describe how these map structures enable the brain to perform its complex functions.

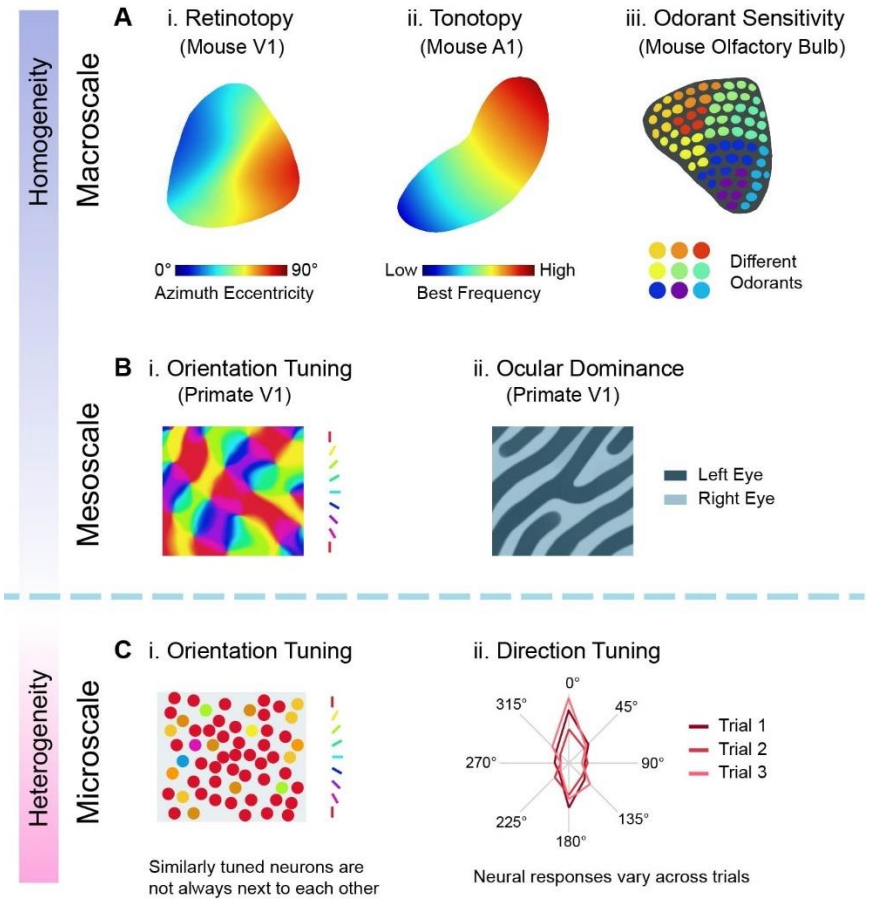

Figure II.1. Nesting of map organization.

Mesoscale structures are often nested within larger macroscale maps, and the level of homogeneity of feature representations vary at different levels. (A) Examples of macroscale maps. (i) Retinotopic mapping of azimuth in mouse primary visual cortex. (ii) Sound characteristic frequency map in the mouse primary auditory cortex. (iii) Olfactory map in the mouse olfactory bulb. Each glomerulus in the olfactory bulb receives inputs expressing a specific odorant receptor type. (B) Examples of mesoscale structures. (i) Orientation tuning in primate V1, showing distinctive “pinwheel” patterns. (ii) Ocular dominance bands in primate V1. (C) Examples of heterogeneity at the microscale level of neural circuits. (i) Orientation tuning in a population of primate V1 cells, showing overall similar tuning within the neighbouring cells with some heterogeneity. (ii) Direction tuning in a single primate V1 cell recorded over three trials, showing a variation in observed tuning across trials.

Development of maps

Do maps serve a necessary biological function, or are they simply an epiphenomenon arising from the mechanisms that permit a circuit to perform functions that do not inherently require patterned circuit organization? While the answer to this question is elusive, one thing we can reliably observe *in vivo* is that biological systems appear to invest considerable resources in establishing and maintaining maps, and the developmental fine-tuning of these maps contributes to the ability of the system to properly respond to the environment.

Maps are thought to emerge from a combination of (1) molecular guidance cues, (2) activity-dependent plasticity in which the circuit applies specific rules to adjust synapses and connections based on spontaneous or evoked neuronal activity, and (3) competition among neurons for available space and resources (Huberman et al., 2008, Feldheim and O'Leary, 2010). While these three mechanisms can act independently of each other and vary in their observed influence on map organization at different developmental timepoints, it is important to note that in natural systems all three mechanisms work in tandem throughout development, and their individual contributions to network organization often cannot be completely isolated from each other.

Molecular guidance cues

The fact that molecular guidance cues play a role in the establishment of maps was demonstrated by Roger Sperry in studies on the retinotectal projection from the eye to the optic tectum of fish and amphibians (Sperry, 1963). Sperry rotated the eyes of frogs by 180 degrees, and observed that the regenerated retinal axons formed an inverted visual field map in the tectum where axons innervated sites corresponding to their original targets within the tectum. Based on this observation, he proposed the "chemoaffinity hypothesis", which states that each retinal axon and tectal neuron relies on unique chemical cues to specify their connectivity, allowing axons to find their original tectal targets even after eye rotation. Membrane stripe assays developed by Bonhoeffer and colleagues provided further evidence for this hypothesis at a cellular level (Walter, Henke-Fahle, et al., 1987, Walter, Kern-Veits, et al., 1987). When chick

temporal retinal ganglion cell (RGC) axons were plated on interleaved stripes of anterior and posterior tectal membranes, temporal axons actively avoided posterior membranes, preferring instead to grow on anterior tectal membranes that correspond with their topographically appropriate target.

Since then, molecular guidance cues of the ephrin/Eph family have been identified as key factors in the establishment of topographic maps in the optic tectum, as well as across multiple other brain areas and sensory systems (reviewed in McLaughlin and O'Leary (2005), Flanagan (2006)). Ephrins and Eph receptors are distributed along anatomical axes in expression gradients, exerting either attractant or repellent activity on axons, depending on concentration, to guide axons into their appropriate target locations (Hansen et al., 2004).

Apart from the well-characterized roles of ephrins, graded expression of morphogens such as Wnt, Sonic hedgehog (Shh), and BMP, as well as cell adhesion molecules such as Sidekicks, Dscam, and cadherins, have also been found to play important roles in topographic map formation (reviewed in Charron and Tessier-Lavigne (2007), Yam and Charron (2013), Missaire and Hindges (2015)).

The origin of ephrin/Eph signaling can be traced back as far as premetazoan choanoflagellates (Arcas et al., 2020), indicating that the elements for creating organized projections have been available since nervous systems first appeared evolutionarily (Anctil, 2015, Burkhardt and Sprecher, 2017). It is reasonable to surmise that the efficiency provided by molecular guidance offers an evolutionary advantage by fast-tracking the assembly of developing sensory circuits based on a genetically encoded template. Rapid circuit formation would be especially important to animals that depend on their sensory systems for survival before the underlying neural circuit is fully developed, as is the case, for example, with vision in externally fertilized frogs and fish (Sakaguchi and Murphey, 1985, Burrill and Easter Jr, 1994, Kita et al., 2015, Li et al., 2022).

Activity-dependent mechanisms for map refinement

The role of activity in the refinement of topographic maps has been studied by

observing map refinement following deprivation of neuronal activity. In fish, intraocular or systemic application of tetrodotoxin (TTX) leads to abnormal local structure of retinotectal maps at relatively late stages in development, as opposed to large-scale topographic mistargeting (Gnuegge et al., 2001; Stuermer et al., 1990), though it appears to cause more extensive disruption to regenerating retinotectal projections (Schmidt and Buzzard, 1990, Olson and Meyer, 1991).

The participation of neural activity in map formation roughly falls into two categories: a permissive role, where neuronal activity is required to enable the signaling of molecular guidance cues; and an instructive role, where activity provides information that is used to direct the refinement of neural projections and the maintenance or elimination of connections.

There are a number of well-established examples of activity exerting a permissive role in circuit formation. In the chick, disrupting rhythmic activity leads to pathfinding errors in the dorsal-ventral motor neuron projections through the regulation of the expression of EphA4 and polysialic acid on NCAM (Hanson and Landmesser, 2004). Axonal responses to chemoattractant guidance molecules such as Netrin-1 can also be regulated by electrical activity through changes in intracellular cAMP levels (Ming et al., 2001). Nicol et al. (2007) established a retinocollicular co-culture preparation that reproduces the topographic ordering of axonal projections. They showed that TTX administration prevented this topographic targeting by altering the underlying retinal growth cone response to ephrin-A5 through calcium-dependent regulation of cAMP oscillations.

In the case of instructive mechanisms, patterned activity, such as visual experience, provides a valuable source of information about the relationship of inputs. Developing neuronal circuits have been found to use this information to instruct the fine-scale organization of maps by applying plasticity rules that exploit patterned sensory activity to regulate the growth and connectivity of neuronal arbors (Kutsarova et al., 2017). Furthermore, simulations with computational models also bolster the idea that biologically realistic molecular cues alone may not be sufficient to produce the precise retinotopic mapping that has been observed *in vivo* (Yates et al., 2004, McLaughlin and

O'Leary, 2005).

In the visual system, patterned activity can either arise from evoked activity in response to visual experience or from spontaneous waves of activity (Pratt et al., 2016). Spontaneous activity has been recorded in the developing retina (Maffei and Galli-Resta, 1990, Meister et al., 1991, Feller et al., 1996, Warland et al., 2006), lateral geniculate nucleus (Weliky and Katz, 1999, Martini et al., 2021), and the cortex (Adelsberger et al., 2005). Spontaneous activity is thought to mimic evoked activity, standing in for its role in instructing circuit plasticity before the developing animal gains access to visual experience (Ackman et al., 2012, Xu et al., 2015, Smith et al., 2018).

There are 3 stages of retinal waves that have been observed in development: the first stage, Stage I, is mediated by gap junctions and takes place prenatally; Stage II occurs primarily during the first postnatal week in mice and depends on cholinergic transmission; and Stage III consists of glutamatergic retinal waves (Arroyo and Feller, 2016). Stage II and III waves coincide with the period of map establishment in the superior colliculus, consistent with their involvement in the process of activity-dependent visual map refinement (reviewed in Assali et al. (2014)).

Cholinergic transmission has been implicated in stage II wave generation. Mice lacking the β2 subunit of the nicotinic acetylcholine receptor exhibit disrupted retinal waves, which results in the degradation of retinocollicular and retinogeniculate topographic projections (McLaughlin et al., 2003, Dhande et al., 2011). In addition, the segregation of RGC axons into eye-specific layers in the lateral geniculate nucleus (LGN) is also believed to result from patterned neural activity and is disrupted in $\beta2^{-/-}$ mutant mice (Sretavan et al., 1988, Bansal et al., 2000, Muir-Robinson et al., 2002, Sun et al., 2008). Following the period of cholinergic waves, between P11 and P15-16, retinal activity blockade by chronic TTX delivery into the vitreous humor prevents the developmental reduction in the number of retinal afferent inputs terminating on individual LGN relay neurons, suggesting a failure of synaptic pruning in the absence of patterned activity during the period dominated by Stage III spontaneous waves (Hooks and Chen, 2006).

N-methyl-D-aspartate (NMDA) type glutamate receptors have been suggested as a

possible molecular detector of correlated activity in the network, due to their requirement of concurrent membrane depolarization and glutamate binding for activation. Preventing glutamatergic transmission through NMDA receptor blockade leads to disorganized afferent projections, supporting the idea that correlated firing are necessary for the development and maintenance of the topographic map (Cline et al., 1987, Simon et al., 1992, Li et al., 2022).

The next level in the hierarchy of visual processing is the primary visual cortex, which also shows input selection by eye preference (ocular dominance). Here we find further evidence for sensory experience shaping developing neural circuits. Wiesel and Hubel (1963) found that, during a developmental critical period, deprivation of normal binocular vision by closing one eye leads to an initial decrease of responsiveness to that eye and strengthening of input from the non-deprived eye. Conversely, artificially inducing strabismus by misaligning the two eyes decorrelates activity between the two eyes, which causes V1 neurons to lose their binocular responses and become driven almost exclusively by monocular inputs (Hubel and Wiesel, 1965).

Rules for activity dependent plasticity

Several plasticity rules apply and act conjointly in the activity-dependent shaping of the neural circuit. Donald O. Hebb postulated that synapses strengthen when neurons “repeatedly or persistently” participate in exciting their postsynaptic partners (Hebb, 1949). Hebbian plasticity is thus often summarized as “neurons that fire together wire together” (Katz and Shatz, 1996). A form of Hebbian plasticity is the spike-timing-dependent long-term potentiation that occurs at retinotectal synapses when there is synchronous firing of inputs from neighboring sites in the eye (Zhang et al., 1998). Structurally, this leads to stabilization of synapses and suppression of exploratory axonal branching (Munz et al., 2014). Hebbian plasticity is therefore useful for promoting the maintenance and reinforcement of topographically appropriate convergent inputs which have a high probability of being coactive (Vislay-Meltzer et al., 2006, Kutsarova et al., 2017, Fassier and Nicol, 2021).

Serving as a corollary to Hebbian mechanisms is Stentian plasticity, wherein “neurons

that fire out of sync lose their link" (Stent, 1973). In this form of plasticity, pre- and postsynaptic neurons that repeatedly fail to fire synchronously experience synaptic long-term depression, which weakens the synapse and increases the rates of axon branch remodeling (Lisman, 1989, Rahman et al., 2020). This destabilizes topographically inappropriate stray inputs and allows them to explore and form new connections. For example, Zhang et al. (2012) optogenetically manipulated retinal activity in mice before eye opening to either increase or decrease the amount of interocular correlation. They found that increasing synchronous activity between the eyes reduced eye-specific segregation in the superior colliculus, whereas asynchronous activation sharpened eye-specific segregation.

In addition, other associative forms of synaptic plasticity that deviate from classic spike-timing-dependent plasticity (STDP) rules or use neuronal signals that extend beyond the timeframe for STDP have also been described (see Suvrathan (2019) for review).

Simulations using computational models have shown that applying plasticity rules alone may be sufficient to allow a model network to self-organize into a biologically plausible map gradient (Fraser and Perkel, 1990, Simpson et al., 2009). For example, in the primary visual cortex, stimulus orientation preference is mapped onto columns nested within the larger macroscale map of visual space (Hubel and Wiesel, 1977), organized as a "pinwheel" arrangement of orientation preferences (Blasdel and Salama, 1986, Bonhoeffer and Grinvald, 1991) (Fig.II.2B(i)). This iconic pinwheel pattern has been reproduced by models implementing Hebbian-based rules (Von der Malsburg, 1973, Willshaw and Von Der Malsburg, 1976, Sirosh and Miikkulainen, 1994, Stevens et al., 2013), as well as reaction-diffusion models (Wolf, 2005, Kaschube et al., 2008, Wilson and Bednar, 2015). Some models show that a patterned map gradient can be produced even from white noise input subjected to bandpass filtering, raising the question of whether certain map patterns are simply a byproduct of the computational filtering performed by the specific microcircuit (Rojer and Schwartz, 1990).

These computational demonstrations suggest that activity-dependent plasticity by itself could be sufficient to direct the wiring of a circuit into the observed patterns. However, given that both nascent and regenerating neural circuits *in vivo* have been found to

extensively rely on molecular guidance for circuit wiring (Fraser and Perkel, 1990, Becker and Becker, 2007, Simpson et al., 2009), it can be surmised that map patterning through plasticity in biological systems is likely too time- and resource-consuming and capricious to serve as the sole mechanism for establishing the wiring of a large-scale neural circuit.

Axon competition and space-filling mechanisms

Along with molecular guidance cues and activity-dependent plasticity, another key mechanism that shapes the organization of neuronal circuits is competition among developing axons for target space and resources (Prestige and Willshaw, 1975, Xiong et al., 1994). Experiments in which molecular gradients are altered or removed provide insight into the nature of interaxonal competition in the absence of molecular guidance cues. In animals in which ephrin-A or EphA gradients have been ablated, the precise targeting of retinal axons along the anteroposterior gradient in the tectum becomes severely disrupted and discontinuous (Feldheim et al., 2000, Feldheim et al., 2004, Cang, Rentería, et al., 2005, Tsigankov and Koulakov, 2006, Cang et al., 2008). Nonetheless, in these animals, bulk labeling of the retinocollicular projection reveals no gaps in the neuropil, suggesting that axons continue to grow to occupy available space. In Islet2-EphA3 knock-in ($EphA3^{ki/ki}$) mice, there are two overlapping retinal EphA gradients, one with high and another with low levels of expression, resulting in the formation of two tandem retinotopic maps (Hansen et al., 2004, Reber et al., 2004). The compression of two maps into the colliculus suggests that it is not absolute levels of ephrin/Eph signaling which determines how the map forms, but rather the signaling relative to other inputs in a given target space. In other words, it is a competitive space-filling mechanism.

Axons seem to be further restricted in space by an upper limit to the size of an individual arbor. In zebrafish *lakritz* mutants that are incapable of generating RGCs, transplanting a blastomere from a wildtype fish allows some of the mutants to develop a single RGC (Gosse et al., 2008). The axonal arbor of the transplanted RGC does not fill the whole tectum, but is targeted to its retinotopically appropriate position where it grows to be larger and more complex than under normal conditions. This experiment demonstrates

that competition constrains the amount of target space occupied by each axon but the potential for arbor expansion is not unlimited.

The existence of such competitive mechanisms may confer an adaptive advantage for matching input to available target space. In animals with a partially ablated retina or tectum/superior colliculus, the resultant projection gradually expands or contracts to more uniformly fill the available target space to form a smooth map of visual space (Finlay et al., 1979, Fraser and Hunt, 1980, Simon et al., 1994). Competition between axons does not only serve to fill the available target space but also maintains the relative rather than absolute spatial relationship between neurons constituting the map.

Roles of maps beyond topography

The mechanisms and phenomenology described above paint a picture of a program in which coarse but consistent map organization emerges under the direction of molecular guidance cues, and subsequent fine-tuning of the map requires activity-dependent mechanisms. These mechanisms additionally appear to be regulated by competition among inputs that ensures proper scaling of the final map to the inputs from which it is composed. Nonetheless, it would be an errant oversimplification to consider the ultimate goal of neural map formation to be the reconstruction in the brain of a precise duplicate of the sensory receptor surface.

Central maps perform at least three additional roles with respect to their inputs, internal organization, and outputs. These roles respectively are the segregation of inputs based on functional properties, higher order feature extraction, and routing of selected outputs forward to higher order processing areas, as well as providing feedback to earlier stations. The visual system serves as an insightful example: both spatial location and feature selectivity are simultaneously encoded by mesoscale structures (e.g., laminae, stripes, and columns) nested within the larger macroscale maps in the thalamus and primary visual cortex (Sedigh-Sarvestani and Fitzpatrick, 2022) (Fig.II.1B).

Input segregation in the thalamus

Input segregation has been one of the most intensively studied aspects of functional brain mapping, primarily because it is strikingly evident at the anatomical and morphological levels. Segregation of retinal inputs from the two eyes into discrete layers of the LGN in mammals is a classic illustration of this phenomenon, but other types of functional segregation are also observed in the thalamus (Huberman et al., 2008). One example is the prominent segregation of ON and OFF RGC axons into leaflets in the LGN of mustelids like minks and ferrets (Stryker and Zahs, 1983, McConnell and LeVay, 1984). Another is the parallel, segregated routing of magnocellular, parvocellular, and koniocellular pathways from retina to cortex. In primates, this segregation results in the anatomical division of the LGN into 6 stacked layers separated by interlaminar cells (Kaplan and Shapley, 1982), while in carnivores, it assorts within the A and C laminae (Linden et al., 1981, Sherman and Spear, 1982, Spear et al., 1989).

Eye segregation is particularly intriguing from a neurodevelopmental perspective, because the optic nerves from the two eyes enter independently and initially intermingle in the early developing thalamus, only to be resegregated into thalamic layers through activity-dependent mechanisms over subsequent days of development (Sretavan and Shatz, 1984, Sretavan et al., 1988, Huberman et al., 2008). Thus, in this case, the developing visual system has committed precious metabolic resources toward re-establishing labeled lines for eye segregation, only to see it all undone in the binocular neurons of the primary visual cortex. This begs the intriguing evolutionary biological question of whether effective processing of visual information in the cortex requires that not just some, but all thalamic inputs be monocular, effectively rendering the thalamus a relay from eye to cortex. Monocular segregation is apparently important for extraction of depth information from binocular disparity, and is consistent with the strong thalamic segregation of monocular inputs in arboreal and predatory mammals like primates and carnivores. Eye segregation in the LGN of less binocular rodents is more subtle, requiring anatomical labeling of retinal inputs for visualization (Muir-Robinson et al., 2002).

Input segregation in the visual cortex

The early segregation of eye preference extends from the thalamus into the input layer 4C of the primary visual cortex in primates and carnivores, where thalamocortical axons sort into eye-specific ocular dominance bands that can be revealed anatomically using transneuronal tracing. The injection of tritiated amino acids or wheat germ agglutinin-conjugated horseradish peroxidase (WGA-HRP) into one eye results in an impressive pattern of alternating right and left eye stripes in layer 4 of Rhesus macaque and many other primates, while periodic eye-specific bead-like patches are observed in area 17 in the cat and ferret (Wiesel et al., 1974, LeVay et al., 1985, Anderson et al., 1988, Law et al., 1988, Horton and Hocking, 1996b). In contrast, the primary visual cortex of rodents does not appear to have anatomical segregation of inputs representing the left and right eyes, instead exhibiting a “salt-and-pepper” distribution of cortical neurons with a range of ocular preferences (Dräger, 1974, Thurlow and Cooper, 1988, Fagiolini et al., 1994, Cang, Kalatsky, et al., 2005, Laing et al., 2015). In addition to ocular dominance, ON and OFF RGC inputs from the thalamus are also segregated in primary visual cortex of the cat, mink, and ferret (McConnell and LeVay, 1984, Zahs and Stryker, 1988, Jin et al., 2008).

In primate cortex, there is a physical segregation of inputs from magnocellular, parvocellular, and koniocellular thalamic sources, with koniocellular inputs specifically targeting cytochrome oxidase (CO) rich “blobs” in extragranular cortical layers (Livingstone and Hubel, 1982, Fitzpatrick et al., 1983, Lachica and Casagrande, 1992, Hendry and Yoshioka, 1994, Solomon, 2002). This segregation is maintained in the form of thick, pale and thin CO stripes in V2, and even into higher cortical areas as the dorsal (“where”) and ventral (“what”) processing streams (Sincich and Horton, 2005, Sedigh-Sarvestani and Fitzpatrick, 2022). Interestingly, while early cortical areas like V1 have pronounced segregation of features like ocular dominance, this is progressively lost in these higher processing areas as visual information processing becomes increasingly specialized. This suggests that multiplexing of segregated input feature representations may facilitate subsequent sorting and routing by information relevance for specialized processing in higher order areas.

An important, largely unresolved question is whether ocular dominance band segregation in the cortex follows a developmental program similar to topographic map refinement, in which some as yet unidentified molecular guidance cue sets the coarse pattern of alternating ocular dominance band formation, with subsequent activity-dependent processes sharpening their boundaries. In seminal experiments in the cat by Stryker and Harris (1986), RGCs were silenced by intraocular injection of tetrodotoxin from the time of eye opening until several weeks later when well-segregated ocular dominance bands are normally anatomically detectable by transneuronal tracing. The experiment showed a failure of eye-specific segregation in the absence of patterned retinal activity. However, subsequent evidence suggested that initial segregation actually predates eye-opening (Horton and Hocking, 1996a, Crair et al., 2001). The retinal silencing may therefore have had the unintended effect of desegregating already patchy ocular dominance bands. Moreover, in the ferret, targeted injections of biotinylated dextran amine into a monocular lamina of the LGN results in patchy tufts of labeled axons in layer 4 of visual cortex as early as P16, just a few days after initial thalamocortical innervation and two weeks before eye opening, considerably earlier than initially reported using transneuronal labeling techniques (Ruthazer et al., 1999, Crowley and Katz, 2000).

This is unsurprising as it has long been appreciated that the segregation of retinogeniculate inputs into eye-specific layers, although believed to be activity-dependent, occurs much earlier in development than eye opening. The discovery that prior to the period of photoreceptor-mediated vision, waves of spontaneous activity sweep across RGCs, as well as the thalamus, in ferrets, rats, and mice during the period of retinogeniculate segregation provides a plausible explanation for how axons are sorted based on their eye of origin, relying on the different patterns of spontaneous neuronal firing in the two eyes (Maffei and Galli-Resta, 1990, Meister et al., 1991, Feller et al., 1996, Warland et al., 2006, Martini et al., 2021). Indeed, retinogeniculate segregation of afferents is severely disrupted when early spontaneous neural activity is blocked either by infusion of TTX into the thalamus in kittens or by intraocular injection of epibatidine in ferrets to prevent the generation of retinal waves (Sretavan et al., 1988, Penn et al., 1998).

The requirement of spontaneous activity for eye-specific segregation is challenged by the observation by Crowley and Katz (1999) that patchy thalamocortical projections are present in animals enucleated shortly after birth, presumably lacking retinal-derived activity cues. However, it should be noted that patchy projections in eyeless animals may not represent a substrate for ocular dominance. Enucleation has been shown to lead to restructuring of thalamic anatomy in the Rhesus macaque, resulting in thalamic lamination into gross magnocellular, parvocellular, and koniocellular layers that target different layers of the cortex and in some cases also segregate into patchy projections (Dehay et al., 1996).

Feature extraction in the visual cortex

Another challenge concerning the function and formation of ocular dominance columns is their heterogeneity across and within species. The characteristic stripe-like ocular dominance bands observed in primate cortex differ from the patchy, bead-like organization of ocular dominance in the cortex of cats and ferrets (Wiesel et al., 1974, LeVay et al., 1985, Anderson et al., 1988, Law et al., 1988, Horton and Hocking, 1996b). A clever model by Jones and coworkers (Jones et al., 1991) proposed that this difference in patterns could emerge as a simple consequence of boundary effects related to the relative shapes of the LGN and V1 in these species. More difficult to account for, however, are the stereotypical heterogeneities in ocular dominance band widths seen in some species. In the ferret, unlike the cat, ocular dominance bands consistently converge into large islands near the area 17/18 border, despite having a more regular patchy appearance in peripheral zones (Law et al., 1988, Redies et al., 1990, Ruthazer et al., 1999). Ocular dominance bands in the squirrel monkey, by comparison, can be quite unpredictable, with the degree of segregation differing across V1, apparently dissipating near the foveal representation in some animals, and with others mysteriously lacking any segregation at all (Adams and Horton, 2003). Another surprising observation is that the periodic distances between ocular dominance stripes in the Rhesus macaque can vary nearly two-fold from one animal to another (Horton and Hocking, 1996b). Perhaps the most extreme case is that of the tree shrew (*Tupaia glis*) in which eye-specific thalamocortical projections from the well-segregated,

laminated LGN do not terminate as alternating columnar bands. Instead, they terminate as uniform sublayers within layer 4 of primary visual cortex, with inputs representing the contralateral eye spanning the entire layer, while ipsilateral eye inputs target only the upper- and lower-most strata of layer 4 (Casagrande and Harting, 1975). Such diversity of organization highlights the convergent evolutionary forces that favor input segregation in the binocular primary visual cortices of many mammalian species.

Orientation and direction selectivity are prominent emergent features extracted by the primary visual cortex. While direction selective neurons are found in the retina (Demb, 2007, Wei and Feller, 2011) and LGN (Shou and Leventhal, 1989), orientation selectivity is a hallmark of the primary cortical visual response. In contrast to the retina and thalamus, spots and full field flashes are very poor stimuli for evoking activity in cortical neurons. As discovered serendipitously by Hubel and Wiesel (1962), cortical neurons respond robustly to oriented edges and lines. Orientation selectivity in the cortex is computed by the interactions of local circuitry and the selection of aligned thalamic inputs (Chapman et al., 1991, Ferster et al., 1996, Ferster and Miller, 2000, Vidyasagar and Eysel, 2015). In carnivore and primate cortex, there is a hypercolumnar organization in which retinotopy, ocular dominance, orientation selectivity, and other visual features are organized in an orthogonal, periodically repeating layout. Hubel and Wiesel initially schematized the hypercolumn using an “ice cube model”: for a particular visual location, orientations were systematically represented along one axis and eye-preference along the orthogonal axis (Hubel and Wiesel, 1977). However, subsequent experiments using voltage sensitive dyes and intrinsic signal optical imaging revealed that orientations were instead organized as a periodic series of “pinwheels” with all orientations radiating from a central axis (Blasdel and Salama, 1986, Bonhoeffer and Grinvald, 1991). Individual neurons located at pinwheel centers were not found to lack orientation selectivity, but are typically more broadly tuned than cells further from the centers (Nauhaus et al., 2008, Koch et al., 2016). Pinwheel centers tended to be located near ocular dominance band centers, thus manifesting an orthogonal relationship of these two feature maps (Crair et al., 1997). An intriguing consequence of this configuration is that more binocular cells should be found at cortical sites where orientation is most narrowly tuned and thus potentially well-suited to compute depth

information from binocular disparity at edges. Thus, the cortical hypercolumn appears to be not just a scheme for multiplexing various feature maps within the same neural substrate, but also creates opportunities for heterogeneity of information processing to extract parallel information streams within a single cortical area.

The question of how the periodic organization of orientation columns arises is fundamental to understanding the multiplexing of feature maps in the brain. On the one hand, there is good precedent for repeating motifs under the control of molecular signaling and mutual transcriptional suppression signals from the development of the eye, perhaps best understood in *Drosophila* eye development (Zipursky, 1989, Chen and Desplan, 2020). It is conceivable that a similar form of local signaling might lead to the periodic waxing and waning of transcriptional regulation across the cortical surface, leading to hypercolumnar organization. On the other hand, in supra- and infragranular layers of primary visual cortex of mammals with hypercolumnar organization, long-range horizontal connections link neighboring hypercolumns and have been shown to connect columns with that prefer similar orientations (Gilbert and Wiesel, 1989, Löwel and Singer, 1992, Bosking et al., 1997). In cats and ferrets, a patchy periodic network of long-range horizontal connections forms prior to eye opening and the maturation of orientation selectivity, and subsequently undergoes further refinement with visual experience (Callaway and Katz, 1990, Durack and Katz, 1996). Interestingly, even in early binocularly enucleated ferrets, this initial clustering of long-range horizontal connections occurs, although infusion of TTX into the developing cortex prevents it entirely, implicating spontaneous patterned activity within the cortex or thalmocortical loop in the establishment of this early earmark of columnar periodicity (Ruthazer and Stryker, 1996). An impressive calcium imaging study performed in the visual cortex of immature ferrets by Smith et al. (2018) confirmed the existence of spontaneous cortical oscillations that exhibited temporal synchrony over very long distances and which predicted the future layout of orientation columns, long before the initial formation of horizontal connections. The long-range spatial periodicity of these oscillations is hypothesized to arise from the local connectivity of excitation and inhibition in the immature cortex. This study provides a compelling proof-of-principle for activity-dependent mechanisms being sufficient to orchestrate the global organization of

hypercolumnar architecture, relying solely on local canonical cortical microcircuitry.

Routing of selected outputs in the visual system

Of course, the most fundamental form of labeled line input segregation is the topographic map itself. Unlike the binary nature of eye-specific laminae, retinotopic maps take the form of smooth, continuous gradients. While it is easy to understand how preserving topographic organization of inputs to visual centers permits the brain to extract critical positional information about where stimuli are located, there is also evidence for ethologically specialized visual processing in different parts of the visual field (Sedigh-Sarvestani and Fitzpatrick, 2022). The most obvious form of topographically specialized visual processing is the photoreceptor composition in the fovea of the primate retina, which consists of such a densely packed array of cones, in the absence of rods, that even the corresponding RGC cell bodies are displaced peripherally (Hendrickson, 1994). Parafoveal RGCs consist disproportionately of color-sensing, small dendritic field midget type cells, in comparison to peripheral retina where large dendritic field, contrast-sensitive parasol cells are found in near equal proportion (Dacey and Petersen, 1992). This heterogeneous retinal organization propagates throughout the visual system of primates leading to a large magnification factor in visual cortex where foveal and parafoveal visual fields are disproportionately represented (Sheth and Young, 2016), as befitting an animal with frontally positioned eyes capable of visual smooth pursuit and having extensive binocular coverage of the visual field. Moreover, differences in the information encoding by midget and parasol type RGCs are converted into complex map features as a result of functional segregation in higher order areas. Thus, midget RGCs constitute the primary source of visual information at CO-rich “blobs” in V1, with the interblob territory receiving innervation downstream of parasol RGCs. These non-homogeneities in the visual maps are further preserved as V1 outputs are targeted to distinct zones in V2 and ultimately culminate in the dorsal and ventral cortical processing streams (Sheth and Young, 2016, Sedigh-Sarvestani and Fitzpatrick, 2022). This segregation of specialized processing pathways leads to dorsal (“where”) extrastriate areas like the middle temporal (MT) area of cortex that exhibit a relatively greater peripheral field representation where parasol-like features

appropriate for motion detection are maintained, and a ventral (“what”) stream with areas like V4, dominated by color-sensitive responses in more central visual fields (Mishkin et al., 1983).

The existence of highly specialized processing by morphologically and transcriptionally distinct cell types in the retina, with the possibility of being propagated and spatially remapped at downstream stations in the visual system, implies a molecular logic akin to Sperry’s chemoaffinity model. Such a mechanism could account not only for topographic organization, but also for the assembly of higher order processing modules, hard-wired to selectively probe for specific features (Kawasaki et al., 2004).

A number of findings suggest the possibility of molecularly defined processing streams. Transgenic mouse lines have been used to identify RGCs with specific functional properties and precise dendritic laminar targeting that extend axonal projections with highly specific subregional and laminar terminations in the dLGN and superior colliculus (Kim et al., 2010). For example, a class of direction-selective ganglion cells (DSGCs), selective for upward motion, have been defined by their expression of junctional adhesion molecule B (JAM-B). These DSGCs selectively target their axonal projections to the superficial layers of the superior colliculus and outer shell of the dLGN, where they have been suggested to account for the presence of direction-selective neurons in these locations (Dräger and Hubel, 1975, Kim et al., 2008). However, it is not known if these classes of cells might mediate information streams that produce direction selectivity in cortical neurons (Dhande and Huberman, 2014).

This also raises the question of whether ocular dominance column segregation in primary visual cortex may be similarly predetermined by the existence of putative molecular cues for sorting out inputs representing the two eyes (Katz and Crowley, 2002). However, in the absence of direct evidence for such molecular cues that definitively explain this kind of functional segregation, activity-dependent developmental plasticity offers a compelling alternative explanation for the emergence of ocular dominance maps.

Maps at the local scale: Local heterogeneity and information coding

In a map with ideal “smooth” topographic organization, neurons would be positioned close to, and be strongly connected to, other similarly tuned neurons, forming a relatively homogeneous population. However, while maps at the macroscale have a stereotyped and smooth organization, local scale circuits are less homogeneous, interspersed with neurons that have disparate responses (Fig.II.1C) (Nauhaus et al., 2008). These incongruous neurons are generally linked by weak connections which are pared during activity-dependent refinement but not completely eliminated (Cossell et al., 2015). Another manifestation of local heterogeneity is the fluctuation in neural responses, in which responses from an individual neuron tend to fluctuate from trial to trial even when presented with the same stimulus.

It is easy to dismiss local heterogeneity as glitches, a result of incomplete circuit refinement. However, increasing evidence points to the possibility that there is information available within this “noise” which the system can potentially utilize in local computation. One such example is the finding that trial-to-trial response fluctuation in pairs of neurons can be correlated, a phenomenon referred to as noise correlation (NC). Zohary et al. (1994) found a positive mean NC in pairs of neurons in area MT of monkeys, on the order of 0.15, a result that was corroborated by subsequent studies in a number of different mammalian species and brain regions (e.g. Ahissar et al. (1992), Bathellier et al. (2012)). In a homogeneous neuronal population, positive NC would amplify errors and impair stimulus decoding. However, when the neuronal population is more heterogeneous, the detrimental effects of NC are mitigated, and in some cases NC can even enhance decoding performance, as shown by theoretical models (e.g. Abbott and Dayan (1999), Averbeck et al. (2006)) as well as experimental evidence (Romo et al., 2003, Graf et al., 2011, Bejjanki et al., 2017). This suggests information available within NC can potentially be exploited by the local circuit to facilitate information processing (see Rothschild and Mizrahi (2015) for review).

A recent study in mouse V1 (Stringer et al., 2021) illustrated how much information discrimination can be encoded with a heterogeneous neural population. Orientation responses in V1 are distributed in a salt-and-pepper fashion (Ohki et al., 2005), in stark

contrast to the orderly organization of orientation selectivity in the primary visual cortex of the cat, ferret, and primates. Stringer and colleagues captured calcium imaging data simultaneously from up to 50,000 mouse V1 neurons, and calculated an impressive stimulus discrimination threshold of 0.35° in an orientation decoding task using a computational model. Comparing this result to decoding performance measured in macaque V1, which generally yielded decoding thresholds of >2° (Vogels and Orban, 1990, Graf et al., 2011), it would seem that the mouse V1 has an encoding capacity comparable to (if not greater!) than that of primate V1, despite being far smaller in size. However, the mouse visual system does not seem to be able to fully utilize this encoded information, as the actual behavioural orientation discrimination threshold in mice is in the range of 20°~30° (Abdolrahmani et al., 2019) compared to ~3° in macaque (Goris et al., 2017).

This begs the question of whether the better behavioural decoding performance in primates is conferred by having an organized orientation map. Koch et al. (2016) provided a possible answer to how properties in the orientation map pattern can be utilized in higher order feature detection: reproducing experimental observations (Nauhaus et al., 2008) with a computational model, they showed that a neuron can gain different properties (e.g., broader orientation tuning, less contrast saturation, and reduced cross-orientation suppression) simply from being located near a pinwheel center.

Recent studies have reported weak spatial clustering of similarly-tuned orientation-selective neurons in mice (Kondo et al., 2016, Ringach et al., 2016), which can potentially represent the beginnings of orientation columns. Ho et al. (2021) showed that the V1 orientation columns in the mouse lemur, one of the smallest living primates, are similar in size and statistics to the macaque, indicating the primate-type orientation map organization may be constrained by a size limitation beyond which substructures such as orientation columns cannot be further miniaturized. The mouse lemur possesses one of the largest V1-to-cortex ratios in primates, presumably to accommodate the orientation map structure within such a small cortex. In comparison, the mouse cortex may be too small to accommodate a similar organization structure without overly

compromising visual field coverage, resulting in the salt-and-pepper organization.

Dimensionality of information

The complexity of the local organization of the primary visual cortex is likely a reflection of the complexity of information processing that the brain must perform. Different maps do not operate in isolation but in combination with each other, enabling coverage and continuity of the input space, but also supporting the emergence of novel response properties, such as orientation tuning and multimodal integration (Rothschild and Mizrahi, 2015). How individual and multiple maps simultaneously encode for both spatial location and feature selectivity has to do with how a neural circuit processes behaviourally relevant information through a population code.

Neurons in the primary visual cortex simultaneously encode for multiple features, forming feature maps that overlap and operate in combination with each other. Given there is an ultimate constraint to the available neuroanatomical resources, the brain must choose between encoding strategies to ensure both the efficiency and robustness of the neural code.

There are two possible directions for population coding in the brain. The first approach is to represent “unique” or non-redundant information by eliminating correlations in the input, as per the efficient coding hypothesis, resulting in high-dimensional and sparse neural code (Barlow, 1961, Atick and Redlich, 1990, Olshausen and Field, 1996, Simoncelli and Olshausen, 2001). This form of encoding is most efficient, requiring only relatively simple downstream networks to read out complex features. On the other hand, neural code can also span a low-dimensional space, where encoding correlated and redundant information allows for more robust computation even in the presence of noise (Shadlen and Newsome, 1998, Reich et al., 2001).

To probe the structure of information encoding in a biological system, Stringer et al. (2019) recorded simultaneous activity from about 10,000 neurons in the mouse visual cortex in response to natural stimuli. Using cross-validated principal component analysis, they characterized the geometry of the population responses in terms of the variance in dimensions encoding increasingly fine features. They found that the

geometry of the neural code allows the representation to be as high-dimensional as possible, while still allowing for smooth rather than fractal encoding. By balancing the need for smoothness and high-dimensionality, the neural code appears to achieve both robustness and efficiency. It is interesting to consider whether the dimensionality of information encoding would be different in animals like primates with more complex feature maps with local map structure, and how this might impact visual perception.

Local computation units

How neural maps achieve sparse and robust coding to produce flexible behaviour is an exciting topic of ongoing investigation. The “canonical cortical microcircuit” (Douglas et al., 1989, Harris and Shepherd, 2015) and the “grid cell-like code” (Constantinescu et al., 2016, Hawkins et al., 2019) have been proposed as models for the local computational units that process information across multiple domains in a map-like representation. The canonical cortical microcircuit models a stereotyped assembly of cells and their connections that constitute the cortical columnar architecture, acting as a neural substrate for predictive processing. The specific connectivity within cortical microcolumns serves as an experience-expectant filter for the extraction of relevant features in the inputs (Kolb and Gibb, 2014). Based on this information, the brain continually updates a generative model of the world that it uses to predict sensory input (Bastos et al., 2012, Keller and Mrsic-Flogel, 2018).

Grid cells are neurons found in the entorhinal cortex that respond to periodically distributed locations in space. Extending this concept into the neocortex, grid-like encoding has been proposed as a substrate for forming models of objects based on their features (Constantinescu et al., 2016). It has been suggested that there exists a repeating pattern of microcircuitry across neocortical areas, with variations for the different types of information each region must process, allowing for the emergence of complex representations like object compositionality and abstractions (Harris and Shepherd, 2015, Hawkins et al., 2019).

Together, multiplexing of information through the superimposition of macroscale and mesoscale maps permits the integration of heterogeneous inputs within the

microcircuitry, allowing for the extraction of behaviourally relevant features from the input space and their integration into rich, multi-dimensional representations.

Evolutionary perspective

We have discussed the mechanisms underlying map development, the phenomenology of multiplexed representations, and the existence of fine-scale microcircuitry that underlies information processing in the brain. It has been proposed that the emergence of feature maps could be a mere artifact of the rules of self-organization (Kaschube et al., 2010). Notably, carnivores (cats, ferret) and ungulates (sheep) share similar orientation map organization with primates (Scholl et al., 2017), but such organization is absent from mice (Ohki & Reid, 2007) and gray squirrels (Van Hooser et al., 2005). Additionally, tree shrews, a close relative to primates, have primate-like orientation columns but ocular dominance organized in layers instead of columns (Fitzpatrick, 1996). This presence of mesoscale feature maps is a common trait among many species with large brains, however, it is unlikely to merely be a result of larger brain size. For example, large rodents like the red-rumped agouti lack periodic cortical orientation columns, whereas one of the smallest primates, the mouse lemur, has archetypal hypercolumns (Schmidt and Wolf, 2021). Thus, the detailed properties of maps appear most likely to be a consequence of evolutionary selection based on adaptive requirements. The ubiquity and diversity of feature maps suggest that they embody principles of organization for more ethologically efficient representations of noisy, multidimensional information from complex environments.

References

Abbott LF, Dayan P (1999), The effect of correlated variability on the accuracy of a population code. Neural computation 11:91-101.

Abdolrahmani M, Lyamzin DR, Aoki R, Benucci A (2019), Cognitive modulation of interacting corollary discharges in the visual cortex. Preprint at biorxiv doi: 101101/615229.

Ackman JB, Burbridge TJ, Crair MC (2012), Retinal waves coordinate patterned activity throughout the developing visual system. Nature 490:219-225.

Adams DL, Horton JC (2003), Capricious expression of cortical columns in the primate brain. Nature neuroscience 6:113-114.

Adelsberger H, Garaschuk O, Konnerth A (2005), Cortical calcium waves in resting newborn mice. Nature neuroscience 8:988-990.

Ahissar E, Vaadia E, Ahissar M, Bergman H, Arieli A, Abeles M (1992), Dependence of cortical plasticity on correlated activity of single neurons and on behavioral context. Science 257:1412-1415.

Anctil M (2015) Dawn of the neuron: the early struggles to trace the origin of nervous systems. McGill-Queen's Press-MQUP.

Anderson PA, Olavarria J, Van Sluyters RC (1988), The overall pattern of ocular dominance bands in cat visual cortex. Journal of Neuroscience 8:2183-2200.

Arcas A, Wilkinson DG, Nieto MÁ (2020), The Evolutionary History of Ephs and Ephrins: Toward Multicellular Organisms. Molecular biology and evolution 37:379-394.

Arroyo DA, Feller MB (2016), Spatiotemporal features of retinal waves instruct the wiring of the visual circuitry. Frontiers in neural circuits 10:54.

Assali A, Gaspar P, Rebsam A, Activity dependent mechanisms of visual map formation-From retinal waves to molecular regulators, Seminars in cell & developmental biology, Elsevier, 2014, pp. 136-146.

Atick JJ, Redlich AN (1990), Towards a theory of early visual processing. Neural computation 2:308-320.

Averbeck BB, Latham PE, Pouget A (2006), Neural correlations, population coding and computation. Nature reviews neuroscience 7:358-366.

Bansal A, Singer JH, Hwang BJ, Xu W, Beaudet A, Feller MB (2000), Mice lacking specific nicotinic acetylcholine receptor subunits exhibit dramatically altered spontaneous activity patterns and reveal a limited role for retinal waves in forming ON and OFF circuits in the inner retina. Journal of Neuroscience 20:7672-7681.

Barlow HB (1961), Possible principles underlying the transformation of sensory messages. Sensory communication 1.

Bastos AM, Usrey WM, Adams RA, Mangun GR, Fries P, Friston KJ (2012), Canonical microcircuits for predictive coding. Neuron 76:695-711.

Bathellier B, Ushakova L, Rumpel S (2012), Discrete neocortical dynamics predict behavioral categorization of sounds. Neuron 76:435-449.

Becker CG, Becker T (2007), Growth and pathfinding of regenerating axons in the optic projection of adult fish. Journal of neuroscience research 85:2793-2799.

Bejjanki VR, Da Silveira RA, Cohen JD, Turk-Browne NB (2017), Noise correlations in the human brain and their impact on pattern classification. PLoS computational biology 13:e1005674.

Blasdel GG, Salama G (1986), Voltage-sensitive dyes reveal a modular organization in monkey striate cortex. Nature 321:579-585.

Bonhoeffer F, Huf J (1980), Recognition of cell types by axonal growth cones in vitro. Nature 288:162-164.

Bonhoeffer F, Huf J (1982), In vitro experiments on axon guidance demonstrating an anterior-posterior gradient on the tectum. The EMBO Journal 1:427-431.

Bonhoeffer F, Huf J (1985), Position-dependent properties of retinal axons and their growth cones. Nature 315:409-410.

Bonhoeffer T, Grinvald A (1991), Iso-orientation domains in cat visual cortex are arranged in pinwheel-like patterns. Nature 353:429-431.

Bosking WH, Zhang Y, Schofield B, Fitzpatrick D (1997), Orientation selectivity and the arrangement of horizontal connections in tree shrew striate cortex. Journal of neuroscience 17:2112-2127.

Burkhardt P, Sprecher SG (2017), Evolutionary origin of synapses and neurons–Bridging the gap. Bioessays 39:1700024.

Burrill JD, Easter Jr SS (1994), Development of the retinofugal projections in the embryonic and larval zebrafish (Brachydanio rerio). Journal of comparative neurology 346:583-600.

Callaway EM, Katz LC (1990), Emergence and refinement of clustered horizontal connections in cat striate cortex. Journal of Neuroscience 10:1134-1153.

Cang J, Kalatsky VA, Löwel S, Stryker MP (2005), Optical imaging of the intrinsic signal as a measure of cortical plasticity in the mouse. Visual neuroscience 22:685-691.

Cang J, Rentería RC, Kaneko M, Liu X, Copenhagen DR, Stryker MP (2005), Development of precise maps in visual cortex requires patterned spontaneous activity in the retina. Neuron 48:797-809.

Cang J, Wang L, Stryker MP, Feldheim DA (2008), Roles of ephrin-as and structured activity in the development of functional maps in the superior colliculus. Journal of Neuroscience 28:11015-11023.

Casagrande VA, Harting JK (1975), Transneuronal transport of tritiated fucose and proline in the visual pathways of tree shrew Tupaia glis. Brain Res 96:367-372.

Chapman B, Zahs KR, Stryker MP (1991), Relation of cortical cell orientation selectivity to alignment of receptive fields of the geniculocortical afferents that arborize within a single orientation column in ferret visual cortex. Journal of Neuroscience 11:1347-1358.

Charron F, Tessier-Lavigne M (2007), The Hedgehog, TGF-β/BMP and Wnt families of morphogens in axon guidance. Axon growth and guidance:116-133.

Chen Y-C, Desplan C (2020), Gene regulatory networks during the development of the Drosophila visual system. Current topics in developmental biology 139:89-125.

Cline HT, Debski EA, Constantine-Paton M (1987), N-methyl-D-aspartate receptor antagonist desegregates eye-specific stripes. Proceedings of the National Academy of Sciences 84:4342-4345.

Constantinescu AO, O'Reilly JX, Behrens TE (2016), Organizing conceptual knowledge in humans with a gridlike code. Science 352:1464-1468.

Cossell L, Iacaruso MF, Muir DR, Houlton R, Sader EN, Ko H, Hofer SB, Mrsic-Flogel TD (2015), Functional organization of excitatory synaptic strength in primary visual cortex. Nature 518:399-403.

Crair MC, Horton JC, Antonini A, Stryker MP (2001), Emergence of ocular dominance columns in cat visual cortex by 2 weeks of age. Journal of Comparative Neurology 430:235-249.

Crair MC, Ruthazer ES, Gillespie DC, Stryker MP (1997), Ocular dominance peaks at pinwheel center singularities of the orientation map in cat visual cortex. J Neurophysiol 77:3381-3385.

Crowley JC, Katz LC (1999), Development of ocular dominance columns in the absence of retinal input. Nature neuroscience 2:1125-1130.

Crowley JC, Katz LC (2000), Early development of ocular dominance columns. Science 290:1321-1324.

Dacey DM, Petersen MR (1992), Dendritic field size and morphology of midget and parasol ganglion cells of the human retina. Proc Natl Acad Sci U S A 89:9666-9670.

Dehay C, Giroud P, Berland M, Killackey HP, Kennedy H (1996), Phenotypic characterisation of respecified visual cortex subsequent to prenatal enucleation in the monkey: development of acetylcholinesterase and cytochrome oxidase patterns. Journal of Comparative Neurology 376:386-402.

Demb JB (2007), Cellular mechanisms for direction selectivity in the retina. Neuron 55:179-186.

Dhande OS, Hua EW, Guh E, Yeh J, Bhatt S, Zhang Y, Ruthazer ES, Feller MB, et al. (2011), Development of single retinofugal axon arbors in normal and β2 knock-out mice. Journal of Neuroscience 31:3384-3399.

Dhande OS, Huberman AD (2014), Retinal ganglion cell maps in the brain: implications for visual processing. Current opinion in neurobiology 24:133-142.

Douglas RJ, Martin KA, Whitteridge D (1989), A canonical microcircuit for neocortex. Neural computation 1:480-488.

Dräger UC (1974), Autoradiography of tritiated proline and fucose transported transneuronally from the eye to the visual cortex in pigmented and albino mice. Brain research 82:284-292.

Dräger UC, Hubel DH (1975), Responses to visual stimulation and relationship between visual, auditory, and somatosensory inputs in mouse superior colliculus. Journal of Neurophysiology 38:690-713.

Durack JC, Katz LC (1996), Development of horizontal projections in layer 2/3 of ferret visual cortex. Cerebral Cortex 6:178-183.

Fagiolini M, Pizzorusso T, Berardi N, Domenici L, Maffei L (1994), Functional postnatal development of the rat primary visual cortex and the role of visual experience: dark rearing and monocular deprivation. Vision research 34:709-720.

Fassier C, Nicol X (2021), Retinal Axon Interplay for Binocular Mapping. Frontiers in Neural Circuits 15.

Feldheim DA, Kim Y-I, Bergemann AD, Frisén J, Barbacid M, Flanagan JG (2000), Genetic analysis of ephrin-A2 and ephrin-A5 shows their requirement in multiple aspects of retinocollicular mapping. Neuron 25:563-574.

Feldheim DA, Nakamoto M, Osterfield M, Gale NW, DeChiara TM, Rohatgi R, Yancopoulos GD, Flanagan JG (2004), Loss-of-function analysis of EphA receptors in retinotectal mapping. Journal of Neuroscience 24:2542-2550.

Feldheim DA, O'Leary DD (2010), Visual map development: bidirectional signaling, bifunctional guidance molecules, and competition. Cold Spring Harbor perspectives in biology 2:a001768.

Feller MB, Wellis DP, Stellwagen D, Werblin FS, Shatz CJ (1996), Requirement for cholinergic synaptic transmission in the propagation of spontaneous retinal waves. Science 272:1182-1187.

Ferster D, Chung S, Wheat H (1996), Orientation selectivity of thalamic input to simple cells of cat visual cortex. Nature 380:249-252.

Ferster D, Miller KD (2000), Neural mechanisms of orientation selectivity in the visual cortex. Annual review of neuroscience 23:441-471.

Finlay BL, Schneps SE, Schneider GE (1979), Orderly compression of the retinotectal projection following partial tectal ablation in the newborn hamster. Nature 280:153-155.

Fitzpatrick D (1996), The functional organization of local circuits in visual cortex: insights from the study of tree shrew striate cortex. Cerebral cortex 6:329-341.

Fitzpatrick D, Itoh K, Diamond IT (1983), The laminar organization of the lateral geniculate body and the striate cortex in the squirrel monkey (Saimiri sciureus). J Neurosci 3:673-702.

Flanagan JG (2006), Neural map specification by gradients. Current opinion in neurobiology 16:59-66.

Fraser SE, Hunt R (1980), Retinotectal plasticity in Xenopus: anomalous ipsilateral projection following late larval eye removal. Developmental biology 79:444-452.

Fraser SE, Perkel DH (1990), Competitive and positional cues in the patterning of nerve connections. Journal of neurobiology 21:51-72.

Fritsch G, Hitzig E (1870), Uber die elektrische Erregbarkeit des Grosshirns. Archiv fur Anatomie und Physiologie 37:300-332.

Gilbert CD, Wiesel TN (1989), Columnar specificity of intrinsic horizontal and corticocortical connections in cat visual cortex. Journal of Neuroscience 9:2432-2442.

Gnuegge L, Schmid S, Neuhauss SC (2001), Analysis of the activity-deprived zebrafish mutantmacho reveals an essential requirement of neuronal activity for the development of a fine-grained visuotopic map. Journal of Neuroscience 21:3542-3548.

Goris RL, Ziemba CM, Stine GM, Simoncelli EP, Movshon JA (2017), Dissociation of choice formation and choice-correlated activity in macaque visual cortex. Journal of Neuroscience 37:5195-5203.

Gosse NJ, Nevin LM, Baier H (2008), Retinotopic order in the absence of axon competition. Nature 452:892-895.

Graf A, Kohn A, Jazayeri M, Movshon JA (2011), Decoding the activity of neuronal populations in macaque primary visual cortex. Nature neuroscience 14:239-245.

Grünbaum AS, Sherrington CS (1902), Observations on the physiology of the cerebral cortex of some of the higher apes.(Preliminary communication.). Proceedings of the Royal Society of London 69:206-209.

Hansen MJ, Dallal GE, Flanagan JG (2004), Retinal axon response to ephrin-as shows a graded, concentration-dependent transition from growth promotion to inhibition. Neuron 42:717-730.

Hanson MG, Landmesser LT (2004), Normal patterns of spontaneous activity are required for correct motor axon guidance and the expression of specific guidance molecules. Neuron 43:687-701.

Harris KD, Shepherd GM (2015), The neocortical circuit: themes and variations. Nature neuroscience 18:170-181.

Hawkins J, Lewis M, Klukas M, Purdy S, Ahmad S (2019), A framework for intelligence and cortical function based on grid cells in the neocortex. Frontiers in neural circuits 12:121.

Hebb DO (1949) The Organization of Behavior. New York, NY: John Wiley and Sons.

Hendrickson AE (1994), Primate foveal development: a microcosm of current questions in neurobiology. Investigative ophthalmology & visual science 35:3129-3133.

Hendry SH, Yoshioka T (1994), A neurochemically distinct third channel in the macaque dorsal lateral geniculate nucleus. Science 264:575-577.

Ho CLA, Zimmermann R, Weidinger JDF, Prsa M, Schottdorf M, Merlin S, Okamoto T, Ikezoe K, et al. (2021), Orientation preference maps in Microcebus murinus reveal size-invariant design principles in primate visual cortex. Current Biology 31:733-741. e737.

Holmes G (1918), Disturbances of vision by cerebral lesions. The British journal of ophthalmology 2:353.

Hooks BM, Chen C (2006), Distinct roles for spontaneous and visual activity in remodeling of the retinogeniculate synapse. Neuron 52:281-291.

Horton JC, Hocking DR (1996a), An adult-like pattern of ocular dominance columns in striate cortex of newborn monkeys prior to visual experience. Journal of Neuroscience 16:1791-1807.

Horton JC, Hocking DR (1996b), Anatomical demonstration of ocular dominance columns in striate cortex of the squirrel monkey. Journal of Neuroscience 16:5510-5522.

Hubel DH, Wiesel TN (1962), Receptive fields, binocular interaction and functional architecture in the cat's visual cortex. The Journal of physiology 160:106.

Hubel DH, Wiesel TN (1965), Binocular interaction in striate cortex of kittens reared with artificial squint. Journal of neurophysiology 28:1041-1059.

Hubel DH, Wiesel TN (1977), Ferrier lecture-Functional architecture of macaque monkey visual cortex. Proceedings of the Royal Society of London Series B Biological Sciences 198:1-59.

Huberman AD, Feller MB, Chapman B (2008), Mechanisms underlying development of visual maps and receptive fields. Annu Rev Neurosci 31:479-509.

Jackson J (1875), Cases of partial convulsion from organic brain disease, bearing on the experiments of Hitzig and Ferrier. Medical Times Gazette 1:578579.

Jin JZ, Weng C, Yeh C-I, Gordon JA, Ruthazer ES, Stryker MP, Swadlow HA, Alonso J-M (2008), On and off domains of geniculate afferents in cat primary visual cortex. Nature neuroscience 11:88-94.

Jones DG, Van Sluyters RC, Murphy KM (1991), A computational model for the overall pattern of ocular dominance. Journal of Neuroscience 11:3794-3808.

Kaplan E, Shapley R (1982), X and Y cells in the lateral geniculate nucleus of macaque monkeys. The Journal of Physiology 330:125-143.

Kaschube M, Schnabel M, Löwel S, Coppola DM, White LE, Wolf F (2010), Universality in the evolution of orientation columns in the visual cortex. science 330:1113-1116.

Kaschube M, Schnabel M, Wolf F (2008), Self-organization and the selection of pinwheel density in visual cortical development. New journal of physics 10:015009.

Katz LC, Crowley JC (2002), Development of cortical circuits: lessons from ocular dominance columns. Nat Rev Neurosci 3:34-42.

Katz LC, Shatz CJ (1996), Synaptic activity and the construction of cortical circuits. Science 274:1133-1138.

Kawasaki H, Crowley JC, Livesey FJ, Katz LC (2004), Molecular organization of the ferret visual thalamus. J Neurosci 24:9962-9970.

Keller GB, Mrsic-Flogel TD (2018), Predictive Processing: A Canonical Cortical Computation. Neuron 100:424-435.

Kim I-J, Zhang Y, Meister M, Sanes JR (2010), Laminar restriction of retinal ganglion cell dendrites and axons: subtype-specific developmental patterns revealed with transgenic markers. Journal of Neuroscience 30:1452-1462.

Kim I-J, Zhang Y, Yamagata M, Meister M, Sanes JR (2008), Molecular identification of a retinal cell type that responds to upward motion. Nature 452:478-482.

Kita EM, Scott EK, Goodhill GJ (2015), Topographic wiring of the retinotectal connection in zebrafish. Developmental neurobiology 75:542-556.

Koch E, Jin J, Alonso JM, Zaidi Q (2016), Functional implications of orientation maps in primary visual cortex. Nat Commun 7:13529.

Kolb B, Gibb R (2014), Searching for the principles of brain plasticity and behavior. Cortex 58:251-260.

Kondo S, Yoshida T, Ohki K (2016), Mixed functional microarchitectures for orientation selectivity in the mouse primary visual cortex. Nature communications 7:1-16.

Kutsarova E, Munz M, Ruthazer ES (2017), Rules for shaping neural connections in the developing brain. Frontiers in neural circuits 10:111.

Lachica E, Casagrande V (1992), Direct W-like geniculate projections to the cytochrome oxidase (CO) blobs in primate visual cortex: Axon morphology. Journal of Comparative Neurology 319:141-158.

Laing R, Turecek J, Takahata T, Olavarria J (2015), Identification of eye-specific domains and their relation to callosal connections in primary visual cortex of long evans rats. Cerebral Cortex 25:3314-3329.

Law MI, Zahs KR, Stryker MP (1988), Organization of primary visual cortex (area 17) in the ferret. Journal of Comparative Neurology 278:157-180.

LeVay S, Connolly M, Houde J, Van Essen DC (1985), The complete pattern of ocular dominance stripes in the striate cortex and visual field of the macaque monkey. Journal of Neuroscience 5:486-501.

Li VJ, Schohl A, Ruthazer ES (2022), Topographic map formation and the effects of NMDA receptor blockade in the developing visual system. Proceedings of the National Academy of Sciences 119:e2107899119.

Linden DC, Guillery R, Cucchiaro J (1981), The dorsal lateral geniculate nucleus of the normal ferret and its postnatal development. Journal of Comparative Neurology 203:189-211.

Lisman J (1989), A mechanism for the Hebb and the anti-Hebb processes underlying learning and memory. Proceedings of the National Academy of Sciences 86:9574-9578.

Livingstone MS, Hubel DH (1982), Thalamic inputs to cytochrome oxidase-rich regions in monkey visual cortex. Proceedings of the National Academy of Sciences 79:6098-6101.

Löwel S, Singer W (1992), Selection of intrinsic horizontal connections in the visual cortex by correlated neuronal activity. Science 255:209-212.

Maffei L, Galli-Resta L (1990), Correlation in the discharges of neighboring rat retinal ganglion cells during prenatal life. Proceedings of the National Academy of Sciences 87:2861-2864.

Martini FJ, Guillamón-Vivancos T, Moreno-Juan V, Valdeolmillos M, López-Bendito G (2021), Spontaneous activity in developing thalamic and cortical sensory networks. Neuron 109:2519-2534.

McConnell SK, LeVay S (1984), Segregation of on-and off-center afferents in mink visual cortex. Proceedings of the National Academy of Sciences 81:1590-1593.

McLaughlin T, O'Leary DD (2005), Molecular gradients and development of retinotopic maps. Annu Rev Neurosci 28:327-355.

McLaughlin T, Torborg CL, Feller MB, O'Leary DD (2003), Retinotopic map refinement requires spontaneous retinal waves during a brief critical period of development. Neuron 40:1147-1160.

Meister M, Wong RO, Baylor DA, Shatz CJ (1991), Synchronous bursts of action potentials in ganglion cells of the developing mammalian retina. Science 252:939-943.

Ming G-l, Henley J, Tessier-Lavigne M, Song H-j, Poo M-m (2001), Electrical activity modulates growth cone guidance by diffusible factors. Neuron 29:441-452.

Mishkin M, Ungerleider LG, Macko KA (1983), Object vision and spatial vision: two cortical pathways. Trends in neurosciences 6:414-417.

Missaire M, Hindges R (2015), The role of cell adhesion molecules in visual circuit formation: from neurite outgrowth to maps and synaptic specificity. Developmental neurobiology 75:569-583.

Muir-Robinson G, Hwang BJ, Feller MB (2002), Retinogeniculate axons undergo eye-specific segregation in the absence of eye-specific layers. Journal of Neuroscience 22:5259-5264.

Munz M, Gobert D, Schohl A, Poquerusse J, Podgorski K, Spratt P, Ruthazer ES (2014), Rapid Hebbian axonal remodeling mediated by visual stimulation. Science 344:904-909.

Nauhaus I, Benucci A, Carandini M, Ringach DL (2008), Neuronal selectivity and local map structure in visual cortex. Neuron 57:673-679.

Nicol X, Voyatzis S, Muzerelle A, Narboux-Nême N, Südhof TC, Miles R, Gaspar P (2007), cAMP oscillations and retinal activity are permissive for ephrin signaling during the establishment of the retinotopic map. Nature neuroscience 10:340-347.

Ohki K, Chung S, Ch'ng YH, Kara P, Reid RC (2005), Functional imaging with cellular resolution reveals precise micro-architecture in visual cortex. Nature 433:597-603.

Ohki K, Reid RC (2007), Specificity and randomness in the visual cortex. Current opinion in neurobiology. Aug 1;17(4):401-7.

Olshausen BA, Field DJ (1996), Emergence of simple-cell receptive field properties by learning a sparse code for natural images. Nature 381:607-609.

Olson MD, Meyer RL (1991), The effect of TTX-activity blockade and total darkness on the formation of retinotopy in the goldfish retinotectal projection. Journal of comparative neurology 303:412-423.

Penfield W, Boldrey E (1937), Somatic motor and sensory representation in the cerebral cortex of man as studied by electrical stimulation. Brain 60:389-443.

Penn AA, Riquelme PA, Feller MB, Shatz CJ (1998), Competition in retinogeniculate patterning driven by spontaneous activity. Science 279:2108-2112.

Pratt KG, Hiramoto M, Cline HT (2016), An evolutionarily conserved mechanism for activity-dependent visual circuit development. Frontiers in Neural Circuits 10:79.

Prestige M, Willshaw D (1975), On a role for competition in the formation of patterned neural connexions. Proceedings of the Royal Society of London Series B Biological Sciences 190:77-98.

Rahman TN, Munz M, Kutsarova E, Bilash OM, Ruthazer ES (2020), Stentian structural plasticity in the developing visual system. Proceedings of the National Academy of Sciences 117:10636-10638.

Reber M, Burrola P, Lemke G (2004), A relative signalling model for the formation of a topographic neural map. Nature 431:847-853.

Redies C, Diksic M, Riml H (1990), Functional organization in the ferret visual cortex: a double-label 2-deoxyglucose study. Journal of Neuroscience 10:2791-2803.

Reich DS, Mechler F, Victor JD (2001), Independent and redundant information in nearby cortical neurons. Science 294:2566-2568.

Ringach DL, Mineault PJ, Tring E, Olivas ND, Garcia-Junco-Clemente P, Trachtenberg JT (2016), Spatial clustering of tuning in mouse primary visual cortex. Nature communications 7:1-9.

Rojer AS, Schwartz EL (1990), Cat and monkey cortical columnar patterns modeled by bandpass-filtered 2D white noise. Biological cybernetics 62:381-391.

Romo R, Hernández A, Zainos A, Salinas E (2003), Correlated neuronal discharges that increase coding efficiency during perceptual discrimination. Neuron 38:649-657.

Rothschild G, Mizrahi A (2015), Global order and local disorder in brain maps. Annual review of neuroscience 38:247-268.

Ruthazer E, Baker G, Stryker M (1999), Development and organization of ocular dominance bands in primary visual cortex of the sable ferret. Journal of Comparative Neurology 407:151-165.

Ruthazer ES, Stryker MP (1996), The role of activity in the development of long-range horizontal connections in area 17 of the ferret. J Neurosci 16:7253-7269.

Sakaguchi D, Murphey R (1985), Map formation in the developing Xenopus retinotectal system: an examination of ganglion cell terminal arborizations. Journal of Neuroscience 5:3228-3245.

Schmidt JT, Buzzard M (1990), Activity-driven sharpening of the regenerating retinotectal projection: effects of blocking or synchronizing activity on the morphology of individual regenerating arbors. Journal of neurobiology 21:900-917.

Schmidt KE, Wolf F (2021), Punctuated evolution of visual cortical circuits? Evidence from the large rodent Dasyprocta leporina, and the tiny primate Microcebus murinus. Current opinion in neurobiology 71:110-118.

Scholl B, Rylee J, Luci JJ, Priebe NJ, Padberg J (2017), Orientation selectivity in the visual cortex of the nine-banded armadillo. Journal of Neurophysiology 117:1395-1406.

Sedigh-Sarvestani M, Fitzpatrick D (2022), What AND Where: Location-dependent feature sensitivity as a canonical organizing principle of the visual system. Frontiers in neural circuits.

Shadlen MN, Newsome WT (1998), The variable discharge of cortical neurons: implications for connectivity, computation, and information coding. Journal of neuroscience 18:3870-3896.

Sherman SM, Spear PD (1982), Organization of visual pathways in normal and visually deprived cats. Physiological reviews 62:738-855.

Sheth BR, Young R (2016), Two visual pathways in primates based on sampling of space: exploitation and exploration of visual information. Frontiers in integrative neuroscience 10:37.

Shou T, Leventhal AG (1989), Organized arrangement of orientation-sensitive relay cells in the cat's dorsal lateral geniculate nucleus. Journal of Neuroscience 9:4287-4302.

Simon DK, Prusky GT, O'leary D, Constantine-Paton M (1992), N-methyl-D-aspartate receptor antagonists disrupt the formation of a mammalian neural map. Proceedings of the National Academy of Sciences 89:10593-10597.

Simon DK, Roskies AL, O'Leary DD (1994), Plasticity in the development of topographic order in the mammalian retinocollicular projection. Developmental biology 162:384-393.

Simoncelli EP, Olshausen BA (2001), Natural image statistics and neural representation. Annual review of neuroscience 24:1193-1216.

Simpson HD, Mortimer D, Goodhill GJ (2009), Theoretical models of neural circuit development. Current topics in developmental biology 87:1-51.

Sincich LC, Horton JC (2005), Input to V2 thin stripes arises from V1 cytochrome oxidase patches. Journal of Neuroscience 25:10087-10093.

Sirosh J, Miikkulainen R (1994), Cooperative self-organization of afferent and lateral connections in cortical maps. Biological Cybernetics 71:65-78.

Smith GB, Hein B, Whitney DE, Fitzpatrick D, Kaschube M (2018), Distributed network interactions and their emergence in developing neocortex. Nature neuroscience 21:1600-1608.

Solomon SG (2002), Striate cortex in dichromatic and trichromatic marmosets: neurochemical compartmentalization and geniculate input. Journal of Comparative Neurology 450:366-381.

Spear PD, McCall MA, Tumosa N (1989), W-and Y-cells in the C layers of the cat's lateral geniculate nucleus: normal properties and effects of monocular deprivation. Journal of Neurophysiology 61:58-73.

Sperry RW (1963), Chemoaffinity in the orderly growth of nerve fiber patterns and connections. Proceedings of the National Academy of Sciences of the United States of America 50:703.

Sretavan D, Shatz CJ (1984), Prenatal development of individual retinogeniculate axons during the period of segregation. Nature 308:845-848.

Sretavan DW, Shatz CJ, Stryker MP (1988), Modification of retinal ganglion cell axon morphology by prenatal infusion of tetrodotoxin. Nature 336:468-471.

Stent GS (1973), A physiological mechanism for Hebb's postulate of learning. Proceedings of the National Academy of Sciences 70:997-1001.

Stevens J-LR, Law JS, Antolík J, Bednar JA (2013), Mechanisms for stable, robust, and adaptive development of orientation maps in the primary visual cortex. Journal of Neuroscience 33:15747-15766.

Stringer C, Michaelos M, Tsyboulski D, Lindo SE, Pachitariu M (2021), High-precision coding in visual cortex. Cell 184:2767-2778. e2715.

Stringer C, Pachitariu M, Steinmetz N, Carandini M, Harris KD (2019), High-dimensional geometry of population responses in visual cortex. Nature 571:361-365.

Stryker MP, Harris WA (1986), Binocular impulse blockade prevents the formation of ocular dominance columns in cat visual cortex. Journal of Neuroscience 6:2117-2133.

Stryker MP, Zahs KR (1983), On and off sublaminae in the lateral geniculate nucleus of the ferret. Journal of Neuroscience 3:1943-1951.

Stuermer C, Rohrer B, Munz H (1990), Development of the retinotectal projection in zebrafish embryos under TTX-induced neural-impulse blockade. Journal of Neuroscience 10:3615-3626.

Sun C, Warland DK, Ballesteros JM, Van Der List D, Chalupa LM (2008), Retinal waves in mice lacking the β2 subunit of the nicotinic acetylcholine receptor. Proceedings of the National Academy of Sciences 105:13638-13643.

Suvrathan A (2019), Beyond STDP—towards diverse and functionally relevant plasticity rules. Current opinion in neurobiology 54:12-19.

Thurlow G, Cooper R (1988), Metabolic activity in striate and extrastriate cortex in the hooded rat: contralateral and ipsilateral eye input. Journal of Comparative Neurology 274:595-607.

Tsigankov DN, Koulakov AA (2006), A unifying model for activity-dependent and activity-independent mechanisms predicts complete structure of topographic maps in ephrin-A deficient mice. Journal of computational neuroscience 21:101-114.

Van Hooser SD, Heimel JAF, Chung S, Nelson SB, Toth LJ (2005), Orientation selectivity without orientation maps in visual cortex of a highly visual mammal. Journal of Neuroscience 25:19-28.

Vidyasagar TR, Eysel UT (2015), Origins of feature selectivities and maps in the mammalian primary visual cortex. Trends in neurosciences 38:475-485.

Vislay-Meltzer RL, Kampff AR, Engert F (2006), Spatiotemporal specificity of neuronal activity directs the modification of receptive fields in the developing retinotectal system. Neuron 50:101-114.

Vogels R, Orban G (1990), How well do response changes of striate neurons signal differences in orientation: a study in the discriminating monkey. Journal of Neuroscience 10:3543-3558.

Von der Malsburg C (1973), Self-organization of orientation sensitive cells in the striate cortex. Kybernetik 14:85-100.

Walter J, Henke-Fahle S, Bonhoeffer F (1987), Avoidance of posterior tectal membranes by temporal retinal axons. Development 101:909-913.

Walter J, Kern-Veits B, Huf J, Stolze B, Bonhoeffer F (1987), Recognition of position-specific properties of tectal cell membranes by retinal axons in vitro. Development 101:685-696.

Warland DK, Huberman AD, Chalupa LM (2006), Dynamics of spontaneous activity in the fetal macaque retina during development of retinogeniculate pathways. Journal of Neuroscience 26:5190-5197.

Wei W, Feller MB (2011), Organization and development of direction-selective circuits in the retina. Trends in neurosciences 34:638-645.

Weliky M, Katz LC (1999), Correlational structure of spontaneous neuronal activity in the developing lateral geniculate nucleus in vivo. Science 285:599-604.

Wiesel T, Hubel D, Lam D (1974), Autoradiographic demonstration of ocular-dominance columns in the monkey striate cortex by means of transneuronal transport. Brain research 79:273-279.

Wiesel TN, Hubel DH (1963), Single-cell responses in striate cortex of kittens deprived of vision in one eye. Journal of neurophysiology 26:1003-1017.

Willshaw DJ, Von Der Malsburg C (1976), How patterned neural connections can be set up by self-organization. Proceedings of the Royal Society of London Series B Biological Sciences 194:431-445.

Wilson SP, Bednar JA (2015), What, if anything, are topological maps for? Dev Neurobiol 75:667-681.

Wolf F (2005), Symmetry, multistability, and long-range interactions in brain development. Physical review letters 95:208701.

Xiong M, Pallas SL, Lim S, Finlay BL (1994), Regulation of retinal ganglion cell axon arbor size by target availability: Mechanisms of compression and expansion of the retinotectal projection. Journal of Comparative Neurology 344:581-597.

Xu HP, Burbridge TJ, Chen MG, Ge X, Zhang Y, Zhou ZJ, Crair MC (2015), Spatial pattern of spontaneous retinal waves instructs retinotopic map refinement more than activity frequency. Developmental neurobiology 75:621-640.

Yam PT, Charron F (2013), Signaling mechanisms of non-conventional axon guidance cues: the Shh, BMP and Wnt morphogens. Current opinion in neurobiology 23:965-973.

Yates PA, Holub AD, McLaughlin T, Sejnowski TJ, O'Leary DD (2004), Computational modeling of retinotopic map development to define contributions of EphA-ephrinA gradients, axon-axon interactions, and patterned activity. Journal of neurobiology 59:95-113.

Zahs KR, Stryker MP (1988), Segregation of ON and OFF afferents to ferret visual cortex. Journal of neurophysiology 59:1410-1429.

Zhang J, Ackman JB, Xu H-P, Crair MC (2012), Visual map development depends on the temporal pattern of binocular activity in mice. Nature neuroscience 15:298-307.

Zhang LI, Tao HW, Holt CE, Harris WA, Poo M-m (1998), A critical window for cooperation and competition among developing retinotectal synapses. Nature 395:37-44.

Zipursky SL (1989), Molecular and genetic analysis of Drosophila eye development: sevenless, bride of sevenless and rough. Trends in Neurosciences 12:183-189.

Zohary E, Shadlen MN, Newsome WT (1994), Correlated neuronal discharge rate and its implications for psychophysical performance. Nature 370:140-143.

Preface to Chapter III

In this chapter, we characterized the emerging retinotopic map in the retinotectal system of *Xenopus laevis* tadpoles, using *in vivo* two-photon microscopy to greatly improve on the level of detail and resolution from previous characterizations provided by classic anatomical and electrophysiology studies. We followed the map longitudinally in the same animals, quantified changes in fine-scale properties of the map, and examined whether NMDAR receptor blockade during development affects properties of the resulting map, contributing to the current base of knowledge on map formation.

Author contributions

Chapter III has been published as: Li, V. J., A. Schohl and E. S. Ruthazer (2022). "Topographic map formation and the effects of NMDA receptor blockade in the developing visual system." Proceedings of the National Academy of Sciences 119(8): e2107899119. https://doi.org/10.1073/pnas.2107899119.

Experiments were designed collaboratively by VJL, AS and ESR. Experiments were performed by VJL. Custom software for data analysis was developed by VJL. Embryological techniques and molecular resources were developed by AS. Funding was provided by VJL and ESR. The paper was written by VJL and ESR.

Chapter III

Topographic map formation and the effects of NMDA receptor blockade in the developing visual system

Author list: Vanessa J. Li, Anne Schohl, Edward S. Ruthazer

Keywords: Xenopus laevis, retinotectal, calcium imaging, topographic maps, development, activity-dependent, mRNA microinjection

Abstract

The development of functional topography in the developing brain follows a progression from initially coarse to more precisely organized maps. To examine the emergence of topographically organized maps in the retinotectal system, we performed longitudinal visual receptive field mapping by calcium imaging in the optic tectum of GCaMP6-expressing transgenic *Xenopus laevis* tadpoles. At stage 42, just one day after retinal axons arrive in the optic tectum, a clear retinotopic azimuth map was evident. Animals were imaged over the following week at stages 45 and 48, over which time the tectal neuropil nearly doubled in length and exhibited more precise retinotopic organization. By microinjecting GCaMP6s mRNA into one blastomere of two-cell stage embryos, we acquired bilateral mosaic tadpoles with GCaMP6s expression in postsynaptic tectal neurons on one side of the animal and in RGC axons crossing to the tectum on the opposite side. Longitudinal observation of retinotopic map emergence revealed the presence of orderly representations of azimuth and elevation as early as stage 42, although presynaptic inputs exhibited relatively less topographic organization than the postsynaptic component for the azimuth axis. Retinotopic gradients in the tectum became smoother between stages 42 and 45. Blocking *N*-methyl-D-aspartate (NMDA) receptor conductance by rearing tadpoles in MK-801 did not prevent the emergence of

retinotopic maps, but produced more discontinuous topographic gradients and altered receptive field characteristics. These results provide evidence that current through NMDA receptors is dispensable for coarse topographic ordering of retinotectal inputs, but does contribute to the fine-scale organization of the retinotectal projection.

Significance Statement

Studying the emergence of topographic organization in sensory maps has been constrained by spatial limitations of traditional anatomical and physiological techniques early in development in many animal models. Here, we have applied a high-resolution, non-invasive, *in vivo* calcium imaging approach to study the nascent retinotopic map in the larval *Xenopus laevis* retinotectal system. We performed longitudinal functional imaging of the three-dimensional organization of emerging retinotopic maps and assessed the effects of NMDA receptor blockade on map formation. Our results provide novel insights into early retinotopic map emergence and the role of NMDARs in the refinement of topographic gradients.

Introduction

Topographic maps are a widespread phenomenon in vertebrate sensory circuits, well documented across multiple species and sensory modalities. Retinotopy in the visual system – the organized projection of retinal ganglion cells (RGC) from the retina to the visual centers of the brain to form an orderly representation of the visual environment – is among the most well-studied examples of topographic sensory mapping (1-4), yet much remains to be unraveled regarding the process and underlying mechanisms of its emergence in early development.

The retinotopic map is first established by molecular guidance cues that direct retinal ganglion cell axons (RGCs) to topographically appropriate positions, establishing a coarse topographic gradient. Neuronal projections are further refined by patterned neural activity into more orderly and precise configurations (5-8). A challenge for studying the activity-dependent refinement process in higher vertebrate models is the

difficulty of visualizing and manipulating the visual system in these early stages: In mammals, the refinement of the retinocollicular map is largely completed before the onset of visual experience, instructed by waves of spontaneous activity (9-11). In contrast, the retinotectal projections of fish and frogs rely directly on patterned visual experience for refinement (5, 12), opening many possibilities for experimental intervention. In particular, Xenopus develop externally from large oocytes, easily subject to pharmacological and genetic manipulation (13, 14). The transparent skin of albino Xenopus tadpoles further permits non-invasive *in vivo* imaging. These traits make Xenopus tadpoles an ideal model for studying the early development of topographic maps.

In the developing tadpole tectum, directing neuronal arbors to their appropriate topographic positions is not a static problem, as the tectum is continuously expanding and adding new cells throughout this process. An added level of complexity arises when considering the patterns by which new cells are added: The tadpole eye adds neurons radially at the peripheral margin of the retina (15), but the tadpole tectum adds new neurons linearly from its caudomedial edge (16). In order to produce a uniform map, the connections between retinal ganglion cells and postsynaptic tectal cells need to shift partners continuously, requiring a high degree of circuit plasticity.

The activity-dependent remodeling of the axonal and dendritic processes of individual neurons has been extensively described in Xenopus (8). However, most of these studies were performed on single neurons or small neuronal populations. To date, characterizations of the evolution of the full retinotectal map in Xenopus have only been done via anatomical tracing (17) or coarse multiunit electrophysiology recordings (18, 19). Therefore, in the present study, we aimed to take advantage of multiphoton microscopy and genetically encoded calcium indicators to obtain a whole-circuit, fine-scale functional characterization of the nascent retinotopic map in *Xenopus* tadpoles. We further sought to repeatedly visualize presynaptic and postsynaptic maps independently over the initial period of map formation and development.

The NMDA receptor is considered a key player in neural circuit refinement, its activity having been shown to affect arbor morphology, branch stability and synaptic plasticity

(20-24). The segregation of retinal afferents into eye specific bands in three-eyed frogs, thought to reflect the influence of differential patterned activity on axonal arborization, is prevented by blockers of NMDA receptors (25, 26). In both frog and mammalian systems, the retinotopic precision of RGC input convergence has been found to be degraded by tectal NMDA receptor blockade (27, 28). Given these results based primarily on anatomical reconstructions of individual or small groups of cells, we sought to assess the contributions of NMDA receptors to development of the map at the whole-circuit level.

Results

Visualizing the retinotopic map in the tadpole tectum

The functional retinotopic map in the optic tectum of developing Xenopus tadpoles was studied by presenting visual mapping stimuli to transgenic Xenopus tadpoles expressing the genetically encoded calcium indicator GCaMP6s (29). Tadpoles were immobilized in agarose in an imaging chamber with a side window to permit viewing of a small LCD video monitor placed next to the animal. The corresponding calcium responses were recorded from the contralateral optic tectum using a resonant scanning two-photon microscope (Fig.III.1A, B). GCaMP6s expression levels in the transgenic tadpoles were sufficient to detect visually evoked responses in the optic tectum in some animals as early as stage 42, as defined by Nieuwkoop and Faber (30).

Animals maintained an adequate level of fluorescence for up to a week after tadpoles had matured to stage 48. This provided a suitable time window for functional characterization of the initial emerging retinotopic map by calcium imaging.

Axonal inputs from RGCs ramify topographically in the tectal neuropil where they synapse upon the dendritic arborizations of postsynaptic tectal neurons (Fig.III.1C). Thus, the organization of inputs is best reflected by the activity in the neuropil region of the tectum, where we carried out the majority of our receptive field map analyses. We devised two independent visual stimulation protocols to extract retinotopic maps: phase mapping and grid mapping. We compared maps independently extracted from the same animals using both methods, the results of which served to validate each other

(*Supplementary* Fig.III.S1).

For phase mapping, we placed an LCD monitor in front of one eye of the tadpole and repeatedly presented a slow-moving dark vertical or horizontal bar that swept across the full span of the monitor every 20 s, with 10 s for the sweep, followed by 10 s pause. The tectal response to this stimulus was a transient wave of elevated GCaMP6s fluorescence intensity that swept across the optic tectum, the response waves occurring with the same periodicity as the sweeping bar. (Fig.III.1D-F, *Supplementary* Movie.III.S1). We generated Fourier power spectra for the fluorescence time courses at each pixel and measured the phase of the response at the stimulus frequency, for bars swept in both directions of the azimuth and elevation axes (31). This creates a phase map which represents the visual field positions that evoked maximal responses at each point in the tectum (Fig.III.1G, *Supplementary* Fig.III.S1, S2). Phase mapping is a highly sensitive method which consistently and robustly revealed functional retinotopy in both the cell body layer and the neuropil.

For grid mapping, we randomly presented a stationary dark vertical or horizontal bar at each of five positions evenly spaced along either the azimuth or elevation axis of the visual field. At these early stages, most locations in the tectum responded to some extent for all five positions, but with a preference for one of the positions (*Supplementary* Fig.III.S1). Therefore, for each pixel within the tectum, we calculated an “optimal stimulus position” by weighting the responses of that pixel to bars at each stimulus position. This value estimates the center of the visual field representation for the responsive pixel (Fig.III.1H middle). Like phase maps, grid maps consistently revealed functional retinotopy in both the cell body and the neuropil layers, albeit showing an apparently smaller range of receptive field positions, especially at the periphery, compared to phase maps from the same animal at roughly the same imaging depth.

In general, phase mapping and grid mapping methods produced retinotopic maps in GCaMP6s transgenic Xenopus tadpoles that broadly matched each other. We quantified pixelwise differences between phase maps and grid maps extracted from the neuropil zone of the same animals and found these differences to be significantly

smaller on average than the mean difference between the phase map and its scrambled version, confirming that maps extracted through the two different methods were consistent with each other (*Supplementary* Fig.III.S1F, G).

We also computed grid maps for the tectal cell somata by calculating “optimal stimulus position” for cell body ROIs instead of single pixels, based on average $\Delta F/F_0$ calcium signal over all pixels within each ROI (Fig.III.1H right). The distribution of optimal stimulus positions in cell body ROIs appeared consistent with the topographic gradient of optimal stimulus positions in the corresponding neuropil region of the pixel-wise grid map.

Changes in retinotopic maps over development

To observe how the retinotopic map evolves during early development, we imaged GCaMP6s transgenic tadpoles at different developmental stages from stage 42 to stage 48 (Fig.III.2A). We performed retinotopic mapping by applying the phase mapping method to multiple optical sections within a tectal volume to extract a 3D representation of functional retinotopy (Fig.III.2, *Supplementary* Fig.III.S3, S4). We were able to visualize maps in tadpoles as young as stage 42, shortly after the first arrival of RGC axons in the optic tectum, and then re-image the same animals repeatedly at later stages. Fig.III.2 shows maps acquired from the same GCaMP6s transgenic animal at stages 42, 45 and 48 (Fig.III.2B, D, F). When raised at 20°C, tadpoles reach stage 42 roughly a week after fertilization; stages 42, 45 and 48 are separated by about 2-3 days each. We assembled 3D maps of the emerging visual field representations in the tectal neuropil at these stages (Fig.III.2E, G; *Supplementary* Figs.III.S3B, D; III.S4B, D, F; Movies.III.S2-5).

In transgenic tadpoles at stage 42, the tectal map already displayed a striking topographic gradient in the azimuth axis, while a gradient for elevation was less apparent (Fig.III.2B, *Supplementary* Fig.III.S4). Over the course of development from stage 42 to 48, the tectal neuropil roughly doubled in length (Fig.III.2C) and the topographic gradients became increasingly defined. At stage 45, a strong gradient in the azimuth map can be seen along the rostral-caudal axis of the tectum (Fig.III.2D-E), consistent with previous reports based on coarse multiunit electrophysiological and

anatomical tracing (17, 19). At this stage a robust gradient for the elevation axis within the 3D volume of the tadpole tectum is also evident. By stage 48, the azimuthal gradient within the 3D tectal volume has rotated with respect to the rostrocaudal axis of the animal (Fig.III.2F-G). We projected the receptive field centers from the tectal neuropil onto the visual field and found that, despite changes in the map orientation within the tectum, the visual field represented in the tectum remained relatively consistent between stage 45 and stage 48, with lower elevation receptive fields more densely represented in the tecta at both stages (Fig.III.2H-I).

An interesting observation was that the orientation of the retinotopic map appeared to undergo an axis rotation in Cartesian coordinates between stages 45 and 48. To estimate the map axes in three dimensions, we calculated the "global topographic gradient" vectors for the azimuth and elevation maps by summing the local gradient vectors in the neuropil, calculated for each pixel as the differences in topographic position (phase) from adjacent pixels in the x, y, and z directions (*Supplementary* Fig.III.S5). Both the azimuth and elevation gradient axes seemed to undergo noticeable changes in orientation between stage 45 and 48. The azimuth gradient initially was nearly aligned with the rostrocaudal axis of the tadpole but shifted toward a more dorsoventral orientation at stage 48, while the elevation gradient shifted from a predominantly dorsoventral orientation towards slightly greater mediolateral axis alignment (*Supplementary* Table III.S1). This observed change may in part be a result of tectal growth between the two stages, displacing previously imaged tectal volumes into different planes of section. Furthermore, the angle between the azimuth and elevation gradient axes became slightly more orthogonal at stage 48 (*Supplementary* Fig.III.S5B,D).

Comparing the retinotopic maps in presynaptic and postsynaptic compartments of the tectum

To observe the emergence of the retinotopic map in the presynaptic (RGC axons) and postsynaptic (tectal neurons) components of the retinotectal circuit, we took advantage of the ability to drive GCaMP expression in one-half of the tadpole (Fig.III.3). Injecting GCaMP6s mRNA into one blastomere of two-cell stage embryos creates animals with

mosaic fluorescent protein expression, which in some cases is restricted to exactly one lateral half of the animal (Fig.III.3A). mCherry mRNA was co-injected with GCaMP6s to aid in visualizing the distribution of fluorescent protein (Fig.III.3B). Because the retinotectal projection is entirely crossed at this developmental stage, these hemimosaic tadpoles will have expression restricted exclusively to the postsynaptic tectal cells on the labeled side and the presynaptic RGC axon terminals within the opposite tectal hemisphere (Fig.III.3C). In mRNA animals we obtained clear retinotopic maps with both phase and grid mapping methods, in both RGC axon terminals and postsynaptic tectal cells (Fig.III.3D). We found that overall GCaMP6s signal strength and signal-to-noise ratio (SNR) were significantly higher in postsynaptic compared to presynaptic compartments (*Supplementary* Fig.III.S6). The period of GCaMP expression was similar between transgenic and mRNA-injected animals, with GCaMP fluorescence persisting for up to a week after tadpoles reached stage 48 before declining in both cases to levels suboptimal for analysis.

Longitudinal imaging of post- and presynaptic topographic map development

We followed the development of retinotopic maps in both the axonal and dendritic compartments over time in the same hemimosaic animals, reconstructing three-dimensional functional map volumes at stage 42, stage 45 and stage 48 (Fig.III.4A, *Supplementary* Fig.III.S7-9, Movie.III.S6-9). Topographic maps were present at all 3 stages imaged, and postsynaptic gradients for the azimuthal visual axis in particular were strikingly evident in stage 42 animals (*Supplementary* Fig.III.S10), less than 24 h after the initial arrival of RGC axons in the tectum at stage 39 (19). At all stages, presynaptic maps appeared to be less well organized than the postsynaptic maps in the opposite hemisphere of the same animal, though this may have been confounded by relatively lower signal strengths in the RGC axons (*Supplementary* Fig.III.S6A,B).

The maturation of topographic organization in the retinotectal circuit is expected to manifest both at the level of the circuit by a progressive refinement of the retinotopic gradient, and at the level of individual cells through sharpening of visual receptive fields. To assess the circuit level organization, we characterized the smoothness of the topographic gradient by measuring “local discontinuity”, defined as the mean difference

in RF position (phase) per pixel to all neighboring pixels within a 15-pixel (7.44 μm) radius. As schematized in Fig.III.4B, a low local discontinuity value indicates a smooth local map gradient. The local discontinuity values were calculated at individual pixels (thresholded for SNR > 0.8), then averaged across the neuropil to obtain a mean discontinuity value for the neuropil azimuth and elevation maps in each animal (*Supplementary* Fig.III.S11A-C). The topographic organization of postsynaptic tectal maps as early as developmental stage 42 was confirmed by the fact that mean local discontinuity in stage 42 postsynaptic maps was significantly lower than that observed when the pixels were randomly scrambled within the neuropil (*Supplementary* Fig.III.S11D). Interestingly for stage 42 axonal maps, only the elevation, but not azimuth, maps had lower local discontinuity than a scrambled version, suggesting that at least for the azimuthal axis, retinotectal axon arbors are initially less topographically distributed within the tectal neuropil than the synapses that they form onto their postsynaptic partners. Two-way ANOVAs revealed an effect of developmental stage on local discontinuity that was significant for elevation ($p = 0.0160$) and exhibited a trend for azimuth ($p = 0.0529$) (Fig.III.4C). In particular, mean discontinuity was significantly lower for maps at stage 45 compared to stage 42. One caveat is that response strength and SNR also exhibited variability across stages, though these did not necessarily correspond to the changes in local discontinuity (*Supplementary* Fig.III.S6A,B).

For both azimuth and elevation, mean discontinuity was significantly greater in presynaptic than in postsynaptic maps across all ages (azimuth: $p = 0.0002$; elevation: $p = 0.0001$). This difference in presynaptic and postsynaptic topographic further supports the idea that tectal neurons can integrate and select inputs from diverse RGCs to transform responses into a more ordered topographic map.

To control for the fact that the tectum changes in size over this period of development (Fig.III.2C), we additionally measured a normalized mean discontinuity by reducing the size of the neighborhood used to calculate local discontinuity in proportion to the different tectal neuropil areas at different stages. This normalized mean discontinuity measure also showed a significant difference between stages 42 and 45 for elevation and for pre- versus postsynaptic maps in both axes (*Supplementary* Fig.III.S11E).

As the circuit becomes more precisely organized, refinement of the map is also expected to manifest at the single cell level in the form of decreased receptive field size (22).We therefore evaluated “receptive field sharpness” as an approximate measure for the size of the receptive field unit (Fig.III.4D). We defined receptive field sharpness as the average response, obtained by grid mapping, to the stimulus positions closest to the optimal stimulus position divided by the average response to the remaining stimulus positions in the periphery (Fig.III.4E). Cumulative probability distributions of single cell receptive field sharpness showed a progressive shift toward higher values with increasing developmental stage for both azimuth and elevation, indicating that visual response fields become more compact as the animals mature (Fig.III.4F).

Elucidating the effects of NMDAR blockade on topographic map development

NMDA receptors are believed to play an important role in retinotectal circuit refinement (20-28) To determine the contributions of NMDA receptors to Xenopus retinotectal map refinement, tadpoles were raised with 10 μM MK-801 added to the rearing solution, starting from stage 39, when RGC axons first innervate the tectum. We compared properties of retinotopic maps in these animals to control tadpoles at the same developmental stage.

Topographic maps in MK-801-treated animals imaged at stage 48 appeared qualitatively similar to maps in control animals at the same stage (Fig.III.5A). We next quantified mean local discontinuity between control and MK-801-treated animals. For both the azimuth and elevation maps, significant main effects, but no interaction, were found by two-way independent measures ANOVA for both drug (MK-801 vs. control) and compartment (presynaptic vs. postsynaptic) (Fig.III.5B). Moreover, no significant differences were found in response power or SNR between chronic MK-801 treated individuals and controls (*Supplementary* Fig.III.S6C,D). These results suggest that MK-801 treatment results in coarser gradients in the topographic map. They also confirm our earlier observation in untreated animals that postsynaptic maps exhibit smoother topographic gradients than presynaptic maps (Fig.III.4C).

Next, we evaluated “receptive field sharpness” for tectal cell bodies in control and MK-801 reared tadpoles. The cumulative distribution curve for azimuthal receptive field

sharpness values was significantly shifted to the left for MK-801 treated animals compared to controls, indicating overall larger, less compact receptive fields (Fig.III.5C). This result is consistent with previous reports of enlarged receptive fields resulting from chronic NMDAR blockade, measured electrophysiologically (22). Interestingly, a comparable shift in receptive field sharpness was not seen in the elevation maps of MK-801 reared animals, despite significant differences in map discontinuity for both azimuth and elevation (Fig.III.5B).

Because MK-801 does not wash out after binding, we performed a control experiment to exclude the possible confound of any acute effects of MK-801 on tectal calcium response and the retinotopic map. We found MK-801 bath perfusion on stage 48 tadpoles significantly reduced the magnitude of calcium responses to our phase mapping stimulus, confirming that acutely applied MK-801 does permeate into the tadpole tectum (*Supplementary* Fig.III.S12A-B). However, extracted phase maps did not change compared to those extracted prior to drug application in overall phase distribution and mean discontinuity (*Supplementary* Fig.III.S12C-F). Thus, the presence of MK-801 in the medium during the imaging period alone does not affect the extracted phase maps and subsequent quantifications.

Overall, MK-801-treated animals developed retinotectal topographic maps with a coarser topographic gradient. As stage 42 maps are coarser than stage 48 maps, this result is consistent with a role for NMDARs in the developmental fine-tuning of topographic maps at the levels of circuit organization and single-cell input selection.

Discussion

Activity-dependent refinement of retinotopic projections, driven by patterned neuronal activity in the form of spontaneous retinal waves in amniotes (32-35) and visually evoked correlated activity in anamniotes (36, 37) is crucial for the establishment of an orderly and precise retinotopic map in the visual system. Disruption or deprivation of patterned activity has been shown to result in altered retinotopic maps in the mature animal, as demonstrated in mice with defects in spontaneous retinal waves (7, 10, 38-

41). NMDA receptors are a key candidate in the processing of patterned visual activity due to their function in detecting correlated activity in converging afferents (23, 24, 26), and the disruption of NMDAR activity has been shown to impact morphology and response properties of individual neurons forming the topographic map (21, 22, 27, 42). Here, we pursued both a circuit and cellular level characterization of this phenomenon in larval Xenopus, which provides an insight into the emergence of functional retinotopic maps during the initial period of activity-dependent refinement.

In this study, we extended the previous literature of anatomical and coarse functional characterizations of topographic map refinement in the Xenopus tadpole by establishing a method to perform retinotopic mapping via *in vivo* two-photon calcium imaging, which allowed us to systematically visualize the developmental emergence of topographic maps across the whole tectal volume while maintaining subcellular resolution. We were able to observe fine-scale retinotopic mapping in tecta of tadpoles as young as Nieuwkoop & Faber stage 42. The non-invasive nature of this imaging method also allowed us to repeatedly image the same animals to follow the progression of the map at several subsequent developmental stages. While early electrophysiological characterizations reported large and overlapping multiunit receptive fields with no clear topographic organization before stage 46 (18), the improved spatial resolution of optical mapping methods allowed us to demonstrate that the tadpole tectum in these early stages already displays a functional topographic gradient. Receptive fields were large but displayed clear preferences for discrete stimulus positions in the visual field, consistent with later reports (19).

Comparing whole-tectum topographic gradients in the same animals at stage 45 and 48, we observed what seemed to be a Cartesian rotation in the representations of both the azimuth and elevation visual axes. This change can likely be explained in part by the growth of the tectum and addition of new tissue: The tadpole tectum expands by adding cells from a caudo-medial proliferative zone, displacing existing tissue laterally and rostrally (16), which would reasonably cause a shift in the retinotopic map layout within the tectal volume. However, since presynaptic RGCs are added radially at the peripheral margin of the retina (15), one might expect the tectal map to grow

increasingly distorted. Instead, we found that the azimuth and elevation axes became increasingly orthogonal to one other compared to stage 45, indicative of a more isotropic map. This observation provides evidence for the idea that presynaptic RGCs and postsynaptic tectal cells may shift their connections during development to minimize distortion of the developing retinotopic map (17, 43, 44). As these maps occupy the full volume of the tectal neuropil, fine-scale three-dimensional analysis of developmental changes in local gradients could shed further light on the mechanisms by which the retinotopic maps shift, but the reduced axial resolution inherent in two-photon microscopy limits its precision for extracting local, rather than global, gradient orientation. A question that could, nonetheless, be raised is which circuit component leads the other in the refinement process: do RGC axons shift their terminals to occupy newly available target space, determining the visual field representation in tectal cells; or do the receptive fields of postsynaptic tectal cells change first, after which presynaptic RGC inputs are then selected for via Hebbian plasticity? Axonal redistribution could be caused by exploratory axonal branch dynamics driven by inter-axonal competition within the expanding tectum for a limited resource such as a neurotrophic factor or postsynaptic availability (6, 8, 26, 45, 46). Additionally, because postsynaptic neurons integrate inputs from multiple converging RGCs, they could use NMDA receptors to detect correlated synaptic inputs and selectively stabilize axons that originate from neighboring RGCs in the eye through Hebbian mechanisms (8, 23).

Using single-cell mRNA blastomere injection at the two-cell stage, we were able to produce hemimorphant mosaic tadpoles expressing GCaMP6s in only one lateral half of the animal. This allowed us to separately image either the presynaptic RGCs or the postsynaptic tectal cells. We were able to visualize retinotopic maps and observed topographic gradients in both pre- and postsynaptic neuropil of stage 48 tadpoles. Applying a measurement of local discontinuity in the retinotopic representation, we found the gradient in postsynaptic neuropil to be smoother than that in the presynaptic inputs. This higher level of postsynaptic refinement preserves the possibility of a model in which the postsynaptic circuit is the driving party in the shifting projections phenomenon, changing their retinotopic representations first towards the direction of a more refined topographic gradient, then recruiting more presynaptic partners to match

their receptive fields.

We used the hemimosaic GCaMP animals to investigate the effects of NMDA receptor blockade early in development on the topographic organization of the map, and whether there is a differential effect in the pre- and post-synaptic circuit components. We found greater discontinuity of the topographic gradient and larger azimuthal receptive field sizes in MK-801-treated animals, consistent with previous reports (22, 27, 47, 48), adding to the evidence of NMDA receptors playing a role in activity-dependent refinement of topographic maps. An important alternative possibility, however, is that rather than freezing maps in an immature crude form, NMDA receptor blockade might actively destabilize connections and promote degradation of the map, consistent with the desegregation of ocular dominance bands seen following tectal APV treatment in postmetamorphic three-eyed frogs (25).

Although NMDA receptor blockade altered some fine-scale properties of the topographic map, the coarse topographic gradient in the functional map remained relatively intact. Combined with our observation of map gradients at the earliest stages of tectal circuit formation, this emphasizes the extent to which the initial formation of the coarse gradient relies on molecular guidance cues instead of patterned activity (49-52). This stands in contrast with regenerating projections, which rely to a much greater extent on activity-dependent mechanisms (53). It would be interesting to apply our technique to see how NMDA receptor blockade alters the restoration of functional retinotopic gradients in regenerating projections.

The mRNA blastomere injection technique can be further expanded by performing injections into the two blastomeres at the two-cell stage, injecting GCaMP mRNA into one blastomere and a different colored calcium indicator (e.g., jRGECO1a) into the other. A co-expressed system would allow simultaneous visualization of the pre- and postsynaptic components of the same tectal circuit, and not just in two hemispheres of the same animal as we have done here, permitting questions about the degree of similarity between the layout of pre- and postsynaptic map gradients to be addressed in the same structure, and about whether reorganization or refinement of the topographic map in the pre- or postsynaptic component leads changes in the other.

Several factors may have impacted our ability to accurately compare receptive field properties and topographic gradients across developmental stages in young tadpoles. On one hand, the small size of the tectal neuropil at the youngest stages provides a more limited substrate in which to construct a topographic gradient. For this reason, we also repeated our measurement of local discontinuity using analysis kernels (pixel neighborhood sizes) normalized to the different tectal neuropil areas at each stage. In addition, the response strength and signal-to-noise ratios were considerably reduced when imaging presynaptic axons, especially in younger animals, which may have limited our sensitivity for detecting topographic gradients in the presynaptic dataset (*Supplementary* Fig.III.S6). Previous evidence has also shown the tadpole eye is not fully developed to resolve crisp images at these stages (54), and consequently our approach of using visually driven activity to characterize functional map organization may be limited by visual acuity of the eye, rather than fully reflecting the anatomical order of the map itself. Nonetheless, the fact that we were able to detect prominent postsynaptic azimuthal gradients in stage 42 tadpoles indicates that our assay was sufficiently sensitive to reveal information about the organization of topographic maps from the earliest stages we were able to image.

The process of circuit refinement can be thought of as a mechanism for increased wiring precision. At the single-cell level this may take the form of greater stimulus selectivity, and in the case of retinotopy, of more compact visual receptive fields to provide the network with greater visual acuity. At the level of circuit anatomy, it often refers to spatial organization of inputs, which for retinotopy means that RGC axons come to closely recapitulate the relative layout of their somata in the eye. We examined the development of receptive field sharpness as a reflection of individual tectal cell fine-tuning. Receptive field size measurements provide an assessment of functional visual acuity at the single cell level, but offer little detail about the anatomical organization of inputs to the network. For example, it is hypothetically conceivable that a network consisting of randomly distributed neurons, each having small, defined receptive fields, might represent stimulus space precisely, but such organization would be energetically inefficient with respect to wiring conservation and not conducive to the input convergence that is needed to generate smaller receptive fields in individual cells.

Therefore, we measured the degree of nearest-neighbor similarity in topographic maps with the local discontinuity measure and associated a high level of similarity with a more anatomically refined topographic map. However, the actual optimizing function used by sensory systems is yet a matter of speculation (55-57). It may therefore be relevant to inquire about additional properties such as the information content stored in the retinotopic map, and its capacity for decoding sensory information (58).

Overall, the present study provided an in-depth four-dimensional characterization of the emergence of functional retinotopic maps in the larval Xenopus retinotectal system and utilized this model to investigate the role of NMDA receptors in the activity-dependent refinement of the topographic map structure. This approach should serve as a valuable basis for future work on the mechanisms underlying functional retinotopic map formation.

Materials and Methods

Animals

All procedures were approved by the Animal Care Committee of the Montreal Neurological Institute at McGill University in accordance with Canadian Council on Animal Care guidelines.

Female albino *Xenopus laevis* frogs (RRID: XEP_Xla300) from our in-house breeding colony were injected with pregnant mare serum gonadotropin (Prospec) and human chorionic gonadotropin (Sigma-Aldrich) to induce ovulation, and eggs were collected for *in vitro* fertilization. To produce GCaMP6s transgenic tadpoles, eggs were fertilized with sperm from Xla.Tg(tubb2b:GCaMP6s)$_{NXR}$ transgenic frogs (National Xenopus Resource, RRID:NXR_0.0107). To produce tadpoles with hemilateral mosaic GCaMP6s and mCherry expression, eggs were fertilized with sperm from male albino *Xenopus laevis* frogs, then blastomere microinjection of GCaMP6s and mCherry mRNA to create bilateral hemimorphant animals was performed as previously described (59, 60). Briefly, a mixture of purified GCaMP6s (500 pg) and mCherry (250 pg) mRNA in 2 nL RNAase-free water was pressure injected into one blastomere of two-cell stage embryos using a

calibrated glass micropipette attached to a PLI-100 picoinjector (Harvard Apparatus). GCaMP and mCherry mRNA were prepared by cloning the coding sequence of GCaMP6s and mCherry into pCS2+, then linearizing plasmids with NotI and transcribing the capped mRNA of GCaMP6s and mCherry with the SP6 mMessage mMachine Kit (Ambion, Thermo Fisher). Developing animals were screened to select individuals with hemilaterally restricted mCherry expression and high levels of GCaMP fluorescence for use in calcium imaging experiments.

All tadpoles were raised in 0.1x Modified Barth's Solution with HEPES (MBSH) on a 12/12-hour light/dark cycle. For transgenic tadpoles, 0.001% PTU was added to the rearing solution to reduce pigmentation. Tadpoles of both sexes were used for all studies. Tadpoles were staged according to Nieuwkoop & Faber (30).

Drugs

For NMDAR inhibition experiments, 10 μM MK-801 (Tocris Bioscience) was added to the tadpoles' rearing solution starting from stage 39. The rearing medium was changed and fresh MK-801 was added every other day. Tadpoles remained in MK-801 until they were imaged at stage 48.

In Vivo Imaging and Visual Stimulation

Tadpoles were immobilized by immersion in 2 mM pancuronium bromide and immobilized in 1% low-melting point agarose in a custom chamber with a glass cover slip window on one side, through which the animal could view visual stimuli presented on an LED screen (Fig.III.1A). The LED display area measured 6.5cm (w) x 4cm (h). The tadpole was positioned so the eye was 2.2 cm from the screen, aligned to the center of the bottom edge of the display area. From this viewpoint, the display area spans roughly 110 degrees visual angle in azimuth and 80 degrees in elevation. Calcium fluorescence images were captured with a high-speed resonance scanner-based 2-photon microscope (Thorlabs) with piezoelectric focusing (Physik Instrumente) of a 1.0 NA 20x water immersion Nikon objective. An excitation wavelength of 910 nm was used for GCaMP6s, and emission signal was collected through a 525/50 nm bandpass filter. A #29 Wratten filter (Kodak) was installed on the LED screen to prevent

light from the display from interfering with the calcium signal. Custom MATLAB scripts based on the Psychophysics Toolbox (Brainard, 1997; Kleiner et al., 2007; RRID:SCR_002881) were used to generate the visual stimuli and synchronize stimulus presentation with image capture. Visual stimuli were presented monocularly, and calcium signal was imaged from the tectum contralateral to the stimulated eye (Fig.III.1B-C). Images (512 x 512 pixels, 0.496 μm/pixel) were collected from a single optical section at 15 Hz or 3-4 optical sections (with 1-2 flyback frames) at 6 Hz. For full neuropil volume mapping, two sequential sets of 7 optical sections (with 3 flyback frames) were collected at 3 Hz with 256 x 256 pixel resolution (0.993μm/pixel).

Receptive Field Mapping and Analysis

Processing and analyses of calcium imaging data were performed with custom scripts in MATLAB (RRID:SCR_001622) and Fiji (RRID:SCR_002285). For analyses comparing two separate recordings, images were aligned using MATLAB *imregtform()* or the *NoRMCorre* algorithm (61).

Visual field representation in the tectum was then estimated with one of two methods:

Phase mapping with drifting bars

Visual stimuli consist of repeated presentations of a single vertical or horizontal 18°-wide black bar drifting at a constant rate along the full span of the anterior-posterior or superior-inferior axis. The bar width was set as a fixed on-screen pixel width that spanned an 18° visual angle on the screen position perpendicular to the eye. In some cases involving stage 42 animals, 36°-wide bar stimuli were used to produce more robust visual responses, but these were not used for quantitative analysis. Typical stimulus-triggered response to a single drifting bar shows a near-Gaussian profile, with slow onset and decay that lasts throughout the stimulus presentation (Fig.III.1D-E). Recorded images were smoothed with a 2D Gaussian filter with $\sigma = 1$. The first differential was calculated for pixel-wise calcium traces, then the following analysis was applied: A Fourier transform (using MATLAB *fft()*) on a response trace converts the signal into a sum of sine waves of different frequencies, and the stimulus-evoked response can be extracted by evaluating the Fourier component at the frequency of

stimulus presentation (31) (Fig.III.1F). The amplitude of this component gives the strength of the peak stimulus-evoked response, and the phase corresponds to the time of the peak response, which converts to the bar position that evoked the response. A drifting bar continuously activates retinotectal neurons as it moves across the tectum, which results in a delay between the bar arriving at the optimal stimulus location and the time the peak response is observed. This response latency is corrected for by conducting pairs of trials where the stimulus bars sweep in opposite directions, and then taking the difference between the peak response phases to obtain an absolute response phase. For an experiment with an interval of t_{blank} between repeated drifting bar presentations, absolute phase φ^+ can be found by

$$\varphi^+=(\varphi_1-\varphi_2-t_{blank}) / 2$$

where φ_1 and φ_2 are the relative phases in the two opposite directions. The signal-to-noise ratio (SNR) of the response is defined as A_r/σ, where A_r is amplitude of the Fourier component at the stimulus frequency, and σ is the standard deviation of all amplitudes at frequencies above the stimulus frequency (62). This approach is justifiable because while pixels in the tectal neuropil exhibited a relatively high degree of direction selectivity on average, preferences for any given direction were homogeneously distributed across the tectum and as a whole the tectum did not strongly favor any one direction (*Supplementary* Fig.III.S1B-D).

Grid mapping with flashing bars

Vertical or horizontal 18°-wide black bars were presented randomly at one of 5 set positions along the azimuth or elevation axis (numbered 1 to 5). Each stimulus bar was flashed for 200 msec. Typical stimulus-triggered calcium signals feature a rapid (<1 s) onset to peak and a slow decay. 15 s intervals where only the background is displayed were placed between stimulus presentations, to allow the GCaMP signal to return to baseline. To extract visual field representations, the pixel-wise $\Delta F/F_0$ response to each stimulus was calculated as the peak calcium signal over 1.5 secs after the onset of the stimulus, subtracted and divided by a baseline of the average calcium signal over 3.3 secs in the blank period before the stimulus. Each pixel was then assigned an “optimal stimulus position” L as a weighted average:

$$L = \Sigma(L_i * F_i) / \Sigma F_i$$

where L_i is the bar position (1 to 5) and F_i is the $\Delta F/F_0$ response evoked by the bar at position L_i.

Comparing phase and grid maps from same animal

To evaluate the consistency between retinotopic maps extracted using the two different methods, phase values from the neuropil area (thresholded for SNR > 1) were scrambled, then both phase map and grid map position values were normalized to the mean of the scrambled phase value. We then compared phase vs grid and phase vs scrambled position values by averaging the absolute differences per pixel over the neuropil.

Computing cell body grid maps

Cell body ROIs were automatically segmented using Cellpose (63) then manually processed to remove non-neuronal elements such as melanophores and radial glia somata. $\Delta F/F_0$ responses were averaged within each ROI, then optimal stimulus position for each ROI was calculated in same way as pixel-wise optimal stimulus positions.

Global topographic gradient

The “global topographic gradient” was calculated from the phase maps within a volume as follows: For each pixel within the neuropil area with SNR > 1.5, a “local gradient vector” was calculated as the vector sum of differences in topographic position (phase) from adjacent pixels in the x, y, and z directions, using the MATLAB function *gradient()*. All local gradient vectors within the volume were then summed and normalized to acquire the global topographic gradient.

Discontinuity

“Local discontinuity” was defined for a given pixel as the mean difference in receptive field position (phase) of the pixel to all neighboring pixels within a 15-pixel (7.44 μm) radius after applying a SNR > 0.8 threshold. Local discontinuity was evaluated at all pixels in the neuropil with SNR > 0.8 and with more than 30% of the pixels in its

neighborhood passing SNR > 0.8. The pixel-wise local discontinuity values were then averaged over the neuropil to obtain the mean discontinuity value for a given animal.

To account for the change in tectal size when comparing discontinuity in the same animal at different developmental stages, a normalized discontinuity measure was calculated by downscaling the radius of the neighborhood evaluated for each pixel. The scaled pixel radius is 15 * the square root of the ratio of neuropil area at the given stage compared to stage 48, rounded to the nearest integer.

Receptive field sharpness

Maps of tectal receptive fields were derived by grid mapping. “Receptive field sharpness” was defined as the average $\Delta F/F_0$ response to the 2 stimulus positions closest to the optimal stimulus position (grid) divided by the average response to the remaining stimulus positions in the periphery. Receptive field sharpness was evaluated for cell body ROIs using average $\Delta F/F_0$ responses within the ROI. Only cell bodies with maximum stimulus response $\Delta F/F_0 > 2$ and optimal stimulus positions falling between the 3 central stimulus positions were evaluated. Animals with less than 30 cell bodies fitting the evaluation criteria were excluded.

Statistical Analysis

Plotted data are presented as mean ± SEM. Statistical tests, as indicated in the figure legends, were performed using Prism 8.0 (GraphPad software, RRID:SCR_002798).

Software Accessibility

MATLAB scripts for data analysis in this paper can be found at www.github.com/RuthazerLab/XenMap

Data Availability

Statistical data used for this paper are included in *Supplementary* Data.III.S1. Additional data generated in this study will be made available upon reasonable request.

Acknowledgments

We would like to thank Dr. Amir Shmuel for providing example MATLAB code for calculating phase maps.

This work was funded by a Foundation Grant from the Canadian Institutes of Health Research (FDN-143238) and a Chaire de recherche from the Fonds de recherche du Québec – Santé (31036) to ER, NSERC Canada Graduate Scholarship – Master's and McGill University Integrated Program in Neuroscience Studentships to VJL.

References

1. U. C. Drager, D. H. Hubel, Topography of visual and somatosensory projections to mouse superior colliculus. *Journal of Neurophysiology* **39**, 91-101 (1976).
2. R. B. Tootell, E. Switkes, M. S. Silverman, S. L. Hamilton, Functional anatomy of macaque striate cortex. II. Retinotopic organization. *Journal of Neuroscience* **8**, 1531-1568 (1988).
3. A. Muto, M. Ohkura, G. Abe, J. Nakai, K. Kawakami, Real-Time Visualization of Neuronal Activity during Perception. *Current Biology* **23**, 307-311 (2013).
4. C. M. Niell, S. J. Smith, Functional Imaging Reveals Rapid Development of Visual Response Properties in the Zebrafish Tectum. *Neuron* **45**, 941-951 (2005).
5. M. Constantine-Paton, H. T. Cline, E. Debski, Patterned Activity, Synaptic Convergence, and the NMDA Receptor in Developing Visual Pathways. *Annual Review of Neuroscience* **13**, 129-154 (1990).
6. T. McLaughlin, D. D. O'Leary, Molecular gradients and development of retinotopic maps. *Annu. Rev. Neurosci.* **28**, 327-355 (2005).
7. J. Cang, L. Wang, M. P. Stryker, D. A. Feldheim, Roles of ephrin-as and structured activity in the development of functional maps in the superior colliculus. *Journal of Neuroscience* **28**, 11015-11023 (2008).

8. E. Kutsarova, M. Munz, E. S. Ruthazer, Rules for Shaping Neural Connections in the Developing Brain. *Front Neural Circuits* **10**, 111-111 (2017).
9. R. O. Wong, Retinal waves and visual system development. *Annual review of neuroscience* **22**, 29-47 (1999).
10. T. McLaughlin, C. L. Torborg, M. B. Feller, D. D. M. O'Leary, Retinotopic Map Refinement Requires Spontaneous Retinal Waves during a Brief Critical Period of Development. *Neuron* **40**, 1147-1160 (2003).
11. S. I. Firth, C.-T. Wang, M. B. Feller, Retinal waves: mechanisms and function in visual system development. *Cell Calcium* **37**, 425-432 (2005).
12. K. G. Pratt, M. Hiramoto, H. T. Cline, An Evolutionarily Conserved Mechanism for Activity-Dependent Visual Circuit Development. *Front Neural Circuits* **10**, 79-79 (2016).
13. B. K. Kay, H. B. Peng, *Xenopus laevis: practical uses in cell and molecular biology* (Academic press, 1992).
14. C. R. Exner, H. R. Willsey, Xenopus leads the way: Frogs as a pioneering model to understand the human brain. *genesis* **59**, e23405 (2021).
15. K. Straznicky, R. Gaze, The growth of the retina in Xenopus laevis: an autoradiographic study. *Development* **26**, 67-79 (1971).
16. K. Straznicky, R. Gaze, The development of the tectum in Xenopus laevis: an autoradiographic study. *Development* **28**, 87-115 (1972).
17. D. S. Sakaguchi, R. K. Murphey, Map formation in the developing Xenopus retinotectal system: an examination of ganglion cell terminal arborizations. *Journal of Neuroscience* **5**, 3228-3245 (1985).
18. R. M. Gaze, M. Keating, S. Chung, The evolution of the retinotectal map during development in Xenopus. *Proceedings of the Royal Society of London. Series B. Biological Sciences* **185**, 301-330 (1974).
19. C. E. Holt, W. A. Harris, Order in the initial retinotectal map in Xenopus: a new technique for labelling growing nerve fibres. *Nature* **301**, 150-152 (1983).
20. L. I. Zhang, H. W. Tao, C. E. Holt, W. A. Harris, M.-m. Poo, A critical window for cooperation and competition among developing retinotectal synapses. *Nature* **395**, 37-44 (1998).

21. I. Rajan, S. Witte, H. T. Cline, NMDA receptor activity stabilizes presynaptic retinotectal axons and postsynaptic optic tectal cell dendritesin vivo. *Journal of Neurobiology* **38**, 357-368 (1999).
22. W. Dong *et al.*, Visual avoidance in Xenopus tadpoles is correlated with the maturation of visual responses in the optic tectum. *Journal of neurophysiology* **101**, 803-815 (2009).
23. M. Munz *et al.*, Rapid Hebbian axonal remodeling mediated by visual stimulation. *Science* **344**, 904-909 (2014).
24. M. Hiramoto, H. T. Cline, NMDARs Translate Sequential Temporal Information into Spatial Maps. *iScience* **23**, 101130-101130 (2020).
25. H. T. Cline, E. A. Debski, M. Constantine-Paton, N-methyl-D-aspartate receptor antagonist desegregates eye-specific stripes. *Proceedings of the National Academy of Sciences* **84**, 4342-4345 (1987).
26. E. S. Ruthazer, C. J. Akerman, H. T. Cline, Control of Axon Branch Dynamics by Correlated Activity in Vivo. *Science* **301**, 66-70 (2003).
27. H. T. Cline, M. Constantine-Paton, NMDA receptor antagonists disrupt the retinotectal topographic map. *Neuron* **3**, 413-426 (1989).
28. D. K. Simon, G. T. Prusky, D. O'leary, M. Constantine-Paton, N-methyl-D-aspartate receptor antagonists disrupt the formation of a mammalian neural map. *Proceedings of the National Academy of Sciences* **89**, 10593-10597 (1992).
29. T.-W. Chen *et al.*, Ultrasensitive fluorescent proteins for imaging neuronal activity. *Nature* **499**, 295-300 (2013).
30. P. Nieuwkoop, J. Faber, Normal Table of Xenopus laevis (Daudin) Garland Publishing. *New York* **252** (1994).
31. V. A. Kalatsky, M. P. Stryker, New Paradigm for Optical Imaging. *Neuron* **38**, 529-545 (2003).
32. D. K. Simon, D. D. O'Leary, Development of topographic order in the mammalian retinocollicular projection. *Journal of Neuroscience* **12**, 1212-1232 (1992).
33. L. M. Chalupa, C. J. Snider, Topographic specificity in the retinocollicular projection of the developing ferret: An anterograde tracing study. *The Journal of Comparative Neurology* **392**, 35-47 (1998).

34. W. T. Wong, J. R. Sanes, R. O. Wong, Developmentally regulated spontaneous activity in the embryonic chick retina. *Journal of Neuroscience* **18**, 8839-8852 (1998).
35. J. B. Ackman, T. J. Burbridge, M. C. Crair, Retinal waves coordinate patterned activity throughout the developing visual system. *Nature* **490**, 219-225 (2012).
36. R. L. Vislay-Meltzer, A. R. Kampff, F. Engert, Spatiotemporal Specificity of Neuronal Activity Directs the Modification of Receptive Fields in the Developing Retinotectal System. *Neuron* **50**, 101-114 (2006).
37. J. A. Demas, H. Payne, H. T. Cline, Vision drives correlated activity without patterned spontaneous activity in developing Xenopus retina. *Developmental neurobiology* **72**, 537-546 (2012).
38. M. S. Grubb, F. M. Rossi, J.-P. Changeux, I. D. Thompson, Abnormal Functional Organization in the Dorsal Lateral Geniculate Nucleus of Mice Lacking the β2 Subunit of the Nicotinic Acetylcholine Receptor. *Neuron* **40**, 1161-1172 (2003).
39. T. D. Mrsic-Flogel *et al.*, Altered map of visual space in the superior colliculus of mice lacking early retinal waves. *Journal of Neuroscience* **25**, 6921-6928 (2005).
40. A. R. Chandrasekaran, R. D. Shah, M. C. Crair, Developmental homeostasis of mouse retinocollicular synapses. *Journal of Neuroscience* **27**, 1746-1755 (2007).
41. O. S. Dhande *et al.*, Development of single retinofugal axon arbors in normal and β2 knock-out mice. *Journal of Neuroscience* **31**, 3384-3399 (2011).
42. H. T. Cline, M. Constantine-Paton, NMDA receptor agonist and antagonists alter retinal ganglion cell arbor structure in the developing frog retinotectal projection. *Journal of Neuroscience* **10**, 1197-1216 (1990).
43. S. S. Easter, Jr., C. A. Stuermer, An evaluation of the hypothesis of shifting terminals in goldfish optic tectum. *Journal of Neuroscience* **4**, 1052-1063 (1984).
44. T. A. Reh, M. Constantine-Paton, Retinal ganglion cell terminals change their projection sites during larval development of Rana pipiens. *Journal of Neuroscience* **4**, 442-457 (1984).
45. B. Alsina, T. Vu, S. Cohen-Cory, Visualizing synapse formation in arborizing optic axons in vivo: dynamics and modulation by BDNF. *Nat Neurosci* **4**, 1093-1101 (2001).

46. T. N. Rahman, M. Munz, E. Kutsarova, O. M. Bilash, E. S. Ruthazer, Stentian structural plasticity in the developing visual system. *Proc Natl Acad Sci U S A* **117**, 10636-10638 (2020).
47. J. T. Schmidt, M. Buzzard, R. Borress, S. Dhillon, MK801 increases retinotectal arbor size in developing zebrafish without affecting kinetics of branch elimination and addition. *Journal of Neurobiology* **42**, 303-314 (2000).
48. K. A. Razak, L. Huang, S. L. Pallas, NMDA receptor blockade in the superior colliculus increases receptive field size without altering velocity and size tuning. *Journal of neurophysiology* **90**, 110-119 (2003).
49. U. Drescher *et al.*, In vitro guidance of retinal ganglion cell axons by RAGS, a 25 kDa tectal protein related to ligands for Eph receptor tyrosine kinases. *Cell* **82**, 359-370 (1995).
50. C. Brennan *et al.*, Two Eph receptor tyrosine kinase ligands control axon growth and may be involved in the creation of the retinotectal map in the zebrafish. *Development* **124**, 655-664 (1997).
51. D. A. Feldheim, D. D. M. O'Leary, Visual map development: bidirectional signaling, bifunctional guidance molecules, and competition. *Cold Spring Harb Perspect Biol* **2**, a001768-a001768 (2010).
52. V. Higenell, S. M. Han, D. A. Feldheim, F. Scalia, E. S. Ruthazer, Expression patterns of Ephs and ephrins throughout retinotectal development in Xenopus laevis. *Developmental neurobiology* **72**, 547-563 (2012).
53. J. T. Schmidt, D. L. Edwards, Activity sharpens the map during the regeneration of the retinotectal projection in goldfish. *Brain Research* **269**, 29-39 (1983).
54. B. A. Richards, J. J. van Rheede, C. J. Akerman, Visuospatial information in the retinotectal system of xenopus before correct image formation by the developing eye. *Developmental Neurobiology* **72**, 507-519 (2012).
55. G. J. Goodhill, T. J. Sejnowski (1996) Quantifying neighbourhood preservation in topographic mappings. in *Proceedings of the 3rd Joint Symposium on Neural Computation* (Citeseer), pp 61-82.
56. M. Kaschube, Neural maps versus salt-and-pepper organization in visual cortex. *Current Opinion in Neurobiology* **24**, 95-102 (2014).

57. S. P. Wilson, J. A. Bednar, What, if anything, are topological maps for? *Developmental Neurobiology* **75**, 667-681 (2015).
58. L. Avitan, Z. Pujic, N. J. Hughes, E. K. Scott, G. J. Goodhill, Limitations of Neural Map Topography for Decoding Spatial Information. *Journal of Neuroscience* **36**, 5385-5396 (2016).
59. P. Kesner, A. Schohl, E. C. Warren, F. Ma, E. S. Ruthazer, Postsynaptic and Presynaptic NMDARs Have Distinct Roles in Visual Circuit Development. *Cell Reports* **32**, 107955 (2020).
60. N. J. Benfey, V. J. Li, A. Schohl, E. S. Ruthazer, Sodium-Calcium Exchanger Mediates Sensory-Evoked Glial Calcium Transients in the Developing Retinotectal System. *bioRxiv* (2020).
61. E. A. Pnevmatikakis, A. Giovannucci, NoRMCorre: An online algorithm for piecewise rigid motion correction of calcium imaging data. *Journal of Neuroscience Methods* **291**, 83-94 (2017).
62. J. Warnking *et al.*, Retinotopical mapping of visual areas by fMRI using a fast cortical flattening algorithm. *NeuroImage* **11**, S646 (2000).
63. C. Stringer, T. Wang, M. Michaelos, M. Pachitariu, Cellpose: a generalist algorithm for cellular segmentation. *Nature Methods* **18**, 100-106 (2021).

Figures

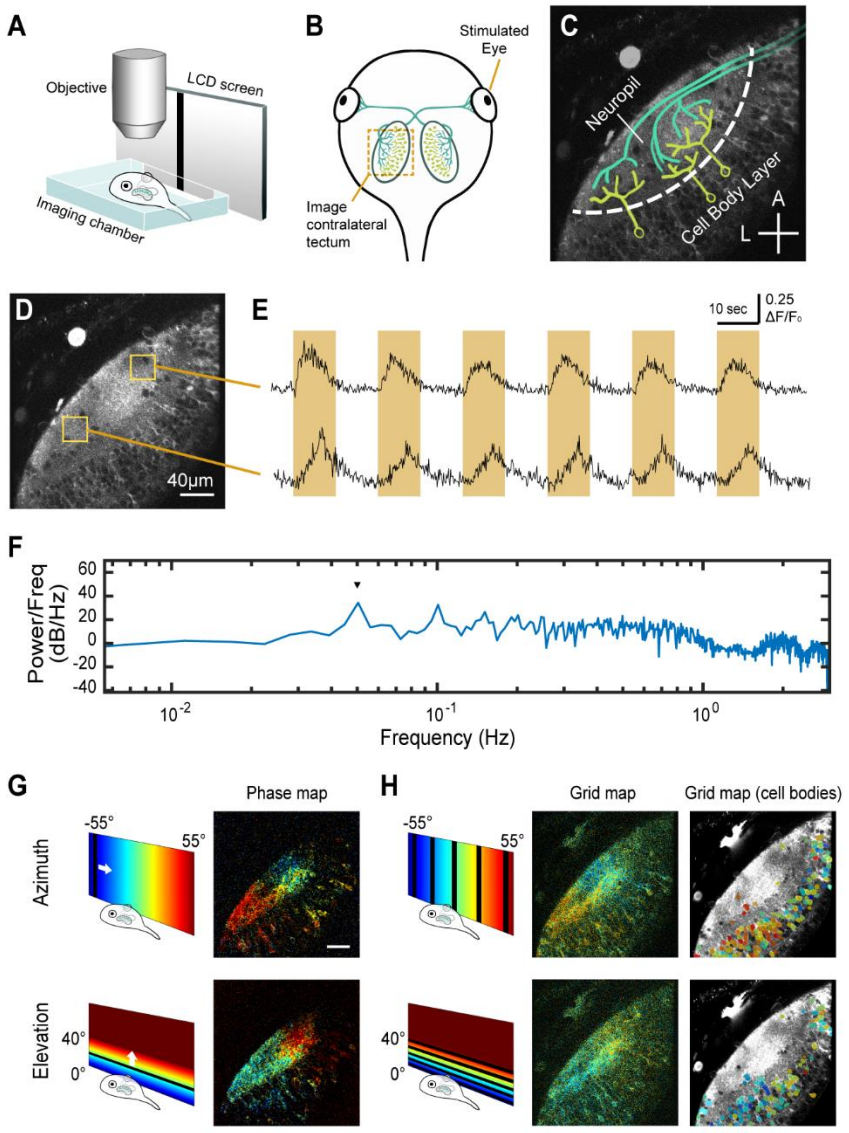

Figure III.1: Experiment setup for visualizing retinotopic maps in the tadpole tectum.

(A) Schematic of imaging setup. The tadpole was immobilized and embedded in agarose in an imaging chamber under the microscope, with one eye viewing visual stimuli on an LCD screen through a glass slide on the side of the imaging chamber.

(B) Schematic of the tadpole retinotectal system. RGC axons innervate the contralateral tectum.

(C) Imaging field in the tadpole tectum, corresponding to the region indicated in B, showing discrete neuropil and cell body layers. RGC axons (green), postsynaptic tectal neurons (yellow). Cross bars = 40 μm, A = anterior, L = lateral.

(D) Two-photon optical section in GCaMP6s transgenic tadpole tectum.

(E) Mean GCaMP6s $\Delta F/F_0$ plots from the anterior and posterior tectal ROIs in D, showing responses to an anterior to posterior drifting bar stimulus. Each cycle consisted of a bar slowly traversing the monitor once over 10 s, followed by 10 s blank, thus repeating every 20 s. Orange highlights indicate when the drifting bar was visible. Signal in the anterior ROI peaked at an earlier time per sweep (phase) than in the posterior ROI.

(F) Fourier power spectrum of the first differential of a calcium response to 10 repeats of the drifting bar stimulus measured over the neuropil (single optical section, 6 Hz acquisition rate). A peak in power (arrowhead) occurs at the stimulus frequency (0.05 Hz).

(G) Examples of retinotopic maps extracted from a stage 48 transgenic animal, color-coded by phase of response to drifting bar stimuli. Pixel brightness in phase maps indicates signal-to-noise ratio (SNR).

(H) “Grid maps” were obtained by flashing a bar at 5 locations across azimuth or elevation. Middle: Pixel-wise grid maps obtained from the same animal in G, color-coded by optimal stimulus position. Pixel brightness reflects the maximal evoked response ($\Delta F/F_0$) divided by mean of evoked responses to the dark bar stimuli. Right: Cell body grid maps from the same animal. Cell body ROIs are color coded by optimal stimulus position and overlaid on a time averaged image of the tectum. Scale bars = 40 μm.

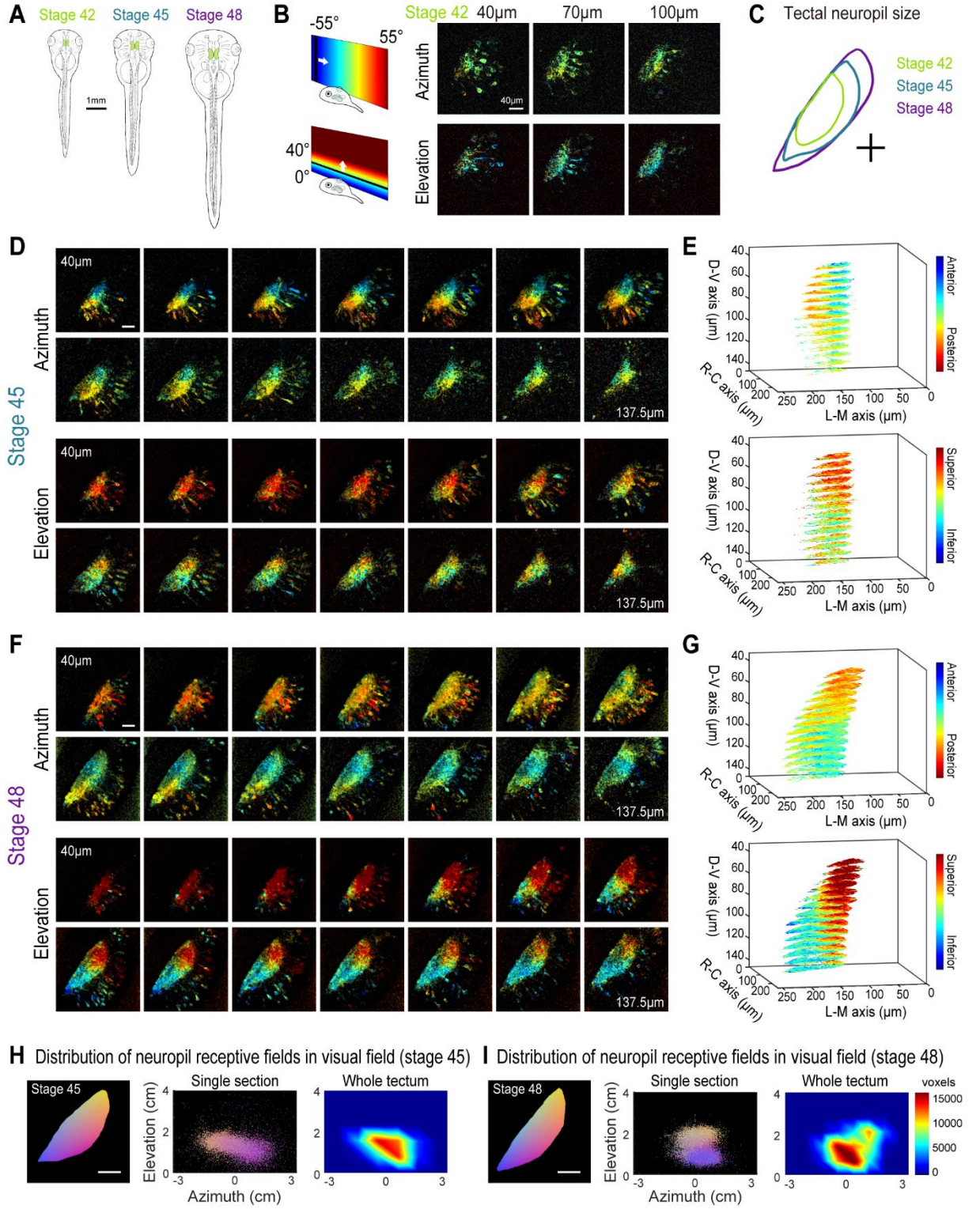

Figure III.2: Retinotopic map over different developmental stages.

(A) Sketches of *X. laevis* tadpole at stage 42, 45 and 48.

(B) Phase maps extracted from a stage 42 GCaMP6s-expressing transgenic tadpole at 3 depths.

(C) Comparison of tectal neuropil outlines, traced from the same animal at stage 42, 45 and 48 (depth ~100 μm from top of tectum).

(D) Phase maps extracted from the same tadpole at stage 45. For both azimuth and elevation, a stack of 14 optical sections is shown (40 μm to 135.75 μm from the top surface of the tectum, 7.5 μm between optical sections). Pixel intensities indicate SNR.

(E) 3D volume rendering of phase maps from D.

(F) Phase maps extracted from the same tadpole at stage 48. Stack of 14 optical sections.

(G) Phase maps from F rendered as a 3D volume. In E and G, only pixels in the neuropil region with SNR > 1.5 are shown.

(H, I) Tectal neuropil positions from an optical section at 100 μm depth (left) mapped onto the stimulus display area (6.5 x 4 cm) (middle) for the tadpole at (H) stage 45 and (I) stage 48. Colors represent tectal neuropil coordinates (left, middle). Density plots (right) show distribution of neuropil receptive fields from the whole tectum mapped onto the stimulus display area (summed from 14 optical sections, 7.5 μm between slices). Scale bars: (A) 1mm, (B-I) 40 μm.

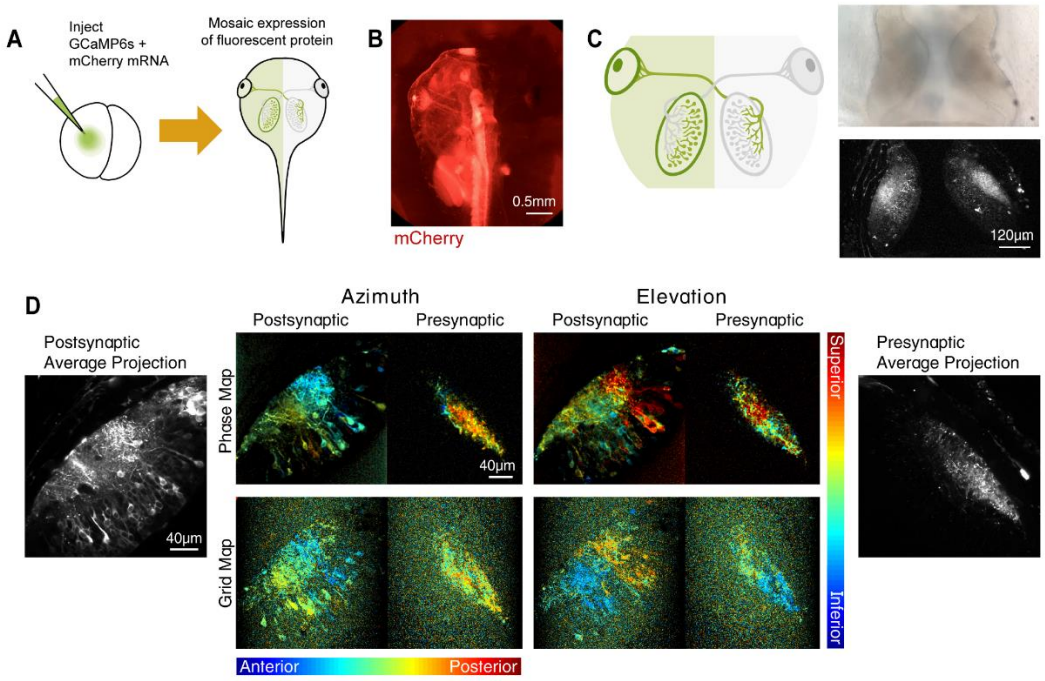

Figure III.3: GCaMP mosaic post- and presynaptic expression in tectum.
(A) Schematic of mRNA injection of 2-cell stage embryos. Injecting GCaMP6s and mCherry mRNA into one blastomere of 2-cell stage tadpole embryos results in mosaic expression of fluorescent protein restricted to one half of the body.

(B) Epifluorescence image of mCherry expression restricted to left half of the tadpole. mCherry was used to confirm half-animal mosaic expression of fluorescent proteins.

(C) Schematic showing restriction of GCaMP expression to post- and presynaptic compartments in the left and right hemispheres respectively. Transmitted light image (top) and 2-photon optical section (bottom) of post- and presynaptic GCaMP expression in the two tectal hemispheres.

(D) Phase maps (top row) and grid maps (bottom row) extracted from the left and right tectal hemispheres in the same GCaMP6s mRNA hemimosaic animal. For phase maps, pixel brightness indicates SNR. For grid maps, pixel brightness reflects the maximal evoked response ($\Delta F/F_0$) divided by mean of all evoked responses. Time averaged images of post- and presynaptic GCaMP expression are shown in the far left and right panels.

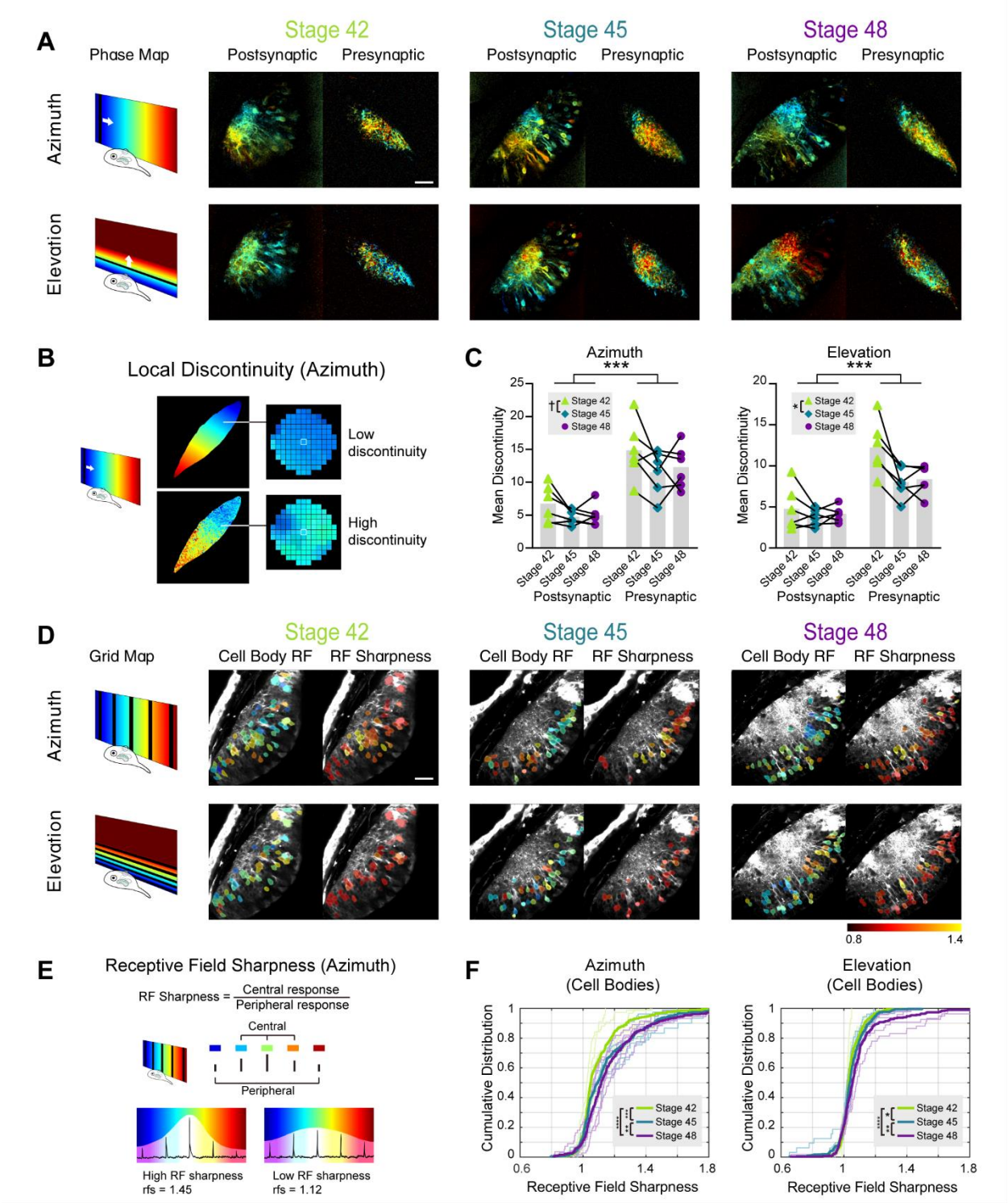

Figure III.4: Longitudinal imaging of post- and presynaptic topographic maps over development

(A) Post- and presynaptic phase maps extracted from the same GCaMP6s mRNA

hemimosaic tadpole at stages 42, 45 and 48.

(B) Local discontinuity is a measure of map smoothness. Local discontinuity for a pixel is low when the pixel is surrounded by neighboring pixels with similar phase values, and high when neighboring pixels display more difference in phase. A low local discontinuity value suggests a smooth map gradient.

(C) Mean discontinuity in tadpoles at stages 42, 45 and 48. Each data point is the mean local discontinuity for the neuropil in one animal from a single optical section approximately 100 μm below the top of the tectum. Linked data points are from the same animal. (n=6) Two-way mixed measures ANOVA for stage vs pre/post compartment showed a significant main effect for compartment in both the azimuth and elevation axes. The main effect for stages was significant in the elevation axis and trended towards significance in the azimuth axis. Azimuth: $F_{compartment}$ (1, 10) = 34.15, ***p = 0.0002; F_{stages} (1.394, 13.94) = 4.059 with Greenhouse-Geisser correction, †p = 0.0529. Elevation: $F_{compartment}$ (1, 10) = 38.22, ***p = 0.0001; F_{stages} (1.146, 11.46) = 7.537 with Greenhouse-Geisser correction, *p = 0.0160. Post-hoc Tukey tests showed significant differences between stage 42 and 45 in both azimuth and elevation axes, azimuth q(11) = 4.723, *p = 0.0167; elevation q(11) = 4.613, *p = 0.0191.

(D) Postsynaptic cell body grid maps and cell body receptive field sharpness at stage 42, 45 and 48, from the same animal as (A). Cell body ROIs are color-coded for optimal stimulus position (left) or RF sharpness (right) and overlaid on an averaged postsynaptic GCaMP6s fluorescence image of the tectum.

(E) Receptive field sharpness is an approximate measure for receptive field size. Receptive field sharpness for a pixel is low when the pixel gives similar responses to the 5 stimulus positions in grid mapping, and high when the pixel exhibits a preference for one stimulus position. A higher receptive field sharpness value suggests a more compact receptive field.

(F) Cumulative distribution of cell body RF sharpness at stages 42, 45 and 48. Thin lines show the cumulative distributions of tectal cell RF sharpness values from individual animals at each stage. Thick lines show the cumulative distribution of the pooled RF

values for each stage (azimuth: stage 42 n_{cells} = 337, stage 45 n_{cells} = 352, stage 48 n_{cells} = 331; elevation: stage 42 n_{cells} = 337, stage 45 n_{cells} = 351, stage 48 n_{cells} = 301). Bonferroni corrected pairwise Kolmogorov-Smirnov tests were significant between the pooled results for all stages for both azimuth and elevation. Azimuth stage 42 vs 45 ***p = 8.92×10^{-4}, 45 vs 48 **p = 0.0083; 42 vs 48 ****p = 1.07×10^{-9}; Elevation stage 42 vs 45 *p=0.049; stage 45 vs 48 **p = 0.0085; stage 42 vs 48 ****p = 2.49×10^{-6})

Scale bars = 40 μm.

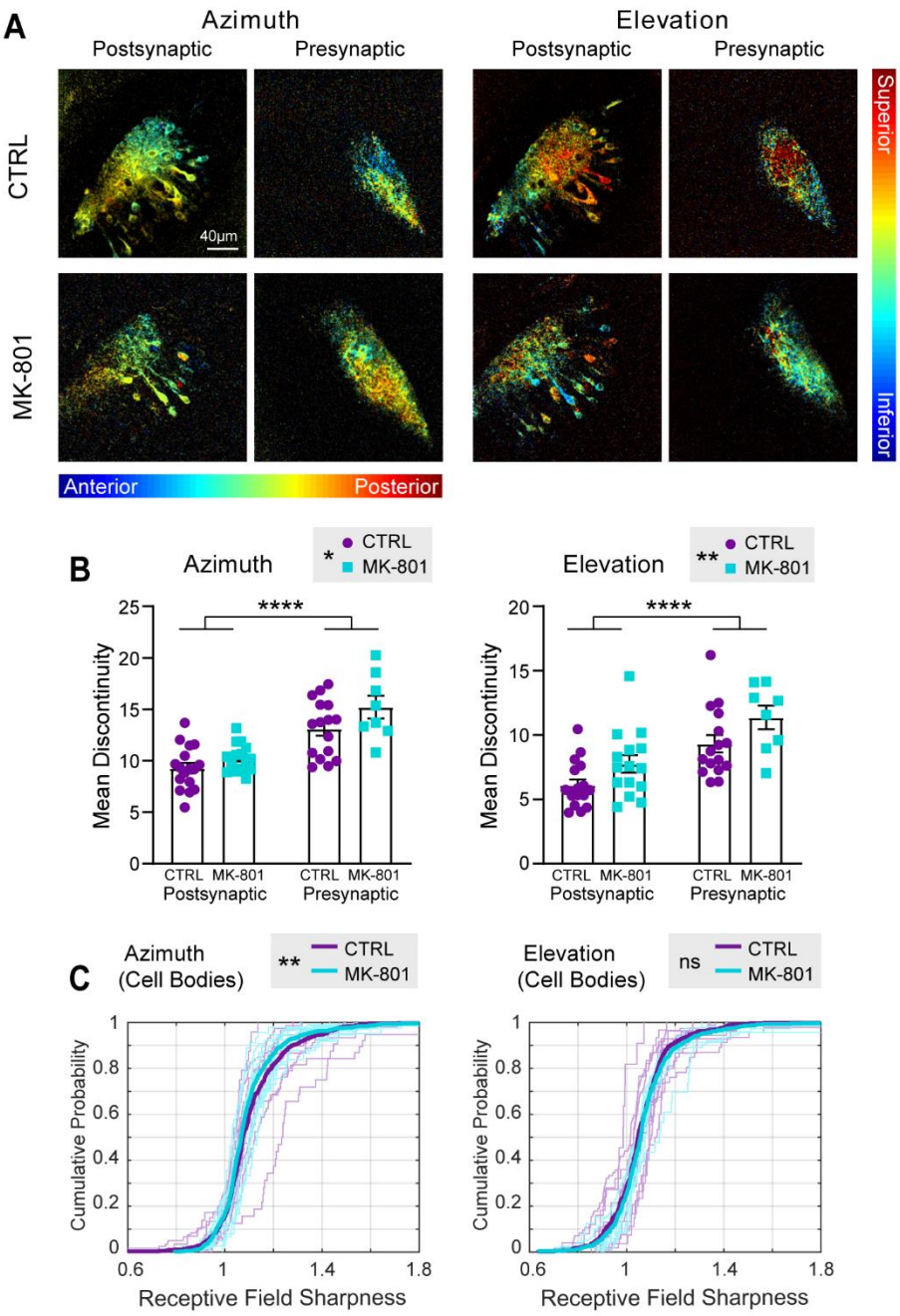

Figure III.5: GCaMP expression in post- and presynaptic compartments and effects of NMDAR blockade on topographic map development.

(A) Examples of retinotopic phase maps from stage 48 animals. Starting at stage 39, animals were reared in either control medium (top) or in medium containing MK-801 (10 μM, bottom).

(B) Mean discontinuity in control vs. MK-801-reared tadpoles, presynaptic vs postsynaptic compartments. Two-way independent measures ANOVA for drug vs compartment shows significant main effects for both drug and compartment, for both the azimuth and elevation axes. (Postsynaptic: CTRL n = 17, MK-801 n = 14; Presynaptic: CTRL n = 16, MK-801 n = 8.) Azimuth: $F_{compartment}$ (1, 51) = 43.94, ****p<0.0001; F_{drug} (1,51) = 5.618, *p=0.0216; Elevation: $F_{compartment}$ (1, 51) =24.29, ****p<0.0001; F_{drug} (1,51) =7.822, **p=0.0073.

(C) Receptive field sharpness in tectal cell bodies of control vs. MK-801-reared animals. In each plot, thin lines show the cumulative distribution of tectal cell RF sharpness values from individual CTRL and MK-801-reared animals (azimuth: CTRL n = 8, MK-801 n = 10; elevation: CTRL n = 6, MK-801 n=7). Thick lines show the cumulative distribution of the pooled RF values for each group (azimuth CTRL n_{cells}=552, MK-801 n_{cells}=594; elevation CTRL n_{cells}=418, MK-801 n_{cells} =518). **p = 0.0016 for azimuth, n.s. for elevation, Kolmogorov-Smirnov test.

Supplementary Information

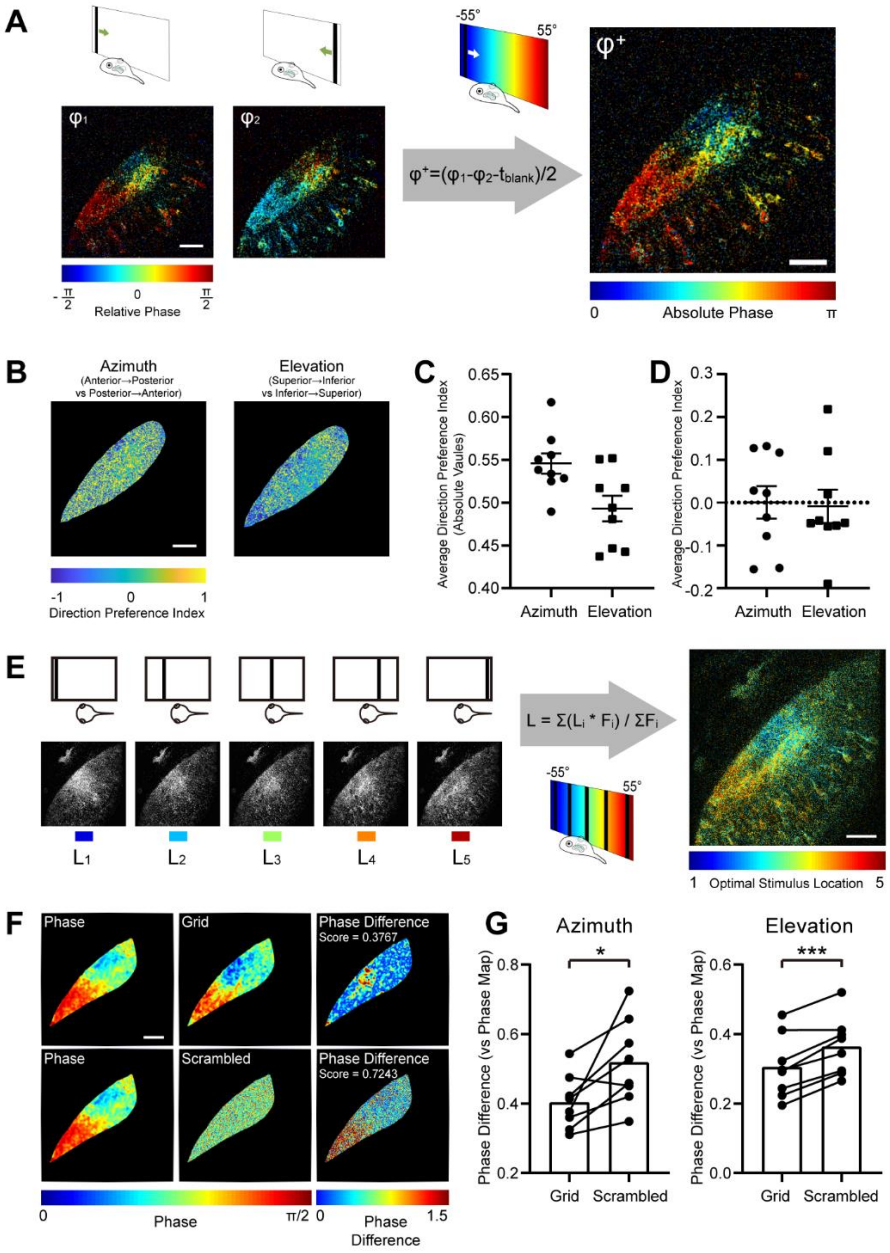

Figure III.S1. Tectal response to positioned stimuli and extraction of the retinotopic map.

(A) Calculating phase maps from responses to drifting bar stimuli (azimuth). Absolute phase (φ_+) was calculated by taking the difference of phase maps extracted from opposite direction drifting bars (φ_1 and φ_2). t_{blank} represents the fixed interval between each bar sweep.

(B) Pixelwise direction preference index values in an example animal. Direction preference index is calculated as the difference between the Fourier power at the stimulation frequency for the responses evoked by opposite direction drifting bars, divided by their sum. While each pixel shows a preference for one of the two directions, pixel-wise direction preference is evenly distributed throughout the tectal neuropil.

(C) Absolute values of pixelwise direction preference index averaged over the tectal neuropil (n = 9 transgenic animals).

(D) Pixelwise direction preference index averaged over the tectal neuropil. The average direction preference indices do not significantly differ from 0 for either azimuth or elevation, indicating no overall direction preference in the neuropil (n = 9 transgenic animals, n.s. by one-sample t-test).

(E) Calculating grid maps from average tectal response to each stimulus position. Each pixel is assigned an “optimal stimulus position” as a number between 1 to 5 based on the pixel’s $\Delta F/F_0$ responses to all 5 stimulus positions, which gives an estimate of the location of the pixel’s receptive field center.

(F) Comparing phase and grid maps extracted from the same animal. A Gaussian filter with $\sigma = 3$ was applied to both the phase and grid maps, optimal stimulus position values in grid maps were converted to equivalent phase values, the two maps were aligned based on time average images, then differences between phase values in the two maps were calculated for each pixel in the neuropil and averaged to obtain a phase difference score. This score was compared to the phase difference score for the phase map compared to a scrambled version of the phase map, in which all phase values in the neuropil region were randomly shuffled.

(G) Phase difference score between phase maps, grid maps and scrambled phase maps. The phase difference score comparing phase and grid maps was significantly smaller than for phase and scrambled phase in both azimuth and elevation maps (n = 8 transgenic animals, paired t-tests, azimuth $t(7) = 2.968$, *$p = 0.021$; elevation $t(7) = 5.947$, ***$p = 0.0006$).

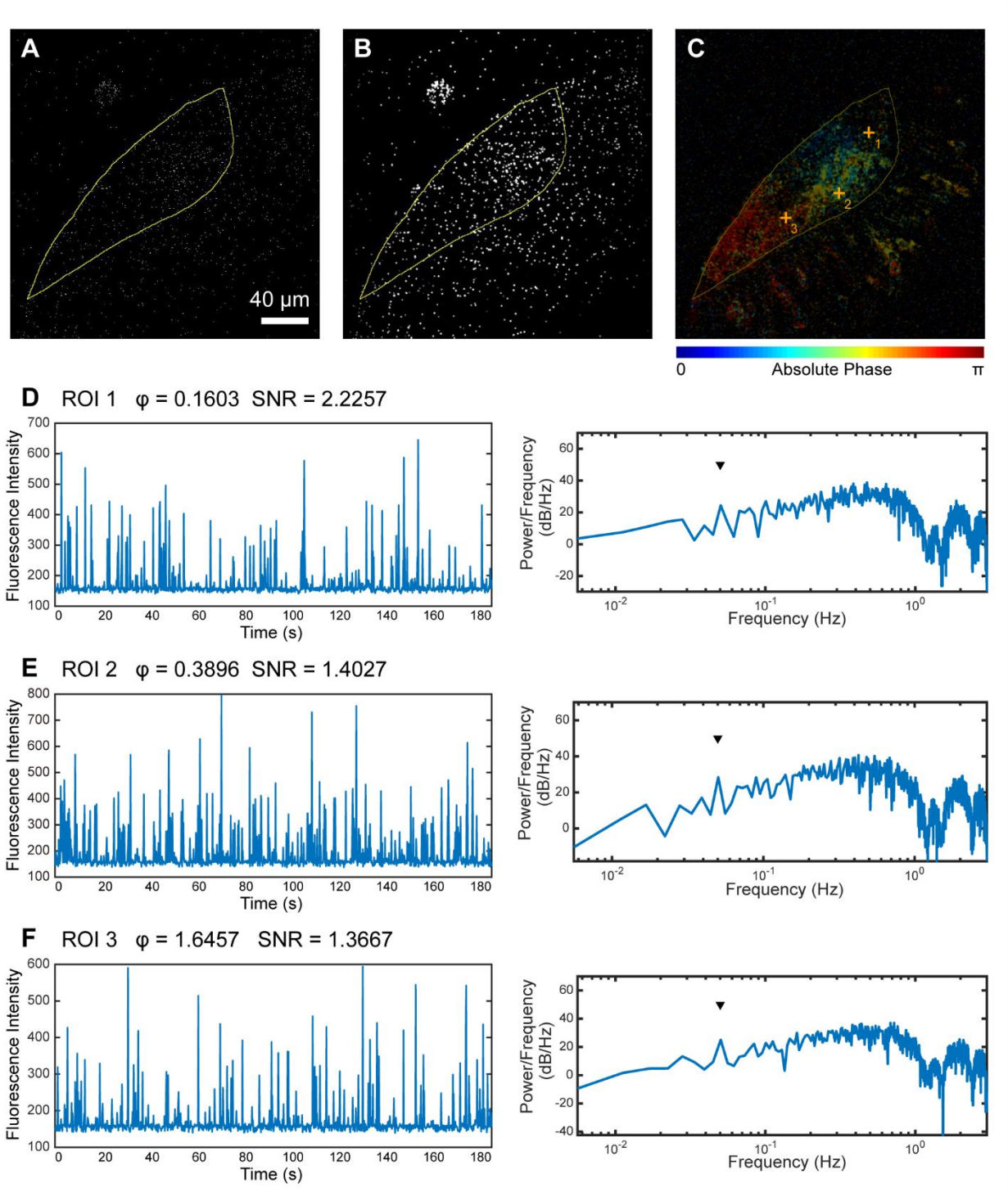

Figure III.S2. Pixel-wise analysis for phase mapping

(A) Single frame of raw calcium signal from a single 2-photon optical plane in a 3D volume in a GCaMP6s transgenic tadpole imaged at 6 Hz, responding to an anterior-to-posterior drifting bar (same animal as Fig.III.1).

(B) Frame in (A) after application of a Gaussian filter with σ = 1.

(C) Absolute phase map color coded for response positions in azimuth. Pixel ROIs labelled for 3 sites.

(D) Raw calcium trace and Fourier power spectrum of its first differential at pixel ROI #1. The relative phase at the stimulus frequency is 0.1603.

(E) Raw calcium trace and Fourier power spectrum of its first differential at pixel ROI #2. The relative phase at the stimulus frequency is 0.3896.

(F) Raw calcium trace and Fourier power spectrum of its first differential at pixel ROI #3. The relative phase at the stimulus frequency is 1.6457.

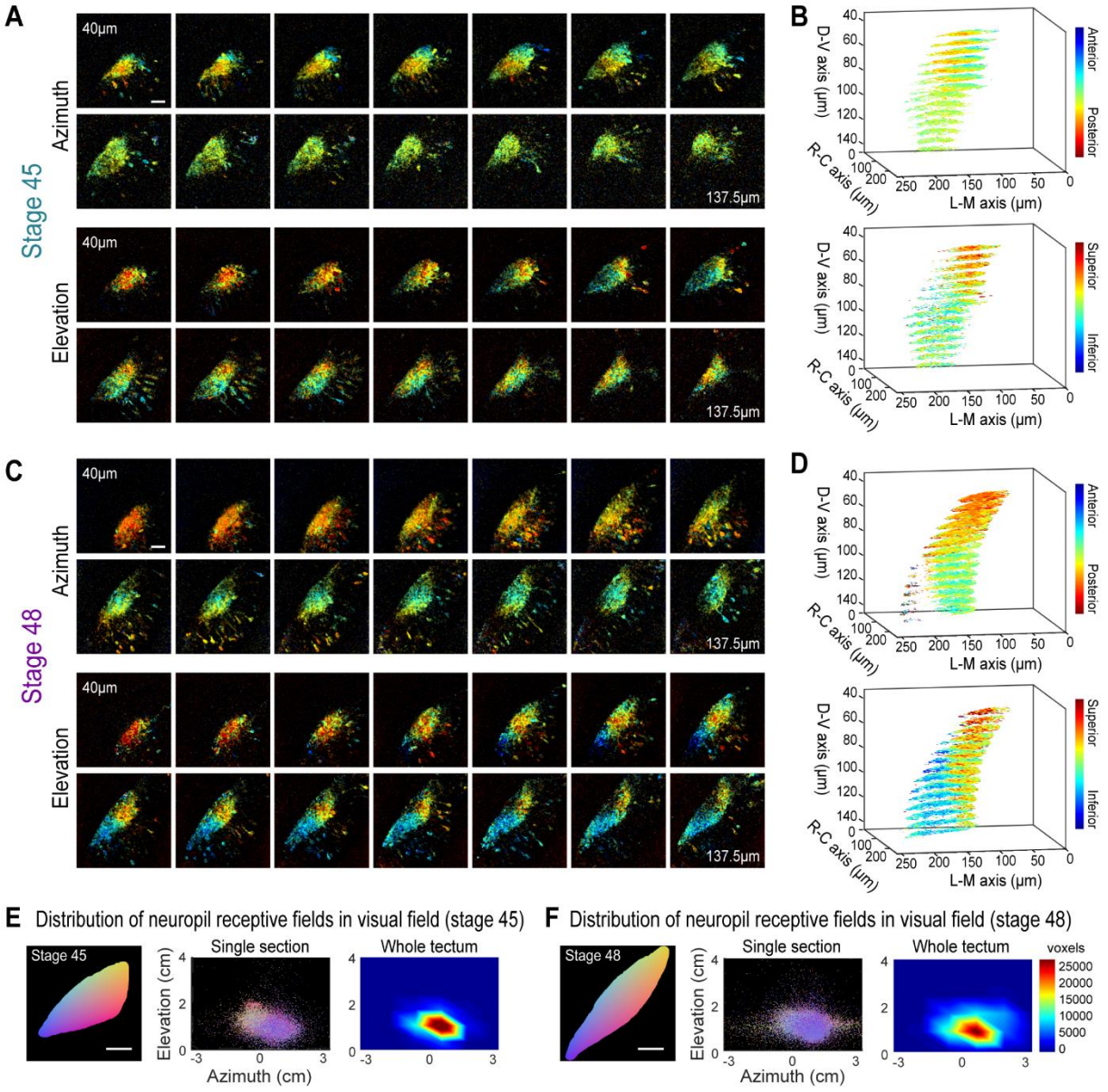

Figure III.S3. Retinotopic map in a transgenic tadpole (tadpole #2) at stage 45 and stage 48.

(A) Phase maps extracted from the tadpole at stage 45. Stack of 14 optical sections with 7.5 μm spacing between slices.

(B) Phase maps in A rendered as 3D volume.

(C) Phase maps extracted from the same tadpole at stage 48. Stack of 14 optical sections with 7.5 μm between slices.

(D) Phase maps in C rendered as 3D volume. In B and D, only pixels in the neuropil region with SNR > 1.5 are shown.

(E, F) Distribution of neuropil receptive fields in the visual field at (E) stage 45 and (F) stage 48. Colors represent tectal neuropil coordinates (left, middle). Density plots (right) show distribution of neuropil receptive fields from the whole tectum mapped onto the stimulus display area (summed from 14 optical sections, 7.5 μm between slices).

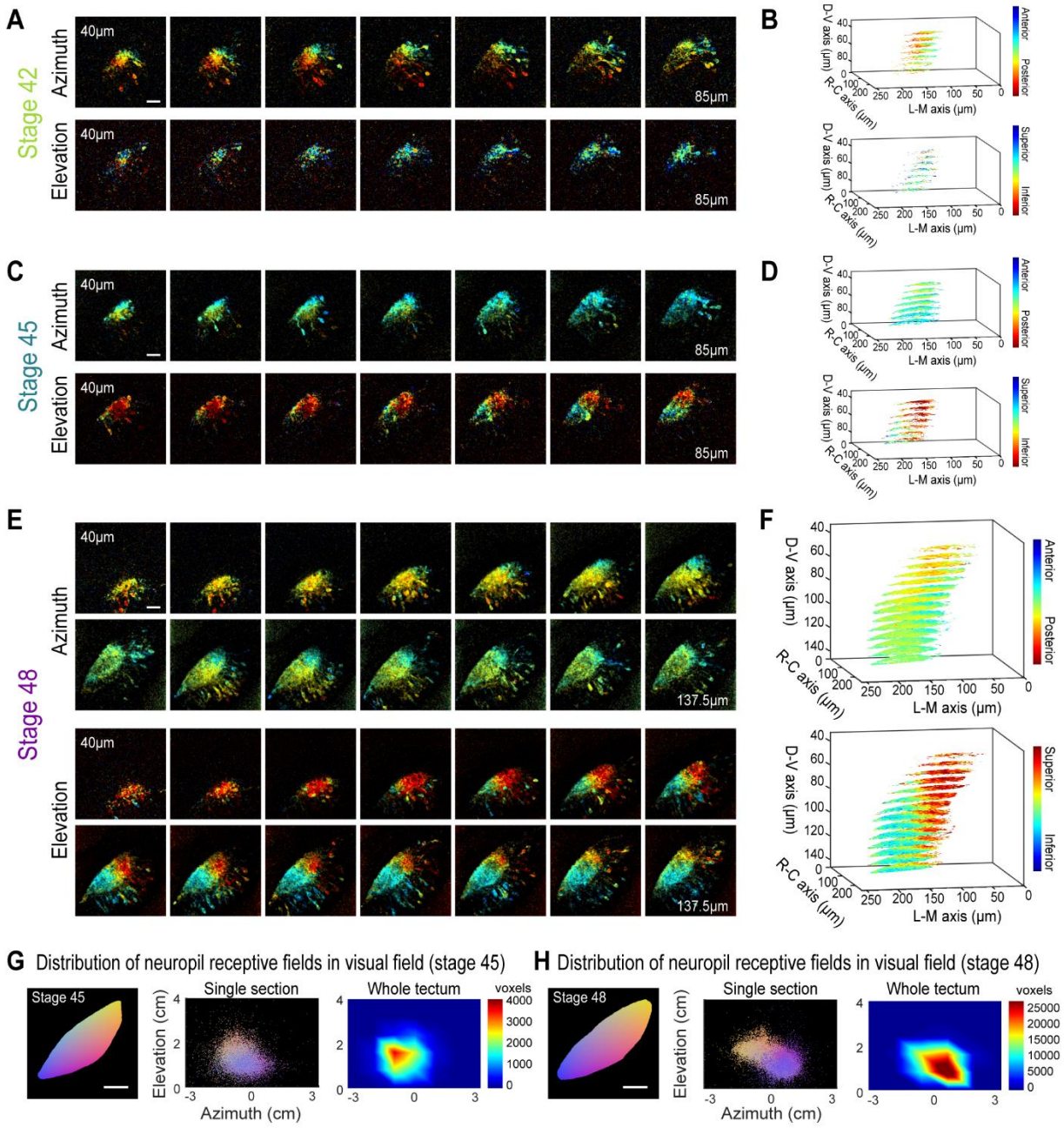

Figure III.S4. Retinotopic map in a transgenic tadpole (tadpole #3) at stage 42, 45 and stage 48.

(A) Phase maps extracted from the tadpole at stage 42. Stack of 7 optical sections, 7.5 μm between slices.

(B) Phase maps in A rendered in 3D volume.

(C) Phase maps extracted from the same tadpole at stage 45. Stack of 7 optical sections, 7.5 μm between slices.

(D) Phase maps in C rendered in 3D volume.

(E) Phase maps extracted from the same tadpole at stage 48. Stack of 14 optical sections, 7.5 μm between slices.

(F) Phase maps in E rendered in 3D volume. In B, D and F, only pixels in the neuropil region with SNR > 1.5 are shown.

(G-H) Distribution of neuropil receptive fields in the visual field at (E) stage 45 and (F) stage 48. Colors represent tectal neuropil coordinates (left, middle). Density plots (right) show distribution of neuropil receptive fields from the whole tectum mapped onto the stimulus display area (summed from 7 optical sections at stage 45 and 14 sections at stage 48, 7.5 μm between slices).

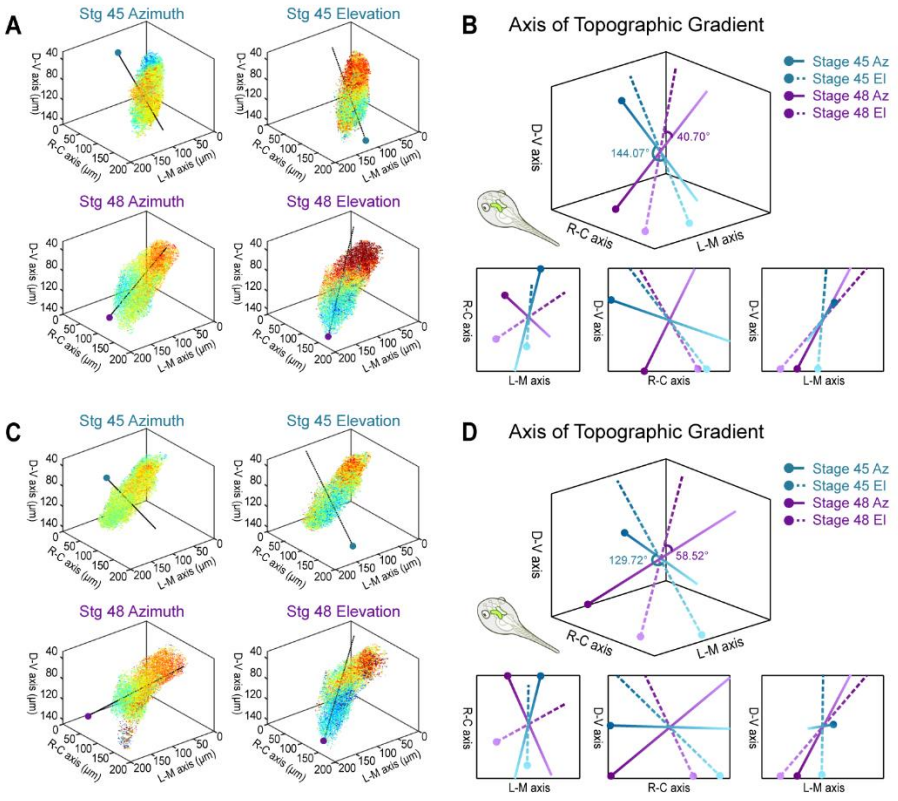

Figure III.S5. Developmental shifting of the topographic gradients at stage 45 and stage 48.

(A) 3D axes of topographic gradients at stage 45 and 48 in a transgenic tadpole (same animal as in Fig.III.2). Phase maps were constructed from 14 optical sections at 7.5 μm intervals. For each optical section, 1000 random pixels in the neuropil region with SNR > 1.5 were plotted as 3D scatter points, with color indicating phase (same scales as in Fig.III.2E,G). A black line in each 3D volume indicates the direction of the mean topographic (phase) gradient. The dot at the end of each line indicates the anterior direction for azimuth and inferior direction for elevation.

(B) Comparison of topographic gradient axes at stage 45 vs 48 in same animal.

(C) 3D axes of topographic gradient at stage 45 and 48 in a transgenic tadpole (same animal as in Fig.III.S2). Phase maps are shown in same manner as panel A.

(D) Comparison of topographic gradient axes at stage 45 vs 48, calculated from the phase maps shown in panel C.

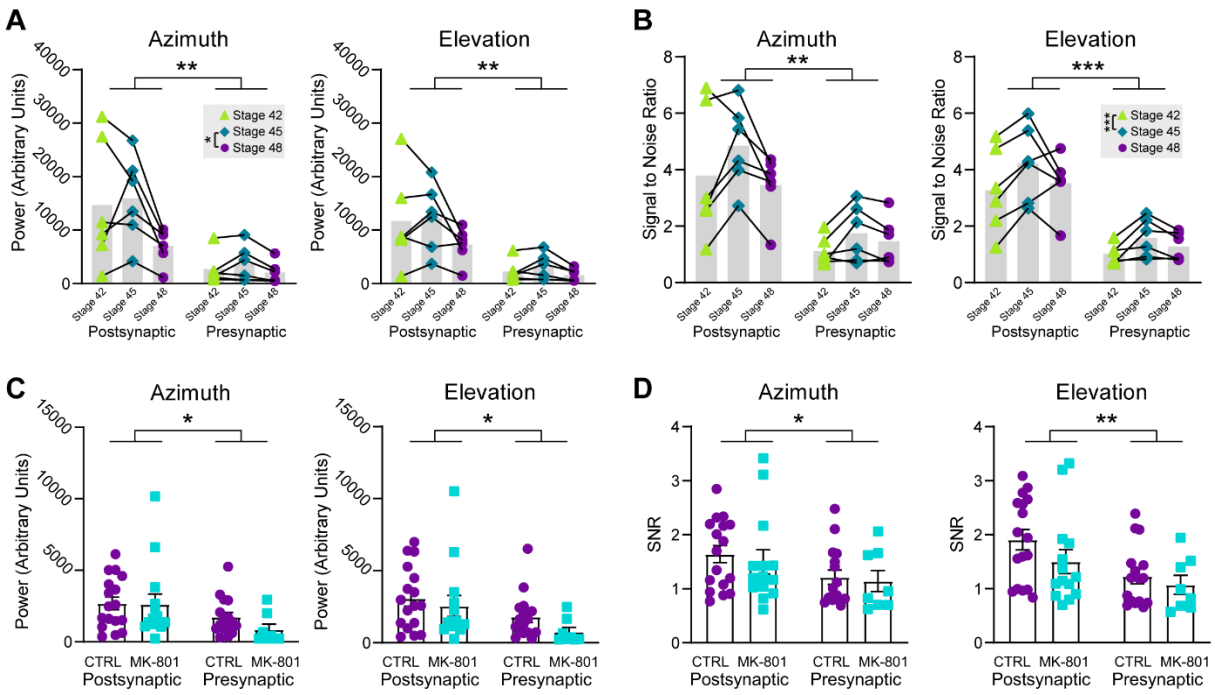

Figure III.S6. Comparison of signal strength and SNR at different developmental stages

(A) Fourier power at the stimulus frequency in response to drifting bar stimuli for GCaMP6s hemimosaic tadpoles at stages 42, 45 and 48 (n = 6 animals). Azimuth measurements were made presenting anterior-to-posterior drifting bars, and elevation with inferior to superior drifting bars. The power is calculated for pixel-wise calcium traces and averaged over the neuropil. Two-way mixed measures ANOVA for stage vs pre/post compartment showed a significant main effect for compartment in both the azimuth and elevation axes. The main effect for stages was significant in the azimuth axis. Azimuth: $F_{compartment}$ (1, 10) = 10.23, **p = 0.0095; F_{stages} (1.362, 13.62) = 5.013 with Greenhouse-Geisser correction, *p = 0.0335. Elevation: $F_{compartment}$ (1, 10) = 11.56, **p = 0.0068; Post-hoc Tukey tests for stages in the azimuth axis showed a significant difference between stage 45 and 48, q(11) = 4.655, *p = 0.0181.

(B) Signal-to-noise ratio for the same tadpoles, calculated pixel-wise and averaged over the neuropil. Two-way mixed measures ANOVA for stage vs pre/post compartment showed a significant main effect for compartment in both the azimuth and elevation axes. The main effect for stages was significant in the elevation axis. Azimuth:

$F_{compartment}$ (1, 10) = 14.88, **p = 0.0032. Elevation: $F_{compartment}$ (1, 10) = 21.47, ***p = 0.0009; F_{stages} (1.370, 13.70) = 6.402 with Greenhouse-Geisser correction, *p = 0.0175. Post-hoc Tukey tests for stages in the elevation axis showed a significant difference between stage 42 and 45, q(11) = 8.197, ***p = 0.0003.

(C) Fourier power at the stimulus frequency for control and MK-801-reared mRNA tadpoles imaged post- or presynaptically at stage 48. (Postsynaptic: CTRL n = 17, MK-801 n = 14; Presynaptic: CTRL n = 16, MK-801 n = 8.) Two-way independent measures ANOVA for drug vs compartment shows significant main effects for compartment, for both the azimuth and elevation axes. Azimuth: $F_{compartment}$ (1, 51) = 6.684, *p = 0.0126; Elevation: $F_{compartment}$ (1, 51) = 6.992, *p = 0.0109.

(D) Signal-to-noise ratio for the same tadpoles in (E), calculated pixel-wise and averaged over the neuropil. Two-way independent measures ANOVA for drug vs compartment shows significant main effects for compartment, for both the azimuth and elevation axes. Azimuth: $F_{compartment}$ (1, 51) = 4.446, *p = 0.0399; Elevation: $F_{compartment}$ (1, 51) = 7.856, **p = 0.0071.

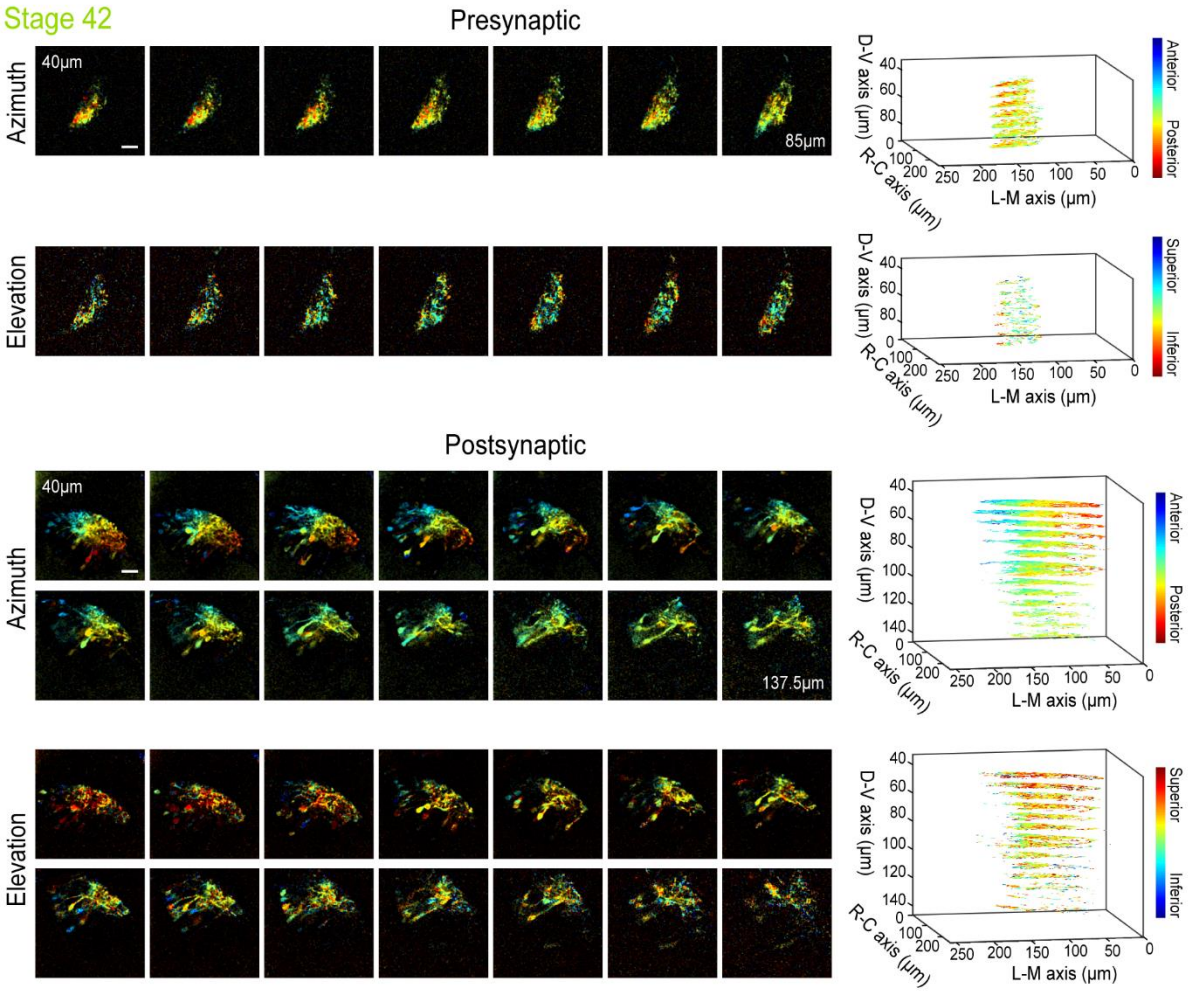

Figure III.S7. Phase maps extracted from a GCaMP6s mRNA hemimosaic tadpole at stage 42.

The animal expressed GCaMP presynaptically in the left tectum, and postsynaptically in the right tectum. The maps were extracted using 36°-wide instead of 18°-wide drifting bars.

Scale bars are 40µm.

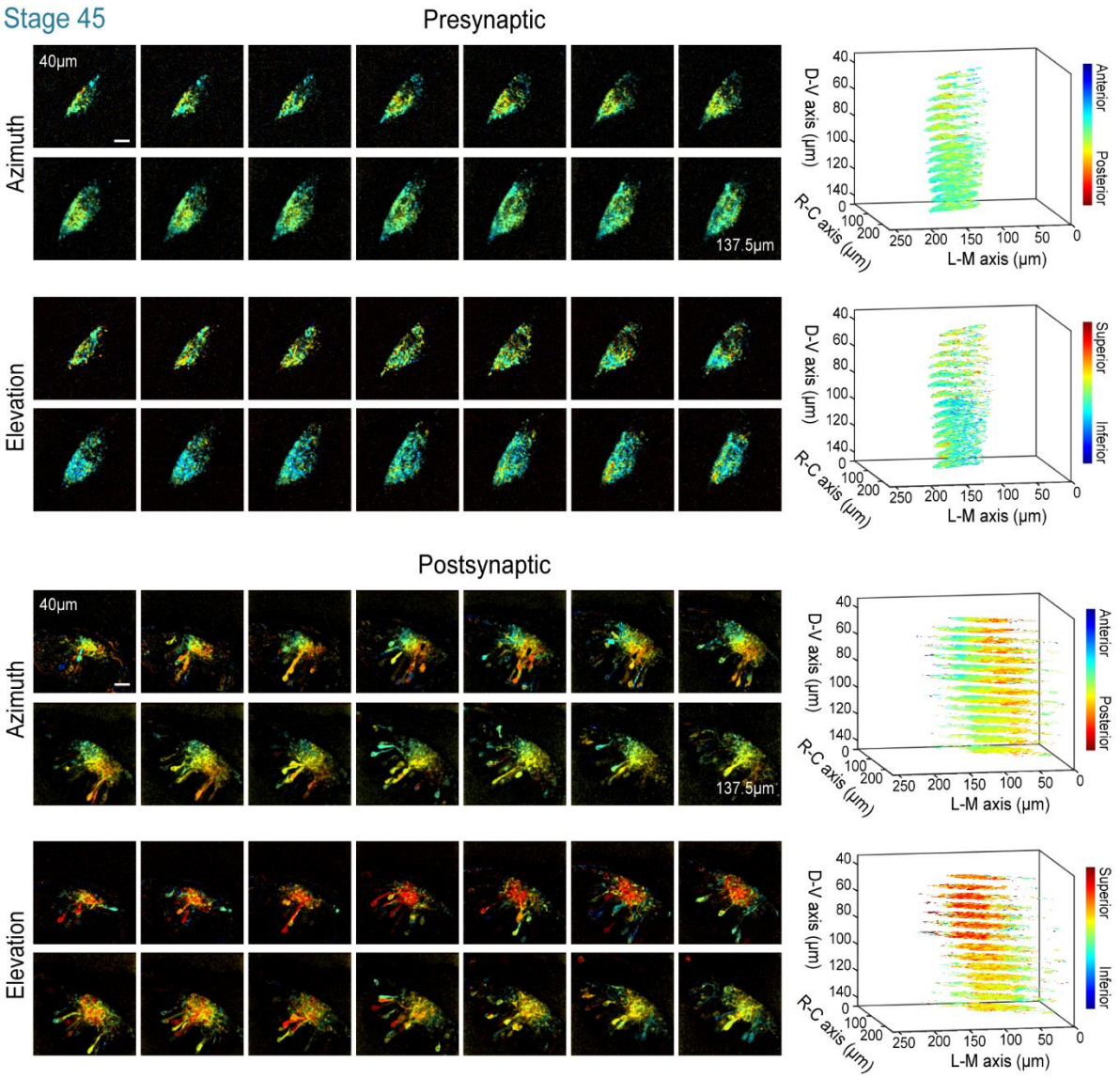

Figure III.S8. Phase maps extracted from a GCaMP6s mRNA hemimosaic tadpole at stage 45

Pre- and postsynaptic phase maps were extracted from the same animal as in Fig.III.S7 at stage 45. The maps were extracted using 18°-wide drifting bars.

Scale bars are 40μm.

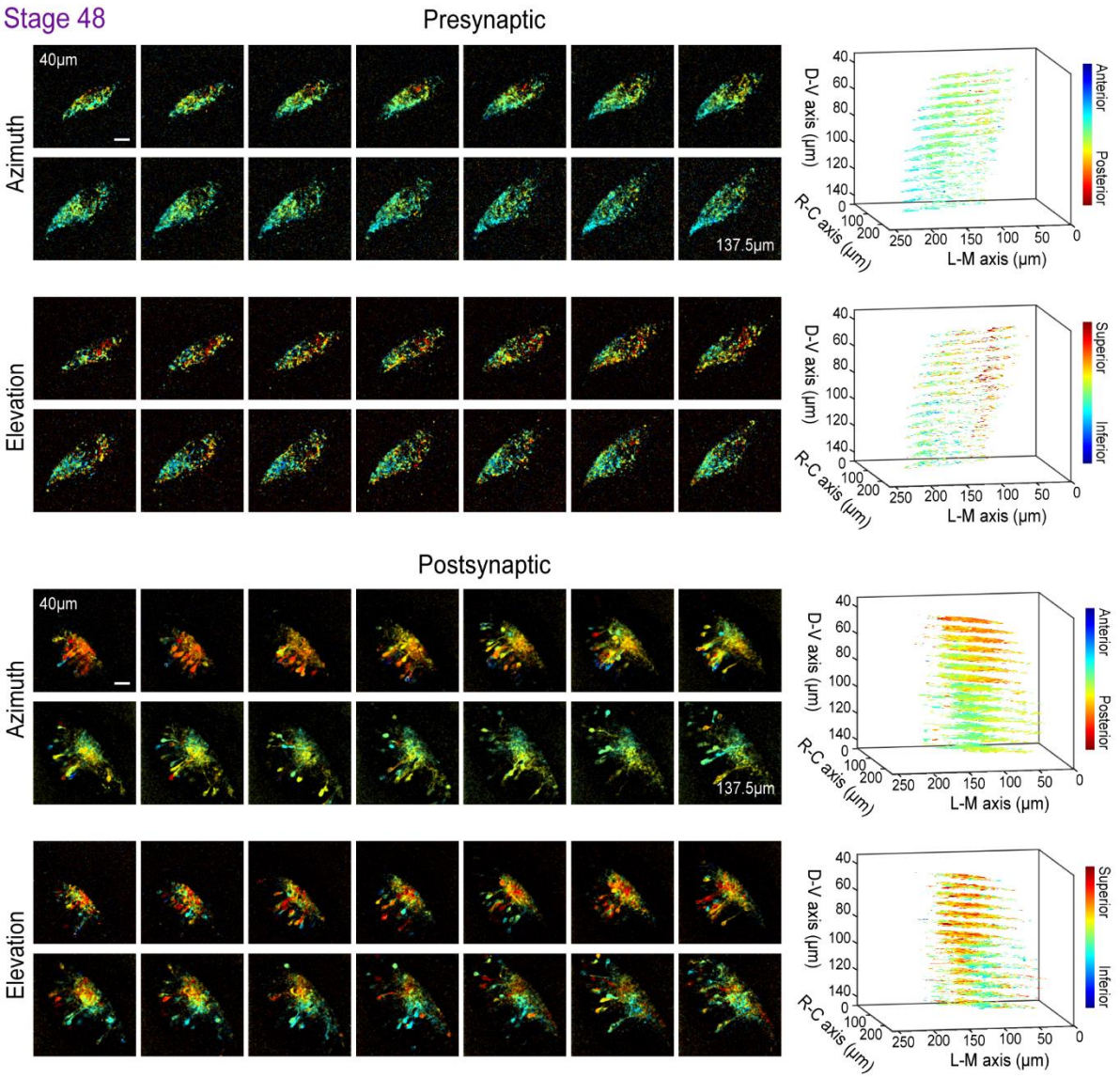

Figure III.S9. Phase maps extracted from a GCaMP6s mRNA hemimosaic tadpole at stage 48

Pre- and postsynaptic phase maps extracted from the same animal as in Figs.III.S7 and III.S8 at stage 48. The maps were extracted using 18°-wide drifting bars.

Scale bars are 40μm.

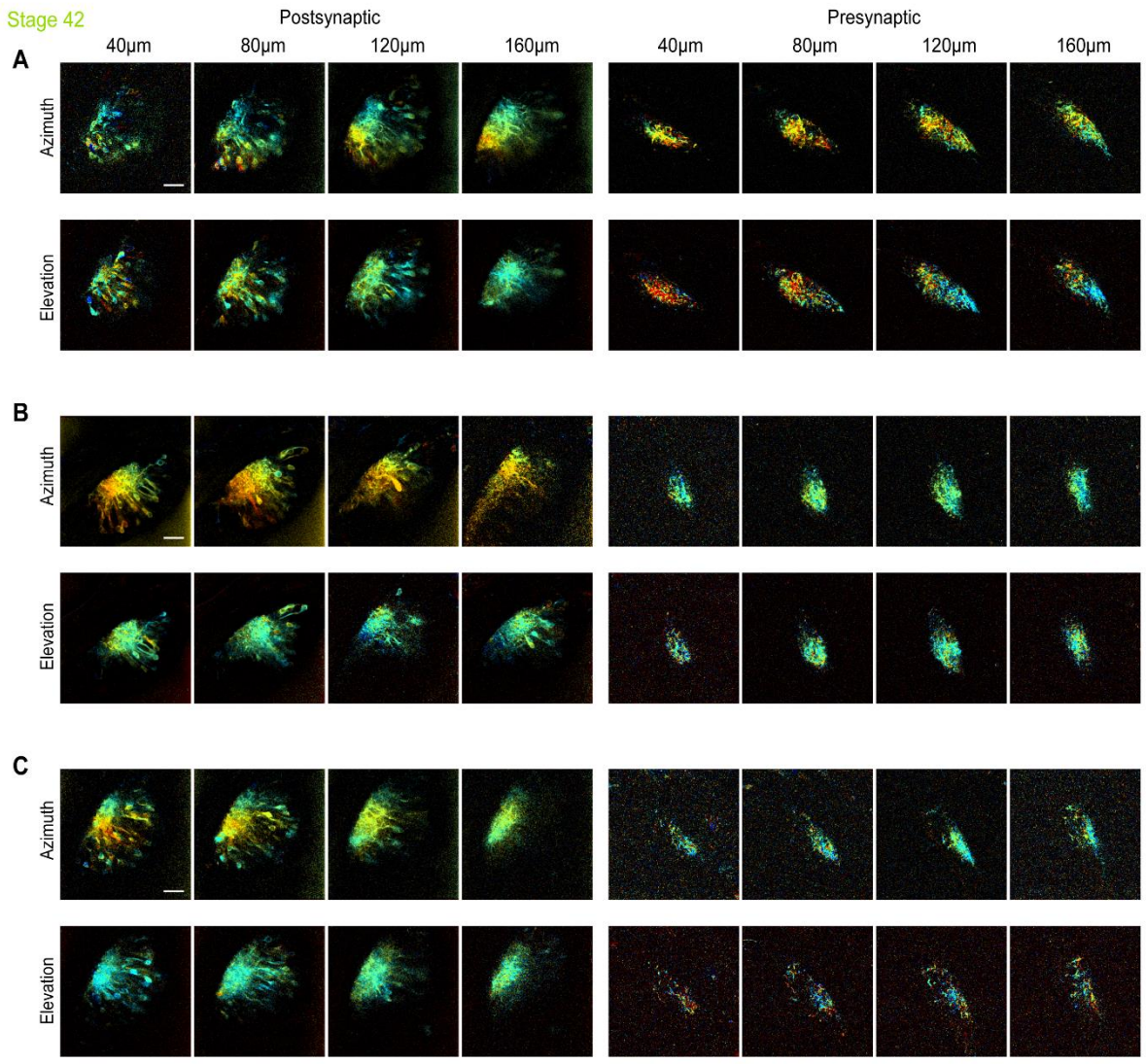

Figure III.S10. Example phase maps from three GCaMP6s mRNA hemimosaic tadpoles imaged at stage 42.

Stacks of 4 optical sections from 40 μm to 160 μm below the surface with 40 μm spacing between slices. For each panel (A, B, C), postsynaptic (left) and presynaptic (right) maps for the azimuth (top) and elevation (bottom) axes were collected in the same animals.

Scale bars are 40μm.

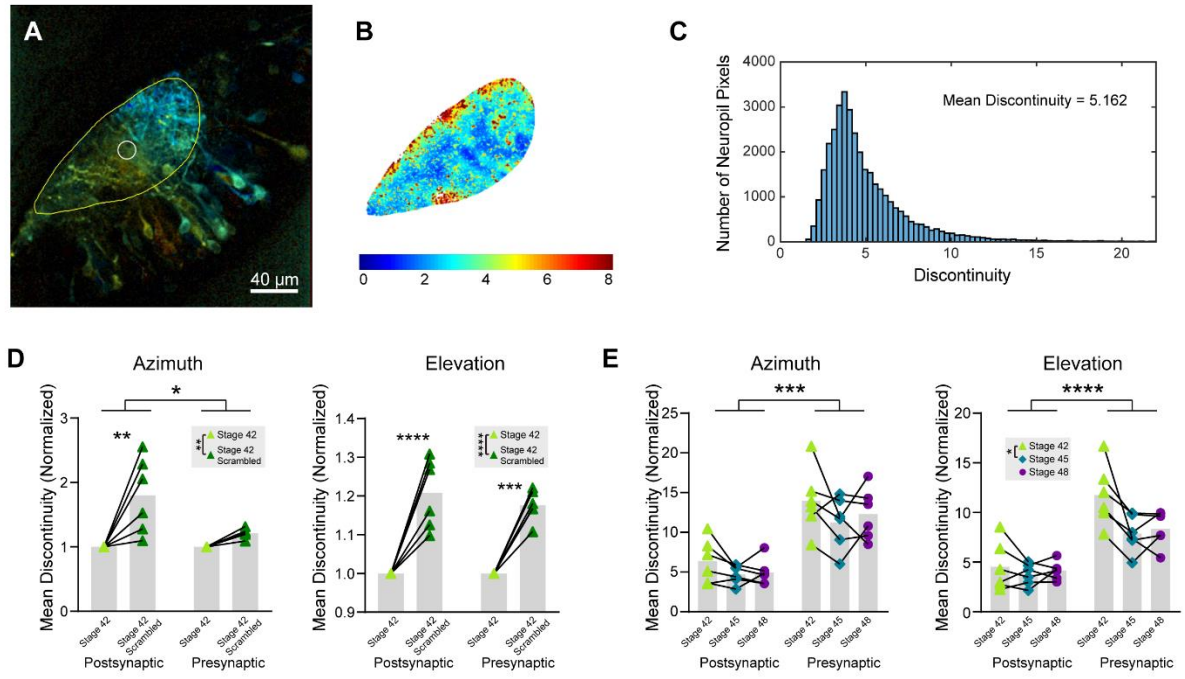

Figure III.S11. Characterization of mean local discontinuity measurements.
(A) Example azimuth phase map for a stage 48 GCaMP6s mRNA tadpole (postsynaptic labelling). Pixel brightness indicates SNR. Yellow outline defines the neuropil area. White outline shows the 15-pixel (7.44 µm) radius region evaluated around a sample pixel.

(B) Scatterplot of neuropil local discontinuity values from the phase map in (A). Dark red corresponds to values greater than 8.

(C) Histogram of the discontinuity values in (B).

(D) Normalized mean discontinuity in stage 42 tadpole maps (same data as in (D)) compared to their scrambled versions (where phase values at different neuropil coordinates were randomly shuffled). Measured discontinuity values were normalized by dividing by mean discontinuity in the original map. Two-way repeated measures ANOVA for shuffling vs compartment showed a significant interaction and significant main effects for both shuffling and compartment for azimuth; and a significant main effect for shuffling for elevation. (n=6) Azimuth: $F_{interaction}(1,10) = 5.955$, *p = 0.0348; $F_{shuffling}(1,10) = 17.60$, **p = 0.0018; $F_{compartment}(1, 10) = 5.955$, *p = 0.0348; Elevation:

$F_{shuffling}(1,10) = 90.49$, ****$p < 0.0001$. Post-hoc t-tests with Sidak correction showed stage 42 discontinuity was significantly lower in original maps compared to scrambled in postsynaptic maps in the azimuth axis; and both pre- and postsynaptic maps in the elevation axis. Azimuth: postsynaptic $t(10) = 4.692$, **$p = 0.0017$; Elevation: postsynaptic $t(10) = 7.286$, ****$p < 0.0001$; presynaptic $t(10) = 6.167$, ***$p = 0.0002$.

(E) Tectal neuropil area-normalized mean discontinuity in tadpoles at stages 42, 45 and 48. The radius of the region evaluated around each pixel was normalized between stages in proportion to the area of the neuropil. Two-way mixed measures ANOVA for stage vs compartment showed significant main effects for compartment in both azimuth and elevation axes, and a significant main effect for stage for elevation. (n=6) Azimuth: $F_{compartment}$ (1, 10) = 34.27, ***$p = 0.0002$; Elevation: $F_{compartment}$ (1, 10) = 39.55, ****$p < 0.0001$; F_{stages} (1.175, 11.75) = 6.134 with Greenhouse-Geisser correction, *$p = 0.0257$. Post-hoc Tukey tests showed a significant difference in discontinuity in the elevation axis between stages 42 and 45, $q(11) = 4.180$, *$p = 0.0323$.

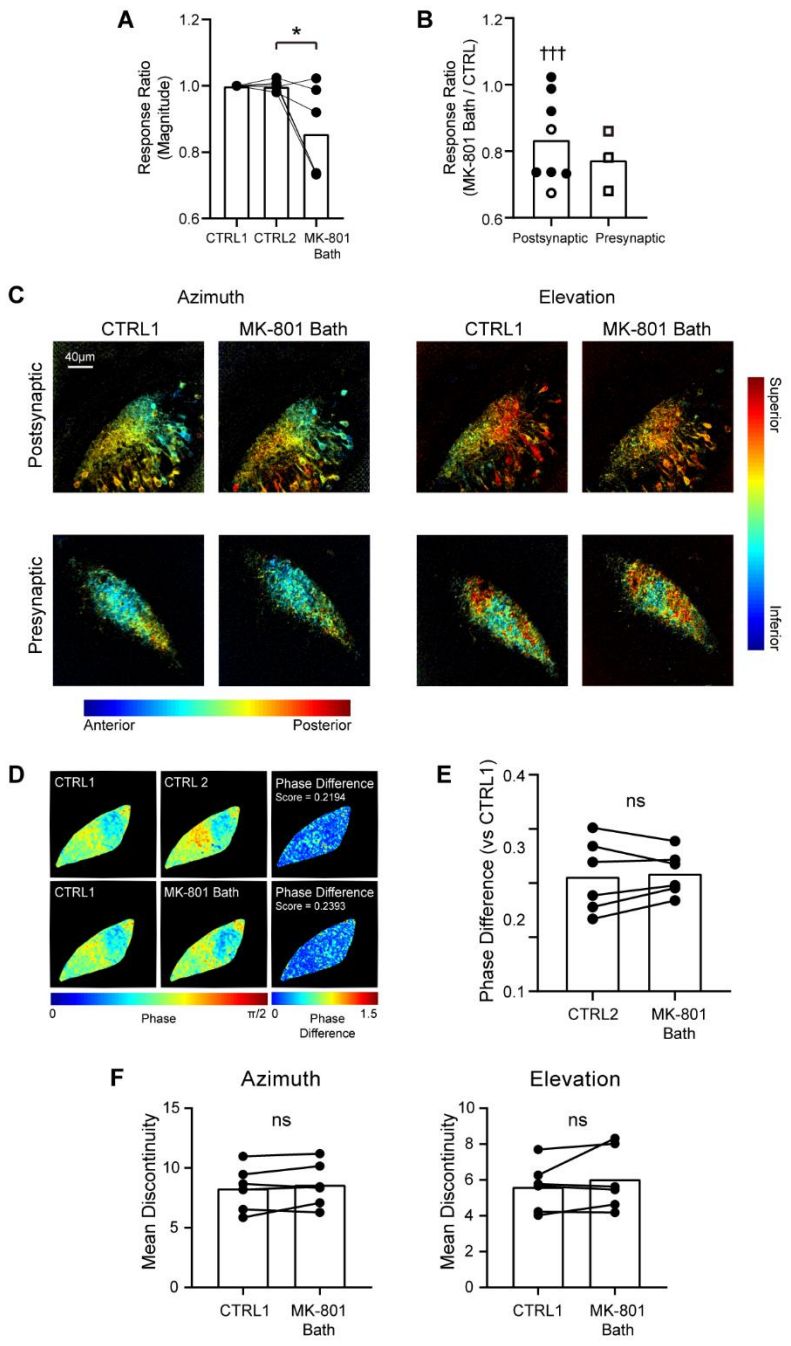

Figure III.S12. Tectal response to drifting bar stimuli after acute MK-801 application.

(A) Two sets of control phase maps were collected approximately 30 min apart, followed by application of MK-801 in the imaging chamber to achieve a final concentration of 10 µM. The Fourier power at the stimulation frequency for the 3 conditions were normalized

by dividing all values by the CTRL1 measurement. Paired t-test showed a significant difference between CTRL2 and MK-801 bath (n = 6, t(5) = 2.616, *p = 0.0471), corresponding to a 14% decrease in response magnitude following acute MK-801 application.

(B) The fractional decrease of Fourier power at the stimulation frequency in response to an anterior to posterior drifting bar after MK-801 bath application was measured for pre- and postsynaptic neuropil. Filled data points indicate data from panel (A); unfilled data points indicate data from additional animals measured without a second control recording. One-sample t-test showed a significant response magnitude decrease after MK-801 bath application in the postsynaptic neuropil (n = 8, t(7) = 4.171, †††p = 0.0042).

(C) Maps extracted from drifting bar experiments before and after acute MK-801 application reveal the robustness of phase mapping to the effects of MK-801 treatment. Phase maps in each row were extracted from the same animal.

(D) Quantifying the difference between azimuth phase maps from drifting bar experiments before and after acute MK-801 application. The phase maps from CTRL2 or acute MK-801 treatment were subtracted from CTRL1 baseline maps, and the resulting phase difference maps were averaged over the neuropil to obtain a phase difference score.

(E) Phase difference scores (versus CTRL1) for azimuth phase maps were used to compare CTRL2 vs MK-801 conditions. A paired t-test showed no significance (n = 6, t(5) = 0.4812, p = 0.651), indicating the maps were not different between these conditions.

(F) Tectal neuropil mean discontinuity does not change following acute MK-801 bath application. (n = 6, azimuth t(5) =1.271, p=0.2598; elevation t(5) = 1.232, p=0.2727, paired t-tests).

		3D Gradient Vectors			Angle with Cardinal Axes		
		x	y	z	x - mediolateral	y - rostrocaudal	z - dorsoventral
tadpole #1	45 Azimuth	79.12	315.71	147.92	77.21	27.98	65.56
	48 Azimuth	-158.52	151.43	-407.45	69.96	70.90	28.28
	45 Elevation	-8.79	-91.68	-158.66	87.25	60.02	30.13
	48 Elevation	-360.91	-241.00	-557.04	59.26	70.04	37.92
tadpole #2	45 Azimuth	44.45	187.01	10.17	76.65	13.70	86.97
	48 Azimuth	-92.36	215.07	-233.99	73.80	49.47	45.01
	45 Elevation	-2.44	-85.10	-110.38	89.00	52.38	37.64
	48 Elevation	-97.91	-53.91	-147.69	58.09	73.08	37.12

Table III.S1. 3D axis gradient vectors and their angles with respect to cardinal axes.

3D azimuth and elevation gradient vectors for the data shown in Fig.III.S5, and their angles with respect to the cardinal axes (in degrees).

Supplementary Movies and Data

The following supplementary movies and dataset can be found at https://doi.org/10.1073/pnas.2107899119.

Movie III.S1. Tectum calcium response to drifting bars.

Example of calcium responses to one cycle of opposite direction drifting bars (left: anterior to posterior; right: posterior to anterior). Images were acquired at 6 Hz (total 20 seconds), then a time average projection was taken for every 10 frames. The clip is looped once for better visibility of calcium response patterns.

Movie III.S2. 3D azimuth phase maps of a transgenic tadpole at stage 45 and stage 48

Rotated views of the 3D azimuth phase maps shown in Fig.III.2E(left) and Fig.III.2G(right).

Movie III.S3. 3D elevation phase maps of a transgenic tadpole at stage 45 and stage 48

Rotated views of the 3D elevation phase maps shown in Fig.III.2E(left) and Fig.III.2G.(right).

Movie III.S4. 3D azimuth phase maps of a transgenic tadpole (tadpole #2) at stage 45 and stage 48

Rotated views of the 3D azimuth phase maps shown in Fig.III.S3B(left) and Fig.III.S3D(right).

Movie III.S5. 3D azimuth phase maps of a transgenic tadpole (tadpole #2) at stage 45 and 48

Rotated views of the 3D elevation phase maps shown in Fig.III.S3B(left) and Fig.III.S3D(right).

Movie III.S6. Presynaptic 3D azimuth phase maps of a GCaMP6s mRNA hemimosaic tadpole at stage 42, 45 and 48

Rotated views of the presynaptic 3D azimuth phase maps shown in Fig.III.S7(left) S8(middle) and S9(right).

Movie III.S7. Presynaptic 3D elevation phase maps of a GCaMP6s mRNA hemimosaic tadpole at stage 42, 45 and 48

Rotated views of the presynaptic 3D elevation phase maps shown in Fig.III.S7(left) S8(middle) and S9(right).

Movie III.S8. Postsynaptic 3D azimuth phase maps of a GCaMP6s mRNA hemimosaic tadpole at stage 42, 45 and 48

Rotated views of the postsynaptic 3D azimuth phase maps shown in Fig.III.S7(left) S8(middle) and S9(right).

Movie III.S9. Postsynaptic 3D elevation phase maps of a GCaMP6s mRNA hemimosaic tadpole at stage 42, 45 and 48

Rotated views of the postsynaptic 3D elevation phase maps shown in Fig.III.S7(left) S8(middle) and S9(right).

Dataset III.S1. Plot data for all figures.

Preface to Chapter IV

In the previous chapter, we observed a dramatic change in the layout of the 3D retinotopic map in the tadpole tectum between developmental stage 45 and 48. This may reflect the drastic adaptations the retinotectal system must undergo during this time, with the continuous addition of cells to the retina and tectum keeping the system in a constantly evolving state. In this chapter, we labelled individual tectal cells to serve as fiducial markers in the tectum and quantified changes in both morphology and functional receptive fields, providing an insight to how developmental changes are unfolding at the single-unit and whole-circuit levels, which may give clues to how the system maintains stable functionality during the turbulent process of development.

Author contributions

Chapter IV is a manuscript in preparation by Li, V. J., D. Foubert, A. Schohl and E. S. Ruthazer.

Experiments were designed collaboratively by VJL, AS and ESR. Experiments were performed by VJL. Custom software for data analysis was developed by VJL. Embryological techniques and molecular resources were developed by AS. CldU immunohistochemistry was performed by DF. Funding was provided by VJL and ESR. The paper was written by VJL and ESR.

Chapter IV

Tracking morphological and functional changes in the developing Xenopus retinotectal system

Author list: Vanessa J. Li, David Foubert, Anne Schohl, Edward S. Ruthazer

Keywords:

Xenopus laevis, retinotectal, calcium imaging, topographic maps, development, mRNA microinjection, single-cell electroporation

Abstract

The retinotectal projection in *Xenopus laevis* is topographically organized. During the early development of the *Xenopus* visual system, the optic tectum increases considerably in volume, and retinotectal axons and dendrites undergo extensive activity-dependent remodelling. We have previously observed marked changes in the three-dimensional layout of the tectal retinotopic functional map over the course of a few days. This raised the question of whether such functional reorganization might be attributable to the migration and structural remodelling of tectal neurons as the brain grows. To examine changes in map topography in the context of individual tectal neuron morphology and location, we performed calcium imaging in the optic tecta of GCaMP6s-expressing tadpoles in parallel with structural imaging of tectal cells that were sparsely labelled with Alexa 594-dextran dye. We performed functional and structural imaging of animals at stages 45-46 and again at stage 48, recording the morphology of the dextran-labelled cells and quantifying the developmental changes in their positions and the spanning volume of their dendritic fields. Comparing anatomical growth to changes in the functional retinotopic map at these early stages, we found that dendritic arbor growth kept pace with the overall growth of the optic tectum, and that individual neurons continued to receive widespread visual field input, even as the tectal retinotopic map evolved markedly over time.

Introduction

Xenopus laevis has historically been a popular model organism in which to study neurogenesis and topographic wiring of neurons in developing circuits (Cline & Kelly, 2012; Liu et al., 2016; McFarlane & Lom, 2012). The Xenopus retinotectal system presents broad similarities with its mammalian homologue, the superior colliculus (SC), sharing basic organizational layout as well as common molecules involved in axon guidance (Mann et al., 2004). Meanwhile, Xenopus offers many advantages compared to mammalian models, including externally developing larvae, readily accessible to genetic and pharmacological manipulations. Albino Xenopus tadpoles have transparent skin allowing non-invasive *in vivo* imaging of tectal cell populations at subcellular resolution (Dunfield & Haas, 2010; Ruthazer et al., 2013). In a previous study (Li et al., 2022), we mapped the three-dimensional (3D) layout of the visuotopic map in the tadpole tectum through calcium imaging over developmental stages 42 through 48 (Nieuwkoop & Faber, 1994), a period of robust growth and circuit refinement for the retinotectal system (Gaze et al., 1972; Holt & Harris, 1983; Kutsarova et al., 2017; Sakaguchi & Murphey, 1985). We saw a marked change in the layout of functional retinotopic maps between stages 45 and 48, with the 3D axes of retinotopic organization undergoing large spatial rotations, prompting questions on how the underlying circuit changed during this process.

Starting from the developmental stages when retinal ganglion cell (RGC) axons first reach the tectum until metamorphosis, both the eye and tectum of the tadpole expand and add cells, requiring the visual system to continuously rewire its circuit to maintain visual encoding functionality so that the tadpole can effectively locate food and avoid predators. To add to the complexity of the problem, the patterns of cell proliferation in the retina and tectum do not match: The retina expands radially by adding cells at its ciliary margin, resulting in the earliest-born retinal ganglion cells being found near the middle of the retina near the head of the optic nerve (Beach & Jacobson, 1979; Hollyfield, 1971; Straznicky & Gaze, 1971); meanwhile the tectum adds new cells at its caudomedial end, displacing older cells toward the rostral end of the tectum (Herrgen & Akerman, 2016; Lazar, 1973; Straznicky & Gaze, 1972). This means that to maintain an

orderly retinotopic map, the circuit must constantly undergo some form of rewiring, by either dynamically shifting physical RGC-to-tectal neuron connections or by functionally changing the receptive field input strengths onto tectal neurons (Chung et al., 1974; Gaze et al., 1979).

In the present study, we sought insights into this rewiring process by following the morphological and functional changes in individual tectal cells and putting them into the context of whole-tectum functional retinotopic map changes. We applied our previously established methods to express the fluorescent calcium indicator GCaMP6s in the tadpole tectum to perform calcium imaging to extract retinotopic maps (Li et al., 2022), but also introduced red fluorescent labelling of individual tectal cells through single-cell electroporation (Haas et al., 2002; Haas et al., 2001). This allowed us to examine developmental changes in the morphology of the labelled cell and its position in the tectum, as well as the functional retinotopy of visual inputs to its dendritic arbor.

Results

Characterizing morphological and functional changes in the growing tadpole tectum

We generated tadpoles expressing the genetically-encoded calcium indicator GCaMP6s (Chen et al., 2013) through mRNA blastomere injection, as described previously (Li et al., 2022). This allowed us to visualize the growing tadpole tectum and analyze its functional properties by recording responses to visual stimuli and extracting visuotopic maps. Injecting GCaMP6s mRNA into one blastomere of two-cell stage embryos produced hemi-mosaic animals with GCaMP expression restricted to one lateral half of the animal. In Xenopus tadpoles, RGC axons from one eye project almost exclusively to the contralateral tectum (Munz et al., 2014). Therefore, the tectal hemisphere in the lateral half with GCaMP expression will contain GCaMP in tectal cells but not incoming RGC axons, ensuring the calcium signal recorded from this tectal lobe primarily reflects postsynaptic neuronal activity. When the animals reached stage 44, we performed single-cell electroporation to fill a single or small number of tectal neurons with Alexa

Fluor 594 dextran dye. This allowed us to observe and follow the morphology of individual tectal cells and their relative anatomical positions in the tectum over time. We performed two-photon calcium imaging on tadpoles at stage 45-46, then again at stage 48 to compare developmental differences in the same animals (Fig.IV.1a,c). During each imaging session, we collected high-resolution z-stack images of the tectum to capture the morphology of both the tectum and Alexa 594 dextran-labelled cell (using basal GCaMP6s fluorescence to visualize overall tectal morphology), then performed retinotopic mapping by presenting drifting visual stimuli and recording the evoked GCaMP signal as previously described (Li et al, 2022).

Morphometric changes in the tectum and postsynaptic tectal cell dendritic fields

We manually segmented the tectum and tectal neuropil to acquire volumetric measurements (Fig.IV.1b), and generated automated 3D reconstructions of the dendritic trees of dextran-labelled tectal neurons to calculate the total branch length and spanning volume of dendritic fields (Fig.IV.1d).

Between stage 45 and stage 48, a period of extensive neurogenesis (Gaze et al., 1972; Herrgen & Akerman, 2016), there was a significant increase in the volume of the tectum and tectal neuropil (Fig.IV.1b). Total branch length and spanning volume of the dendritic fields of individual tectal neurons increased significantly (Fig.IV.1e,g), and Sholl analysis showed an increase in branch complexity (Supplementary Fig.IV.S1a). However, we did not detect a significant change in dendritic branch length per total neuropil volume nor in dendrite spanning volume divided by total neuropil volume, indicating that there was not a significant change in the proportion of total neuropil covered by a single cell's dendritic field due to matched growth of the dendritic arbor and tectal volume (Fig.IV.1f,h).

We measured the soma position of the dextran-labelled cells along the long axis of the tectal lobe, and found that from stage 45 to 48 the cell somata consistently shifted rostrally and ventrally (Fig.IV.1i-j), consistent with new tectal cells being added from the caudal end of the tectum (Herrgen & Akerman, 2016). To confirm the pattern of proliferation of tectal neurons, we performed chlorodeoxyuridine (CldU) labelling to lable cells that were dividing at the time of administration (Fig.IV.1k). CldU administered for 2 hours at stage 45 resulted in CldU labelling distributed in a laminar fashion in the middle

of the cell body layer of the tectum at stage 48, consistent with tectal cells being added linearly in the tectum.

Previous studies of Golgi impregnated cells in slightly older animals reported that morphological features of tectal cells may be correlated to the position of the cell along the rostrocaudal (R-C) axis due to more mature cells being situated in more rostral positions (Lazar, 1973; Wu et al., 1996). However, for the cells in our dataset we observed no consistent correlation between soma position in the tectum and morphological complexity, including dendrite spanning volume, total branch length, dendrite coverage (measured as dendrite spanning volume divided by total neuropil volume) or dendrite growth rate (Supplementary Fig.IV.S1b-d).

Changes in functional retinotopic representations in the tectal neuropil

To characterize the functional representation of the visual field in the tectum, we presented tadpoles with repeated drifting bar stimuli across the azimuth and elevation axes of the visual field and recorded calcium responses ($\Delta F/F_0$) in the tectum to estimate receptive field (RF) positions. A Fourier power spectrum analysis of the calcium signal fluctuations at the stimulus repetition frequency (0.05 Hz) was used to extract the stimulus-driven neural responses. The phase of the response signal at the stimulation frequency corresponds to the time of the peak response and thus the receptive field position on the stimulation screen. Retinotopic mapping was performed by rapidly imaging at multiple depths in one tectal hemisphere to obtain a 3D functional visuotopic map. We regularly observed marked changes in the 3D layouts of azimuth and elevation topographic gradients in the same animal between stage 45 and stage 48 (Fig.IV.2a-c).

Using the dextran-labelled cells as fiducial markers in the tectum, we matched 3 optical sections containing the labelled cells at early (stage 45-46) and late (stage 48) stages, with 15 μm depth between optical sections, and quantified the topographic gradients along the R-C axis of the neuropil for each optical section (Supplementary Fig.IV.S2a-c). The dorsalmost sections were 40~70 μm from the dorsal surface of the tectum, depending on the position of the labelled cell. The topographic gradients, as measured by the slope of the linear regression fitted to the RF values, differed considerably

between early and late stages. In the dorsalmost section imaged, the gradient of the elevation axis map consistently shifted toward alignment with the R-C axis from early to late stages. However, in deeper optical sections, the directions that topographic gradients shifted were not consistent between animals (Supplementary Fig.IV.S2d). This observation indicates a high degree of lability of the retinotopic map during these developmental stages.

Despite the striking lability in the layout of the topographic gradients within the tectum between early and late stages, when we compared total visual field representations throughout the tectal neuropil for each animal, there was no overall shift in the mean receptive field center of either the azimuth or elevation axes (Fig.IV.2d). However, the overall distribution for all measured RFs showed a slight but significant shift towards higher phase values in azimuth (corresponding to more representations in the posterior field) and lower phase values in elevation (corresponding to more representations in the inferior field) in late-stage recordings (Fig.IV.2e).

Given the surprising amount of map reorganization observed, we wondered how the inputs to individual tectal neurons might be changing across these time points. Therefore, we next examined the RFs of voxels colocalizing with the dendritic arbors of the dextran-labelled postsynaptic cells (Fig.IV.3a) and their relationship to the RF coverage in the rest of the tectal neuropil. Cumulative distribution plots of pooled RF phase values from voxels colocalized with the dendritic fields of dextran-labelled cells showed a developmental shift towards more coverage in anterior visual fields (lower phase values) in azimuth and a small shift towards superior visual fields (higher phase values) in elevation (Fig.IV.3b) at the later stage, opposite to the trend that was seen for the whole neuropil (Fig.IV.2e). This points to a scenario where the RFs of individual tectal cells are shifting gradually, but this change in mature cells may be offset by newer cells being added to the tectum, preserving the overall RF distribution in the whole tectum.

The fact that we did not see a morphometric change in the dendritic coverage of labelled cells as a proportion of total neuropil volume (Fig.IV.1h) led us to ask if this would also be reflected functionally in RF representations in the dextran-labelled cells

compared to the whole neuropil. We binned RF phase values recorded from the total neuropil and dendrites of dextran-labelled cells into 2D histograms, and found a high degree of similarity between the two histograms (Fig.IV.3c-e). This degree of similarity did not change significantly between early and late stages, suggesting high levels of visual input convergence to each tectal neuron that was preserved over these developmental stages.

Changes in visual response properties in individual tectal neurons

Receptive field analysis based on drifting bar responses in individual tectal cell soma regions-of-interest (ROIs) yielded retinotopic maps with topographic gradients that were generally consistent with the corresponding neuropil retinotopic maps from the same animals (Fig.IV.4a). The distribution of cell body RF positions along the neuropil R-C axis largely matched the neuropil RF distribution (Supplementary Fig.IV.S3-4). As in the neuropil, the mean RF phase of all cell body ROIs from the whole tectum of individual animals revealed no significant shift between early and late stages (Fig.IV.4b), but the overall distribution of RF centers of individual cells showed a very slight but significant posterior shift in azimuth and a small downward shift in elevation (Fig.IV.4c).

Because we expressed GCaMP6s by mRNA microinjection into blastomeres at the 2-cell stage, one possible alternative explanation for the lability of RF gradients and distributions could be that degradation of mRNA and protein over time might lead to less reliable responses in older animals. We therefore quantified the signal-to-noise ratio (SNR) and direction selectivity index (DSI) of cell body responses to drifting bars and their degree of direction preference for drifting bars presented in opposite directions (Fig.IV.5). Comparing pools of cell body responses recorded at early vs late stages, we saw an increase in SNR at the later stage compared to younger animals. Additionally, we found that direction selectivity significantly decreased with age. Thus, GCaMP6s protein expression was likely sufficiently high at both the early and late experimental time points to obtain robust visual responses, and adequate to reveal developmental changes in stimulus selectivity.

Discussion

In this study, we examined the *Xenopus laevis* retinotectal system over a key period of rapid growth in early visual system development. We characterized morphological and functional changes at both the whole-tectum and single-cell levels to gain a better understanding of the potential ways morphology translates to function, and how changes at the single-cell level contribute to changes in the whole circuit. Our method of expressing GCaMP in tadpoles through mRNA blastomere injection produced hemi-mosaic animals with GCaMP expression in one of the two tectal hemispheres restricted to postsynaptic tectal cells, with no GCaMP in the presynaptic retinal ganglion cell arbors. This ensured that calcium signal recorded from this tectal hemisphere was comprised exclusively of postsynaptic somatic and dendritic components of the retinotectal map, without contamination from presynaptic RGC axonal signals that would instead reflect axonal morphologies. Next, by labelling individual neurons in this tectal lobe by single-cell electroporation of dextran-conjugated dye, we established a system where the morphology and functional activity of the whole tectum and individual postsynaptic cells within the tectum could be observed in parallel. We examined the developmental changes in the position, morphology, and functional visual field representations in the labelled individual cells, and compared them to changes seen in the whole tectum.

Our morphometric measurements showed that while both the whole tectum and dextran-labelled postsynaptic dendritic arbors saw significant increases in volume, the proportion of total tectal volume occupied by the dendritic field of the labelled cell remained relatively constant. These observations were echoed in functional aspects: While there were considerable shifts in the layout of retinotopic gradients within the whole tectum, there was relatively little change in the distribution of total visual field inputs to the dendrites of individual labelled tectal neurons.

Notably, regarding developmental refinement in the retinotectal circuit, Sakaguchi and Murphey (1985) reported that while RGC axons continue to grow and increase in complexity over development, their expansion is slower than that of the overall tectal neuropil, thereby resulting in each axon occupying a progressively smaller fraction of

the total neuropil over time. In contrast, our morphometric observations of tectal cell dendritic arborization showed ongoing but matched growth of tectal cell dendritic arbors and whole tectal neuropil. Functionally, we found the range of visual field representations found in tectal cell dendritic arbors to be quite wide, and evidence of topographic refinement within the observed developmental stages was subtle. This suggests an overall scenario where the presynaptic portion of the retinotectal circuit is becoming more precise, but the postsynaptic portion maintains a relatively large input range and does not follow the same pattern of refinement as the presynaptic component.

A recent study in adult mouse superior colliculus (Molotkov et al., 2023) found RGC axon terminals to form near-perfect retinotopic tiling in the SC, with retinotopic precision measured in RGC axon terminals found to be higher than that in local SC neuron somata. Based on these results, the authors suggested that retinotopic precision in the SC arises from topographically precise input from presynaptic cells rather than from computational reconstruction performed by postsynaptic circuitry. We believe it is likely that the adult Xenopus tectum functions in a similar fashion, which will be consistent with the developmental trend of more prominent topographic refinement in the presynaptic side. However, our observations suggest the transmission and processing of retinotopic information in the developing tectum deviates from what is seen in the adult tectum: inputs received by tectal cell dendrites in the developing tectum are broad and imprecise, and the animal would likely need to rely on computations in postsynaptic tectal cells to recover sufficient (albeit coarse) visual information to guide behaviour.

The Xenopus tectum in early development faces two prominent challenges that could determine its strategy for encoding and processing visual information. On one hand, computational power in the developing tectum is much more limited, both in terms of the total number of available tectal neurons and the ability of these neurons to resolve spatial information. In the developmental stages examined in this study, the volume of the tectum is only about one-hundredth of what it will grow to in adult animals (Gaze et al., 1974; Roth & Walkowiak, 2015), and tectal neurons at these stages have been shown to have very large receptive fields (Dong et al., 2009; Gaze et al., 1974;

Hiramoto & Cline, 2024; Van Horn et al., 2017; Vislay-Meltzer et al., 2006). On the other hand, the developing tectum needs to reconcile with the constant integration of newly proliferated cells into the tectal circuit and the resulting need to adjust local connections to maintain stable and behaviourally relevant visual processing output. With individual tectal neurons lacking the ability to encode precise retinotopic information through single stimulus-evoked responses, the animal likely needs to integrate the responses of multiple tectal cells to recover spatial relationships. Under these circumstances, the topographically precise wiring of retinal inputs to tectal targets become less important, which could explain the apparent lack of topographic refinement observed in tectal cell dendrites over a short period of time. An inherently wide input range and reduced requirement for topographically precise connections can in turn become beneficial when integrating new cells into the circuit: the amount of branch rewiring necessary to reestablish working order in the circuit would be reduced, cutting down on metabolic expenses involved in the process.

It should be noted that in the present study, our measurements of calcium signals from voxels overlapping with dendrites of dextran-labelled tectal cells are likely a close reflection of the range of retinal inputs available to that cell, but they do not give us precise information on the computational output from that tectal cell, which would be most reliably measured at the cell soma. Functional analyses on somatic signal from the dextran-labelled cells in our dataset was unfortunately not possible as a large proportion of the dextran-labeled tectal neurons had poor GCaMP signal strength from their cell bodies. We performed our single-cell electroporations blind to GCaMP responsiveness, resulting in many dextran-labeled cells that had little or no somatic calcium signal. The harsh process of membrane disruption required for electroporation may have also perturbed GCaMP activity within the cell. However, based on the increased SNR we measured from somatic responses of other cells in the tectum, we expect that had we been able to evaluate somatic responses in these dextran-labelled cells, we would see an increase in their ability to reliably decode visual information despite the lack of topographic refinement in the input they are receiving. We also expect that later in development, as the size of the tectal neuron population surpasses a certain threshold, the system would switch from favoring broad integration over diffuse inputs to favoring

focused connections from selected inputs, at which point developmental refinement in topographic precision in tectal neurons would become much more prominent.

Materials and Methods

Animals

All procedures were approved by the Animal Care Committee of the Montreal Neurological Institute at McGill University and carried out in accordance with Canadian Council on Animal Care guidelines.

Female albino *Xenopus laevis* frogs (RRID: XEP_Xla300) from our in-house breeding colony were injected with pregnant mare serum gonadotropin (Prospec) and human chorionic gonadotropin (Sigma-Aldrich) to induce ovulation. Eggs were collected and fertilized with sperm from male albino X. laevis frogs. Blastomere microinjection of GCaMP6s mRNA to create animals with hemilateral GCaMP expression was performed as previously described (Li et al., 2022). Briefly, a solution of purified GCaMP6s (500 pg) mRNA in 2 nL RNase-free water was pressure injected into one blastomere of two cell–stage embryos using a calibrated glass micropipette attached to a PLI-100 picoinjector (Harvard Apparatus). GCaMP mRNA was prepared by cloning the coding sequence of GCaMP6s into pCS2+, then linearizing plasmids with NotI, and transcribing the capped mRNA of GCaMP6s with the SP6 mMessage mMachine Kit (Ambion; Thermo Fisher). Developing animals were screened to select individuals with bright and unilaterally restricted GCaMP fluorescence. When these animals reached stage 44, single-cell electroporation was performed on the tectal hemisphere with postsynaptic GCaMP expression to label a single or small group (2~3) of postsynaptic tectal cells with Alexa Fluor 594 dextran.

All tadpoles were reared in biological oxygen demand incubators on a 12/12-h light/dark cycle. Rearing medium was 0.1x Modified Barth’s Solution with 4-(2-hydroxyethyl)-1-piperazineethanesulfonic acid (HEPES) buffer. Tadpoles of both sexes were used for all studies. Tadpole developmental stages were determined according to Nieuwkoop and Faber (1994).

CldU labelling and whole mount immunofluorescence

Animals were placed in rearing solution with 10mM CldU (5-Chloro-2'-deoxyuridine) (Sigma-Aldrich) for 2 h at stage 45, then sacrificed at stage 48. Brains were extracted and fixed with 4% paraformaldehyde in phosphate-buffered saline (PBS, Sigma) overnight at 4°C, washed in PBS, then incubated in PBS-T (0.1% Triton X-100 (VWR) in PBS) for 10 min, followed by 0.5% Triton X-100 in PBS for 1 h. Samples were then treated with 2N hydrochloric acid at 37°C for 20 min for epitope retrieval, rinsed in PBS-T, then placed in blocking buffer (1% bovine serum albumin (Fisher) and 5% normal goat serum (Qiagen) in PBS-T) for 24 h at 4°C. Next, the samples were incubated with primary antibodies (rat anti-BrdU, Abcam, 1:500) for CldU, and β-tubulin (chicken anti-β-tubulin, Chemicon, 1:1000) diluted in blocking buffer for 24 h at 4°C, washed in PBS-T, then incubated in secondary antibodies (Alexa Fluor 555 goat anti-rat (Invitrogen) for BrdU, Alexa Fluor 488 goat anti-chicken (Invitrogen) for β-tubulin) overnight at 4°C. Finally, the brains were washed with PBS-T, mounted with half a drop of Aqua-Poly/Mount (Polyscience) onto slides fitted with custom mounting spacers (4 layers of scotch tape with a hole punched in the center of the tape square) and sealed with a coverslip for imaging.

In vivo imaging

Fluorescence images were captured with a high-speed resonance scanner-based two-photon microscope (Thorlabs) with piezoelectric focusing (Physik Instrumente) on a 1.0 NA 20x water immersion objective (Nikon). Emission signal was collected in 2 channels through 525/50 and 630/92 bandpass filters, respectively. For morphometric imaging, an excitation wavelength of 840 nm was used to simultaneously image GCaMP6s and Alexa Fluor 594. For functional imaging with GCaMP6s, an excitation wavelength of 910 nm was used. For imaging CldU immunofluorescence, 990 nm was used for Alexa Fluor 488 and 555.

Morphometric imaging and analysis

Tadpoles were imaged at stage 45 and again at stage 48. In each imaging session, tadpoles were anesthetized by immersion in 0.02% MS-222 (Sigma-Aldrich) and placed on a block of Sylgard 184 silicone elastomer (Dow Silicones) with a carved indentation

to hold the animal immersed in a small amount of medium. Stacks of 512 x 512 pixel images stepping through the tectum were collected at two magnifications: low magnification 1.492 µm per pixel to show both tectal hemispheres; high magnification 0.482 µm per pixel to focus on one tectal hemisphere. Low magnification images were first denoised using the CANDLE algorithm (Coupé et al., 2012) implemented in MATLAB (MathWorks, RRID: SCR_001622), then segmented in 3D Slicer (Fedorov et al., 2012) to obtain volume measurements of the tectum and tectal neuropil. High magnification images were used to reconstruct the dendritic trees of the dextran-labelled cells using the TREES Toolbox (Cuntz et al., 2010) in MATLAB. Total branch length, dendrite spanning volume and Sholl analyses of the reconstructed dendritic trees were calculated using TREES Toolbox functions.

Functional imaging and visual stimulation

Tadpoles were immobilized by immersion in 2 mM pancuronium bromide (Abcam) and embedded in 1% low melting point agarose in a custom chamber with a glass coverslip window on one side, through which the animal could view visual stimuli presented on an LCD screen. The LCD display area measured 6.5 cm (width) × 4 cm (height). The tadpole was positioned so the eye was 2.2 cm from the screen, aligned to the center of the bottom edge of the display area. From this viewpoint, the display area spans roughly 110° of visual angle in azimuth and 80° in elevation. A #29 dark red Wratten filter (Kodak) was installed on the LCD screen to prevent light from the display from interfering with the calcium signal. Custom MATLAB scripts based on the Psychophysics Toolbox (Brainard, 1997; Kleiner et al., 2007; Pelli, 1997) (RRID: SCR_002881) were used to generate the visual stimuli and synchronize stimulus presentation with image capture. Visual stimuli were presented monocularly, and calcium signal was imaged from the tectum contralateral to the stimulated eye. Images were captured by rapidly scanning through 10 optical sections (with 3 flyback frames) at 4.5 Hz and 256 × 256-pixel resolution (0.963 µm per pixel).

Receptive field mapping and analysis

Processing and analyses of calcium imaging data were performed with custom scripts in MATLAB and Fiji (RRID: SCR_002285). ROI segmentation and fluorescence trace

extraction for postsynaptic tectal cells were performed with Suite2P (Pachitariu et al., 2016). Image alignment and motion correction were performed with either the MATLAB imregtform() library function, NoRMCorre (Pnevmatikakis & Giovannucci, 2017) implemented in MATLAB, or Suite2P.

Receptive field mapping

Receptive field mapping using drifting bar stimuli was performed as previously described (Li et al., 2022). Briefly, a mapping stimulus consisting of a single vertical or horizontal black bar drifting at a constant rate along the full span of the anterior-posterior or superior-inferior axis of the LCD screen was presented repeatedly at regular intervals while recording calcium responses in the tectum. A Fourier transform was applied to the first differential of response traces, the Fourier component at the stimulus frequency yielding the amplitude and phase of the peak response to the stimulus. The phase of the peak stimulus response converts to receptive field position.

To correct for latency in the response due to the continuous activation of retinotectal neurons by the stimulus, mapping experiments were conducted in pairs of trials where the stimulus bars sweep in opposite directions, then a difference was taken between the response phases from the two trials to obtain an absolute response phase. For an experiment with an interval of t_{blank} between repeated drifting bar presentations, absolute phase φ^+ can be found by

$$\varphi^+ = (\varphi_1 - \varphi_2 - t_{blank}) / 2$$

where φ^1 and φ^2 are the relative phases in the two opposite directions.

Signal to noise ratio

Signal to noise ratio (SNR) of a stimulus-evoked response is defined as A_r/σ, where A_r is the amplitude of the Fourier component at the stimulus frequency, and σ is the standard deviation of all amplitudes at frequencies above the stimulus frequency. When using SNR as thresholds for data analysis and display in Fig.IV.2 through 5, the smaller of the two SNR values from a pair of mapping experiments was used. For evaluating SNR levels in cell body ROIs in Fig.IV.5a and 5c, the larger of the two SNR values from a pair of mapping experiments was used.

Direction selectivity index

Direction selectivity index (DSI) was calculated for a pair of drifting bar directions (azimuth: forward vs reverse; elevation: upwards vs downwards) as

$$DSI = 1 - (A_{nonpreferred} / A_{preferred})$$

where $A_{preferred}$ is the amplitude of the response to the preferred direction, and $A_{nonpreferred}$ is the amplitude of the response to the opposite direction.

Comparing RF phase distributions via histogram intersection

To compare the distribution of RF phase values recorded from the whole neuropil versus the dendrites of dextran-labelled cells, we evaluated the similarity between the two distributions by computing their histogram intersection, as defined by Swain and Ballard (1991).

We mapped RF phase values for all voxels from the neuropil and dextran groups onto the stimulus display field and binned them into 2D histograms with 50 bins along each visual axis (azimuth and elevation), totaling n=2500 bins (Fig.IV.3c). Bin counts for each individual bin were normalized so that the sum of all bin counts in the 2D histogram equaled 1.

The intersection between the histogram for RF phase values for dextran-labelled voxels, *D*, and the histogram for RF phase values from all neuropil voxels, *M*, is defined to be

$$\sum_{i=1}^{n} \min (D_i, M_i)$$

The match value between the two histograms is defined as

$$H(D, M) = \frac{\sum_{j=1}^{n} \min (D_i, M_i)}{\sum_{j=1}^{n} M_j}$$

The match value *H(D, M)* is a fractional value between 0 and 1, where higher match values indicate greater similarity between the two distributions.

Mean centering correction for phase values

We expected inter-animal variability to affect early-late stage comparisons disproportionately more when looking at the dendritic fields of single cells compared to

when looking at the whole neuropil. We therefore performed corrections on the phase data shown in Fig.IV.3b as follows:

For each animal, calculate the mean phase of all voxels colocalized with the dendritic fields of dextran-labelled cells at early and late stages, X_{dex_early} and X_{dex_late}, and the mean phase of all voxels in the neuropil at early and late stages, X_{np_early} and X_{np_late}.

For early-stage data, the corrected phase value $\varphi_{corrected}$ is calculated from the raw phase value φ_{raw} as

$$\varphi_{corrected} = \varphi_{raw} - X_{dex\_early.}$$

For late-stage data, the corrected phase $\varphi_{corrected}$ is calculated from the raw phase φ_{raw} as

$$\varphi_{corrected} = \varphi_{raw} - X_{dex\_early} - (X_{np\_late} - X_{np\_early})$$

Statistical analysis

Statistical tests, as indicated in the figure legends, were performed using Graphpad Prism 10 (GraphPad software, RRID: SCR_002798).

Acknowledgements

This work was funded by a Natural Sciences and Engineering Research Council of Canada grant (RGPIN-2024-05306) and Canadian Institutes of Health Research grant (PJT-180478) to ESR, a Molson Neuro-Engineering Award, Shuk-Tak Liang Fellowship and McGill University Integrated Program in Neuroscience Studentship to VJL.

References

Beach, D., & Jacobson, M. (1979). Patterns of cell proliferation in the retina of the clawed frog during development. *Journal of Comparative Neurology*, *183*(3), 603-613.

Brainard, D. H. (1997). The Psychophysics Toolbox. *Spatial Vision*, *10*(4), 433-436. https://doi.org/10.1163/156856897x00357

Chen, T.-W., Wardill, T. J., Sun, Y., Pulver, S. R., Renninger, S. L., Baohan, A., Schreiter, E. R., Kerr, R. A., Orger, M. B., Jayaraman, V., Looger, L. L., Svoboda, K., & Kim, D. S. (2013). Ultrasensitive fluorescent proteins for imaging neuronal activity. *Nature*, *499*(7458), 295-300. https://doi.org/10.1038/nature12354

Chung, S.-H., Keating, M., & Bliss, T. (1974). Functional synaptic relations during the development of the retino-tectal projection in amphibians. *Proceedings of the Royal Society of London. Series B. Biological Sciences*, *187*(1089), 449-459.

Cline, H. T., & Kelly, D. (2012). Xenopus as an experimental system for developmental neuroscience: introduction to a special issue. In (Vol. 72, pp. 463-464).

Coupé, P., Munz, M., Manjón, J. V., Ruthazer, E. S., & Collins, D. L. (2012). A CANDLE for a deeper in vivo insight. *Medical image analysis*, *16*(4), 849-864.

Cuntz, H., Forstner, F., Borst, A., & Häusser, M. (2010). One rule to grow them all: a general theory of neuronal branching and its practical application. *PLoS computational biology*, *6*(8), e1000877.

Dunfield, D., & Haas, K. (2010). In vivo single-cell excitability probing of neuronal ensembles in the intact and awake developing Xenopus brain. *Nature protocols*, *5*(5), 841-848.

Fedorov, A., Beichel, R., Kalpathy-Cramer, J., Finet, J., Fillion-Robin, J.-C., Pujol, S., Bauer, C., Jennings, D., Fennessy, F., & Sonka, M. (2012). 3D Slicer as an image computing platform for the Quantitative Imaging Network. *Magnetic resonance imaging*, *30*(9), 1323-1341.

Gaze, R., Chung, S., & Keating, M. (1972). Development of the retinotectal projection in Xenopus. *Nature New Biology*, *236*(66), 133-135.

Gaze, R., Keating, M., Ostberg, A., & Chung, S. (1979). The relationship between retinal and tectal growth in larval Xenopus: implications for the development of the retino-tectal projection. *Development*, *53*(1), 103-143.

Gaze, R. M., Keating, M., & Chung, S. (1974). The evolution of the retinotectal map during development in Xenopus. *Proceedings of the Royal Society of London. Series B. Biological Sciences*, *185*(1080), 301-330.

Haas, K., Jensen, K., Sin, W. C., Foa, L., & Cline, H. T. (2002). Targeted electroporation in Xenopus tadpoles in vivo–from single cells to the entire brain. *Differentiation*, *70*(4-5), 148-154.

Haas, K., Sin, W.-C., Javaherian, A., Li, Z., & Cline, H. T. (2001). Single-cell electroporationfor gene transfer in vivo. *Neuron*, *29*(3), 583-591.

Herrgen, L., & Akerman, C. J. (2016). Mapping neurogenesis onset in the optic tectum of Xenopus laevis. *Developmental neurobiology*, *76*(12), 1328-1341.

Hollyfield, J. G. (1971). Differential growth of the neural retina inXenopus laevis larvae. *Developmental biology*, *24*(2), 264-286.

Holt, C. E., & Harris, W. A. (1983). Order in the initial retinotectal map in Xenopus: a new technique for labelling growing nerve fibres. *Nature*, *301*(5896), 150-152. https://doi.org/10.1038/301150a0

Kleiner, M., Brainard, D., & Pelli, D. (2007). What's new in Psychtoolbox-3?

Kutsarova, E., Munz, M., & Ruthazer, E. S. (2017). Rules for Shaping Neural Connections in the Developing Brain. *Frontiers in neural circuits*, *10*, 111-111. https://doi.org/10.3389/fncir.2016.00111

Lazar, G. (1973). The development of the optic tectum in Xenopus laevis: a Golgi study. *Journal of anatomy*, *116*(Pt 3), 347.

Li, V. J., Schohl, A., & Ruthazer, E. S. (2022). Topographic map formation and the effects of NMDA receptor blockade in the developing visual system. *Proceedings of the National Academy of Sciences*, *119*(8), e2107899119.

Liu, Z., Hamodi, A. S., & Pratt, K. G. (2016). Early development and function of the Xenopus tadpole retinotectal circuit. *Current Opinion in Neurobiology*, *41*, 17-23.

Mann, F., Harris, W. A., & Holt, C. E. (2004). New views on retinal axon development: a navigation guide. *The International journal of developmental biology*, *48*, 957.

McFarlane, S., & Lom, B. (2012). The Xenopus retinal ganglion cell as a model neuron to study the establishment of neuronal connectivity. *Developmental Neurobiology*, *72*(4), 520-536.

Molotkov, D., Ferrarese, L., Boissonnet, T., & Asari, H. (2023). Topographic axonal projection at single-cell precision supports local retinotopy in the mouse superior colliculus. *Nature communications*, *14*(1), 7418.

Munz, M., Gobert, D., Schohl, A., Poquerusse, J., Podgorski, K., Spratt, P., & Ruthazer, E. S. (2014). Rapid Hebbian axonal remodeling mediated by visual stimulation. *Science*, *344*(6186), 904-909. https://doi.org/10.1126/science.1251593

Nieuwkoop, P. D., & Faber, J. (1994). *Normal Table of Xenopus Laevis (Daudin): A Systematical and Chronological Survey of the Development from the Fertilized Egg Till the End of Metamorphosis*. Garland Pub.

Pachitariu, M., Stringer, C., Schröder, S., Dipoppa, M., Rossi, L. F., Carandini, M., & Harris, K. D. (2016). Suite2p: beyond 10,000 neurons with standard two-photon microscopy. *bioRxiv*, 061507.

Pelli, D. G. (1997). The VideoToolbox software for visual psychophysics: Transforming numbers into movies. *Spatial Vision*, *10*, 437-442.

Pnevmatikakis, E. A., & Giovannucci, A. (2017). NoRMCorre: An online algorithm for piecewise rigid motion correction of calcium imaging data. *Journal of*

Neuroscience Methods, *291*, 83-94. https://doi.org/10.1016/j.jneumeth.2017.07.031

Roth, G., & Walkowiak, W. (2015). The influence of genome and cell size on brain morphology in amphibians. *Cold Spring Harbor perspectives in biology*, *7*(9), a019075.

Ruthazer, E. S., Schohl, A., Schwartz, N., Tavakoli, A., Tremblay, M., & Cline, H. T. (2013). In vivo time-lapse imaging of neuronal development in Xenopus. *Cold Spring Harbor Protocols*, *2013*(9), pdb. top077156.

Sakaguchi, D. S., & Murphey, R. K. (1985). Map formation in the developing Xenopus retinotectal system: an examination of ganglion cell terminal arborizations. *Journal of Neuroscience*, *5*(12), 3228-3245. https://doi.org/10.1523/JNEUROSCI.05-12-03228.1985

Straznicky, K., & Gaze, R. (1971). The growth of the retina in Xenopus laevis: an autoradiographic study. *Development*, *26*(1), 67-79.

Straznicky, K., & Gaze, R. (1972). The development of the tectum in Xenopus laevis: an autoradiographic study. *Development*, *28*(1), 87-115.

Swain, M. J., & Ballard, D. H. (1991). Color indexing. *International journal of computer vision*, *7*(1), 11-32.

Wu, G.-Y., Malinow, R., & Cline, H. (1996). Maturation of a central glutamatergic synapse. *Science*, *274*(5289), 972-976.

Figures

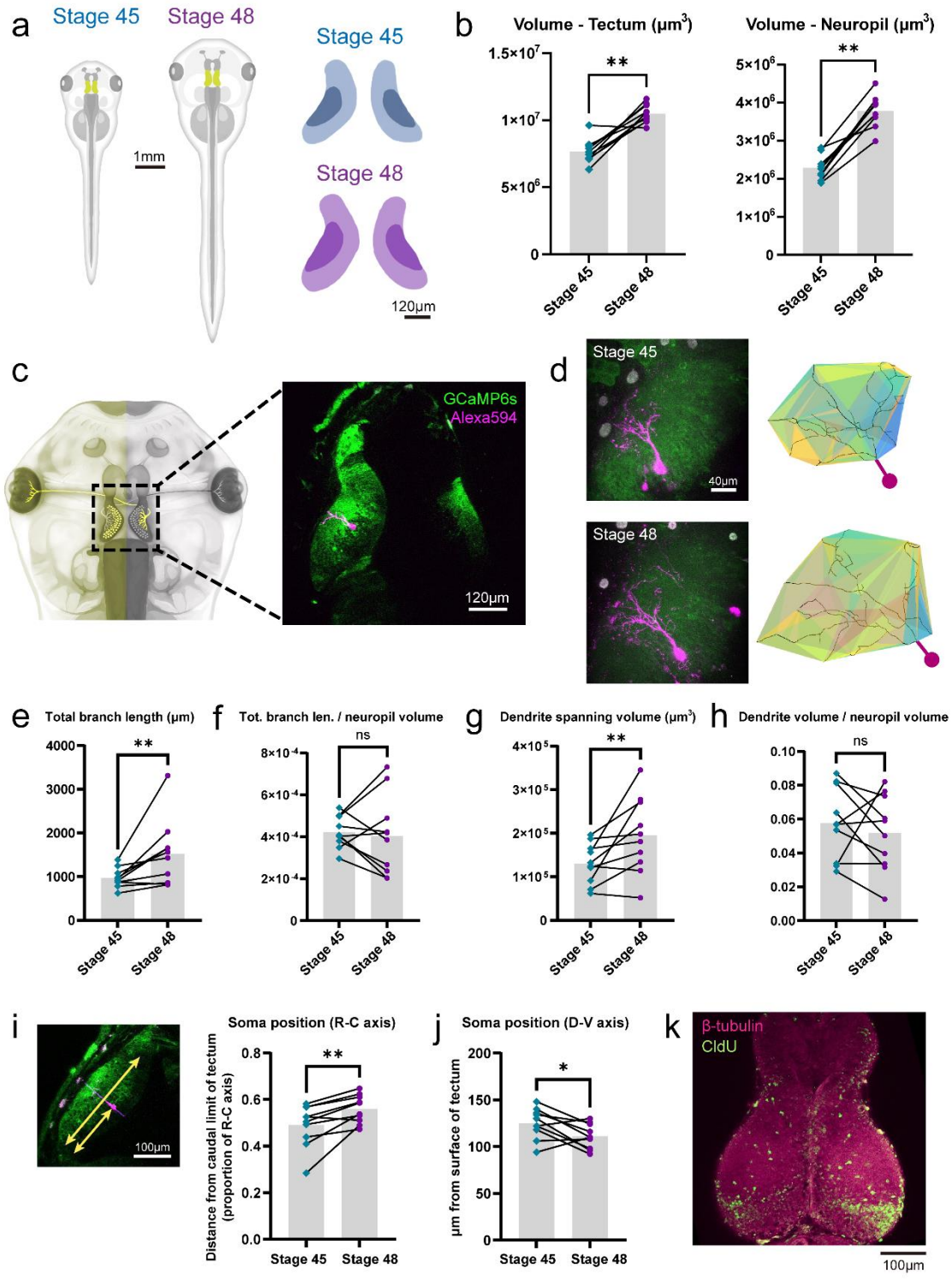
a
Stage 45
Stage 48
1mm
Stage 45
Stage 48
120µm
b
Volume - Tectum (µm3)
Volume - Neuropil (µm3)
**
**
Stage 45
Stage 48
c
GCaMP6s
Alexa594
120µm
d
Stage 45
40µm
Stage 48
e
Total branch length (µm)
**
f
Tot. branch len. / neuropil volume
ns
g
Dendrite spanning volume (µm3)
**
h
Dendrite volume / neuropil volume
ns
i
100µm
Soma position (R-C axis)
Distance from caudal limit of tectum (proportion of R-C axis)
**
j
Soma position (D-V axis)
µm from surface of tectum
*
k
β-tubulin
CldU
100µm

Figure IV.1. Morphometric changes in the tadpole tectum between stages 45 and 48.

(a) Illustration of the tadpole and tadpole tectum at stages 45 and 48. The neuropil of the tectum is represented by darker colors.

(b) Volume of the tectum and tectal neuropil increased significantly from stage 45 to 48 (Wilcoxon matched pairs test, n=10 animals, tectum **p=0.0039; neuropil **p=0,0020)

(c) (Left) Schematic of a tadpole with hemimosaic GCaMP6s expression restricted to the left half of the animal. (Right) Two-photon image showing GCaMP6s expression limited to tectal cells in the left and RGC axons in the right tectal hemisphere. A single postsynaptic cell in the left tectal hemisphere was labelled with Alexa Fluor 594 dextran fluorescent dye.

(d) (Left) Maximum projection images of the left tectal hemisphere of the same tadpole at stages 45 and 48, with a single postsynaptic tectal neuron labelled with Alexa 594 dextran. (Right) Reconstructions of the dendritic tree of the dextran-labelled cell, with colored patches showing the boundaries of its 3D spanning volume.

(e) Dendritic total branch length increased from stage 45 to 48 (Wilcoxon matched pairs test, n=10 animals, **p=0.0039)

(f) Dendrite density, calculated as total branch length divided by neuropil volume, did not change significantly (p=0.7695)

(g) Dendrite spanning volume increased from stage 45 to 48 (**p=0.0098)

(h) Dendrite coverage, calculated as dendrite spanning volume divided by neuropil volume, did not change significantly (p=0.3750)

(i) Position of the cell soma along the rostrocaudal (R-C) axis was calculated as the distance from the soma to the caudal limit of the tectum divided by the full length of the R-C axis. Labeled neuronal somata shifted rostrally from stage 45 to stage 48 (**p=0.0039).

(j) Position of the cell soma along the dorsoventral (D-V) axis. From stage 45 to stage 48, cell somata shifted deeper below the dorsal surface of the tectum (*p=0.0430).

(k) β-tubulin and CldU labelling in the tectum of an animal treated with 10 mM CldU for 2 h at stage 45 and sacrificed at stage 48. CldU labelling can be seen distributed in the cell body layer in a laminar fashion, revealing the linear proliferation pattern of tectal neurons. CldU puncta can also be seen sparsely distributed in the tectal neuropil.

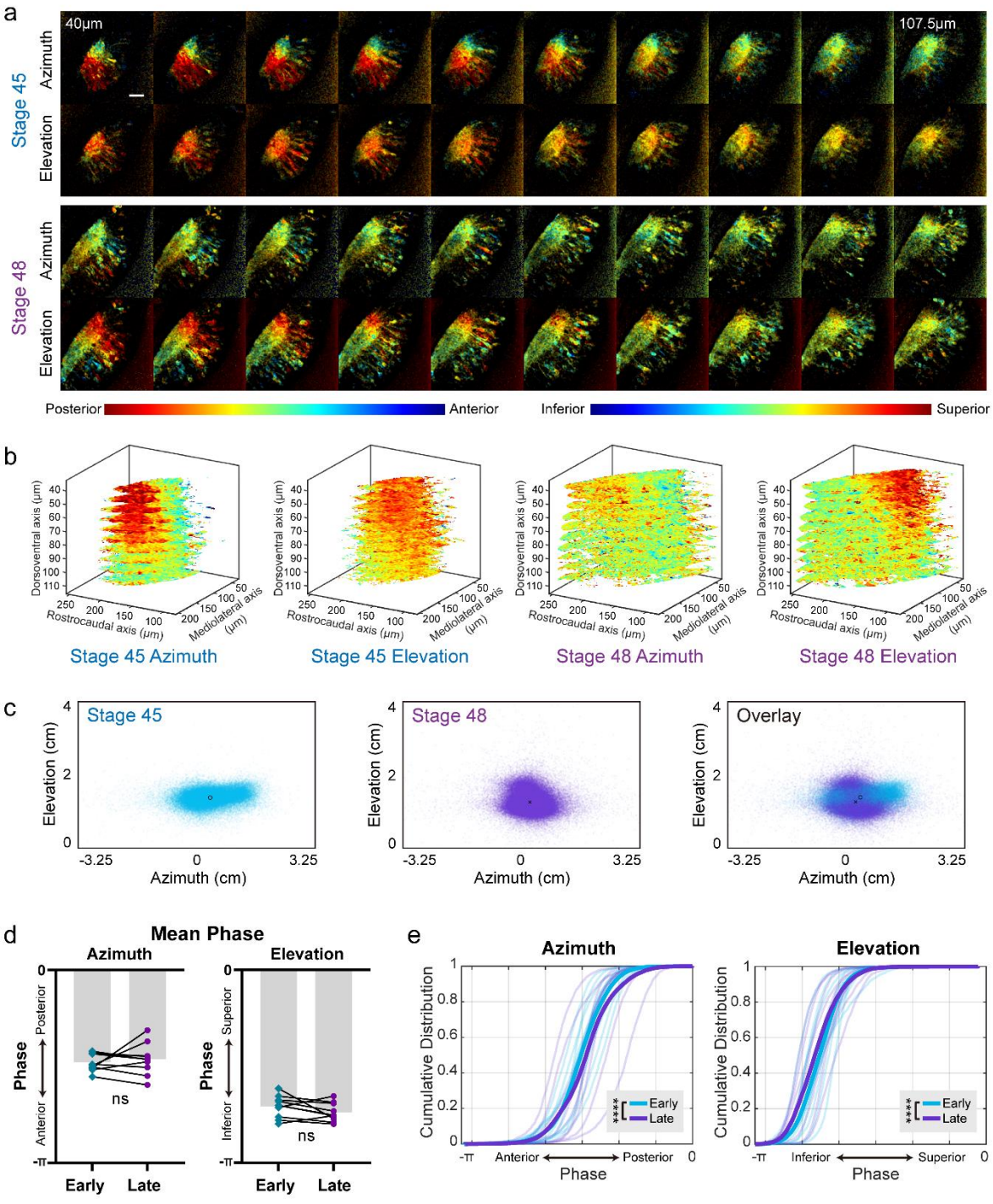

Figure IV.2. Visual receptive fields represented in the tectal neuropil at different developmental stages.

(a) Azimuth and elevation receptive field maps from the same animal at stage 45 and stage 48. Receptive field (RF) positions were calculated as the phase of the response to

a repeated drifting bar stimulus in the corresponding axis. Pixel intensities indicate signal-to-noise ratio (SNR). Images were taken in stacks of 10 optical sections starting at approximately 40 μm depth from the surface of the tectum, at 7.5 μm intervals between sections.

(b) 3D renderings of the phase maps from (a), showing only voxels in the neuropil with SNR > 2.

(c) Neuropil receptive field positions from (b) (all optical sections) mapped onto the stimulus display field.

(d) Mean neuropil phase did not differ between early and late stages for both azimuth and elevation axes (Wilcoxon matched pairs test, n=9 animals, azimuth p=0.7695, elevation p=1934)

(e) Cumulative probability distribution of neuropil receptive field phase values. Thin lines show data from individual animals (n=9), down sampled to 2000 random datapoints for each animal. Thick lines show pooled data from all animals. Kolmogorov–Smirnov tests on pooled data show a small but significant shift in the RF distributions between early and late stages for both azimuth and elevation (****p<0.0001).

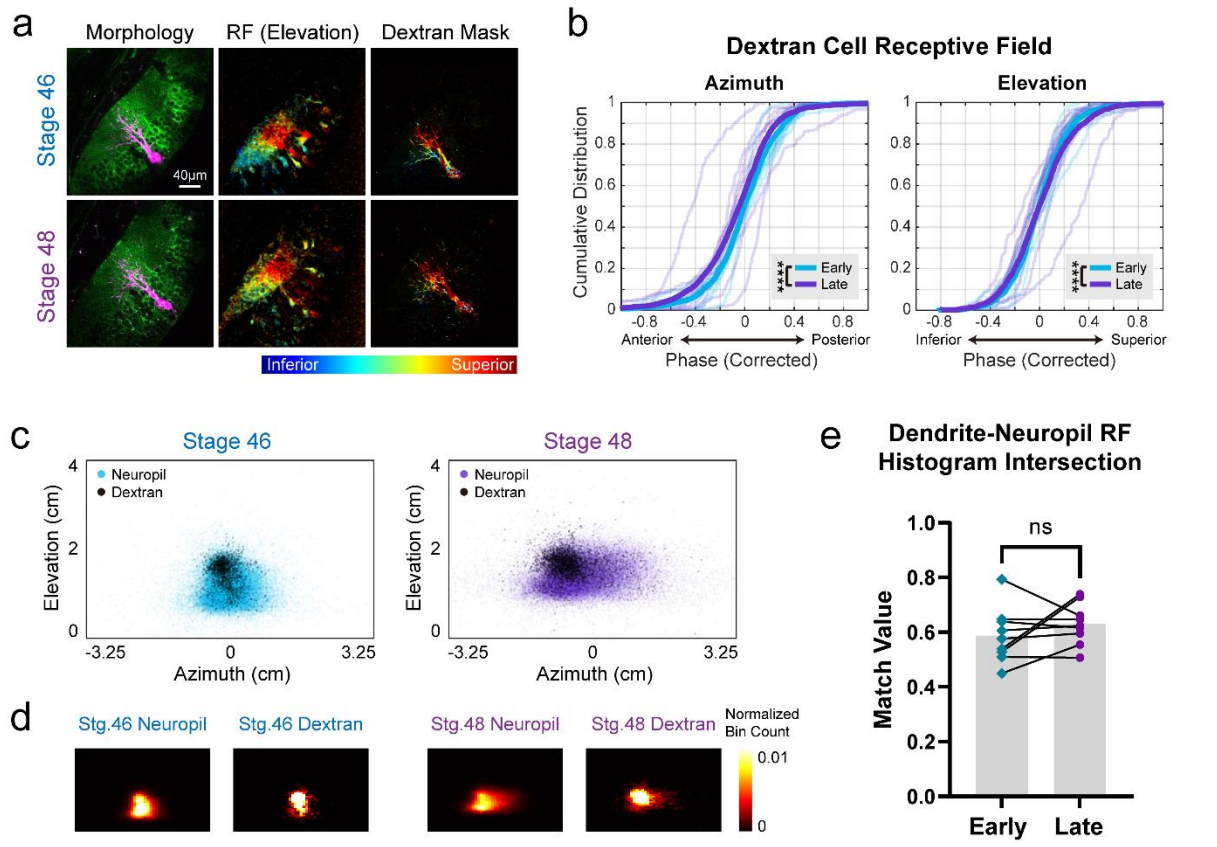

Figure IV.3. Receptive fields measured at the dendrites of single tectal neurons at different developmental stages.

(a) Example optical section from the same animal imaged at stage 46 and 48: (Left) Morphology of the tectum with a single-cell electroporated dextran-labelled neuron. (Middle) Elevation receptive field maps (pixel intensities indicate SNR). (Right) Elevation receptive field maps overlaid with mask of dextran labelling.

(b) Cumulative distribution of receptive field phase values recorded from areas in the neuropil with dextran labelling (data from 10 optical sections for each animal). Thin lines show data from individual animals (n=9), down sampled to 200 datapoints for each animal. Thick lines show pooled data from all animals. Phase values were corrected by mean centering (see Methods). Kolmogorov–Smirnov tests on data pooled from all 9 animals show significant difference between early and late stages for both azimuth and elevation (****p<0.0001).

(c) RF phase values from the animal in (a) (data from 10 optical sections) mapped onto the stimulus display field. Colored scatter points represent data points from the neuropil; black scatter points represent datapoints from areas in the neuropil with dextran labelling.

(d) Heat maps showing the data from (c) binned into 2D histograms (50 x 50 bins. Bin counts were normalized so that the sum of all bin counts in each histogram equals 1).

(e) The match value (see Methods) between RF histograms for neuropil and dextran-labelled cells was high, and didn't change significantly between early and late stages (Wilcoxon matched pairs test, n=9 animals, p=0.4258).

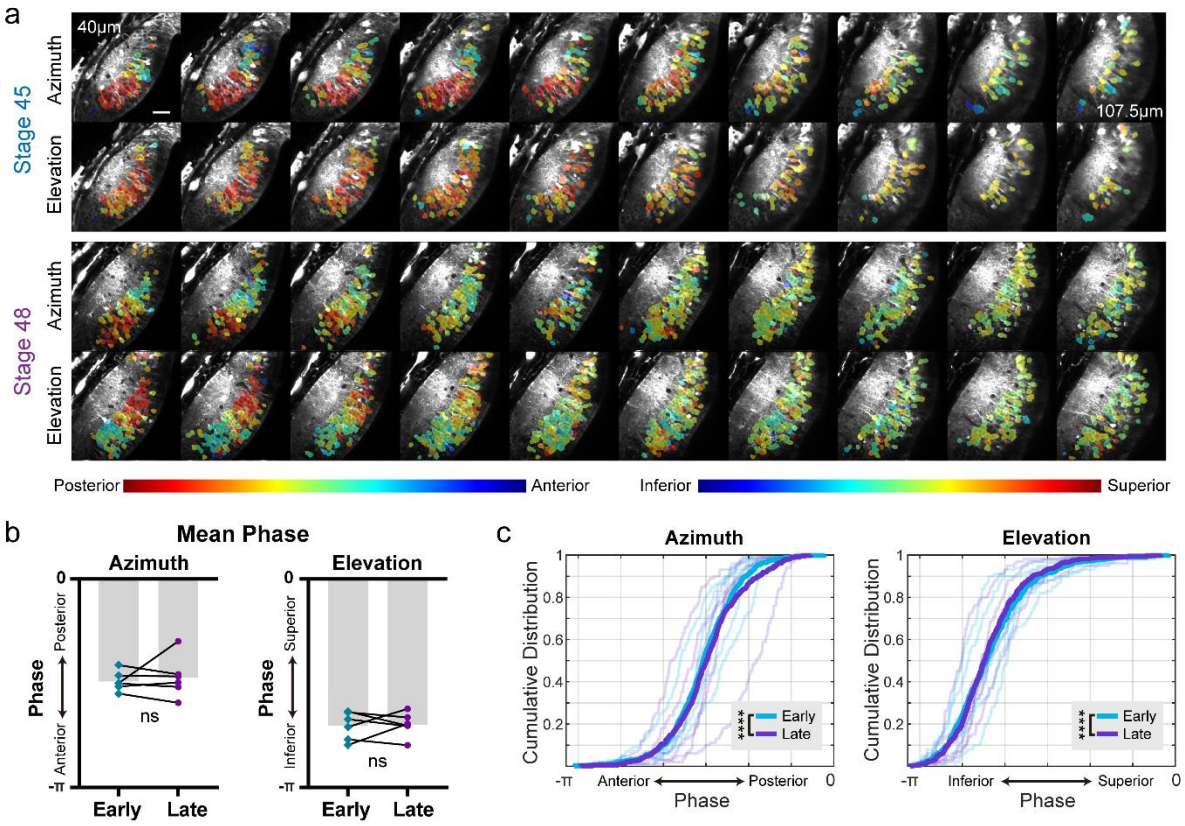

Figure IV.4. Receptive fields of tectal neuron cell bodies across developmental stages.

(a) Azimuth and elevation cell body receptive field maps from the same animal and showing the same optical sections as in Fig.IV.2a. RF phase values were calculated from the mean ΔF/F trace for each cell body ROI. Only cells with SNR > 2 are shown.

(b) Mean RF phase for each animal (n = 6). No significant difference between early and late stage animals (Wilcoxon matched pairs test, azimuth p=0.8438, elevation p>0.9999)

(c) Cumulative probability distributions of cell body RF phase values. Thin lines show data from individual animals (n=6), down sampled to 120 cells for each animal. Thick lines show pooled data from all animals. Kolmogorov–Smirnov tests on pooled data reveal a small difference between early and late stages for both azimuth and elevation (****p<0.0001).

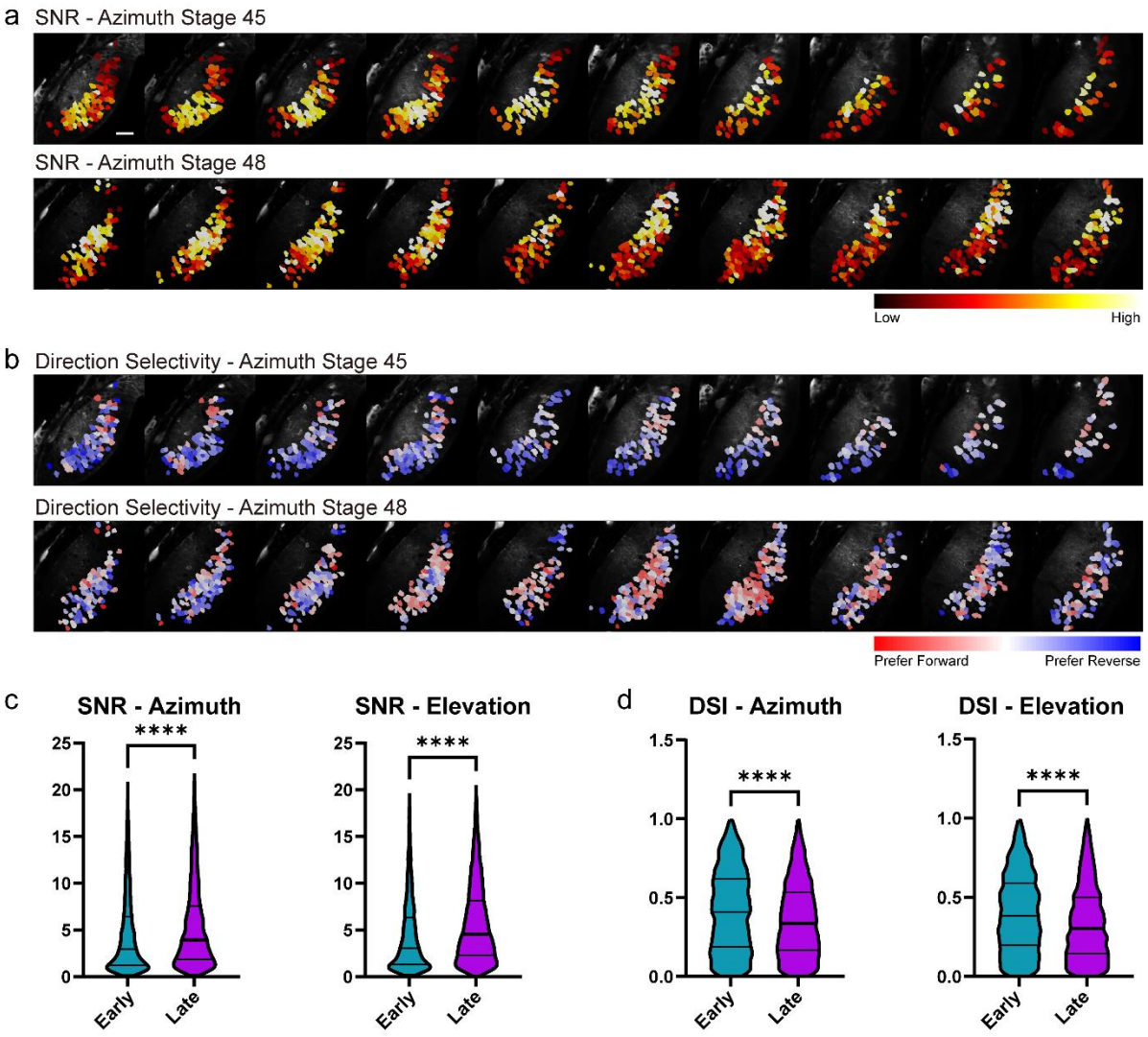

Figure IV.5. Signal to noise ratio and direction selectivity in postsynaptic tectal cells.

(a) SNR of cell body responses to drifting bars in the same animal at stage 45 and 48.

(b) Direction selectivity of tectal cells. Darker colors indicate a higher direction selectivity index (DSI).

(c) SNR of cell body responses to drifting bars at early (stage 45-46) and late (stage 48) stages, cells pooled from 5 animals. SNR was significantly higher at late stage for both azimuth and elevation (two-tailed Mann-Whitney test, azimuth $U= 5.931x10^6$, ****$p<0.0001$, $median_{early}=2.958$, $n=3679$, $median_{late}=3.943$, $n=3781$; elevation $U=5.559$

x10^6, ****p<0.0001, $median_{early}$=3.047, n=3633, $median_{late}$=4.532, n=3886)

(d) DSI of tectal cells at early and late stages, pooled from 5 animals. Only cells with SNR>2 were included. DSI was significantly lower at late stage for both azimuth and elevation (two-tailed Mann-Whitney test, azimuth U= 2.609x10^6, ****p<0.0001, $median_{early}$=0.4097, n=2185, $median_{late}$=0.3363, n=2704; elevation U= 2.818x10^6, ****p<0.0001, $median_{early}$=0.3816, n=2206, $median_{late}$=0.3022, n=2999)

Supplementary Figures

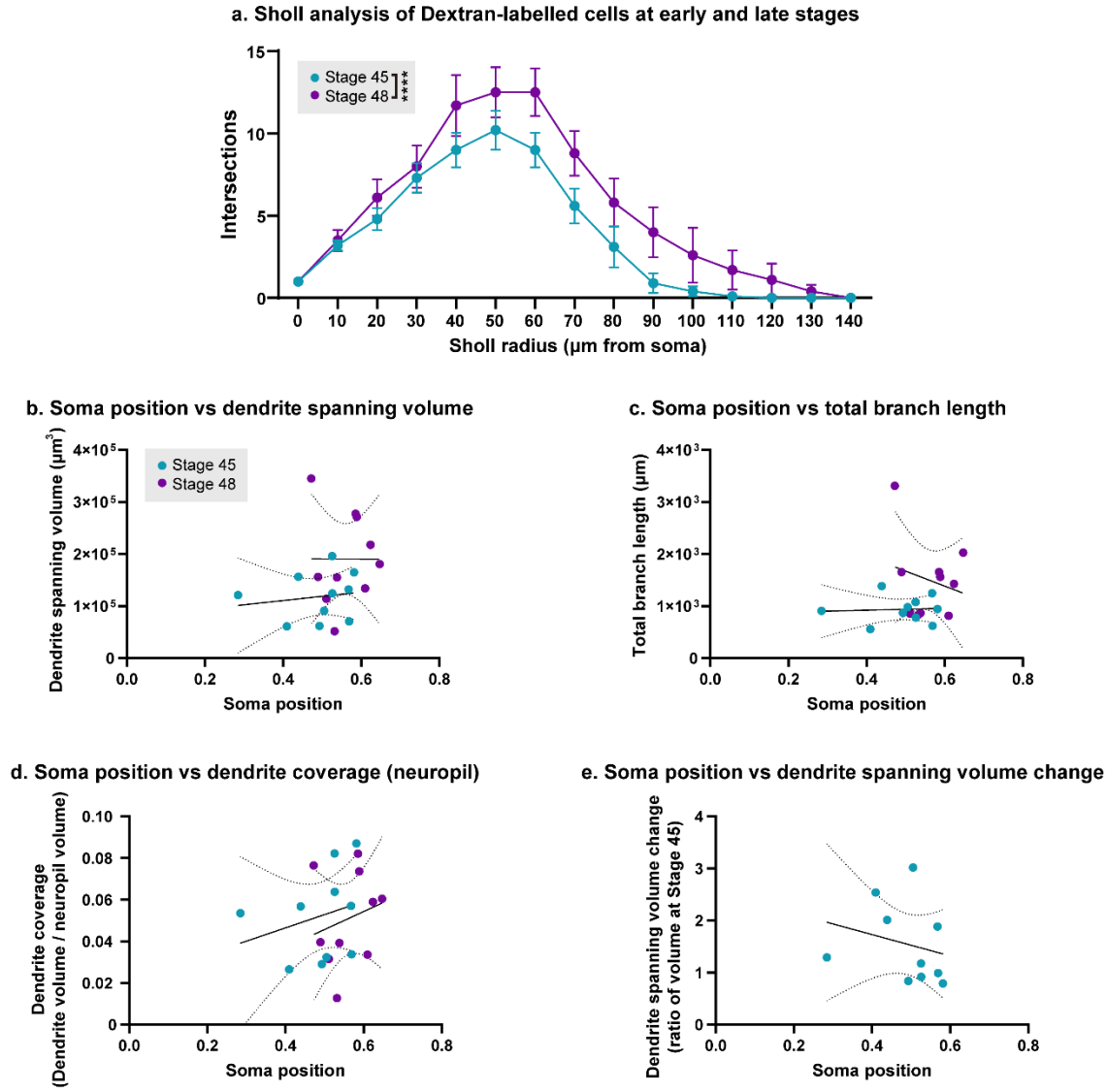

Figure IV.S1. Morphometric changes in dextran-labelled cells between stages 45 and 48.

(a) Sholl analysis for dextran-labelled cells at Stage 45 and 48 (mean ± SEM number of intersections, n=10 animals). Two-factor repeated measures ANOVA for stage and Sholl radius found significant main effects for both stage and Sholl radius (Stage $F(1,135) = 35.55$, ****$p<0.0001$); Sholl radius $F(14,135) = 22.45$, ****$p<0.0001$). **(b~e)** Relationships between various morphometric measurements of dextran-labelled cells and the position of their cell soma along the rostro-caudal axis of the tectum. Solid and dotted lines show linear regressions (performed separately for stage 45 and 48 data) and their 95% confidence intervals.

(b) Soma position vs dendrite spanning volume. Slopes for linear regressions were not significantly different from zero ($p_{45} = 0.6594$, $p_{48} = 0.9950$).

(c) Soma position vs total branch length. Slopes for linear regressions were not significantly different from zero ($p_{45} = 0.8643$, $p_{48} = 0.5366$).

(d) Soma position vs dendrite coverage (dendrite spanning volume divided by total neuropil volume). Slopes for linear regressions were not significantly different from zero ($p_{45} = 0.4535$, $p_{48} = 0.5310$).

(e) Soma position at Stage 45 vs change in dendrite coverage between Stage 45-48. Slope for linear regression was not significantly different from zero ($p = 0.5045$).

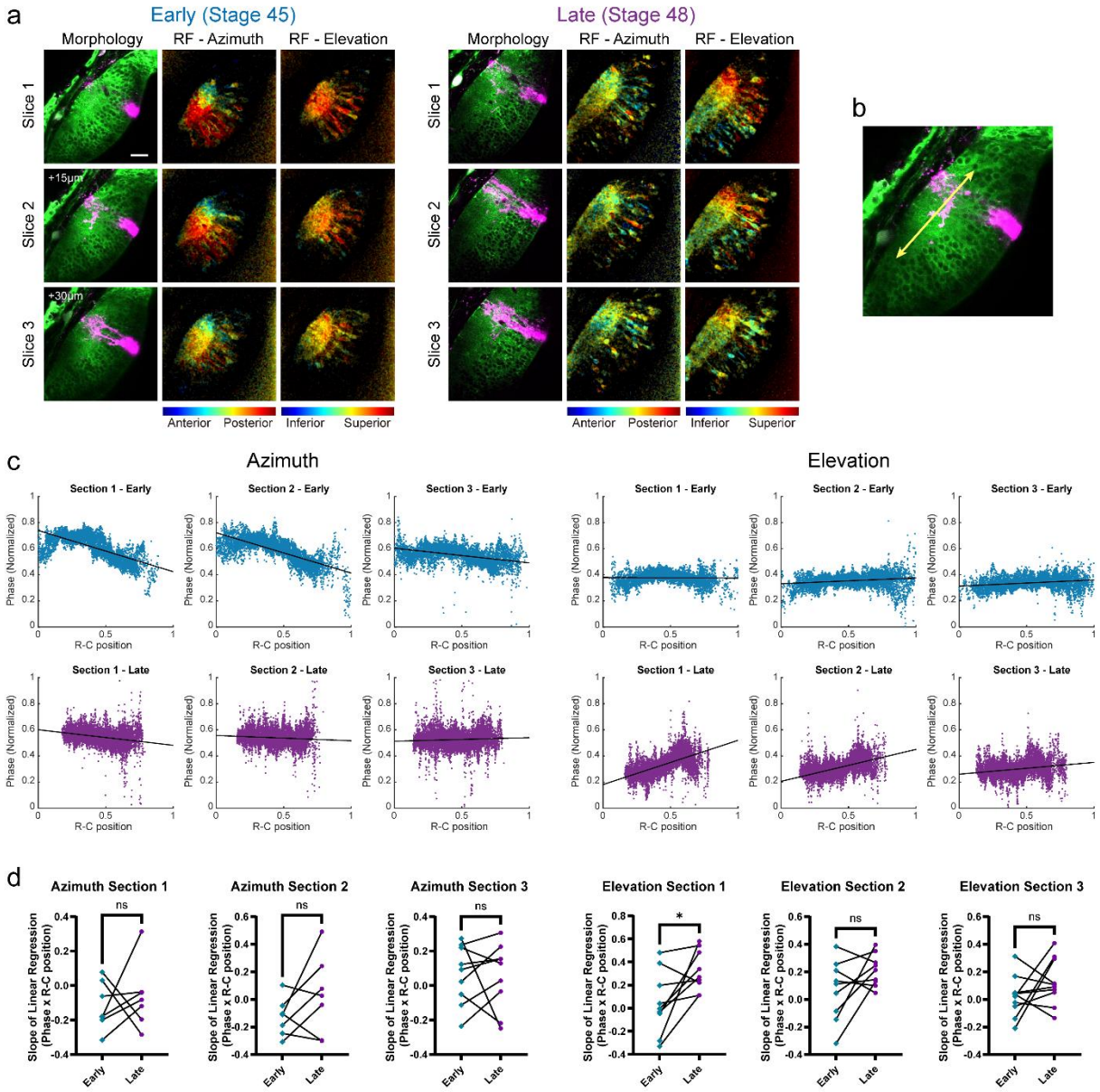

Figure IV.S2: Comparing retinotopic gradients in three matched optical sections from the same animal at early and late stages.

(a) Example images from one animal. Scale bar in upper left image is 40 µm. The three optical sections are spaced 15 µm in depth from each other, with Section 3 at the bottommost depth. In each row of 3 images for each optical section: (Left) Morphology of the tectum showing dextran-labelled cell. (Middle) Azimuth receptive field map (pixel intensities indicate SNR). (Right) Elevation receptive field map.

(b) For each stage, the rostrocaudal axis of the neuropil of the center section Section 2 was used as the reference R-C axis when quantifying the topographic gradients along the R-C axis. An R-C position of 0 is closest to the caudal edge of the neuropil, 1 is closest to the rostral end.

(c) Distribution of receptive field phase values along the R-C axis for the example animal and optical sections shown in (a). Black line shows simple linear regressions fitted to the data. Phase values are scaled from the original range of [-pi, 0] to a range of [0, 1], so that a linear regression slope of 1 or -1 indicates a topographic gradient that is perfectly perpendicular to the R-C axis.

(d) Comparing slopes of linear regressions fitted to phase vs R-C position (n=10 animals). Data for animals/sections where the linear regression wasn’t a good fit (i.e. an F-test shows the regression did not fit significantly better than a constant model) was excluded. Comparing slope values at early vs late stages yielded no significant direction of change for all cases except for the elevation gradients in Section 1, which showed a significant increase (Wilcoxon matched-pairs test, $p = 0.0273$).

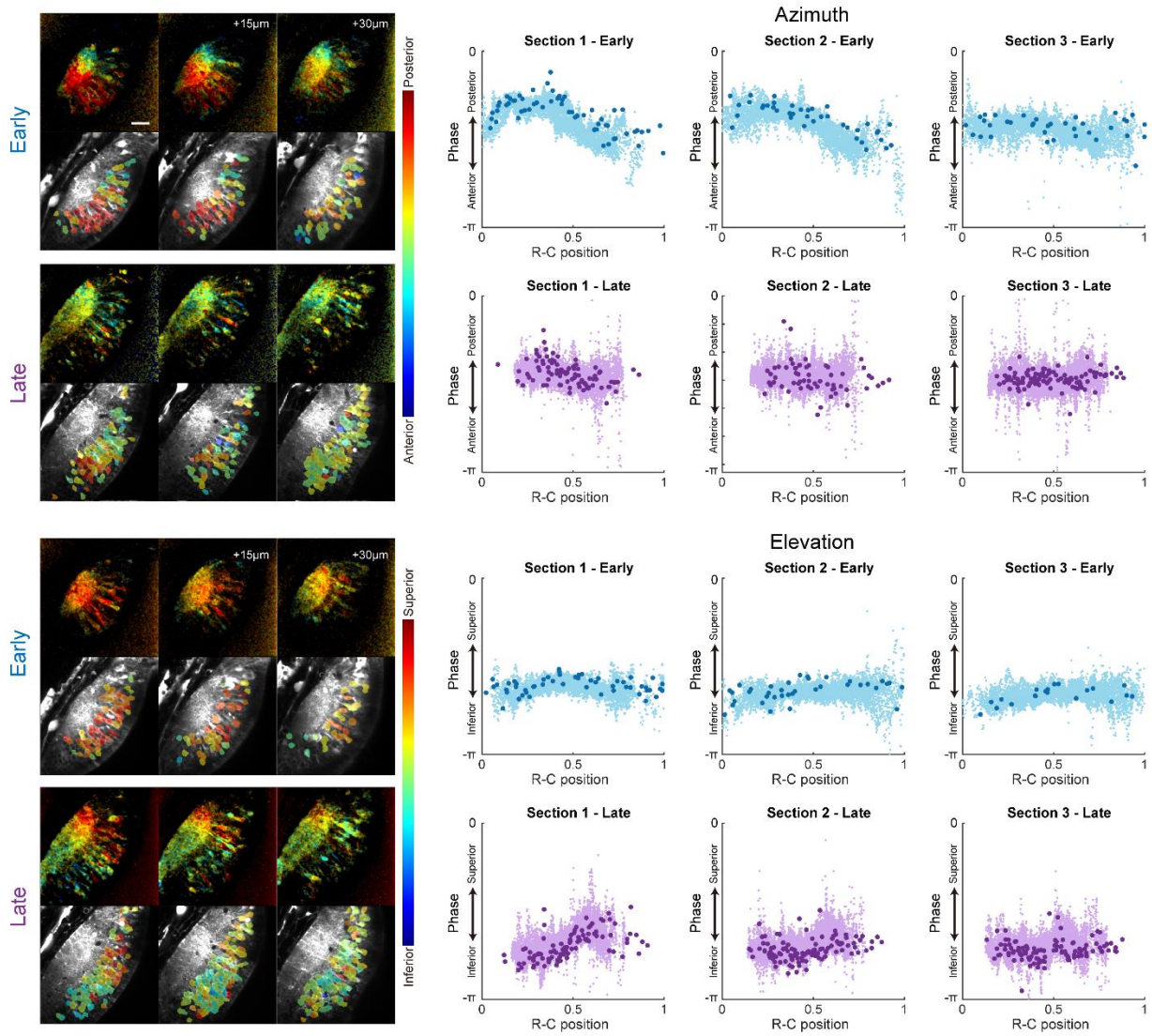

Figure IV.S3. Comparing the distribution of retinotopic representations from the neuropil and cell bodies.

Data from same animal and optical sections shown in Fig.IV.S2(a-c). Scale bar in upper left image is 40 μm. Dark points in scatterplots denote data from cell bodies, lighter points denote data from the neuropil.

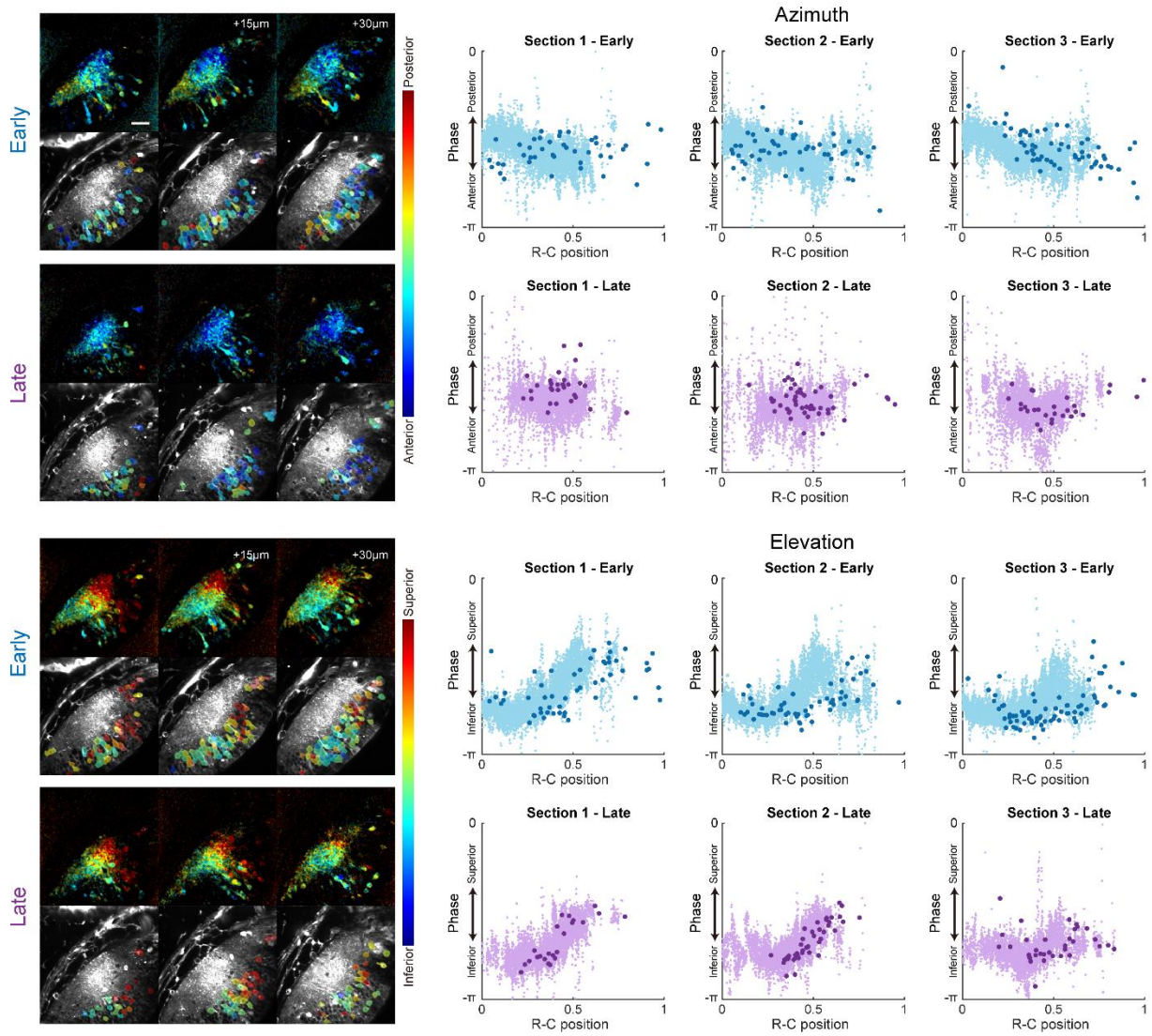

Figure IV.S4. Comparing the distribution of retinotopic representations from the neuropil and cell bodies, showing data from a second animal.

Scale bar in upper left image is 40 μm. Dark points in scatterplots denote data from cell bodies, lighter points denote data from the neuropil.

Chapter V: Discussion

Author contributions

Vanessa Li wrote this chapter, with revisions by Edward Ruthazer.

Characterizing the developing retinotopic map in the tadpole tectum

What does the retinotopic map in the Xenopus tadpole tectum look like in its early days of development, how does it change as the tadpole grows, and what are the underlying mechanisms that can affect its outcome? Focusing on a time range between developmental stage 42 to 48, a period of robust growth and refinement in the retinotectal circuit, we developed a procedure to perform retinotopic mapping in tadpoles with calcium imaging, which gave us a detailed view of 3D functional retinotopy in the young tadpole tectum and how it changes over several days. To our knowledge, this is the first example of a longitudinal study on visual receptive field map development for the earliest moments of retinotectal innervation and visual responsiveness in Xenopus. The use of two-photon calcium imaging allowed us to detect neuronal activity and perform retinotopic mapping at a much higher spatial resolution than previous electrophysiology studies (Gaze et al., 1974; Holt & Harris, 1983). The improved spatial resolution was essential for capturing topographic features in the tadpole tectum, a tiny structure that is only a few hundred microns wide in these early developmental stages. We saw coarse topographic gradients at stage 42 that became smoother at stage 45 and 48, while receptive field sharpness estimated at cell body ROIs grew less diffuse, indicating refinement in the map during this period.

Role of activity-dependent plasticity

The role of activity-dependent mechanisms in the establishment and refinement of the retinotopic map was one of the key themes we wished to address in this project. Our

results showed that blocking NMDA receptor activity did not prevent the formation of retinotopic maps in the tectum by stage 48, but there was a subtle reduction in the smoothness of the topographic gradient and enlargement of tectal cell receptive fields. Molecular guidance cues, notably ephrin-A and EphB, are present in prominent gradients in the frog tectum during stage 45-48 (Higenell et al., 2012; Mann et al., 2002; Scalia et al., 2009). Our results support the notion that molecular guidance cues and other “hard-wired” activity-independent mechanisms play the main role in establishing the macroscopic retinotopic gradient during these stages, while activity-dependent refinement is mostly responsible for fine-scale tuning in local neighborhoods.

The extent that guidance from sensory activity is involved in the wiring of sensory circuits seems to vary under different scenarios. On one hand, the role of activity is heavily implicated in many aspects of cortical circuit wiring, such as the precise tuning of axon targeting in fish tectum (Gnuegge et al., 2001; Olson & Meyer, 1991) and rat superior colliculus (Simon & O'Leary, 1992); sharpening of receptive fields in the tadpole tectum (Dong et al., 2009; Van Horn et al., 2017; Vislay-Meltzer et al., 2006) and hamster superior colliculus (Razak & Pallas, 2006); the segregation of input in multimodal sensory circuits in the mouse superior colliculus (Guillamón-Vivancos et al., 2022); as well as the development of orientation and direction selectivity in the ferret visual cortex (Chapman & Stryker, 1993; Li et al., 2006). Computational models have shown that patterned neuronal activity alone is hypothetically capable of establishing ocular dominance and orientation selectivity maps displaying the signature “stripe” and “pinwheel” motifs (Goodhill, 1993; Obermayer et al., 1990; Swindale, 1996). On the other hand, recent studies have shown that fully functional circuits exhibiting normal response properties and behavioural output can be established in the absence of sensory activity (Barabási et al., 2024; Pietri et al., 2017).

It is worth noting that the most pronounced activity-dependent effects, where activity or the lack thereof drastically altered patterning in the resulting sensory map, were demonstrated in sensory deprivation experiments, specifically those that introduced an unbalanced sensory input substantially deviating from what the system would receive under normal circumstances. Examples are the classic monocular deprivation

experiments performed by Hubel and Wiesel (Hubel & Wiesel, 1970; Wiesel & Hubel, 1963) where absence of input from the deprived eye resulted in dramatic reduction in its cortical representation, and the “three-eyed frog” experiments (Cline et al., 1987; Constantine-Paton & Law, 1978; Reh & Constantine-Paton, 1985) where artificially introducing an additional line of visual input via implantation of a third eye produced ocular dominance columns in the normally monocular frog tectum. In contrast, bilateral deprivation of visual input left cortical visual maps surprisingly intact (Arcaro et al., 2018; Butt et al., 2013; Wiesel & Hubel, 1965). In the absence of sensory input, it would be hard-wired molecular guidance mechanisms and innate spontaneous activity leading the establishment of these cortical maps. In context, the relationship between innate “hard-wired” and activity-dependent mechanisms seems to be a complementary and dynamic one: in normal development with typical sensory experience, innate guidance mechanisms lay the groundwork for the topography of sensory maps, and activity-dependent plasticity are only depended on for auxiliary fine-tuning of the local circuit. However, when the developing sensory system receives aberrant sensory input indicating the need of compensatory corrections to default wiring plans, activity-dependent plasticity is then promoted to a leading role in the guidance process as it is now the sole avenue that would allow the circuit to reconcile with the unexpected perturbations in the input stream and reestablish normal sensory processing functions.

Input convergence and response homeostasis in the developing circuit

In Chapter IV, we showed that despite considerable tectal growth and tectal dendrite arbor elaboration occurring over developmental stages 45~48, the proportion of total tectal neuropil volume occupied by individual tectal dendritic fields remained unchanged. In contrast, RGC axon terminals also become more elaborate over the same developmental stages, yet the relative proportion of tectal neuropil they cover is reduced (Sakaguchi & Murphey, 1985). Functionally, we observed that the dendritic fields of tectal neurons each received inputs covering a large proportion of the total visual field representation present in the tectum, a proportion which remained stable over the observed developmental stages, pointing to an overall conservation of input

convergence from RGC afferents to tectal neurons in this early developmental period. The retinotectal circuit at this period of development faces dramatic nonlinear expansion of neuron populations in both the retina and the tectum, which would require the circuit to adapt quickly by shifting connections to preserve topographic organization (Gaze et al., 1979). Having tectal neurons consistently integrate from a large pool of presynaptic inputs during this process may be necessary for the circuit to maintain a stable information flow for visual processing computations, while also serving as a substrate for synaptic plasticity needed to perform the necessary adjustments to connectivity.

Homeostasis in input convergence can be commonly observed in developing neural circuits. In hamsters with partial SC ablation at birth, RGCs project to form a compressed retinotopic map in remaining SC fragment, yet neurons in the ablated colliculus showed similar RF sizes and spatial tuning properties compared to wild type as a result of a reduced number of RGC axons innervating the colliculus and reduced RGC arbor sizes (Pallas & Finlay, 1991; Xiong et al., 1994). In the SC of $\beta2^{-/-}$ mice lacking retinal waves, neurons had larger receptive fields, but for each neuron the sum of visual responses over their whole RF was also weaker, keeping the integrated response across the RF same as wild type (Chandrasekaran et al., 2005). Interestingly, this homeostasis in integrated response was maintained through different mechanisms at different developmental phases: in P6~P7 neurons sampled over a larger number of weaker inputs, but in P21~P25 they changed to having fewer retinal inputs with stronger synaptic strength over the same area (Chandrasekaran et al., 2007).

Tao and Poo (2005) performed whole cell voltage-clamp recordings in tectal neurons while visually stimulating different areas in the retina in Xenopus tadpoles from stage 44 to 48. The authors found a reduction in receptive field sizes accompanied by a reduction of integrated response over the whole RF, which they attributed to pruning of retinal inputs to the RF periphery. However, our observations in the dendritic fields of tectal neurons suggest that connections from these retinal inputs may in fact still be present, but computation is performed within the tectal neuron after receiving the inputs to produce the more restricted receptive field in the somatic response.

From microscale to macroscale: Organizational patterns and information encoding in sensory circuits

Sensory circuits are in essence multiscale architectures. From single synapses to the whole circuit, there is a typical transition from heterogeneity at local scales to homogeneity at global scales (Rothschild & Mizrahi, 2015), but spatial patterns can be found at every level of organization.

At the level of individual synapses, a common phenomenon is spatial clustering of synaptic responses, where neighboring synapses are more likely to be coactive than synapses further away. Synaptic clustering has been observed in mammalian hippocampus (Kleindienst et al., 2011; Takahashi et al., 2012) and visual cortex (Iacaruso et al., 2017; Leighton et al., 2024; Niculescu et al., 2018; Wilson et al., 2016; Winnubst et al., 2015), as well as Xenopus tectum (Podgorski et al., 2021). Leighton et al. (2024) found that synapses in the neonatal mouse V1 initially assemble in confined segments in dendrites, leaving other dendritic segments devoid of synapses; then as synapse number increases during development, dendrites eventually become covered with domains of co-active synapses. Numerous studies have found that synaptic clustering is driven by activity-dependent mechanisms (Niculescu et al., 2018; Podgorski et al., 2021; Winnubst et al., 2015).

Topographic order can be seen in the spatial preference of dendritic subfields in neurons in mouse primary visual cortex (V1) (Iacaruso et al., 2017) and Xenopus tectum (Bollmann & Engert, 2009), which is reflected in our observations in Chapter IV. Interestingly, this pattern of organization is not universal, as (Scholl et al., 2017) reported that spatial preference in dendritic spines of ferret V1 neurons display considerable variance with no apparent topographic distribution.

Mesoscale organizations at the level of neuron populations within a circuit often occur in the form of columnar patterns, as seen with orientation and direction selectivity maps in mammalian V1. Again, there is a species and brain area variation in how columnar patterns are manifested, as orientation/direction selectivity maps in rabbits and many rodent species show a salt-and-pepper organization with no columnar patterning

(Schmidt & Wolf, 2021). Jang et al. (2020) compared orientation maps in 8 mammalian species and found that whether a species displays salt-and-pepper or columnar orientation is related to their size ratio of V1-to-retina. However, this concept is challenged by recent observations of orientation columns in a small primate with low V1-to-retina ratio (Ho et al., 2021), and salt-and-pepper orientation organization in a large rodent with high V1-to-retina ratio (Ferreiro et al., 2021). Taken together with observations of columnar organization in the V1 of marsupials (Jung et al., 2022) and orientation tuning patterns in mouse SC (Feinberg & Meister, 2015), it is likely that there is an evolutionarily common genetic substrate for producing elements in the circuit necessary to form columnar organization, such as long-range horizontal connections (Kaschube et al., 2010; Schmidt & Galuske, 2023), and these genes are expressed divergently in different evolutionary branches to produce different results. Notably, Smith et al. (2018) showed that local, heterogeneous connections generated long-range correlations in spontaneous activity that predicted the structure of orientation columns in mature animals, suggesting that columnar organization can also form in an activity-dependent, self-organizing manner from activity patterns arising spontaneously from local circuit connections.

Ultimately, organizational patterns in sensory circuits are surface manifestations of the connectivity and synaptic interaction mechanisms that contribute to visual computation in the circuit. As such, developmental “refinement” may be better understood in the context of improvement in information encoding at different organizational levels in the circuit.

In a recently published study, Munn et al. (2024) surveyed neural coding in brains of five phylogenetically diverse species (*C.elegans*, Drosophila, zebrafish, mice and macaques) and found a common hierarchical structure in neuronal ensembles that balances efficiency and resiliency of information encoding. The authors used a computational method to identify ensembles within neurons in the whole brain (or sensory cortex in the case of Drosophila, mouse and macaque) by greedily pairing neurons based on pairwise correlation in their activity, then iteratively pairing smaller ensembles to form larger ensembles. This creates a microscale-to-macroscale ladder of

ensemble sizes from which to evaluate population encoding at different scales within the system. When evaluating fine-scale ensembles containing only a few correlated neurons, the level of correlation between ensembles was very low, translating to low levels of information redundancy that supports high encoding efficiency. However, when grouping neurons into increasingly larger ensembles, the level of information redundancy across ensembles increased exponentially with ensemble size, which supports a population code that is resilient to local change.

The tadpole tectum offers a very limited substrate for hierarchical encoding structures with its small size, and the large receptive field representations we observed in our mapping results suggest high levels of information redundancy starting at the dendritic scale. However, in the work presented in this thesis we have only looked at a single type of visual stimulus with a limited range of parameters, during early visual system development. It would be interesting to look into information encoding in the tectum with a larger battery of stimuli with different visual features, and evaluate whether developmental progression is accompanied by a change in information volume and redundancy.

Technical details and caveats

Visual response properties before developmental stage 44

In Chapter III we recorded visually-evoked responses and performed receptive field mapping in tadpoles at stage 42. We found that large stimuli presented at high contrast were required to drive visual responses, whereas at stage 45 and later the same animals responded readily to small stimuli presented at lower contrasts, consistent with previous reports (Holt & Harris, 1983). This difference may indicate functional immaturity of tectal neurons, but may also be a product of the optics of the eye: The tadpole eye is hyperopic at stage 42, and only becomes emmetropic after stage 45 (Richards et al., 2019).

Spike timing dependent plasticity (STDP) has been well characterized in tectal cells of Xenopus tadpoles, and studies have demonstrated its robust ability to modify receptive

field properties including direction selectivity and receptive field shape (Mu & Poo, 2006; Vislay-Meltzer et al., 2006; Zhang et al., 1998; Zhou et al., 2003). However, these studies were mostly performed in wild-type animals younger than stage 44. A study in our lab (Tsui et al., 2010) has shown that standard STDP protocols can only invoke lasting plasticity changes in tadpoles before stage 44, and other stimulation protocols must be used to induce plasticity in older tadpoles. In addition, STDP could not be reliably induced in albino tadpoles during the same STDP-sensitive period for wild-type animals.

In an electrophysiological analysis, van Rheede et al. (2015) also observed that many tectal neurons at stage 41~44 do not generate sensory-evoked spikes, and only convert to exhibiting spiking activity after receiving sensory experience. In all, stage 44 seems to be a diverging point for two different sets of visual processing and synaptic plasticity mechanisms, and there is also a potential difference between wild-type and albino tadpoles that must be considered when evaluating receptive field mapping results from this developmental period.

Diversity in tectal neurons

When analyzing tectal neuron responses in Chapter III and IV, we treated tectal neurons as a uniform group, though they are in fact a diverse population with cells varying greatly in morphology (Lazar, 1973) and response profiles (Ciarleglio et al., 2015). In addition, neurons vary in maturity along the R-C axis of the tectum, as newer cells are concentrated near the caudal proliferative zone (Herrgen & Akerman, 2016; Lazar, 1973; Straznicky & Gaze, 1972). Our morphometric analysis on tectal dendritic arbors of individual neurons in Chapter IV drew from cells located in roughly the same part of the tectum, but the population analyses of cell body receptive field sharpness in Chapter III and receptive field positions in Chapter IV included cells from all positions along the R-C axis. As such, there may be obscured experimental effects in the population analyses that can be parsed by sorting tectal cells through functional clustering and analysing different functional groups separately.

Inter-animal variability

We observed a considerable amount of variability between our animals, notably in the layout of topographic gradients. While both azimuth and elevation gradients can generally be found to lay across the rostrocaudal axis, the precise orientation of gradients within the tectal volume, as well as its range and steepness can vary wildly. Most gradients seen in a single optical section are unidirectional, but some animals displayed partial reversals in the gradient, which can be attributed to a wrapping topography in the map in three dimensions. This reversal may reflect the inclusion in the imaging field of pretectal areas, which are not easily segmented anatomically from the main input field in the Xenopus tectum. Another possibility source of this variability is differing levels of maturation in these animals: tadpoles from the same clutch raised in identical conditions can still be seen to mature at different rates, with some tadpoles lagging a full developmental stage behind others. Tadpoles were also staged by morphological criteria with an emphasis at stage 42-48 on the morphology of the gut (Nieuwkoop & Faber, 1994; Zahn et al., 2022), which may not be a good indicator of the maturity of the tectum. Another factor that may have not been adequately controlled for is the circadian cycle, which has been implied to affect retinal function (Anderson & Green, 2000). Our tadpoles were reared in incubators under controlled light-dark cycles, but imaging sessions last up to several hours and were carried out in a dark environment, and tadpoles remain under the effect of paralytic for up to 24 hours, which may perturb circadian rhythm.

Quantitative characterization of topographic gradient

The direction and steepness of the topographic gradient in the tectum for retinotopy in the cardinal visual axes were among the key properties we wished to compare between developmental stages. This proved to be complicated due to the shape of the tectal neuropil, elongated along the rostrocaudal axis and pinched at the rostral and caudal extremities. We devised two methods to describe the topographic gradient, one by summing local three-dimensional gradient vectors throughout the neuropil volume to acquire a “global” gradient vector, and the second by collapsing two-dimensional space in an optical section onto the rostrocaudal axis of the neuropil and calculating a linear fit

to the distribution of RF positions along the R-C axis. Both methods are susceptible to skew from nonuniform distribution of datapoints in space due to neuropil shape, as well as uneven distribution of SNR in the neuropil that tends to be higher in more superficial optical sections and near the center of the rostrocaudal axis, and fall off at deeper sections and near rostral and caudal extremities. An additional layer of complexity is introduced by significant change in tectum shape between developmental stages, making it difficult to align positional coordinates for comparison. A potential direction to solve these issues is to register images to a morphological template of the tadpole tectum, a process that has been widely performed in the creation of digital brain atlases in different species including the zebrafish (Légaré et al., 2023).

Use of GCaMP6s to visualise neuronal activity

Among the genetically encoded calcium indicators available to us at the time of our experiments, we chose GCaMP6s over GCaMP6f in the same family, with GCaMP6s having a higher signal-to-noise ratio but slower dynamics compared to GCaMP6f (Chen et al., 2013). The slow decay time of GCaMP6s (1.8sec $\tau_{1/2}$ after 10 APs) presents a caveat to our retinotopic mapping experiments, especially with the method using continuously drifting bars. To correct for response latency from the combination of slow GCaMP dynamics and tectal cell response profiles to continuous stimulation, we performed mapping with drifting bars in pairs of trials in opposite directions and took the difference between extracted peak response phase values to obtain the final estimate for receptive field position. However, tectal cells generally show preference for one of the two directions (see Chapter III Fig.III.S1C-D and Chapter IV Fig.IV.5), which can potentially lead to skewed results in our RF position estimates.

Another experimental concern is potential side-effects from chronic GCaMP expression in our tadpoles starting from birth. The calmodulin in GCaMP variants including GCaMP6 interferes with L-type calcium channels, disrupting calcium dynamics and gene expression (Yang et al., 2018). Reported side effects for chronic GCaMP expression include cytotoxicity (Resendez et al., 2016; Tian et al., 2009) and aberrant brain activity (Steinmetz et al., 2017). While we did not observe higher rates of morphological deformations in our GCaMP tadpoles compared to wild type animals, nor

any abnormal changes in GCaMP activity over imaging sessions, there remains the possibility of chronic GCaMP expression in our tadpoles introducing undetected artefacts to our experimental data.

Dual-color GECI expression paradigm for imaging pre- and postsynaptic tectal circuitry

In Chapter III we took advantage of lateral hemi-mosaic expression of GCaMP induced by mRNA blastomere injection to separately visualise calcium activity in RGC axon terminals and tectal cells in opposite tectal hemispheres in the same animal. It is possible to extend this technique to visualise the pre- and postsynaptic components of the retinotectal pathway within the same tectal hemisphere by expressing two differently colored calcium indicators. To this end, we have tested injecting jRGECO1a (a red genetically encoded calcium indicator (Dana et al., 2016)) mRNA into one blastomere of two-cell stage embryos of GCaMP6s transgenic animals, and successfully obtained tadpoles with general GCaMP6s expression and jRGECO1a expression restricted to one lateral half (Fig.V.1). Under the two-photon microscope we were able to see clear jRGECO1a fluorescence in RGC axon terminals and GCaMP6s fluorescence in tectal cells in the same tectal hemisphere, and visually evoked responses recorded with both indicators were robust. However, the signal-to-noise ratio in the axon terminals was considerably lower than in tectal cells, likely due to sparser distribution of axonal fibers in the neuropil compared to tectal cell dendrites. Furthermore, it was difficult to find a suitable optical filter for stimulus presentation that blocks both red and green wavelengths for simultaneous two-photon imaging of GCaMP and jRGECO, while still passing through sufficient light for visual stimulation. We tested visual stimulation through a Wratten #47 deep blue filter, which left considerable amounts of light bleed-through into the red channel even at low illumination levels. Regardless, our preliminary results present this method as a promising avenue to study map formation in different compartments of the tectal circuitry, which can be made viable in the future by improved calcium indicators and optical filters that provide more specific bandpass filtering. The issue of stimulus illumination bleed-through can also be circumvented by staggering the timing of image capture and visual stimulus presentation to illuminate the monitor only

during the flyback periods of the scanned laser.

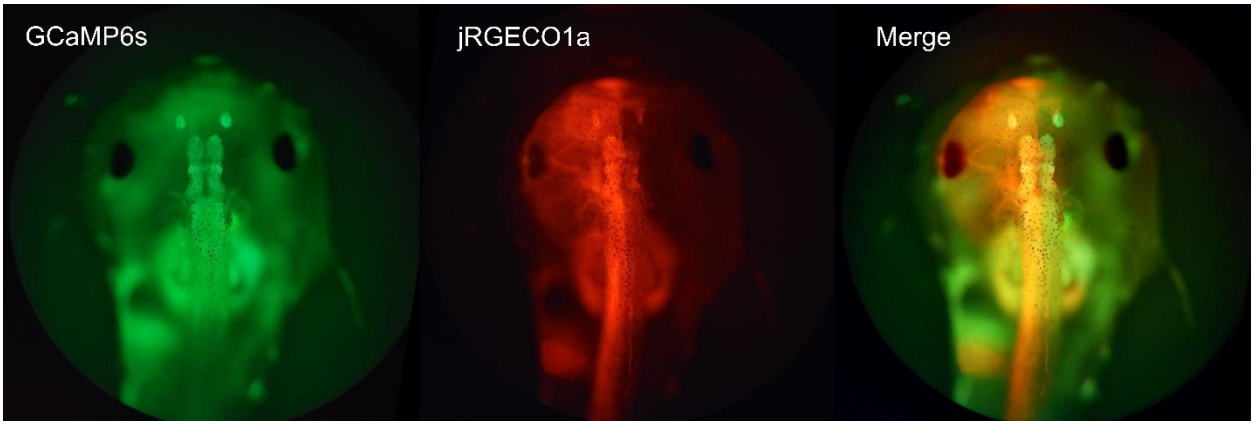

Figure V.1. GCaMP6s transgenic tadpole with jRGECO1a expression on left side. Widefield epifluorescence images of a GCaMP6s transgenic tadpole with hemi-mosaic jRGECO1a expression from mRNA blastomere injection. jRGECO fluorescence is restricted to the left half of the animal.

Conclusion and future directions

In the work presented in this thesis, we characterized the layout of the functional retinotopic map in the Xenopus tadpole tectum at developmental stages 42 through 48, and quantified whether blocking NMDA receptor activity has an effect in fine-scale properties of map organization. We also evaluated the relationship between individual tectal cells and the whole tectum in the context of development between stages 45 and 48, comparing how morphometric changes translate to functional changes in retinotopic representation at single-cell versus whole-circuit levels of organization.

There are several potential avenues for further research or improvement of existing methods used in these studies:

In Chapter III, we compared functional retinotopy in pre- and postsynaptic components of the tectal circuit by imaging RGC axon terminals and tectal cells separately in tadpoles with hemilateral GCaMP expression. It is potentially feasible to image activity in RGC axon terminals and tectal cells in the same tectal hemisphere by labelling RGCs

and tectal cells with different colored calcium indicators. However, difference in the density of RGC axonal and tectal dendritic arbors must be taken into account when evaluating fine-scale differences in map organization.

In Chapter IV, we labeled individual tectal cells in GCaMP-expressing tadpoles and evaluated visual receptive fields within their dendritic arbors, but we were unable to acquire receptive field measurements from their cell soma. This experimental setup can potentially be improved by labelling single cells with a suitable red fluorescent calcium indicator, which should provide more pronounced somatic signals and additionally allow us to evaluate dendritic responses without signal contamination from neighboring dendrites.

In both studies we only evaluated visual receptive fields in response to flashed or drifting bars, but the tadpole tectum may have different encoding schemes for different types of visual stimuli. It would be interesting to examine a wider range of feature space and perform a more comprehensive evaluation on the amount of information encoded in the tectum, and explore how the structure and performance of information encoding changes with development.

References

Anderson, F. E., & Green, C. B. (2000). Symphony of rhythms in the Xenopus laevis retina. *Microscopy research and technique*, *50*(5), 360-372.

Arcaro, M., Schade, P., & Livingstone, M. (2018). Preserved cortical organization in the absence of early visual input. *Journal of Vision*, *18*(10), 27-27.

Barabási, D. L., Schuhknecht, G. F., & Engert, F. (2024). Functional neuronal circuits emerge in the absence of developmental activity. *Nature communications*, *15*(1), 364.

Bollmann, J. H., & Engert, F. (2009). Subcellular topography of visually driven dendritic activity in the vertebrate visual system. *Neuron*, *61*(6), 895-905.

Butt, O. H., Benson, N. C., Datta, R., & Aguirre, G. K. (2013). The fine-scale functional correlation of striate cortex in sighted and blind people. *Journal of Neuroscience*, *33*(41), 16209-16219.

Chandrasekaran, A. R., Plas, D. T., Gonzalez, E., & Crair, M. C. (2005). Evidence for an instructive role of retinal activity in retinotopic map refinement in the superior colliculus of the mouse. *Journal of Neuroscience*, *25*(29), 6929-6938.

Chandrasekaran, A. R., Shah, R. D., & Crair, M. C. (2007). Developmental homeostasis of mouse retinocollicular synapses. *Journal of Neuroscience*, *27*(7), 1746-1755. https://doi.org/10.1523/JNEUROSCI.4383-06.2007

Chapman, B., & Stryker, M. P. (1993). Development of orientation selectivity in ferret visual cortex and effects of deprivation. *Journal of Neuroscience*, *13*(12), 5251-5262.

Chen, T.-W., Wardill, T. J., Sun, Y., Pulver, S. R., Renninger, S. L., Baohan, A., Schreiter, E. R., Kerr, R. A., Orger, M. B., Jayaraman, V., Looger, L. L., Svoboda, K., & Kim, D. S. (2013). Ultrasensitive fluorescent proteins for imaging neuronal activity. *Nature*, *499*(7458), 295-300. https://doi.org/10.1038/nature12354

Ciarleglio, C. M., Khakhalin, A. S., Wang, A. F., Constantino, A. C., Yip, S. P., & Aizenman, C. D. (2015). Multivariate analysis of electrophysiological diversity of Xenopus visual neurons during development and plasticity. *elife*, *4*, e11351.

Cline, H. T., Debski, E. A., & Constantine-Paton, M. (1987). N-methyl-D-aspartate receptor antagonist desegregates eye-specific stripes. *Proceedings of the National Academy of Sciences*, *84*(12), 4342-4345.

Constantine-Paton, M., & Law, M. I. (1978). Eye-specific termination bands in tecta of three-eyed frogs. *Science*, *202*(4368), 639-641.

Dana, H., Mohar, B., Sun, Y., Narayan, S., Gordus, A., Hasseman, J. P., Tsegaye, G., Holt, G. T., Hu, A., & Walpita, D. (2016). Sensitive red protein calcium indicators for imaging neural activity. *elife*, *5*, e12727.

Dong, W., Lee, R. H., Xu, H., Yang, S., Pratt, K. G., Cao, V., Song, Y.-K., Nurmikko, A., & Aizenman, C. D. (2009). Visual avoidance in Xenopus tadpoles is correlated with the maturation of visual responses in the optic tectum. *Journal of neurophysiology*, *101*(2), 803-815. https://doi.org/10.1152/jn.90848.2008

Feinberg, E. H., & Meister, M. (2015). Orientation columns in the mouse superior colliculus. *Nature*, *519*(7542), 229-232.

Ferreiro, D. N., Conde-Ocazionez, S. A., Patriota, J. H., Souza, L. C., Oliveira, M. F., Wolf, F., & Schmidt, K. E. (2021). Spatial clustering of orientation preference in primary visual cortex of the large rodent agouti. *iScience*, *24*(1).

Gaze, R., Keating, M., Ostberg, A., & Chung, S. (1979). The relationship between retinal and tectal growth in larval Xenopus: implications for the development of the retino-tectal projection. *Development*, *53*(1), 103-143.

Gaze, R. M., Keating, M., & Chung, S. (1974). The evolution of the retinotectal map during development in Xenopus. *Proceedings of the Royal Society of London. Series B. Biological Sciences*, *185*(1080), 301-330.

Gnuegge, L., Schmid, S., & Neuhauss, S. C. (2001). Analysis of the activity-deprived zebrafish mutantmacho reveals an essential requirement of neuronal activity for the development of a fine-grained visuotopic map. *Journal of Neuroscience*, *21*(10), 3542-3548.

Goodhill, G. J. (1993). Topography and ocular dominance: a model exploring positive correlations. *Biological Cybernetics*, *69*(2), 109-118.

Guillamón-Vivancos, T., Aníbal-Martínez, M., Puche-Aroca, L., Moreno-Bravo, J. A., Valdeolmillos, M., Martini, F. J., & López-Bendito, G. (2022). Input-dependent

segregation of visual and somatosensory circuits in the mouse superior colliculus. *Science*, *377*(6608), 845-850.

Herrgen, L., & Akerman, C. J. (2016). Mapping neurogenesis onset in the optic tectum of Xenopus laevis. *Developmental neurobiology*, *76*(12), 1328-1341.

Higenell, V., Han, S. M., Feldheim, D. A., Scalia, F., & Ruthazer, E. S. (2012). Expression patterns of Ephs and ephrins throughout retinotectal development in Xenopus laevis. *Developmental neurobiology*, *72*(4), 547-563. https://doi.org/10.1002/dneu.20930

Ho, C. L. A., Zimmermann, R., Weidinger, J. D. F., Prsa, M., Schottdorf, M., Merlin, S., Okamoto, T., Ikezoe, K., Pifferi, F., & Aujard, F. (2021). Orientation preference maps in Microcebus murinus reveal size-invariant design principles in primate visual cortex. *Current Biology*, *31*(4), 733-741. e737.

Holt, C. E., & Harris, W. A. (1983). Order in the initial retinotectal map in Xenopus: a new technique for labelling growing nerve fibres. *Nature*, *301*(5896), 150-152. https://doi.org/10.1038/301150a0

Hubel, D. H., & Wiesel, T. N. (1970). The period of susceptibility to the physiological effects of unilateral eye closure in kittens. *The Journal of Physiology*, *206*(2), 419-436.

Iacaruso, M. F., Gasler, I. T., & Hofer, S. B. (2017). Synaptic organization of visual space in primary visual cortex. *Nature*, *547*(7664), 449-452.

Jang, J., Song, M., & Paik, S.-B. (2020). Retino-cortical mapping ratio predicts columnar and salt-and-pepper organization in mammalian visual cortex. *Cell Reports*, *30*(10), 3270-3279. e3273.

Jung, Y. J., Almasi, A., Sun, S. H., Yunzab, M., Cloherty, S. L., Bauquier, S. H., Renfree, M., Meffin, H., & Ibbotson, M. R. (2022). Orientation pinwheels in

primary visual cortex of a highly visual marsupial. *Science Advances*, *8*(39), eabn0954.

Kaschube, M., Schnabel, M., Löwel, S., Coppola, D. M., White, L. E., & Wolf, F. (2010). Universality in the evolution of orientation columns in the visual cortex. *Science*, *330*(6007), 1113-1116.

Kleindienst, T., Winnubst, J., Roth-Alpermann, C., Bonhoeffer, T., & Lohmann, C. (2011). Activity-dependent clustering of functional synaptic inputs on developing hippocampal dendrites. *Neuron*, *72*(6), 1012-1024.

Lazar, G. (1973). The development of the optic tectum in Xenopus laevis: a Golgi study. *Journal of anatomy*, *116*(Pt 3), 347.

Légaré, A., Lemieux, M., Desrosiers, P., & De Koninck, P. (2023). Zebrafish brain atlases: a collective effort for a tiny vertebrate brain. *Neurophotonics*, *10*(4), 044409-044409.

Leighton, A. H., Cheyne, J. E., & Lohmann, C. (2024). Clustered synapses develop in distinct dendritic domains in visual cortex before eye opening. *elife*, *12*, RP93498.

Li, Y., Fitzpatrick, D., & White, L. E. (2006). The development of direction selectivity in ferret visual cortex requires early visual experience. *Nature neuroscience*, *9*(5), 676-681.

Mann, F., Ray, S., Harris, W. A., & Holt, C. E. (2002). Topographic mapping in dorsoventral axis of the Xenopus retinotectal system depends on signaling through ephrin-B ligands. *Neuron*, *35*(3), 461-473.

Mu, Y., & Poo, M.-m. (2006). Spike timing-dependent LTP/LTD mediates visual experience-dependent plasticity in a developing retinotectal system. *Neuron*, *50*(1), 115-125.

Munn, B. R., Müller, E. J., Favre-Bulle, I., Scott, E., Lizier, J. T., Breakspear, M., & Shine, J. M. (2024). Multiscale organization of neuronal activity unifies scale-dependent theories of brain function. *Cell*.

Niculescu, D., Michaelsen-Preusse, K., Güner, Ü., van Dorland, R., Wierenga, C. J., & Lohmann, C. (2018). A BDNF-mediated push-pull plasticity mechanism for synaptic clustering. *Cell Reports*, *24*(8), 2063-2074.

Nieuwkoop, P. D., & Faber, J. (1994). *Normal Table of Xenopus Laevis (Daudin): A Systematical and Chronological Survey of the Development from the Fertilized Egg Till the End of Metamorphosis*. Garland Pub.

Obermayer, K., Ritter, H., & Schulten, K. (1990). A principle for the formation of the spatial structure of cortical feature maps. *Proceedings of the National Academy of Sciences*, *87*(21), 8345-8349.

Olson, M. D., & Meyer, R. L. (1991). The effect of TTX‐activity blockade and total darkness on the formation of retinotopy in the goldfish retinotectal projection. *Journal of Comparative Neurology*, *303*(3), 412-423.

Pallas, S., & Finlay, B. (1991). Compensation for population size mismatches in the hamster retinotectal system: alterations in the organization of retinal projections. *Visual neuroscience*, *6*(3), 271-281.

Pietri, T., Romano, S. A., Pérez-Schuster, V., Boulanger-Weill, J., Candat, V., & Sumbre, G. (2017). The emergence of the spatial structure of tectal spontaneous activity is independent of visual inputs. *Cell Reports*, *19*(5), 939-948.

Podgorski, K., Toth, T. D., Coleman, P., Opushnyev, S., Brusco, J., Hogg, P., Edgcumbe, P., & Haas, K. (2021). Comprehensive imaging of synaptic activity reveals dendritic growth rules that cluster inputs. *bioRxiv*, 2021.2002. 2011.430646.

Razak, K. A., & Pallas, S. L. (2006). Dark rearing reveals the mechanism underlying stimulus size tuning of superior colliculus neurons. *Visual neuroscience*, *23*(5), 741.

Reh, T., & Constantine-Paton, M. (1985). Eye-specific segregation requires neural activity in three-eyed Rana pipiens. *Journal of Neuroscience*, *5*(5), 1132-1143.

Resendez, S. L., Jennings, J. H., Ung, R. L., Namboodiri, V. M. K., Zhou, Z. C., Otis, J. M., Nomura, H., McHenry, J. A., Kosyk, O., & Stuber, G. D. (2016). Visualization of cortical, subcortical and deep brain neural circuit dynamics during naturalistic mammalian behavior with head-mounted microscopes and chronically implanted lenses. *Nature protocols*, *11*(3), 566-597.

Richards, B. A., Lillicrap, T. P., Beaudoin, P., Bengio, Y., Bogacz, R., Christensen, A., Clopath, C., Costa, R. P., de Berker, A., & Ganguli, S. (2019). A deep learning framework for neuroscience. *Nature neuroscience*, *22*(11), 1761-1770.

Rothschild, G., & Mizrahi, A. (2015). Global order and local disorder in brain maps. *Annual Review of Neuroscience*, *38*, 247-268.

Sakaguchi, D. S., & Murphey, R. K. (1985). Map formation in the developing Xenopus retinotectal system: an examination of ganglion cell terminal arborizations. *Journal of Neuroscience*, *5*(12), 3228-3245. https://doi.org/10.1523/JNEUROSCI.05-12-03228.1985

Scalia, F., Currie, J. R., & Feldheim, D. A. (2009). Eph/ephrin gradients in the retinotectal system of Rana pipiens: developmental and adult expression patterns. *Journal of Comparative Neurology*, *514*(1), 30-48.

Schmidt, K. E., & Galuske, R. A. (2023). Functional columnar organization and long-range circuits in different cortical systems. In (Vol. 17, pp. 1168606): Frontiers Media SA.

Schmidt, K. E., & Wolf, F. (2021). Punctuated evolution of visual cortical circuits? Evidence from the large rodent Dasyprocta leporina, and the tiny primate Microcebus murinus. *Current Opinion in Neurobiology*, *71*, 110-118.

Scholl, B., Wilson, D. E., & Fitzpatrick, D. (2017). Local order within global disorder: synaptic architecture of visual space. *Neuron*, *96*(5), 1127-1138. e1124.

Simon, D. K., & O'Leary, D. D. (1992). Development of topographic order in the mammalian retinocollicular projection. *Journal of Neuroscience*, *12*(4), 1212-1232. https://doi.org/10.1523/JNEUROSCI.12-04-01212.1992

Smith, G. B., Hein, B., Whitney, D. E., Fitzpatrick, D., & Kaschube, M. (2018). Distributed network interactions and their emergence in developing neocortex. *Nature neuroscience*, *21*(11), 1600-1608.

Steinmetz, N. A., Buetfering, C., Lecoq, J., Lee, C. R., Peters, A. J., Jacobs, E. A., Coen, P., Ollerenshaw, D. R., Valley, M. T., & De Vries, S. E. (2017). Aberrant cortical activity in multiple GCaMP6-expressing transgenic mouse lines. *eneuro*, *4*(5).

Straznicky, K., & Gaze, R. (1972). The development of the tectum in Xenopus laevis: an autoradiographic study. *Development*, *28*(1), 87-115.

Swindale, N. (1996). The development of topography in the visual cortex: a review of models. *Network: Computation in neural systems*, *7*(2), 161-247.

Takahashi, N., Kitamura, K., Matsuo, N., Mayford, M., Kano, M., Matsuki, N., & Ikegaya, Y. (2012). Locally synchronized synaptic inputs. *Science*, *335*(6066), 353-356.

Tao, H. W., & Poo, M.-m. (2005). Activity-dependent matching of excitatory and inhibitory inputs during refinement of visual receptive fields. *Neuron*, *45*(6), 829-836.

Tian, L., Hires, S. A., Mao, T., Huber, D., Chiappe, M. E., Chalasani, S. H., Petreanu, L., Akerboom, J., McKinney, S. A., & Schreiter, E. R. (2009). Imaging neural activity

in worms, flies and mice with improved GCaMP calcium indicators. *Nature Methods*, *6*(12), 875-881.

Tsui, J., Schwartz, N., & Ruthazer, E. S. (2010). A developmental sensitive period for spike timing-dependent plasticity in the retinotectal projection. *Frontiers in synaptic neuroscience*, *2*, 1392.

Van Horn, M. R., Strasser, A., Miraucourt, L. S., Pollegioni, L., & Ruthazer, E. S. (2017). The gliotransmitter d-serine promotes synapse maturation and axonal stabilization in vivo. *Journal of Neuroscience*, *37*(26), 6277-6288.

van Rheede, J. J., Richards, B. A., & Akerman, C. J. (2015). Sensory-evoked spiking behavior emerges via an experience-dependent plasticity mechanism. *Neuron*, *87*(5), 1050-1062.

Vislay-Meltzer, R. L., Kampff, A. R., & Engert, F. (2006). Spatiotemporal Specificity of Neuronal Activity Directs the Modification of Receptive Fields in the Developing Retinotectal System. *Neuron*, *50*(1), 101-114. https://doi.org/10.1016/j.neuron.2006.02.016

Wiesel, T. N., & Hubel, D. H. (1963). Single-cell responses in striate cortex of kittens deprived of vision in one eye. *Journal of neurophysiology*, *26*(6), 1003-1017.

Wiesel, T. N., & Hubel, D. H. (1965). Comparison of the effects of unilateral and bilateral eye closure on cortical unit responses in kittens. *Journal of neurophysiology*, *28*(6), 1029-1040.

Wilson, D. E., Whitney, D. E., Scholl, B., & Fitzpatrick, D. (2016). Orientation selectivity and the functional clustering of synaptic inputs in primary visual cortex. *Nature neuroscience*, *19*(8), 1003-1009.

Winnubst, J., Cheyne, J. E., Niculescu, D., & Lohmann, C. (2015). Spontaneous activity drives local synaptic plasticity in vivo. *Neuron*, *87*(2), 399-410.

Xiong, M., Pallas, S. L., Lim, S., & Finlay, B. L. (1994). Regulation of retinal ganglion cell axon arbor size by target availability: Mechanisms of compression and expansion of the retinotectal projection. *Journal of Comparative Neurology*, *344*(4), 581-597.

Yang, Y., Liu, N., He, Y., Liu, Y., Ge, L., Zou, L., Song, S., Xiong, W., & Liu, X. (2018). Improved calcium sensor GCaMP-X overcomes the calcium channel perturbations induced by the calmodulin in GCaMP. *Nature communications*, *9*(1), 1504.

Zahn, N., James-Zorn, C., Ponferrada, V. G., Adams, D. S., Grzymkowski, J., Buchholz, D. R., Nascone-Yoder, N. M., Horb, M., Moody, S. A., & Vize, P. D. (2022). Normal Table of Xenopus development: a new graphical resource. *Development*, *149*(14), dev200356.

Zhang, L. I., Tao, H. W., Holt, C. E., Harris, W. A., & Poo, M.-m. (1998). A critical window for cooperation and competition among developing retinotectal synapses. *Nature*, *395*(6697), 37-44. https://doi.org/10.1038/25665

Zhou, Q., Tao, H. W., & Poo, M.-m. (2003). Reversal and stabilization of synaptic modifications in a developing visual system. *Science*, *300*(5627), 1953-1957.

Appendix

Reprint license for Fig.I.1 (Configuration of the retinotectal map)

Order Details

1. Annual review of cell and developmental biology

Article: Retinotectal mapping: new insights from molecular genetics.

Billing Status: Open

Print License

Order License ID	1558835-1	**Type of Use**	Republish in a thesis/dissert...
Order detail status	Completed	**Publisher**	ANNUAL REVIEWS
ISSN	1530-8995	**Portion**	Image/photo/illustration

0.00 CAD

Republication Permission

Hide Details

Publisher Terms and Conditions

LICENSED CONTENT

Publication Title	Annual review of cell and de...	**Publication Type**	e-Journal
Article Title	Retinotectal mapping: new i...	**Start Page**	551
Author / Editor	ANNUAL REVIEWS, INC.	**End Page**	580
Date	01/01/1995	**Issue**	1
Language	English	**Volume**	21
Country	United States of America	**URL**	http://arjournals.annualrevi...
Rightsholder	Annual Reviews, Inc.		

REQUEST DETAILS

Portion Type	Image/photo/illustration	**Distribution**	Worldwide
Number of Images / Photos / Illustrations	1	**Translation**	Original language of publica...
		Copies for the Disabled?	No
Format (select all that apply)	Electronic	**Minor Editing Privileges?**	No
Who Will Republish the Content?	Academic institution	**Incidental Promotional Use?**	No
		Currency	CAD
Duration of Use	Life of current edition		
Lifetime Unit Quantity	Up to 250,000		
Rights Requested	Main product		

NEW WORK DETAILS

Title	With a bright young mind an...	**Institution Name**	McGill University
Instructor Name	Edward S. Ruthazer	**Expected Presentation Date**	2024-12-22

ADDITIONAL DETAILS

The Requesting Person / Organization to Appear on the License	Vanessa Li

REQUESTED CONTENT DETAILS

Title, Description or Numeric Reference of the Portion(s)	Figure 1	**Title of the Article / Chapter the Portion Is From**	Retinotectal mapping: new i...
Editor of Portion(s)	Lemke, Greg; Reber, Michaël	**Author of Portion(s)**	Lemke, Greg; Reber, Michaël
Volume / Edition	21	**Issue, if Republishing an Article From a Serial**	1
Page or Page Range of Portion	551-580		
		Publication Date of Portion	2005-11-10

Reprint license for Fig.I.2 (Schematic of an NMDA receptor)

License Number	5936660389410
License date	Dec 26, 2024

Printable Details

Licensed Content

Licensed Content Publisher	Elsevier
Licensed Content Publication	Behavioural Brain Research
Licensed Content Title	Overlap in the neural circuitry and molecular mechanisms underlying ketamine abuse and its use as an antidepressant
Licensed Content Author	Saurabh S. Kokane,Ross J. Armant,Carlos A. Bolaños-Guzmán,Linda I. Perrotti
Licensed Content Date	Apr 20, 2020
Licensed Content Volume	384
Licensed Content Issue	n/a
Licensed Content Pages	1

Order Details

Type of Use	reuse in a thesis/dissertation
Portion	figures/tables/illustrations
Number of figures/tables/illustrations	1
Format	electronic
Are you the author of this Elsevier article?	No
Will you be translating?	No

About Your Work

Title of new work	With a bright young mind and a map to see: Imaging topographic map reorganization in the developing visual system
Institution name	Edward S. Ruthazer
Expected presentation date	Dec 2024

Additional Data

Portions	Figure 1
The Requesting Person / Organization to Appear on the License	Vanessa Li

Requestor Location

Requestor Location	Vanessa Li 3801 Rue University Montréal, QC H3A 2B4 Canada

Tax Details

Publisher Tax ID	GB 494 6272 12